THE INFLUENCE OF THERMAL MODIFICATION ON THE RESISTANCE TO WATER IMPACT PROPERTIES AND STRENGTH OF WOOD USED IN OUTDOOR CONDITIONS

Darius Albrektas, Milda Jucienė, Vaida Dobilaitė
Raimondas Bliūdžius
Kaunas University of Technology
Lithuania

ABSTRACT

In this study the influence of thermal modification on the resistance of wood to the impact of water and mechanical properties and to compare the durability of thermally modified and coated wood products operating in wet conditions was investigated. It was found that the weight of thermally unmodified non-coated oak wood after 48 h of soaking increased on average up to ~ 15%, and the weight of coated oak wood increased up to ~ 8%. If wood was thermally modified, the weight of non-coated oak wood increased up to ~ 9%, and the weight of coated oak wood increased up to ~ 5%. After 168 h of soaking these change is about 2 times larger. In the case of pine wood compared to oak wood these change of weight after 48 h is about 2.0 – 2.4 times and after 168 h about 1.4 - 2.0 larger. It can be stated that wooden constructions intended to be used in very wet conditions should be made of thermally modified wood without coating. Thermally modified wood will have greater dimensional and shape stability. Thermal modification reduces the swell up to 1.6 times in the case of oak, more than 2 times in the case of pine.

KEYWORDS: Coating, sorption properties, strength, thermal modification, wood.

INTRODUCTION

The problem of the durability of the wood becomes relevant as the wood is exposed to the atmosphere impacts, rains on it, and therefore has the ability to absorb large amounts of water. This causes wood deformation, swelling, and, after longer exposure of these factors, wood is vulnerable to destructive fungus and biological pests. In construction, the durability of wood in the open atmosphere is usually enhanced by the chemical treatment of the wood or by coating

with various coatings. The effect of moisture can be reduced by coating wood with various paints, waxes, oils, biocides or a combination of thereof (Wood Handbook 2010, Zlahtic-Zupanc et al. 2018). However, this way of treating wood in the paths is undesirable in valuable natural areas, as chemicals washed out of wood can damage the environment and coating is not compatible with the natural environment. Therefore, there is a search for alternative ways of increasing the durability of outdoor wood that would be suitable for use in natural environment conditions.

One of the most effective modifications to increase the resistance and durability of wood is thermal modification. It has been found that thermal modification improves the resistance of the wood to the atmospheric impact, the surface of the thermally modified wood, which is naturally worn due to the environmental impact, is better than that of the thermally unmodified (Deka et al. 2007). Although not moderately, thermally modified at 170-230°C, wood swelling factors due to structural changes are significantly reduced (Esteves et al. 2008, Cao et al. 2011). This is relevant to wooden structures operating under extremely wet and changing conditions.

It is known that the biological durability of thermally modified wood is superior to unmodified wood. The main factor is the thermochemical modification of cell wall polymers (predominantly hemicellulose) (Sustersic et al. 2010, Candelier et al. 2013, Mohareb et al. 2011). The resistance to biological effects correlates well with weight loss and chemical composition of wood after thermal modification. Therefore, knowing how much wood has lost its weight or its chemical composition or its biological durability can be predicted. Thermal modification of the wood first causes the breakdown of hemicellulose and the removal of many extractive substances. It is known that the hydroxyl groups, which are in hemicellulose, are the main determinants of the process of wood shrinkage - swelling. In addition, hemicellulose is one of the main 'nutrients' for biological pests that destroy wood. Some of wood mechanical properties, which in many cases deteriorate are changing in a positive direction due to thermal modification of the wood. In many cases, after heat treatment chemical changes influenced structure of the cell walls, density of wood and e.g. content of resin in conifer wood, etc.

However, thermal modification changes the mechanical properties of wood, which often deteriorate (Jimenez et al. 2011, Borrega and Karenlampi 2007, Kol et al. 2015). The reduction in the resistance of thermally modified wood to static bending and tension perpendicular to the grain correlates with the level of hemicellulose depolymerisation reactions, which mostly depend on the temperature of the process (Borrega and Karenlampi 2007, Hannouz et al. 2015, Younsi et al. 2010). Mechanical strength is not the most important feature of thermally modified wood and therefore there is no change in the mechanical properties of wood after thermal analysis. There is also a lack of research on thermally modified wood behaviours under very humid conditions.

The aim of the work is to evaluate the influence of thermal modification on the resistance of wood to the impact of water and mechanical properties and to compare the durability of thermally modified and coated wood products operating in wet conditions.

MATERIALS AND METHODS

Oak and pine wood samples with dimensions of 100 × 100 × 15 mm and density of 515 - 655 kg·m^{-3} and 435 - 470 kg·m^{-3} were used for research according to standard EN 323. Humidity varied between 8.5% and 10.2% (determined by a humidity meter according to standard EN 13183-2). Wood fibre direction was random; semi-tangential, semi-radial incision prevailed.

A summary of the research is presented in Fig. 1. Before the test, all samples were conditioned for 14 days in a room with a temperature of $20 \pm 2°C$, relative humidity within the range was of 60-62% (standard EN 408, point 8). After conditioning, the parts of the oak and pine wood samples were left in the conditioned room and the rest were dried to a constant weight at 103°C. In order to avoid drying defects during thermal modification according to standard EN 13183-1 and heated at temperatures of 140°C, 165°C, 190°C and 215°C for 3 hours. After thermal modification, the samples were cooled in a conditioned room.

The temperature and duration of the thermal modification has been selected after analysing other works and changes in the wood due to temperature effects (Younsi et al. 2010, Kol 2010, Albrektas and Navickas 2017). Samples for heating were selected randomly.
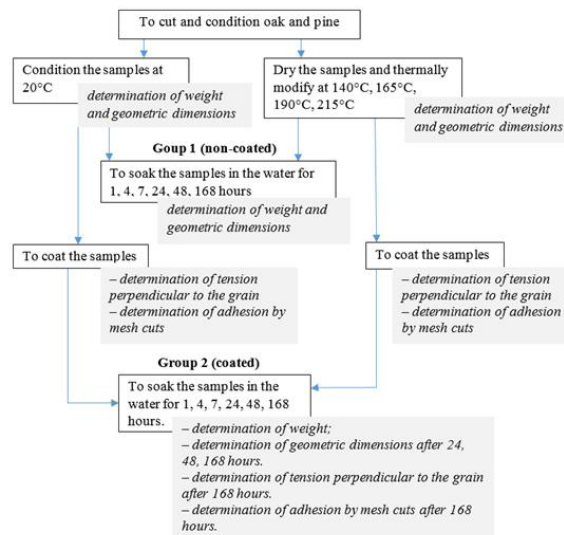

Fig. 1: A summary of the experimental plan.

Thermally modified and unmodified samples were divided into 2 groups. Samples in group 1 were not coated with paints. The surface of group 2 samples was grounded manually, the graininess of used abrasive material is P120 according to FEPA (Federation of European Producers of Abrasives), then the samples were coated on all sides with 2-layer brush with commercial paints intended for various surfaces for outdoor coating, water-based paints, where non-volatile materials are 62.6% (ISO 3251, 2008), density is 1.451 $g \cdot cm^{-3}$ (ISO 2811-1, 2016). Samples were coated according to the manufacturer's recommendations. The second layer was coated, when the first one completely dried, after one day. The coated samples were dried in a conditioned room for 7 days. Subgroup codes and sample processing methods are presented in Tab. 1.

Tab. 1: Marking of samples.

Thermal modification temperature (°C)	Subgroup name (oak wood)		Subgroup name (pine wood)	
	Group 1 Non-coated	Group 2 Coated	Group 1 Non-coated	Group 2 Coated
20 (unmodified)	O.I.20	O.II.20	P.I.20	P.II.20
140	O.I.140	O.II.140	P.I.140	P.II.140
165	O.I.165	O.II.165	P.I.165	P.II.165
190	O.I.190	O.II.190	P.I.190	P.II.190
215	O.I.215	O.II.215	P.I.215	P.II.215

Samples of O.I.20, O.II.20, P.I.20 and P.II.20 subgroups are samples that were in air-conditioned state. Five samples of each subgroup were randomly selected and their geometric parameters (accuracy of 0.02 mm), weight (accuracy of 0.01 g) were determined. Thermally modified and unmodified samples of Group 1 and Group 2 were soaked in distilled water. During the entire soaking period, the samples were completely immersed in water at a temperature of 20°C ± 2°C under atmospheric pressure.

After 1, 4, 7, 24, 48 and 168 hours, the weight of samples was fixated. After 24, 48 and 168 hours, the dimensions of the samples were recorded. The relative change in weight and dimensions across and along the grain was calculated.
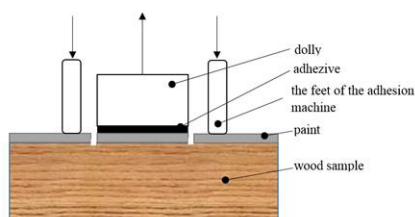

Fig. 2: Test of tension perpendicular of the samples to the grain.

Tension perpendicular of the sample to the grain and adhesion by the mesh cut method was determined before the soaking process and after 168 hours (7 days) of soaking. According to ISO 4624 (2016), tension perpendicular of the sample to the grain was determined in each sample by tearing 4 zones, using dollies of 2 cm diameter (Fig. 2). A visual inspection of the tearing site was performed to determine the mechanism of failure.

Determination of adhesion by mesh cuts was done according to standard ISO 2409 (2013). Cut direction is 45° to grain. The distance between the cuts is 3 mm taking into account that the thickness of the coating is > 120 μm (thickness is measured according to EN ISO 2808 (2019), method 4A). Peeled off coating particles were removed using a pressure sensitive adhesive tape. The test was carried out according to the requirements of the standard EN ISO 13076 (2012), with an average illumination of 900 lx. The coefficient of variation of the test results did not exceed 8%.

RESULTS AND DISCUSSION

Influence of thermal modification and coating on the sorption properties of wood

The modified, unmodified and coated specimens were soaked in water. The relative change in weight of coated and non-coated oak and pine wood samples, when soaking in water, is shown in Fig. 3.
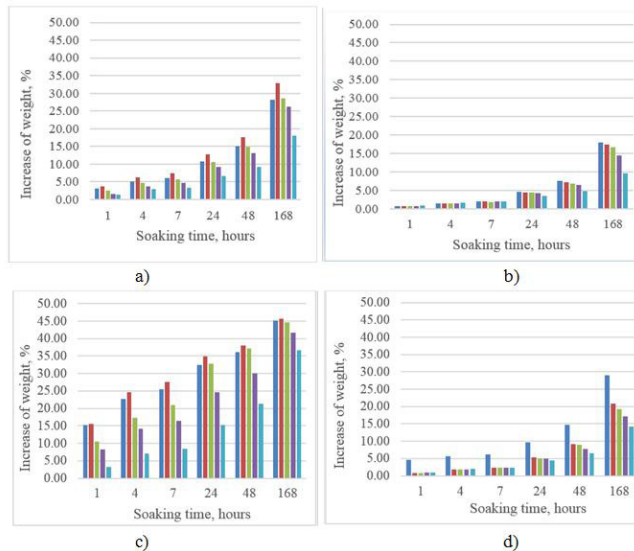

Fig. 3: The increase of oak wood O.I (a) and O.II (b) and pine wood P.I (c) and P.II (d) samples weight (%), when soaking them in the water, when the samples are thermally unmodified at 20°C and thermally modified at temperatures (°C):

■ 20 ■ 140 ■ 165 ■ 190 ■ 215

It can be seen, in the case of oak wood (Fig. 3a,b), the weight of thermally unmodified non-coated wood after 48 h of soaking increased on average up to ~ 15%, and the weight of coated wood increased up to ~ 8%. If wood was thermally modified at ~ 215°C, the weight of non-coated wood increased up to ~ 9%, and the weight of coated wood increased up to ~ 5%. The difference (of thermally unmodified and thermally modified) was about 1.7 and 1.6 times, respectively.

After 168 h of soaking, the weight of thermally unmodified non-coated wood increased up to 28%, and the weight of coated wood rose up to 18%. If wood was thermally modified at 215°C, its weight (non-coated and coated) increased approximately to 18 and 10% respectively. The difference between thermally unmodified and thermally modified oak wood is about 1.6 and 1.8 times.

In the case of pine wood (Fig. 3c,d), more significant changes in results are seen after 48 hours of soaking. The weight of thermally unmodified non-coated wood has increased up to ~ 36%, the weight of thermally unmodified coated pine increased approximately to ~ 15%. If wood was thermally modified at 215°C, the weight of non-coated and coated pine increased up to 21 and 7% respectively. The difference between thermally unmodified and thermally modified wood samples was 1.7 and 2.1 times.

After 168 h of soaking, the weight of thermally unmodified non-coated wood increased up to ~ 45% and coated wood samples up to ~ 29%. If wood was thermally modified at 215°C, the weight of non-coated and coated pine increased up to 37 and 14% respectively. In this case, the

difference between thermally unmodified and thermally modified wood samples (non-coated and coated) was 1.2 and 2.1 times. The results of these tests could be explained by differences in the structure of pine and oak wood.

In the case of non-coated wood, thermally modified samples at 140°C can be excluded. They soaked more water than thermally non-coated thermally unmodified and modified wood samples at higher temperatures (Fig. 3a,c). The wood, after heating at 140°C, is very dry (to get completely dry wood, it can be dried and at 103°C, as indicated in the standard EN 13183-1). However, when heating at this temperature, there are no significant changes in the structure of wood or chemical composition, determining its hygroscopicity (Sundqvist 2004, Yildiz et al. 2006, Garrote et al. 1999). Thus, it can be stated that at this temperature the wood is dried rather than modified (almost no increase in hydrophobicity). Unmodified wood had a higher moisture content (about 10.3 - 11.2%) before soaking. This resulted in a greater increase in the weight of the soaked dry wood, i.e. it absorbed more water at the same time. The coating has significantly slowed down the sorption process of samples, when taking into account thermally modifying the samples at all temperatures.

Swelling along and across the grain

In the case of both oak and pine, irrespective of the coating and thermally modifying temperature, the swelling along the grain was up to 1%. The variation in the dimensions of the oak and pine samples transversely soaking "across" in water is shown in Fig. 4.
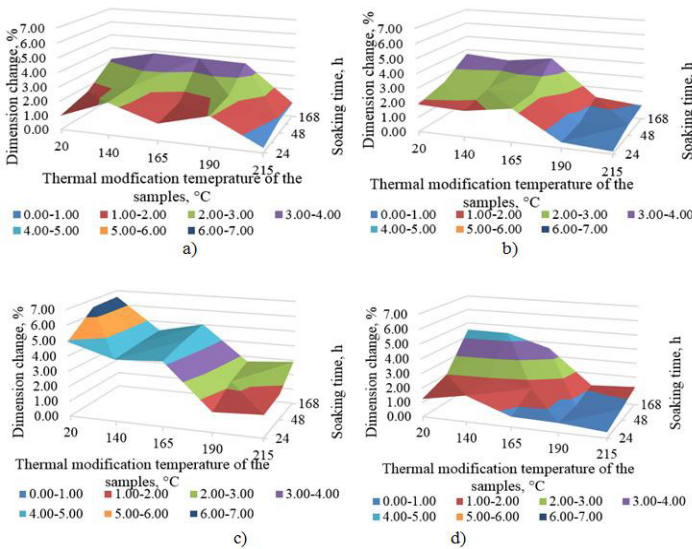

Fig. 4: The change in dimensions of oak wood O.I (a) and O.II (b) and pine wood P.I (c) and P.II (d) samples across the grain, after soaking in water.

After 48 hours of soaking oak wood, as the thermally modifying temperature increases, the swelling decreases from approximately ~ 1.6% (when the wood was thermally unmodified) to 1% (thermally modified samples at 215°C). In the case of pine wood, slightly higher results were obtained: from ~ 6.5% for non-heated pine wood to 7% for heated wood at 215°C.

When increasing heating temperature from ambient temperature to 215°C, in the case of oak wood, the average swell during 168 hours was approximately ~ 1%. In this case, the coated and non-coated samples have similar values.

In the case of pine wood, the average swell during 168 hours of non-coated samples ranged from 6.6% (for thermally unmodified wood) to 2.9% (for thermally modified wood). In the case of coated pine samples, the same range was from 4.5 to 1.3%.

It was identified that the weight, of the samples during the soaking increased more than dimensions. The biggest change in the weight of oak was 32% and pine 45%, respectively. In this case, the dimensions of the oak across the grain increased up to 4%, the pine up to 6.5%. The change in the mass of the wood is related to the change in both free and bound moisture. It is known that the dimension of wood across the fibre can usually vary within a few percent (Esteban et al. 2005). It is only related to the change in the bound moisture, which is usually found in the cell walls (microcapillaries) of wood. Drying-swelling processes usually occur in wood, with humidity ranging from 0 to 30%. The change in the mass of the wood is related to the change in both free and bound moisture. The maximum moisture content of the wood depends on the density of the wood (higher density wood may contain less free moisture due to the smaller volume of macrocapillary where the free moisture builds up) and can reach 100% and more (Hrčka 2017, Shi et al. 2000). This can be explained by the greater change in the mass of pine trees compared to oak wood.

Tension perpendicular of the wood to the grain.

Generally, if oak wood was thermally modified from ambient temperature to 215°C, the force required to tear the wood across the grain reduces about 2.5 times, in the case of pine wood up to 10 times. As mentioned, the cut of the coated samples varied (mixed, tangential, and radial). In the case of thermally unmodified samples, tearing off the coating, the degradation of "wood - coating" composite varied. It decomposes both in the "wood-coating" area and the wood. Such degradation is most likely associated with diverse and uneven wood structure (Yildirim et al. 2015). Characteristic examples of degradation of the "wood - coating material" composite are shown in Fig. 5.
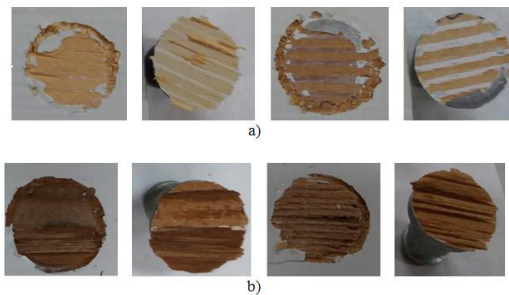

a)

b)

Fig. 5: Degradation options of composite "wood – coating material": a) "mixed" degradation through wood and between wood and coating, b) degradation through wood.

It was obtained that when the degradation was only through the wood, it usually happened through the early wood. This is probably due to the fact that early wood is mostly made of thin-walled elements with a lower density and worse mechanical properties compared to late wood. Examples of such degradation are shown in Fig. 5a. Early wood inserts are characterized by inferior quality of wood, which is commonly used for observation paths and passages.

In all cases of thermally modified wood, this composite "wood - coating material" degraded only through wood (Fig. 5b). This is due to the fact that the tension perpendicular of thermally modified wood to the grain is significantly reduced (Younsi et al. 2010). Fig. 6 shows the dependence of the wood resistance to tension perpendicular to the grain on thermally modifying temperature.

Generally, in the case of oak wood, the wood tension perpendicular increased from 4.5 to 1.8 MPa by increasing the thermally modifying temperature. In the case of pine wood, the range was from 3.5 to 0.2 MPa.

After soaking for 168 hours, the tension perpendicular of thermally unmodified oak and pine fell 5 times (oak) and 7 times (pine). The tension perpendicular of both thermally modified oak and pine wood to the grain, irrespective of thermally modifying temperature varies from 0.2 to 0.3 MPa (Dahle et al. 2017, Ardalany et al. 2011).

After the analysis of the results, it can be said that the difference in tension perpendicular to the grain of the thermally modified and unmodified wood, is significant in case of both types (Fig. 6a,b).
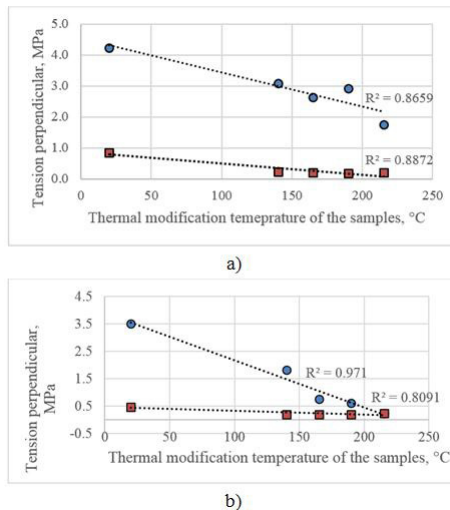

a)

b)

Fig. 6: The dependence of tension perpendicular to the grain on thermal modification temperatures in oak wood (a) and pine wood (b) samples, before soaking, after 168 hours of soaking.

The results of adhesion testing of the mesh cuts of thermally modified coated oak and pine samples at different temperatures and modified at different times indicate that in fact, in all cases, a tier 0 was obtained, i.e. there are no coat splits, which means that the finishing layer is firmly adhered to the wood surface. As the thermal modification temperature increases, the bond strength between the coating material and the coating surface remains stronger than the tension perpendicular of the wood to the grain, except for pine samples that have been thermally modified at 215°C and soaked for one week, when adhesion is reduced (Tier 2: small coat splits in the incision areas, the damage area does not exceed 15%).

Adhesion between the coating material used in the research and the surface of oak and pine wood is strong regardless the thermal modification temperature and soaking time.

During the research it was found that the coating reduces the absorption of unmodified and modified wood several times during short-term moisture, but the difference of absorption of both types of wood, (coated and non-coated) is reduced as the soak time increases.

Resistance of tensile perpendicular to the grain of unmodified and thermally modified coated and non-coated wood samples, under moisture for a long period of time, significantly reduces and becomes approximately equal for all samples. It can be stated that wooden constructions intended to be used in very wet conditions (soil that is not exposed to rain and snow) should be made of thermally modified wood without coating. Thermally modified wood will have greater dimensional and shape stability and biological resistance. Strength in this direction will vary slightly, with mechanical impact; the coating will quickly peel off with a small layer of wood, so the appearance of the wood will soon become much worse than non-coated wood. Thermally treated non-coated wood will perform its functional purpose longer.

CONCLUSIONS

1. Water absorption of thermally modified wood under long-term moisture conditions is lower than that of unmodified wood. Thermally modified wood, is less deformed (pine swell ~ 3%, oak ~ 1%).
2. Water absorption of thermally modified wood with coating is significantly lower than that of non-coated wood, but this difference decreases with the increase of soaking time. At the beginning of the soak, the impregnation of the coated and non-coated oak and pine samples varied about 3 times, and after 168 hours of soaking, varied only 1.5 times.
3. Tension perpendicular of thermally modified dry wood to the grain is significantly less than that of unmodified wood (for oak wood it decreased from 4.2 MPa to 1.8 MPa, for pine wood it decreased from 3.5 MPa to 0.2 MPa). However, after long-term soaking, tension perpendicular of thermally modified and unmodified wood to the grain is significantly reduced (for oak from 0.8 MPa to 0.2 MPa, for pine wood becomes practically the same, in range of 0.2 - 0.3 MPa).
4. The mesh cut method has shown that thermally modified and unmodified wood at all temperatures (140 - 215°C) has good adhesion in the tests when coatings are used. Only the adhesion of the samples with the coating material modified at 215°C slightly deteriorates, therefore it is not appropriate in this case to use coatings.
5. Under wet conditions coated wood only reduces the water absorption of the wood at the initial stage of operation, and then the wood is soaked. The coated layer slows the drying of the wood.
6. Due to reduced resistance of tension perpendicular to the grain, the mechanically exposed coating tears off with the wood layer and may even reduce the service life of the wood.

REFERENCES

1. Albrektas, D., Navickas, P., 2017: An evaluation of modulus of elasticity, dimensional stability and bonding strength of bonded heat - treated wood. Drvna Industrija 68(2): 137-144.
2. Ardalany, M., Deam, B., Fragiacomo, M., Crews, K.I., 2011: Tension perpendicular to grain strength of wood, laminated veneer lumber (LVL), and cross-banded LVL (LVL-C). In: Incorporating sustainable practice in mechanics of structures and materials (eds. Fragomeni, Venkatesan, Lam & Setunge). Pp 891-896, Taylor & Francis Group. London.

3. Borrega, M., Karenlampi, P.P., 2007: Mechanical behavior of heat-treated spruce (*Picea abies*) wood at constant moisture content and ambient humidity. European Journal of Wood and Wood Products 66(1): 63-69.
4. Candelier, K., Dumarçay, S., Pétrissans, A., Desharnais, L., Gérardin, P., Pétrissans, M., 2013: Comparison of chemical composition and decay durability of heat treated wood cured under different inert atmospheres: Nitrogen or vacuum. Polymer Degradation And Stability 98(2): 677-681.
5. Cao, Y., Lum, J., Huang, R., Jiang, J., 2011: Increased dimensional stability of Chinese fir through steam-heat treatment. European Journal of Wood and Wood Products 70(4): 441-444.
6. Dahle, G.A., James, K.R., Kane, B., Grabosky, J.C., Detter, A., 2017: A review of factors that affect the static load-bearing capacity of urban trees. Arboriculture & Urban Forestry 43(3): 89-106.
7. Deka, M., Humar, M., Rep, G., Kricej, B., Sentjurc, M., Petric, M., 2007: Effects of UV light irradiation on colour stability of thermally modified, copper ethanolamine treated and non-modified wood: EPR and DRIFT spectroscopic studies. Wood Science And Technology 42(1): 5-20.
8. Esteban, L., Gril, J., De Palacios, P., Casasus, A.G., 2005: Reduction of wood hygroscopicity and associated dimensional response by repeated humidity cycles. Annals of Forest Science 62: 275–284.
9. Esteves, B., Domingos, I., Pereira, H., 2008: Pine wood modification by heat treatment in air. BioResources 3(1): 142-154.
10. Garrote, G., Domınguez, H., Parajo, J. C., 1999: Hydrothermal processing of lignocellulosic materials. Holz als Roh- und Werkstoff 57(3): 191–202.
11. Hannouz, S., Collet, R., Butaud, J.C., Bleron, L., Candelier, K., 2015: Mechanical characterization of heat-treated ash wood in relation with structural timber standards. Pro Ligno 11(1): 3-10.
12. Hrčka, R., 2017: Model of free water in wood. Wood Research 62(6): 831-838.
13. Jimenez, Jr., J.P., Acda, M.N., Razal, R.A., Madamba, P.S., 2011: Physico-mechanical properties and durability of thermally modified malapapaya (*Polyscias nodosa* (Blume) Seem.) wood. Philippine Journal of Science 140(1): 13-23.
14. Kol, H.S., 2010: Characteristics of heat-treated Turkish pine and fir wood after ThermoWood processing. Journal of Environmental Biology 31(6): 1007-1011.
15. Kol, H.S., Sefil, Y., Keskin, S., 2015: Effect of heat treatment on the mechanical properties, and dimensional stability of fir wood. In: Proceedings of the 27th International Conference: Research for Furniture Industry, Ankara, Pp 269-279.
16. Mohareb, A., Sirmah, P., Pétrissans, M., Gérardin, P., 2011: Effect of heat treatment intensity on wood chemical composition and decay durability of *Pinus patula*. European Journal of Wood and Wood Products 70(4): 519-524.
17. Shi, S.Q., Gardner, D.J., Wang, J., 2000: Estimating maximum water absorption of wood fiber/polymer fluff composites. Wood und Fiber Science 32(3): 269-277.
18. Sundqvist, B., 2004: Colour changes and acid formation in wood during heating, 50 pp.
19. Sustersic, Z., Mohareb, A.Z., Chaouch, M., Petrissans, M., Petric, M., Gérardin, P., 2010: Prediction of the decay resistance of heat treated wood on the basis of its elemental composition. Polymer Degradation and Stability 95(1): 94-97.
20. Wood Handbook 2010: Wood as an Engineering Material, General Technical Report FPL-GTR-190, Madison, 509 pp.

21. Yildirim, M.N., Uysal, B., Ozcifci, A., Ertas, A.H., 2015: Determination of fatigue and static strength of scots pine and beech wood. Wood Research 60(4): 679-686.
22. Yildiz, S., Gezer, D.E., Yildiz, C.U., 2006: Mechanical and chemical behavior of spruce wood modified by heat. Building and Environment 41: 1762-1766.
23. Younsi, R., Kocaefe, D., Poncsak, S., Kocaefe, Y., 2010: Computational and experimental analysis of high temperature thermal treatment of wood based on ThermoWood technology. International Communications in Heat and Mass Transfer 37(1): 21-28.
24. Zlahtic-Zupanc, M., Lesar, B., Humar, M., 2018: Changes in moisture performance of wood after weathering. Construction and Building Materials 193: 529-538.
25. EN 13183-1, 2003: Moisture content of a piece of sawn timber. Part 1: Determination by oven dry method.
26. EN 13183-2, 2003: Moisture content of a piece of sawn timber. Part 2: Estimation by electrical resistance method.
27. EN 323, 1999: Wood-based panels. Determination of density.
28. EN 408, 2010: Timber structures. Structural timber and glued laminated timber. Determination of some physical and mechanical properties.
29. EN ISO 2808, 2019: Paints and varnishes. Determination of film thickness.
30. EN ISO 13076, 2012: Paints and varnishes. Lighting and procedure for visual assessments of coatings.
31. ISO 2409, 2013: Paints and varnishes. Cross-cut test.
32. ISO 2811-1, 2016: Paints and varnishes. Determination of density Pycnometer method.
33. ISO 4624, 2016: Paints and varnishes. Pull-off test for adhesion.

Darius Albrektas
Kaunas University of Technology
Faculty of Mechanical Engineering and Design
Studentu St. 56
Lt – 51424 Kaunas
Lithuania

Milda Jucienė*, Vaida Dobilaitė, Raimondas Bliūdžius
Kaunas University of Technology
Institute of Architecture and Construction
Tunelio St. 60
Lt – 44405 Kaunas
Lithuania
*Corresponding author: milda.juciene@ktu.lt

RESONANCE AND TIME-OF-FLIGHT METHODS FOR EVALUATING THE MODULUS OF ELASTICITY OF PARTICLEBOARDS AT DIFFERENT HUMID CONDITIONS

Sheikh Ali Ahmed, Stergios Adamopoulos, Francesco Poggi
Linnaeus University
Sweden

Thomas Walther
Ikea Industry AB
Sweden

ABSTRACT

Non-destructive testing of wood panels by either resonance or time-of-flight (TOF) methods provides possibilities for predicting their static bending properties. In the present study, three non-destructive devices (BING - Beam Identification by Non-destructive Grading by CIRAD, Montpellier, France, Fakopp Ultrasonic Timer and Sylvatest TRIO) were used for measuring the dynamic stiffness of different particleboard types. Fakopp Ultrasonic Timer and Sylvatest TRIO produce ultrasonic pulses to measure the sound velocity while BING uses resonance frequencies. Commercially produced particleboards with different thickness and densities were used to measure the dynamic modulus of elasticity (MOE_{dyn}) in two directions (parallel and perpendicular to the production line) and at three different humidity levels (dry - 35%, standard - 65% and wet - 85% RH in constant temperature of 20°C). MOE_{dyn} of particleboards were correlated with the static moduli of elasticity (MOE_{stat}) and rupture (MOR_{stat}). It was found that the non-destructive methods gave higher MOE_{dyn} values in both production directions than that of MOE_{stat} values. MOE_{dyn} was found to decrease from dry to wet conditions. A very strong and statistically significant correlation existed between MOE_{dyn} and static bending properties. MOE_{dyn} correlated stronger to MOE_{stat} than MOR_{stat}. At different humidity level, all three methods- Fakopp Ultrasonic Timer, BING and Sylvatest TRIO analyses showed good predicting capabilities to estimate MOE_{stat} and MOR_{stat} of different particleboard types with high level of accuracy.

KEYWORDS: Ultrasonic velocity, vibration methods, static bending, dynamic modulus of elasticity, wood panels.

INTRODUCTION

Wood panels are widely used in furniture manufacturing and for construction purposes. In wood-based panel industry, the main goal is to produce panels with high and consistent quality. An understanding of the fundamental mechanical properties is needed in order to specify their particular applications. One of the properties is modulus of elasticity (MOE), which describes the material's stiffness and it is a key indicator used for evaluating the mechanical properties of wood panels. A high value of MOE indicates a high resistance of the material to deformation (Liang and Fu 2007). To determine the stiffness and strength properties of materials, small samples are destructively tested in a testing machine according to standard methods. This type of evaluation process is time-consuming, expensive and more importantly destructive in nature. Thus, special attention was given on different types of non-destructive tests, and mainly acoustic methods have been applied within the last decade for standing trees (Tsehaye et al. 2000a, Amishev and Murphy 2008, Lindström et al. 2009, Wang 2013), logs (Jang 2000, Tsehaye et al. 2000b, Matheson et al. 2002, Dickson et al. 2004, Edlund et al. 2006), lumber (Brancheriau and Baillères 2003, Baltrušaitis and Mišeikytė 2011, Øvrum 2013). On the contrary, little attention has been paid on the non-destructive evaluation of wood panels (Dunlop 1980, Bekhta and Marutzky 2007, Niemz and Mannes 2012, Guan et al. 2015).

Usually, non-destructive testing is carried out by using two acoustic methods; the time-of-flight (TOF) and the resonance method. TOF relies on the evaluation of propagation time of a pulse of ultrasound or a stress wave across the material while the resonance method is based on the free vibration frequency of the material under forced harmonic vibration. The resonance method provides more information on the elastic properties of materials and it is more reliable than the TOF method. Most of the resonance-based acoustic tools have a built-in fast Fourier transformation program that can analyze the acoustic signals. The dynamic modulus of elasticity (MOE_{dyn}) is obtained from the acoustic velocity or the resonance frequency data. It is reported that the ultrasonic pulse transit time gives the highest MOE_{dyn}, which is followed by the stress wave transit time, and then the longitudinal and flexural vibration frequency (Hassan et al. 2013, Wang 2013, Chauhan and Sethy 2016, Legg and Bradley 2016). Acoustic tools based on the two non-destructive methods have proved to provide a rapid, reliable and simple measure of MOE_{dyn} for trees, logs, lumber and wood-based panels, and have also shown good potential to predict their static bending properties (static moduli of elasticity MOE_{stat} and rupture MOR_{stat}).

Several researchers have compared MOE_{dyn} or acoustic wave velocity with MOE_{stat} or MOR_{stat} of wood panels, and have reported good to strong association between them (Ross and Pellerin 1988, Han et al. 2006, Guan et al. 2015). However, values of MOE_{dyn} varied depending on the method used. Moreover, moisture has an influence on the sound wave and resonance properties of wood panels as they can swell considerably in humid conditions. However, moisture influence is more predictable for solid wood than wood panels. As for example, the stress wave velocity in solid wood is affected by about 1% per percent of MC change in the hygroscopic range (Han et al. 2006). However, such linear relationship is not observed in wood panels due their complex nature and large thickness swelling in humid conditions and thus are less predictable in higher moisture range.

Swelling of wood panels is complicated as it is often accompanied with internal bond failures that lead to changes of their internal structure (Wu and Piao 1999). It is thus needed to establish correlations between the acoustic properties and stiffness/strength of wood panels in different humid conditions, which will enable more safe predictions of their behavior in the intended end uses. Temperature also influences the bending strength and stiffness of wood-based panels

(Bekhta and Marutzky 2007), so it should be taken into account for a proper non-destructive evaluation by acoustics. Several other factors need to be considered in non-destructive testing of wood panels, such as the size, shape and variability of the particles, the spatial variation in orientation, the distribution of binder and additives, the size, shape and variation of cavities, and the layering and density variation through the panel thickness (Bodig 2000). Since wood panels are multiphase products, intensive care should be taken in selecting the proper non-destructive method for a specific panel type that more closely responds to the controlling variables of interest (e.g. wave velocity, MOE_{dyn}, shear modulus).

Application of non-destructive acoustic testing for wood-based panels is still in infancy but could be very useful in contemporary quality control of the production for fast determinations of stiffness and strength properties of different panel types. The main objective of this paper was to evaluate the potential of three acoustic tools based on TOF and resonance methods for assessing the mechanical performance (static bending properties) of commercially produced particleboards as effected by their moisture content. Predictions of MOE_{stat} and MOR_{stat} of the particleboards exposed to three humid conditions (dry, standard and wet) were based on MOE_{dyn} values determined by TOF and resonance methods.

MATERIALS AND METHODS

Commercial wood panels

Four (4) types of commercially produced particleboards with different binders, thicknesses and densities were used in this study. The particleboards were collected from factories in Slovakia, Sweden and Poland. Their details are presented in the following Tab. 1.

Tab. 1: Types of particleboards used in the study. Values in parenthesis are the standard deviation of density measured after conditioning at 20˚C and 65% RH.

Type of particleboard	Type of glue used	Thickness (mm)	Density (g·cm⁻³)
Standard particleboard (PB1)	UF	16	0.60 (0.03)
High density particleboard (PB2)	UF	20	0.72 (0.01)
Non-load bearing particle board (PB3)	pMDI	19	0.66 (0.00)
Load bearing particle board (PB4)	pMDI	19	0.69 (0.01)

PB: particleboard; UF: urea formaldehyde; pMDI: polymeric diphenylmethane diisocyanate.

Three climatic conditions were considered for this study: dry (20˚C, 35% RH), standard (20˚C, 65% RH) and wet (20˚C, 85% RH). Both static (MOE_{stat} and MOR_{stat}) and dynamic MOE_{dyn} were measured in samples acclimatized at those three climatic conditions. The samples were considered to be acclimatized when the difference between two weightings within 24 hours were smaller than 0.1% mass of the sample. Moisture content MC (SS-EN 322) and density (SS-EN 323) of the samples were measured after acclimatization at dry, standard and wet conditions.

Two panel directions were considered for determining the bending (static and dynamic) properties viz. parallel and perpendicular. Two different directions, three climatic conditions and six replications produced a total of 36 samples for each board type (see Tab. 2).

Tab. 2: *Dimensions (length × width × thickness) and number of samples for different tests in three different climatic conditions.*

Board type	Direction	Dimension (mm)	Number of samples
PB1	∥ & ⊥	370 × 50 × 16	36
PB2	∥ & ⊥	450 × 50 × 20	36
PB3	∥ & ⊥	430 × 50 × 19	36
PB4	∥ & ⊥	430 × 50 × 19	36

∥: parallel direction; ⊥: perpendicular direction.

Non-destructive testing
Resonance method

For the resonance method, the BING system was used. This is a non-destructive testing device designed to evaluate the mechanical properties of rigid materials using vibration analysis (Brancheriau and Baillères 2002). Main element of the system is the measurement software BING® (version 9.6.2), which controls a data acquisition logger (PicoScope 4224, UK), processes data and delivers results. In this purpose, a free-free flexural vibration test setup was used (Fig. 1).
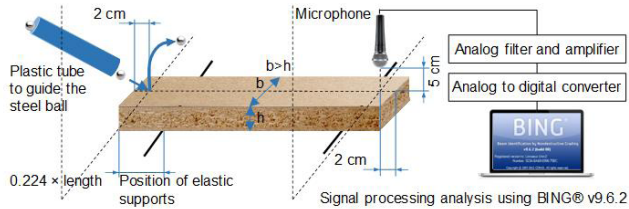

Fig. 1: *Schematic representation of the experimental setup for measuring the vibrational properties of particleboards. Note: b and h are the width and height of the sample, respectively.*

Each test piece was placed on two elastic supports on nodal points (0.224 × length) from the both ends of the sample to allow free vibrations. A small stainless steel ball (diameter 14 mm and mass 11.2 g) was dropped at one flat end to produce an exciting impulse. On the other end, an omnidirectional microphone was placed to measure the acoustic signal radiated by the impact. The signals were transmitted via PicoScope, and acoustic classification and signal-processing analysis was performed by the BING® software at a signal sampling frequency of 40000 Hz and with a spectral acquisition of 16384 points.

The first four modes of vibration were used for determining the dynamic modulus of elasticity (MOE_{dyn}). More details about the motion equation and method can be found in Hein et al. (2012). The test was repeated four times for every sample with two times in each side and the average was calculated.

Time-of-flight method

Two different ultrasonic testing devices were used for the TOF method; Fakopp Ultrasonic Timer (Fakopp Enterprise Bt., Hungary) and Sylvatest TRIO (CBS-CBT, France). Both devices use a single pass measurement of time and involve two transducers (sender and receiver) connected to the testing equipment with cables. The devices create ultrasonic excitation and then it is measured the time needed for the ultrasonic impulse to travel from one transducer to another. For Sylvatest TRIO, the result (ultrasonic propagation time) was the average of four impulses in

a sequence. To get a more accurate result, three measurements were performed; two at the top and bottom surface layers and one at the core layer of the particleboard samples (Fig. 2). The average data of the three measurements were used for the calculation of velocity. For Fakopp Ultrasonic Timer, two special triangle-shaped piezoelectric sensors were placed on the flat sides of the samples. Measurements of the propagation time were performed on both the top and bottom surfaces of the samples and the average data was used for the calculation of the ultrasonic wave velocity (Fig. 2).
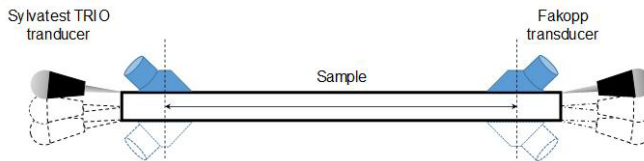

Fig. 2: Measurement of ultrasonic wave velocity on different positions of the particleboard sample by Sylvatest TRIO and Fakopp Ultrasonic Timer.

The acoustic velocity for each sample was calculated using the following formula:

$$V = \frac{D}{T} \times 1000 \qquad (1)$$

where: V is the ultrasonic velocity (m·s⁻¹), D is the distance of the transducers (mm) and T is the time needs to travel from the sender to the receiver transducer (µs). Then, V (m·s⁻¹) and density ρ (g·cm⁻³) were used to calculate the MOE_{dyn} (MPa) with the following formula:

$$MOE_{dyn} = \rho V^2 \qquad (2)$$

Static bending test

A universal testing machine (MTS 810, MTS System Corporation, USA) was used for the three-point bending test following the standard SS-EN 310. Uniaxial load was applied on the flat side of the samples. The loading rate was adjusted so that the maximum load was reached within 60 ± 30 s. During the bending test, the deflection and load were recorded until the fracture of the sample. From the load-deflection curve, the modulus of elasticity (MOE_{stat}) and modulus of rupture (MOR_{stat}) were calculated.

Data analysis

The MOE_{dyn} data of different samples in three climatic conditions were analyzed using the statistical software package IBM SPSS Statistics, Version 23 (IBM Corporation, New York, USA). One-way analysis of variance (ANOVA) was applied to determine whether MOE_{dyn} were significantly different among the sample categories. A 5% level of significance was used to detect differences and when a significant difference was found, Duncan's multiple-range test was performed. To measure the significance of relationships among the static and dynamic data, regression analysis was performed at 95% confidence level using Microsoft Excel 2016 program (Microsoft, Redmond, WA, USA).

RESULTS AND DISCUSSION

Static bending

MOE_{stat} and MOR_{stat} are important properties that measure respectively the elastic behavior and resistance to bending when the particleboard is under static load. Therefore, these properties determine largely the applicability of particleboards as structural components in furniture and other constructions. Tab. 3 summarizes the moisture content, density, static bending MOE_{stat} and MOR_{stat} in both parallel and perpendicular of particleboard's production line at the three selected humid conditions.

Tab. 3: Equilibrium moisture content (EMC), density, static bending strength (MOR$_{stat}$) and stiffness (MOE$_{stat}$) of the particleboard types after conditioning in three different humid conditions at constant temperature 20°C. Values in parenthesis are the standard deviations.

Board type		Dry, 35% RH				Standard, 65% RH				Wet, 85% RH			
		EMC (%)	Density (g·cm⁻³)	MOE_{stat} (MPa)	MOR_{stat} (MPa)	EMC (%)	Density (g·cm⁻³)	MOE_{stat} (MPa)	MOR_{stat} (MPa)	EMC (%)	Density (g·cm⁻³)	MOE_{stat} (MPa)	MOR_{stat} (MPa)
PB1	‖	6.7 (0.01)	0.60 (0.03)	2891 (225)	11.36 (1.04)	9.9 (0.04)	0.60 (0.03)	2421 (233)	10.91 (1.37)	14.0 (0.12)	0.60 (0.02)	1871 (157)	8.89 (0.84)
	⊥		0.59 (0.00)	2381 (167)	10.35 (1.17)		0.60 (0.00)	2067 (110)	9.61 (0.97)		0.61 (0.01)	1498 (235)	7.69 (0.95)
PB2	‖	7.1 (0.03)	0.72 (0.01)	3943 (110)	19.61 (1.31)	9.7 (0.02)	0.73 (0.01)	3503 (103)	19.25 (0.90)	13.3 (0.26)	0.73 (0.01)	2812 (71)	17.04 (0.82)
	⊥		0.72 (0.01)	3788 (41)	19.19 (0.48)		0.72 (0.01)	3319 (29)	18.29 (0.71)		0.73 (0.01)	2675 (31)	16.11 (0.36)
PB3	‖	7.2 (0.02)	0.65 (0.00)	2657 (43)	12.51 (1.21)	10.2 (0.05)	0.65 (0.00)	2324 (43)	12.04 (0.70)	13.6 (0.04)	0.66 (0.00)	1913 (42)	10.01 (0.61)
	⊥		0.65 (0.01)	2452 (101)	12.65 (1.17)		0.65 (0.01)	2140 (133)	11.71 (0.66)		0.66 (0.01)	1746 (51)	9.33 (0.85)
PB4	‖	6.7 (0.08)	0.69 (0.01)	2954 (112)	15.17 (1.02)	10.0 (0.05)	0.70 (0.01)	2655 (166)	14.56 (0.99)	13.7 (0.13)	0.70 (0.01)	2132 (80)	11.63 (0.57)
	⊥		0.68 (0.03)	2685 (54)	14.40 (0.53)		0.70 (0.01)	2285 (40)	12.98 (0.71)		0.70 (0.01)	1870 (32)	10.63 (0.98)

‖: parallel direction; ⊥: perpendicular direction.

In all particleboards, static bending properties parallel to the production line showed higher values than perpendicular to the production line. As expected the high-density particleboard (PB2) had the highest values than the other types. At standard condition (20°C and 65% RH), MOE_{stat} and MOR_{stat} values for PB2 boards were 8-11% and 8-14% higher, respectively. With increasing humidity and consequently MC from the dry to the wet condition, the bending properties decreased for all types of particleboards. The reduction was more pronounced from the standard to wet condition. Similar humidity and MC effects were also found elsewhere for wood panels (Wu and Suchsland 1997, Pritchard 2001) as well as for wood (Gerhards 1982). Particleboards are formed under pressure and the adhesive holds the particles in a compressed state, which means that they are self-stressed in compression perpendicular to the grain of the wood fibers. MC changes lead to relaxation of stresses and recovery of the locked-in deformations resulting in increase of board dimensions and some change in the moment of inertia (Oliver 1981). In addition, the decrease of stiffness and strength is directly affected by the humidity changes but the magnitude depends on the type of adhesive. An experiment by Dinwoodie (1978) reported that urea-formaldehyde bonded boards subjected to humidity change from 30% to 90% RH retained only 58% and 45% of their initial MOR_{stat} and MOE_{stat} respectively, whilst boards

bonded with melamine urea-formaldehyde, phenol formaldehyde and sulphite liquor retained at least 73% and often more than 90% of their initial property value.

The reduction in strength properties is due to the effect of mechanical stressing set up by alternate swelling and shrinkage of adjacent particles (Halligan and Schniewind 1974, Dinwoodie 1978). Both MOE_{stat} and MOR_{stat} are affected by various processing parameters like the board density, surface density and particle size, particle alignment, moisture content, and particularly by the nature of adhesives used (Kollmann et al. 1975, Jian and Lu 2017). The higher MOE_{stat} and MOR_{stat} values observed in the parallel than in the perpendicular direction for all particleboard types in all humid conditions could be explained by the particle orientation in respect to the direction of the production line. Parallel to the production line, the orientation of particles with their fibers along the grain provide increased strength and stiffness to resist stress while loading of particles against the grain in the perpendicular direction results in lower flexure values (Han et al. 2006, Buyuksari 2012, Ayrilmis et al. 2010). In addition, the fine particles of the panel's face layers need the core layer as a strengthening element. Panels with core layer particles with parallel orientation affects and enables the core layer to resist it from deformation and failure when subjected to the bending loads (Benthien and Ohlmeyer 2018).
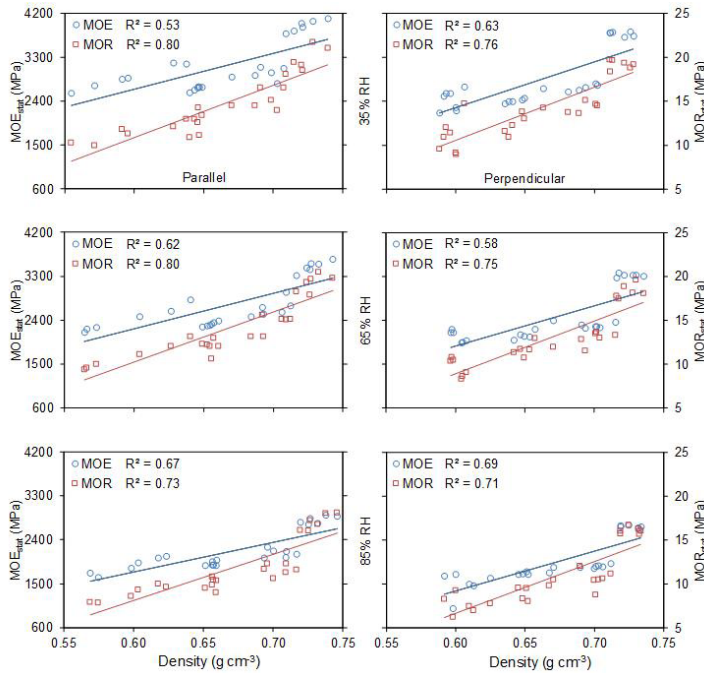

Fig. 3: Relationship of static bending properties (MOE_{stat}, MOR_{stat}) with density for the particleboard types acclimatized at three humid conditions.

Fig. 3 shows the relationship of MOE_{stat} and MOR_{stat} with the density of all particleboard types at each humid condition. In every humid condition, linear regression models of MOE_{stat} and MOR_{stat} with the density showed significant positive relationships ($p < 0.05$).

As revealed by the coefficients of determination, the relationship of density was stronger with MOR_{stat} than with MOE_{stat}. Our findings are in agreement with previous studies (Wong

et al. 1998, Rachtanapun et al. 2012, Guan et al. 2016), which reported an increase in MOE_{stat} and MOR_{stat} with increasing board density. The surface board density plays an important role on the MOR_{stat} since bending stresses are higher at the surfaces. Furthermore, MOR_{stat} values are highly dependent on the vertical density gradient where different values can be obtained for equal average board densities simply by changing the processing parameters (Wong et al. 1998).

However, in this study, the mean board density was used for analysis, and therefore no conclusions can be made on the effect of density gradient on the bending performance of the particleboard types. Linear regressions model was used to determine how well the MOR_{stat} is related with MOE_{stat} values in parallel and perpendicular samples (Fig. 4). It showed strong positive and significant relationships ($p < 0.05$) for every humid condition, particleboard direction (parallel and perpendicular) as well as when all data were grouped together. Strong correlation between bending strength and modulus of elasticity is also reported for wood (Olsson et al. 2012, Baar et al. 2015) and wood-based panels (McNatt et al. 1990, Jian and Lu 2017).
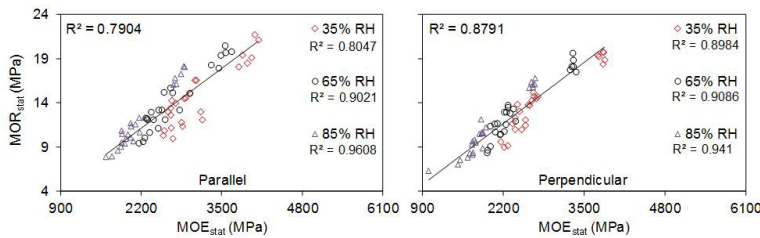

Fig. 4: Relationship of MOE_{stat} and MOR_{stat} for the particleboard types acclimatized at three humid conditions.

Dynamic modulus of elasticity

MOE_{dyn} represents the mean stiffness value of a sample whilst MOE_{stat} represents the local stiffness of the material at the highly stressed areas of a specific test setup. The MOE_{dyn} values measured for the different particleboard types at dry, standard and wet conditions by the different resonance and TOF methods are presented in Tabs. 4-6.

Tab. 4: Dynamic modulus of elasticity (MOE_{dyn}) of the particleboard types, after conditioning in three different humid conditions at constant temperature 20°C, measured by BING in transversal vibration (resonance method). Values in parenthesis are the standard deviations.

Board type	Direction of board	Dry, 35% RH MOE_{dyn} (MPa)	Standard, 65% RH MOE_{dyn} (MPa)	Wet, 85% RH MOE_{dyn} (MPa)
PB1	‖	3631a (212)	3376a (189)	2683b (132)
	⊥	3294a (274)	3048a (242)	2398b (195)
PB2	‖	5754a (71)	5408b (54)	4461c (62)
	⊥	5301a (217)	4980a (202)	4102b (191)
PB3	‖	3527a (142)	3260b (146)	2721c (101)
	⊥	3185a (58)	2945b (39)	2432c (37)
PB4	‖	3808a (66)	3428b (58)	2867c (28)
	⊥	3615a (17)	3250b (14)	2689c (17)

‖: parallel direction; ⊥: perpendicular direction.

Mean values followed by different letter within a row indicate that there is a significant difference ($p \leq 0.05$) as determined by ANOVA and Duncan's multiple range test.

Tab. 5: Dynamic modulus of elasticity (MOE$_{dyn}$) of the particleboard types, after conditioning in three different humid conditions at constant temperature 20°C, measured by Fakopp Ultrasonic Timer (TOF method). Values in parenthesis are the standard deviations.

Board type	Direction of board	Dry, 35% RH MOE_{dyn} (MPa)	Standard, 65% RH MOE_{dyn} (MPa)	Wet, 85% RH MOE_{dyn} (MPa)
PB1	‖	4184a (207)	3944a (174)	3316b (126)
	⊥	3606a (165)	3276b (163)	2897c (144)
PB2	‖	5822a (110)	5617b (103)	4870c (69)
	⊥	5383a (53)	5327a (166)	4505b (161)
PB3	‖	3918a (132)	3732a (127)	3222b (132)
	⊥	3520a (61)	3353b (98)	2948c (59)
PB4	‖	4469a (95)	4102b (78)	3525c (63)
	⊥	4132a (39)	3846b (25)	3307c (22)

‖: parallel direction; ⊥: perpendicular direction.

Mean values followed by different letter within a row indicate that there is a significant difference (p ≤ 0.05)
as determined by ANOVA and Duncan's multiple range test.

Tab. 6: Dynamic modulus of elasticity (MOE$_{dyn}$) of the particleboard types, after conditioning in three different humid conditions at constant temperature 20°C, measured by Sylvatest TRIO (TOF method). Values in parenthesis are the standard deviations.

Board type	Direction of board	35% RH MOE_{dyn} (MPa)	65% RH MOE_{dyn} (MPa)	85% RH MOE_{dyn} (MPa)
PB1	‖	3273a (200)	3230a (179)	2713b (121)
	⊥	3000a (195)	2925a (162)	2449b (112)
PB2	‖	4815a (115)	4905a (103)	4251b (102)
	⊥	4556a (99)	4604a (105)	3987b (128)
PB3	‖	3400a (112)	3223a (161)	2864b (119)
	⊥	2998a (51)	2923a (62)	2603b (60)
PB4	‖	3903a (167)	3652a (119)	3307b (122)
	⊥	3647a (57)	3416b (52)	3095c (40)

‖: parallel direction; ⊥: perpendicular direction.

Mean values followed by different letter within a row indicate that there is a significant difference (p ≤ 0.05)
as determined by ANOVA and Duncan's multiple range test.

As expected, the increase of humidity from dry to wet conditions resulted in decreased MOE_{dyn} due to the elevated EMC of particleboards. The trend was noticed in each particleboard type for all the acoustic methods used (Tab. 4-6). At 85% RH, MOE_{dyn} of the particleboard types determined by both the resonance and TOF methods was found significantly lower than that was in 35% and 65% RH (ANOVA and Duncan's multiple range test, P ≤ 0.05). MOE_{dyn} in TOF methods is directly related to the acoustic velocity (see formula 2). Resonance frequency and ultrasonic velocity of wood panels decrease with an increase in moisture content, and thus proportionally influence the MOE_{dyn} (Bucur 2006). A similar trend has also been reported for solid wood (Llana et al. 2014). This phenomenon can be explained by the hypothesis that at dryer state, molecular chains in the amorphous regions of the cell wall are unusually distorted with the presence of microvoids between the molecular chains resulting in lower internal friction, which corresponds to higher MOE_{dyn}. With increasing moisture content, water molecules are embedded

in the microvoids and rearrange the distorted molecular chains. However, with further increase in moisture content, water acts as a plasticizer allowing additional molecular movement and the cohesive forces between molecules are decreased. That results in a higher internal friction leading to a decrease in MOE_{dyn} (Akitsu et al. 1993).

Like MOE_{stat}, higher MOE_{dyn} was observed in samples parallel to the production line than perpendicular (Tabs. 4-6). The reason behind this result is the highest resonance frequency and ultrasonic velocity parallel to the grain (Bucur 2006, Han et al. 2006). The higher values of MOE_{dyn} parallel to the production line of particleboards meant that higher number of wood particles along the grain were aligned in this direction. When different methods were compared, the mean values of the MOE_{dyn} based on flexural vibration and TOF methods (Tabs. 4-6) were higher than MOE_{stat} (Tab. 3) for each particleboard type and humid condition. As average, BING, Fakopp Ultrasonic Timer and Sylvatest TRIO gave respective MOE_{dyn} values 29%, 37% and 27% higher than MOE_{stat} values. Moduli of elasticity determined using speed of sound measurements are in general higher than values determined by static experiments (Bucur 2006, Niemz and Mannes 2012, Hassan et al. 2013, Guan et al. 2015, Chauhan and Sethy 2016). Like wood, the difference between MOE_{dyn} and MOE_{stat} is attributed to the viscoelastic behaviour and damping properties of particleboards. According to Halabe et al. (1997), materials exhibit elastic behaviour when a force is applied for a very short duration and behave as a viscous liquid when a force is applied for longer time. As static bending test takes long duration compared to the TOF or resonance test, higher moduli of elasticity are obtained by the later methods. MOE_{stat} represents a local stiffness while the MOE_{dyn} represents a mean value over the full specimen. Overall, MOE_{dyn} was found to be the highest when Fakopp Ultrasonic Timer was used, and it was about 11% and 16% higher respectively than MOE_{dyn} obtained by BING and Sylvatest TRIO. The considered layer for the measurements might explain the difference between the two ultrasonic TOF methods (Fakopp Ultrasonic Timer, Sylvatest TRIO) on a three-layered particleboard, which is not characteristic and does not represent the whole section (Dunlop 1980). Low-density middle layers have the greatest effect on sound propagation time. A sound wave needs more time to travel across a low-density middle layer, and thus provides different results than the surface layers of higher density. In this contrast, Fakopp Ultrasonic Timer sound velocity results were the average of measurements done on both surfaces of the particleboards whilst an average of three layers (two faces and core layer) was used for Sylvatest TRIO. The addition of the low-density core layer into the final average in Sylvatest TRIO might explain the differences noted between the two ultrasonic testing methods. However, the prediction of MOE_{stat} from MOE_{dyn} values depends on the good correlation between them. Barbu et al. (2014) showed strong correlations between the density of the surface layer and the MOE_{stat} and MOR_{stat} for particleboards and medium density fibreboards (MDF). Sound velocity in the panel direction is dominated by the surface layers with higher densities and mainly influence MOE_{stat} and MOR_{stat} (Kruse 1997) whilst the porous core layer influences sound velocity perpendicular to the panel surface (Hilbers et al. 2009). However, both methods tested here were able to capture the structural differences among the particleboards types. As for example, the high-density particleboard (PB2) gave the highest values.

Linear regression analysis was employed to determine how well a particular acoustic method could predict the MOE_{stat} or MOR_{stat} values by the MOE_{dyn} values on samples with different directions (parallel and perpendicular) and EMC levels (Tab. 7). Significant positive relationships (confidence level of 0.05) were found between MOE_{dyn} and MOE_{stat} for samples in the parallel and perpendicular production directions acclimatized in different humid conditions. This result is in well agreement with a previous study (Han et al. 2006). The coefficients of determination (R^2) ranged from 0.889 to 0.995 for the different acoustic methods. All three methods, Fakopp

Ultrasonic Timer, BING and Sylvatest TRIO, performed well to predict MOE_{stat}. Linear regression models between MOR_{stat} and MORdyn also showed positive relationships. Those developed regression models were found statistically significant at the 0.05 confidence level for most of the relationships on samples at different relative humidity levels. The coefficients of determination (R^2) ranged from 0.852 to 0.994. Sylvatest TRIO performed better than the other two methods in predicting MOR_{stat}.

Tab. 7: Regression analysis results on the relationships between static moduli of elasticity (MOE_{stat}) and rupture (MOR_{stat}), and dynamic modulus of elasticity (MOE_{dyn}). Model: MOE_{stat} or MOR_{stat} = Intercept + Slope × MOE_{dyn}.

Testing method	RH (%)	Parallel direction			p-value	Perpendicular direction			p-value
		Intercept	Slope	R²		Intercept	Slope	R²	
MOR_{stat} - MOE_{dyn} relationship									
BING	35	880.030	0.534	0.981	0.006*	282.620	0.661	0.992	0.004*
Fakopp		33.816	0.669	0.991	0.004*	-306.220	0.753	0.978	0.011*
Sylvatest		163.850	0.766	0.888	0.058ns	-237.760	0.863	0.945	0.028*
BING	65	749.930	0.511	0.960	0.020*	291.790	0.608	0.991	0.005*
Fakopp		26.165	0.621	0.988	0.006*	42.640	0.610	0.986	0.007*
Sylvatest		196.120	0.674	0.995	0.002*	-72.960	0.728	0.975	0.013*
BING	85	587.210	0.501	0.970	0.015*	152.600	0.618	0.961	0.019*
Fakopp		88.143	0.561	0.981	0.010*	-337.180	0.669	0.971	0.015*
Sylvatest		130.090	0.625	0.988	0.006*	-240.300	0.721	0.962	0.019*
MOR_{stat} - MOE_{dyn} relationship									
BING	35	1.148	0.003	0.869	0.068ns	0.454	0.036	0.875	0.064ns
Fakopp		-4.202	0.004	0.899	0.052ns	-3.185	0.004	0.912	0.045*
Sylvatest		-5.425	0.005	0.996	0.002*	-3.322	0.005	0.935	0.032*
BING	65	1.345	0.003	0.852	0.077ns	0.160	0.004	0.894	0.055ns
Fakopp		-3.442	0.004	0.886	0.059ns	-1.893	0.004	0.959	0.021*
Sylvatest		-2.959	0.005	0.961	0.020*	-2.594	0.005	0.946	0.027*
BING	85	-1.198	0.004	0.950	0.026*	-1.906	0.004	0.958	0.021*
Fakopp		-5.223	0.005	0.952	0.024*	-5.473	0.005	0.974	0.013*
Sylvatest		-5.181	0.005	0.994	0.003*	-4.873	0.005	0.978	0.011*

* Significant regression equation at the 0.05 level (two-tailed); ns- non significant regression equation; R^2- coefficient of determination.

Previous studies (Liang and Fu 2007, Chauhan and Sethy 2016) showed better relationships of MOE_{stat} and MOE_{dyn} when MOE_{dyn} was measured with resonance frequency by the Fast Fourier Transform (FFT) technique than with the TOF techniques (ultrasonic, stress wave). This is because the resonance speed by the vibration method is the function of the volume weighted average stiffness of the entire sample whilst in TOF methods, the high frequency waves travels at a relatively faster speed in stiffer and denser material (Chauhan et al. 2005). However, for particleboard, notifiable differences among the tested methods were not observed. In addition, this study showed that the differences in MOE_{dyn} measured by any of these three methods was not constant over the entire MOE_{stat} or MOR_{stat} range. The slope of the equations relating MOE_{dyn} to MOE_{stat} or MOR_{stat} was different in all three cases and was the lowest in BING and the highest in Sylvatest TRIO, which is in agreement with Chauhan and Sethy (2016). Previous studies (Bos

and Casagrande 2003, Hassan et al. 2013) showed that the correlation coefficients between the MOE_{dyn} and MOE_{stat} are higher than those between the MOE_{dyn} and MOR_{stat}. This fact was also observed in the current study.

CONCLUSIONS

This study investigated the potential for predicting the bending properties of different particleboard types by using resonance and time-of-flight methods at three different humid conditions (dry, standard and wet). The overall conclusions of the study are given below:

(1) Both MOE_{stat} and MOR_{stat} decreased with increases in particleboards' moisture content. Bending properties increased with the density of the particleboards. Linear relationships were found between both MOE_{stat} and MOR_{stat} with density for every humid condition.

(2) At a given humid condition, higher MOE_{stat} and MOR_{stat} values were observed in samples parallel compared to samples perpendicular to the production line. Overall, samples parallel to production line had MOE_{stat} and MOR_{stat} respectively 12% and 8% higher than the samples perpendicular to the production line.

(3) Positive linear relationships were found between MOE_{stat} and MOR_{stat} at dry ($R^2 = 0.83$), standard ($R^2 = 0.90$) and wet ($R^2 = 0.93$) conditions.

(4) All three methods (BING, Fakopp Ultrasonic Timer and Sylvatest TRIO) showed higher MOE_{dyn} values in samples parallel than in samples perpendicular to the production line. MOE_{dyn} of particleboards decreased as their moisture content increased, and was statistically significant lower at the wet than at the dry condition.

(5) The mean values of MOE_{dyn} were higher than MOE_{stat} for each particleboard type and humid condition. Overall, MOE_{dyn} was found 29%, 37% and 27% higher than MOE_{stat} when BING, Fakopp Ultrasonic Timer Sylvatest TRIO were used respectively.

(6) The obtained strong and statistically significant MOE_{stat}-MOE_{dyn} and MOR_{stat}-MOE_{dyn} linear relationships at almost every humid condition and production direction suggested that the resonance and TOF methods could be useful in practical quality control for predicting the static bending properties of particleboards. All tools showed exceptional ability to predict MOE_{stat} while Sylvatest TRIO provided better MOR_{stat} prediction results than Fakopp Ultrasonic Timer and BING.

ACKNOWLEDGEMENTS

REFERENCES

1. Akitsu, H., Norimoto, M., Morooka, T., Rowell, R.M., 1993: Effect of humidity on vibrational properties of chemically modified wood. Wood and Fiber Science 25(3): 250-260.

2. Amishev, D., Murphy, G.E., 2008: In-forest assessment of veneer grade douglas-fir logs based on acoustic measurement of wood stiffness. Forest Products Journal 58(11): 42-47.

3. Ayrilmis, N., Buyuksari, U., As, N., 2010: Bending strength and modulus of elasticity of wood-based panels at cold and moderate temperatures. Cold Regions Science and Technology 63(1-2): 40-43.

4. Baar, J., Tippner, J., Rademacher, P., 2015: Prediction of mechanical properties- modulus of rupture and modulus of elasticity- of five tropical species by nondestructive methods. Maderas. Ciencia y tecnología 17(2): 239-252.

5. Baltrušaitis, A., Mišeikytė S., 2011: Strength and stiffness properties of the lithuanian grown scots pine (*Pinus sylvestris*): non-destructive testing methods vs. static bending. Wood Research 56(2): 157-168.

6. Barbu, M.C., Hasener, J., Bernardy, G., 2014: Modern testing of wood-based panels, process control, and modelling. In: Research developments in wood engineering and technology (eds. Aguilera, A., Davim, J.P.). IGI Global, PA, USA, Pp 90-130.

7. Bekhta, P.; Marutzky, R. 2007. Bending strength and modulus of elasticity of particleboards at various temperatures. Holz als Roh- und Werkstoff 65(2): 163-165.

8. Benthien, J.T.; Ohlmeyer, M., 2018. Enhancement of low-density particleboard properties by core layer particle orientation. European Journal of Wood and Wood Products 76(3): 1087–1091.

9. Bodig, J., 2000: The process of NDE research for wood and wood composites. In: 12th International symposium on nondestructive testing of wood, University of Western Hungary, Sopron, Pp 7-22.

10. Bos, F., Casagrande, S.B., 2003: On-line non-destructive evaluation and control of wood-based panels by vibration analysis. Journal of Sound and Vibration 268(2): 403-412.

11. Brancheriau, L., Baillères, H., 2002: Natural vibration analysis of clear wooden beams: a theoretical review. Wood Science and Technology 36(4): 347-365.

12. Brancheriau, L., Baillères, H., 2003: Use of the partial least squares method with acoustic vibration spectra as a new grading technique for structural timber. Holzforschung 57(6): 644-652.

13. Bucur, V., 2006: Acoustics of wood. 2nd ed. Springer Series in Wood Science, Springer-Verlag Berlin Heidelberg, Berlin, 393 pp.

14. Buyuksari, U., 2012. Physical and mechanical properties of particleboard laminated with thermally compressed veneer. BioResources 7(1): 1084-1091.

15. Chauhan, S., Sethy, A., 2016: Differences in dynamic modulus of elasticity determined by three vibration methods and their relationship with static modulus of elasticity. Maderas. Ciencia y tecnología 18(2): 373-382.

16. Chauhan, S.S., Entwistle, K.M., Walker, J.F.C., 2005: Differences in acoustic velocity by resonance and transit-time methods in an anisotropic laminated wood medium. Holzforschung 59(4): 428-434.

17. Dickson, R.L., Matheson, A.C., Joe, B., Ilic, J., Owen, J.V., 2004: Acoustic segregation of *Pinus radiata* logs for sawmilling. New Zealand Journal of Forestry Science 34(2): 175-189.

18. Dinwoodie, J.M., 1978: The properties and performance of particleboard adhesives. Journal of the Institute of Wood Science 8(2): 59-68.

19. Dunlop, J.I., 1980: Testing of particle board by acoustic techniques. Wood Science and Technology 14(1): 69-78.

20. Edlund, J., Lindström, H., Nilsson, F., Reale, M., 2006: Modulus of elasticity of Norway spruce saw logs vs structural lumber grade. Holz als Roh- und Werkstoff 64(4): 273-279.

21. Gerhards, C.C., 1982: Effect of moisture content and temperature on the mechanical properties of wood: an analysis of immediate effects. Wood and Fiber 14(1): 4-36.

22. Guan, C., Zhang, H., Hunt, J.F., Yan, H., 2016: Determining shear modulus of thin wood composite materials using a cantilever beam vibration method. Construction and Building Materials 121: 285-289.

23. Guan, C., Zhang, H., Zhou, L., Wang, X., 2015: Dynamic determination of modulus of elasticity of full-size wood composite panels using a vibration method. Construction and Building Materials 100: 201-206.

24. Halabe, U.B., Bidigalu, G.M., GangaRao, H.V.S., Ross, R.J., 1997: Nondestructive evaluation of green wood using stress wave and transverse vibration techniques. Materials Evaluation 55(9): 1013-1018.

25. Halligan, A.F., Schniewind, A.P., 1974: Prediction of particleboard mechanical properties at various moisture contents. Wood Science and Technology 8(1): 68-78.

26. Han, G., Wu, Q., Wang, X., 2006: Stress-wave velocity of wood-based panels: Effect of moisture, product type, and material direction. Forest Products Journal 56(1): 28-33.

27. Hassan, K.T.S., Horáček, P., Tippner, J., 2013: Evaluation of stiffness and strength of scots pine wood using resonance frequency and ultrasonic techniques. BioResources 8(2): 1634-1645.

28. Hein, P.R.G., Lima, J.T., Gril, J., Rosado, A.M., Brancheriau, L., 2012: Resonance of scantlings indicates the stiffness even of small specimens of Eucalyptus from plantations. Wood Science and Technology 46(4): 621-635.

29. Hilbers, U., Thoemen, H., Barbu, M.C., Hasener, J., 2009: Ultrasonic inspection of wood composites: How process parameters influence the transmission signal. In: Proceeding of 43rd International Wood Composites Symposium, Academic Press, Seattle, USA, Pp 614-624.

30. Jang, S.S., 2000: Evaluation of lumber properties by applying stress waves to larch logs grown in Korea. Forest Products Journal 50(3): 44-48.

31. Jian, J., Lu, X., 2017: Effect of blocked polyurethane prepolymer on properties of MUF-particleboard made from high moisture particles. International Journal of Adhesion and Adhesives 78: 189-194.

32. Kollmann, F.F.P., Kuenzi, E.W., Stamm, A.J., 1975: Principles of wood science and technology- II wood based materials. Springer-Verlag, Berlin Heidelberg New York, 703 pp.

33. Kruse, K., 1997: Modern techniques for efficient process control of wood-based panel production. In: Proceedings of workshop on non-destructive testing of panel products. Academic Press, Llandudno, Wales, Pp 1-9.

34. Legg, M., Bradley, S., 2016: Measurement of stiffness of standing trees and felled logs using acoustics: A review. The Journal of the Acoustical Society of America 139(2): 588-604.

35. Liang, S.-Q., Fu, F., 2007: Comparative study on the three dynamic modulus of elasticity and static modulus of elasticity for Lodgepole pine lumber. Journal of Forestry Research 18(4): 309-312

36. Lindström, H., Reale, M., Grekin, M., 2009: Using non-destructive testing to assess modulus of elasticity of *Pinus sylvestris* trees. Scandinavian Journal of Forest Research 24(3): 247-257.

37. Llana, D.F., Iñiguez-Gonzalez, G, Arriaga, F., P. Niemz, P. 2014: Influence of temperature and moisture content on non-destructive measurements in Scots pine wood. Wood Research 59(5): 769-780.

38. Matheson, A.C., Dickson, R.L., Spencer, D.J., Joe, B., Ilic, J., 2002: Acoustic segregation of *Pinus radiata* logs according to stiffness. Annals of Forest Science 59(5-6): 471-477.

39. McNatt, J.D., Wellwood, R.W., Bach, L., 1990: Relationships between small-specimen and large panel bending tests on structural wood-based panels. Forest Products Journal 40(9): 10-16.

40. Niemz, P., Mannes, D., 2012: Non-destructive testing of wood and wood-based materials. Journal of Cultural Heritage 13S(3): S26-S34.

41. Oliver, J.F., 1981: Adhesion in cellulosic and wood-based composites. Plenum Press, New York, 261 pp.

42. Olsson, A., Oscarsson, J., Johansson, M., Källsner, B., 2012: Prediction of timber bending strength on basis of bending stiffness and material homogeneity assessed from dynamic excitation. Wood Science and Technology 46(4): 667-683.

43. Øvrum, A., 2013: In-forest assessment of timber stiffness in Norway spruce (*Picea abies* (L.) Karst.). European Journal of Wood and Wood Products 71(4): 429-435.

44. Pritchard, J., Ansell, M.P., Thompson, R.J.H., Bonfield, P.W., 2001: Effect of two relative humidity environments on the performance properties of MDF, OSB and chipboards. Wood Science and Technology 35(5): 395-423.

45. Rachtanapun, P., Sattayarak, T., Ketsamak, N., 2012: Correlation of density and properties of particleboard from coffee waste with urea–formaldehyde and polymeric methylene diphenyl diisocyanates. Journal of Composite Material 46(15): 1839-1850.

46. Ross, R.J., Pellerin, R.F., 1988: NDE of wood-based composites with longitudinal stress waves. Forest Products Journal 38(5): 39-45.

47. SS-EN 310, 1993: Wood-based panels- determination of modulus of elasticity in bending and of bending strength.

48. SS-EN 322, 1993: Wood-based panels- determination of moisture content.

49. SS-EN 323, 1993: Wood-based panels- determination of density.

50. Tsehaye, A., Buchanan, A.H., Walker, J.C.F., 2000a: Selecting trees for structural timber. Holz als Roh- und Werkstoff 58(3): 162-167.

51. Tsehaye, A., Buchanan, A.H., Walker, J.C.F., 2000b: Sorting of logs using acoustics. Wood Science and Technology 34(4): 337-344.

52. Wang, X., 2013: Acoustic measurements on trees and logs: a review and analysis. Wood Science and Technology 47(5): 965-975.

53. Wong, E.D., Zhang, M., Wang, Q., Kawai, S., 1998: Effects of mat moisture content and press closing speed on the formation of density profile and properties of particleboard. Journal of Wood Science 44(4): 287-295.

54. Wu, Q., Piao, C., 1999: Thickness swelling and its relationship to internal bond strength loss of commercial oriented strandboard. Forest Products Journal 49(7/8): 50-55.

55. Wu, Q., Suchsland, O., 1997: Effect of moisture on the flexural properties of commercial oriented strandboards. Wood and Fiber Science 29(1): 47-57.

Sheikh Ali Ahmed, Stergios Adamopoulos*, Francesco Poggi
Linnaeus University
Faculty of Technology
Department of Forestry and Wood Technology
Georg Lückligs Plats 1
351 95 Växjö
Sweden
*Corresponding author: stergios.adamopoulos@lnu.se

Thomas Walther
Ikea Industry AB
Malmö
Sweden

EFFECT OF THE METALLIZATION TREATMENT ON THE SURFACE PROPERTIES OF *POPULUS EUPHRATICA*

Ruyuan Yang, Xiaofeng Zhang, Youfu Sun, Tingting Zhou, Quan Yuan
Nanjing Forestry University
China

ABSTRACT

To improve the surface-finishing performance and enhance the protection of surface coatings, this study employed metallization treatment of fast-growing poplar through an orthogonal experiment. The poplar specimens were impregnated using a low-melting point alloy at different temperatures (75°C, 85°C, 95°C), pressures (0.5MPa, 1 MPa, 1.5 MPa), and times (0.5h, 1h, 2h) to obtain the optimum process parameters and determine the paint film adhesion of metalized poplar. The test results showed that the impregnation effect was obvious with an increase in the pressure and time. The optimum process parameters were 0.5 MPa, 85°C, and 1 h. Contact angle of the treated wood increased, the surface free energy dropped to some extent, wetting property of tread wood decreased. Whether the treated wood or the untreated wood, film adhesion of treated wood got a higher level. After anti-aging treatment, the treated poplar still had a higher level of film adhesion.

KEYWORDS: Fast-growing poplar (*Populus*), metallization, contact angle, mechanical property, paint film properties.

INTRODUCTION

Poplar wood, which is widely distributed in China, grows fast, has a strong adaptability to environmental changes, and is suitable for wide applications (Zhang and Yang 2012, Kou 2006). The properties of various poplar wood species are not very different. Generally, sapwood is a pale yellow to light fawn color (*Populus euphratica* is light red) and heartwood is darker in color than sapwood. Diffuse-porous or semi diffuse-porous wood has many pores, and the density of air-dried wood is between 0.30 kg·m⁻³ and 0.55 kg·m⁻³. The texture of the wood is detailed and uniform, and therefore it is easy to dry and has a good processing performance (He et al. 2008, Sun and Yang 2011). However, the formed material is loose, soft, and weak with a low surface hardness; low wear resistance, low content of extractives in the heartwood, poor durability, and poor corrosion resistance, which limit the applications of poplar (Li et al. 2018).

The metallization treatment of wood is intended to improve the dimensional stability and surface finishing performance of wood-based materials, and thus enhance the protection of the surface finishing (Gobakken and Westin 2008 , Kielmann et al. 2016), reduce decay, prolong the service life, meet the demands for wood products (Jirous-Rajkovic et al. 2004, Hakkou et al. 2005), and expand the application range of fast-growing poplar.

During World War II, metalized wood was used as a bearing for ships and helicopter propellers in Germany. The density of metalized wood can reach 0.95 kg·m^{-3} to 3.83 kg·m^{-3}, with a considerable increase in the hardness and wear resistance upon combining with alloys, such as Sn, Bi, Pb, etc. (Si 2003). Metallization is an effective way to improve the wood dimensional stability and biological durability, and is an environmentally friendly wood preservation method (Hill 2006, Yildiz and Gümüşkaya 2007, Aytin and Korkut 2016, Toker et al. 2016, Turkoglu et al. 2017, Kucuktuvek et al. 2017, Kart et al. 2019). After metallization, the properties of wood are favorable for making outdoor furniture, floor materials, various instruments for outdoor and indoor applications, and cladding for wood buildings (Homan and Jorissen 2004). Okon et al. (2018) used a low-melting point alloy to metalize Masson pine (*Pinus massoniana*) to study the change in its strength characteristics, contact angle, color, etc. Scanning electron microscopy was used to evaluate the effectiveness of the treatment (Okon et al. 2018). A preliminary study of metalized wood was done by Li J. and Li G. (1994) and Li (1995) by injecting molten metal or alloy into porous wood to form wood-metal composites (also called metalized wood). If the wood was compressed after impregnation with metal, metalized compact wood could be obtained (Lu and Chen 2003). Wang et al. (2006) used the electroless nickel plating method to metalize wood and studied the influence of the amount of plating solution, treatment time, and temperature on the surface resistivity and electromagnetic shielding effectiveness of wood.

In this study, a pressurized impregnation method was used to metalize fast-growing poplar. The air-dried wood was impregnated using a low-melting point alloy under various temperatures, pressures, and impregnation ratios, and the density and surface impregnation area of the wood were calculated. Before and after the metallization treatment, the contact angles of distilled water on the surfaces of untreated and treated poplar specimens were measured. The surface paint film adhesion grades of all of the painted specimens that were treated and not treated with an anti-aging treatment were then evaluated.

MATERIAL AND METHODS

Materials

The experiments were performed in a laboratory at the Material Science and Engineering School of Nanjing Forestry University in Nanjing, China. During the experiment, the ambient temperature was between 26°C and 28°C and the relative humidity was between 42% and 45%.

The pressure vessel used for metallization of the wood was a series of high-pressure reactors, which consisted of a reactor body and controller produced by Zhuoqun Instrument Equipment Co. Ltd. (Zhaoyuan, China). The reactor body consisted of a reaction vessel, safety device, heating furnace, etc. The section and top views of the reactor are shown in Fig. 1.

The wood used for this study was fast-growing *Populus euramericana*, purchased from a wood sales plant in Yibei Township of Guanyun (China). The tree age was 12 years and the diameter at breast height was approximately 350 mm. The other characteristics included a loose tree-texture, light yellow sapwood, light brown heartwood, following the standard ISO 3131-1975 (ISO 3131 1975), an air-dry density of 0.5034 kg·m^{-3}. The wet untreated poplar was cut by a bandsaw into

quarter-sawn timber with the dimensions 950 × 120 × 30 mm. The quarter-sawn poplar timber was then dried to approximately 10% of its original water content. The quarter-sawn poplar timber was planed after drying and then cut into specimens with the desired dimensions by a circular saw. The dimensions of the specimens were 20 × 20 × 20 mm, 30 × 20 × 20 mm, and 60 × 60 × 6 mm.
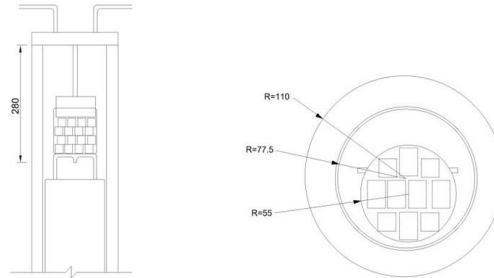

Fig. 1: Section view and top view of the reactor.

Following the standard ISO 3129-2012 (ISO 3129 2012), the minimum number of specimens required at a P of 5% was calculated using Eq. 1 based on a confidence level of 0.95:

$$n_{min} = \frac{v^2 t^2}{P^2} \qquad (1)$$

where: n_{min} - the minimum number of specimens required; v - the coefficient of variability of the measured properties (%); t - the reliability index, taking 1.96 as per the 0.95 confidence level; and P - the test accuracy index (5%).

The results were rounded to a single digit based on the rules of rounding off for numerical values and expression, and judgement of the limiting values (GB/T 8170 2008). Based on the tree species, the required specimen characteristics for testing the related properties are shown in Tab. 1.

Tab. 1: Wood samples.

Wood property	CV (%)	n_{min}	Dimensions (mm)
Density	10	15	30 × 20 × 20
Shrinkage (linear)	28	20	20 × 20 × 20
Compression strength parallel to the grain	13	15	30 × 20 × 20

CV - coefficient of variation.

The low-melting point alloy used for impregnation was provided by Pujiang Alloy Materials Co., Ltd. (Nanjing, China). The main components were Sn, Bi, and Pb, the density was approximately 39.6 kg·m⁻³, and the melting point was approximately 70°C. This alloy had a silver white color while solid and bright silver white color after melting. The alloy existed as a solid at room temperature, and exhibited the desired strength, hardness, corrosion resistance, and other properties. Two kilograms of the alloy when placed in 75°C water began to melt after 40 min and melted completely in approximately 4 h; in 85°C water, the alloy melted completely in 0.5 h; and in 95°C water, the alloy melted completely in 10 min. The molten alloy did not solidify at a temperature of 75°C to 95°C. In air, a gray oxide film formed on the surface of the molten metal alloy. At higher temperatures, this film oxidized easily.

A static drop contact angle or interfacial tension measuring instrument (JC2000A, Zhongchen Digital Technology Equipment Co. Ltd., Shanghai, China) was used for wettability testing of the surface of the impregnated wood. The instrument had DH-CG400 image card driving software (China Daheng Co. Ltd., Beijing, China). The main interface and other supporting components included a microsyringe (1-ml syringe), 3D platform, dimming knob, and focusing control panel. The test material used was fast-growing untreated and metal-impregnated poplar specimens with the dimensions 20 (radial) × 20 (tangential) × 30 mm (length). The specimen samples were prepared using three technical conditions, which were named Group B (0.5 MPa for 1 h at 85°C and a density of 3.19 kg·m^{-3}); Group C (0.5 MPa for 2 h at 95°C and a density of 3.08 kg·m^{-3}); and Group G (1.5 MPa for 2 h at 75°C and a density of 3.73 kg·m^{-3}). The surfaces of all of the specimens were polished with #320 abrasive paper before impregnation.

For paint film adhesion testing of the impregnated wood, a QFH cross-cut tester (Jingkelian Material Testing Machine Co. Ltd., Tianjin, China), HSRO25 artificial climate box with ultraviolet lamp (Nanjing Experimental Instrument Factory, Nanjing, China), wool brush, plastic bucket, and electronic scale (with a precision of 0.01 g) were used. The test materials included alkyd varnish and phenolic enamel (Changjiang Paint Company Ltd., Jiangsu, China), a two-component polyurethane resin varnish (Taicang Lugong Special Coating Factory, Suzhou, China), and poplar specimens (60 × 60 × 6 mm) that underwent the metallization treatment.

Methods
Impregnating metallization treatment of the wood

The reactor setup for the metal impregnation of the poplar specimen is shown in Fig. 1. The stainless-steel reactors, which contained the low-melting point alloy and specimens, were kept in an autoclave. The liner support heating jacket set by the reactor continuously transferred heat to the reactor, and the heat was transmitted to the stainless-steel container using water as the medium. Pressure was applied when the set temperature was reached.

Poplar wood is a diffuse-porous or semi diffuse-porous wood with many holes and has a loose texture; thus, it exhibits a good wettability. In this experiment, the poplar specimens were impregnated and metalized by the pressure impregnation method according to the L9 (34) orthogonal table. The pressure, temperature, and time were selected as influencing factors on the impregnation effect. The temperature and time had three levels, and the pressure had five levels. A total of 11 experiments were conducted. The factor levels are shown in Tab. 2.

Tab. 2: Levels of the factors.

Level	Factor		
	Pressure (MPa)	Temperature (°C)	Time (h)
1	0.5	75	0.5
2	1	85	1
3	1.5	95	2
4	0.1	-	-
5	0.3	-	-

Surface wettability test of the impregnated wood

Surface wettability of wood-based materials plays an important role in the coating of wood surfaces and the movement of moisture in wood. The surface wettability values indicate the effect of wetting, spreading, and adhesion of various liquids or reagents (water, adhesive, oxidizer, crosslinker, water repellent, dyeing agent, paint, and treatment solutions for various

modifications) on the surface (Teng 2009). The contact angle between wood and liquids is an important parameter to measure the diffusion of water-soluble paint on wood surfaces.

Various methods for determining the contact angle include the light point reflection, tilting plate, sessile drop, drooping, and capillary rise methods. In general, the contact angle of wood is often determined by the sessile drop and capillary rise methods (Gu 1999). The sessile drop method was used in this experiment, with distilled water as the testing liquid. A JC2000A static drop contact angle or interfacial tension measuring instrument (Zhongchen Digital Technology Equipment Co., Ltd., Shanghai, China) was used and the average value for each test block was taken. The measurement was divided into two parts, which were the collection of specimen images in the wet state and measurement of the contact angle.

Paint film adhesion test of the impregnated wood

The paint film adhesion refers to the adhesion property between a paint film and surface of a coated substrate. It is one of the important indices to measure the performance of paint. The untreated and treated poplar wood specimens were first polished using #180 coarse and #320 fine abrasive paper to obtain a relatively smooth surface. The specimens were not treated with putty in the experiment. All of the specimens were painted twice, where the second coat was applied after the first coat was nearly dry. The painted specimens are shown in Fig. 2. The paint film adhesion of the painted specimens was measured after two weeks of air drying.

The paint film adhesion test was performed as per the standard method BS 3962-6-1980 (BS 3962-6 1980). First, the surfaces of the untreated and treated wood specimens were coated with the alkyd varnish, phenolic enamel, and polyurethane resin varnish for a total of six specimens. The specimen numbers are shown in Tab. 3.

Fig. 2: Painted specimens.

Tab. 3: Specimen numbers for the adhesion test.

Impregnation process	Alkyd varnish	Phenolic enamel	Polyurethane resin varnish
Untreated	1	2	3
Treated	4	5	6

Second, the center of each specimen was used as the test area to measure the thickness of the two-point paint films and the arithmetic mean value was obtained. Third, two groups of rectangular marks were cut on the surface of the paint films, each of which included 11 parallel cuts with a length of 35 mm and spacing of 2 mm. All of the cuts penetrated into the surface of the base material, and the cut marks were angled approximately 45° in the direction of the wood grain. Fourth, the scraps were dusted with a paint brush and a rubber paste was pressed by hand onto the cut parts of the test area. Finally, the rubber paste was exposed abruptly in the diagonal direction to carefully check the damage of the paint film with a magnifying glass under an observation lamp.

After the adhesion test, anti-aging testing was done. For this purpose, the surfaces of the untreated and treated wood were coated with alkyd varnish, phenolic enamel, and polyurethane resin varnish for a total of six specimens. The specimen numbers are shown in Tab. 4.

Tab. 4: Specimen numbers for the anti–aging test.

Impregnation process	Alkyd varnish	Phenolic enamel	Polyurethane resin varnish
Untreated	7	8	9
Treated	10	11	12

The specimens were installed in an aging tester (HSR025, Nanjing Test Instrument Factory, Nanjing, China) at 45°C ± 5°C with a relative humidity of 65% to 90%. The specimens were sprayed with a water jet once an hour with a spray time of 3 min. The specimens were removed after 72 h in the aging tester, and then wiped and cleaned with clean absorbent gauze containing a small amount of alcohol. Finally, the cracks on the surfaces of the specimens were observed under natural light. The measured value of the paint film adhesion was compared with the results before the aging test.

RESULTS AND DISCUSSION

Impregnating metallization treatment of the wood

Following the L9 (3⁴) orthogonal table, 11 groups of experiments were performed. The factors studied included the pressure, temperature, and time. The pressure values were 0.1 MPa, 0.3 MPa, 0.5 MPa, 1 MPa, and 1.5 MPa; the temperatures were 75°C, 85°C, and 95°C; and the time intervals were 0.5 h, 1 h, and 2 h. The impregnation effect on the poplar wood under the various experimental conditions is shown in Tab. 5.

Tab. 5: Effect of impregnation with different conditions.

No.	Pressure (MPa)	Temperature (°C)	Time (h)	ρ (kg·m^{-3})	β (%)
Untreated	-	-	-	0.5034	100
A	0.5	75	0.5	2.6600	100
B	0.5	85	1	3.1885	100
C	0.5	95	2	3.0827	100
D	1	75	1	3.3624	100
E	1	85	2	3.4471	100
F	1	95	0.5	2.8933	100
G	1.5	75	2	3.7269	100
H	1.5	85	0.5	3.3830	100
I	1.5	95	1	4.0485	100
J	0.1	85	0.5	2.2231	82
K	0.3	85	0.5	2.2811	90

ρ – density, β – surface impregnation rate.

The surface impregnation rate was calculated by the number grid method. The area ratio of the surface layer impregnated is the result measured by observing the impregnated specimen on the macro level. The place where the metal was impregnated on the surface of the specimen

presents the metal color, which was different from the place where the specimen was not impregnated. A transparent sheet with a 2 × 2 mm grid was placed on the surface of the specimen, and the number of grids showing the metal color was calculated. The part less than one grid shall be roughly calculated according to the proportion. The impregnation surface area ratio is expressed as follows:

$$\beta = \frac{n_1}{n_2} \times 100\% \qquad (2)$$

where: n_1 - the number of grids showing the metal color,
         n_2 - the number of grids occupied by the specimen.

Tab. 5 revealed that the density increased considerably after metallization under the various conditions, and was approximately four to eight times more than that before the treatment. The main reason for this result was attributed to the larger density of the low-melting point alloy. When the poplar specimens were immersed in the alloy, the density of the specimens increased. When the pressure was greater than 0.5 MPa, the surface impregnation of the specimen was good, which showed that under the orthogonal experimental design conditions, the impregnation effect was obvious and a favorable impregnation surface was obtained. However, when the pressure was less than 0.5 MPa, impregnation of the poplar specimen was not sufficient and hence the surface impregnation effect of the specimen was not good.

Variance and range analyses of the impregnation test results were analyzed by using Orthogonal Design Assistant Software. The results were as follows. The F ratios of the pressure and time were greater than 19 and the F ratio of the pressure was greater than that of the time (Tab. 6), which indicated that the pressure and time have a significant influence on the impregnation effect. The impact of the pressure on impregnation was greater than that of the time. Because the F ratio of the temperature was less than 19, the temperature range of the orthogonal design had no obvious effect on the impregnation of the specimen.

Tab. 6: Variance analysis of the effect of impregnation.

Factor	Square of deviance	Degree of freedom	F ratio	Critical F-values	Significance
Pressure (MPa)	0.853	2	34.120	19.000	*
Temperature (℃)	0.016	2	0.640	19.000	–
Time (h)	0.514	2	20.560	19.000	*
Error	0.03	2	–	–	–

This conclusion was reached because of the differences in the ranges for each factor in Tab. 7. For the factors in the orthogonal experiment, the density ranges of the metalized poplar specimen with the pressure and time were large, which indicated that the pressure and time significantly influenced the impregnation effect.

Tab. 7: Range analysis of the effect of impregnation.

Factor	Pressure (MPa)			Temperature (℃)			Time (h)		
Level	0.5	1	1.5	75	85	95	0.5	1	2
Average	2.977	3.234	3.719	3.250	3.340	3.341	2.979	3.533	3.419
Range	0.742			0.091			0.554		

However, the density range of the metalized poplar specimen with the temperature was small, which indicated that the effect of the temperature on the impregnation effect was not significant. The specific analysis of the various factors is shown in Fig. 3.
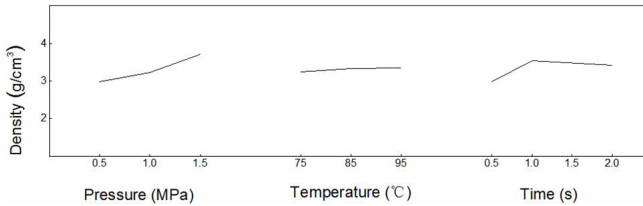

Fig. 3: Visual analysis of the effect of impregnation.

Pressure

The influence of the pressure on the impregnation was noticeable. As the pressure increased from 0.5 MPa to 2 MPa, the density of the specimen obviously increased and the impregnation was gradually improved, as is shown in Fig. 3. To further investigate the effect of the pressure, experiments 10 and 11 were done. It was found that the specimen can also be impregnated under a pressure of 0.1 MPa and 0.3 MPa at 85°C and a time of 0.5 h, but the impregnation effect was not as good as that of the other test groups. The surface impregnation effect was reduced because of inadequate impregnation. Therefore, a pressure of 0.5 MPa was chosen as the best process parameter for a good impregnated surface.

Temperature

The temperature range of 75°C to 100°C for the orthogonal experiment guaranteed the alloy was in a molten state and avoided a negative influence on the properties of the molten alloy and poplar specimens because of the high temperature. However, the temperature range had little effect on the impregnation of the specimen, as is shown in Fig. 3. The density of the treated specimen was relatively unchanged. To ensure that the alloy was in a molten state and the energy loss was reduced, a temperature of 85°C was chosen as the best process parameter.

Time

Under pressure, when the impregnation time was longer, the sample exhibited a better impregnation effect. For the impregnated samples, a time of 2 h was able to attain a good impregnation effect. Fig. 3 shows that the impregnation effect improved with an increase in the time; after 1 h, the impregnation effect instead decreased, which may have been because of the comprehensive function of the other factors. Therefore, a time of 1 h was selected as the optimum process parameter.

Surface wetting experiments of the impregnated materials

The contact angle changes of the radial and tangential sections of the untreated and treated wood using distilled water with time are shown in Tab. 8 and Tab. 9 and Fig. 4. The contact angle measurements were done through the collection of pictures of the morphological change of the static liquid drop on the sample surface and angle measurements from the pictures. Because of the fast changes in the contact angle on the radial section of the untreated wood, the measurement was done in 2-s intervals, while for the tangential section, it was done in 1-s intervals. The contact angle for the treated wood with distilled water changed relatively slowly, so the contact angle was measured with a 12-s interval.

Tab. 8: Change in the contact angle with time for the untreated specimens.

Time (s)	2	4	6	8	10	12	14	16
Contact angle of the radial section (°)	56.83	44.42	36.08	31.50	27.50	23.75	19.08	15.58
Time (s)	1	2	3	4	5	6	7	8
Contact angle of the tangential section (°)	62.75	45.75	36.00	28.25	22.25	17.50	14.75	11.75

Tab. 9: Change in the contact angle with time for the treated specimens.

Time (s)	Contact angle (°)					
	Radial section (Group B)	Tangential section (Group B)	Radial section (Group C)	Tangential section (Group C)	Radial section (Group G)	Tangential section (Group G)
12	73.10	88.67	71.33	74.50	97.50	95.00
24	62.30	78.33	62.67	65.33	84.67	63.17
36	59.30	76.00	60.67	60.50	78.83	56.17
48	57.00	73.75	58.00	56.83	76.17	52.33
60	54.30	70.83	54.83	53.17	74.00	47.33
72	51.20	68.67	52.17	49.50	70.83	41.17
84	48.50	65.83	49.17	45.33	68.50	35.33
96	45.50	63.17	46.67	41.17	66.67	28.00
108	42.90	60.00	44.00	36.83	62.67	20.67
120	40.30	56.33	41.33	31.67	59.50	9.67

Because of some definite variations in the size selected for the initial distilled water hanging drop, the initial wetting angles were different. Hence, for those experiments, the contact angle and its change rate were taken as the wetting judgment standard and were used to evaluate the wettability of the untreated and treated wood specimens in the combined analysis.

Figs. 4a to 4f show that the contact angle changed with distilled water had a good exponential regression relationship with the time for both the untreated and treated poplar specimens. For the untreated poplar specimens, the wettability in the tangential section was larger than that in the radial section, and the rate of contact angle change for the tangential section was larger than that for the radial section. However, for the treated samples, the rates of contact angle change for the radial and tangential sections with distilled water tended to be the same (Figs. 4a to 4d). After insufficient alloy impregnation of the samples, the rate of contact angle change for the tangential section was larger than for the radial section (Fig. 4d) because the tangential void ratio of the untreated poplar was larger than the radial porosity. When the sample was not completely impregnated by the metal, the radial and tangential void ratios tended to be the same, and showed a similar change trend for the wetting angle. However, when the sample was completely impregnated, its absorption of distilled water relied on the hydrophilic xylem, where the tangential wettability was larger than the radial wettability. The change rate for the tangential section with distilled water was larger than that for the radial section.
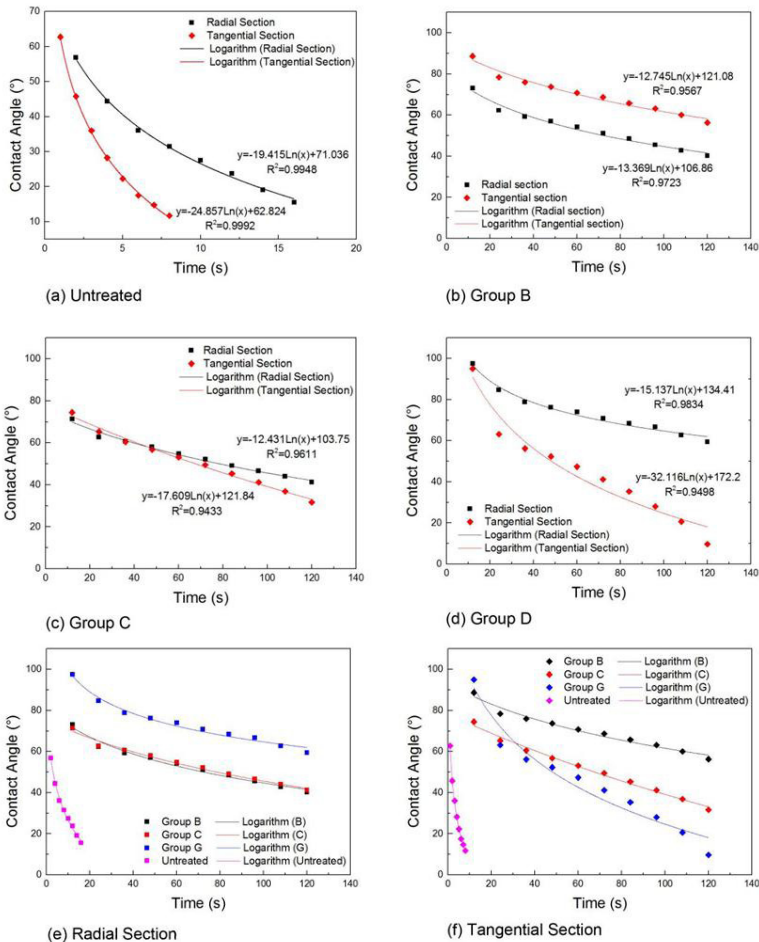
Fig. 4: Change in the contact angle with time for: (a) the untreated specimens, (b) Group B; (c) Group C; (d) Group G; (e) radial section, and (f) tangential section.

Fig. 4e shows that the wettability of the radial section of the treated poplar sample was smaller than that of the untreated wood. Also, as the wetting effect improved, the radial section had a poorer wettability. Group G displayed the best impregnation effect with a weakened wettability in the radial section. Groups B and C exhibited equivalent impregnation effects, with equivalent section wetting properties.

Fig. 4f shows that the wettability of the radial section of the treated wood sample was smaller than that of the untreated wood. Moreover, as the wetting effect improved, the wettability in the radial section weakened. Groups B and C had equivalent impregnation effects, with an equivalent wettability for the tangential sections. Group G had the best impregnation effect and theoretically the poorest wettability because of the roughness of the sample surface treatment.

Coating adhesion test after painting the metalized poplar surface

The experimental results are shown in Tab. 10 and Tab. 11:

Tab. 10: Grading standards for the film adhesion test.

Grade	Description
1	The cut marks were smooth, no paint film peeling.
2	There was paint film flaking at the intersection of the cut, and there was a small amount of intermittent peeling of the paint film.
3	There was intermittent or continuous peeling of the paint film along the cut marks.
4	In under 50% of the rectangular cut marks, the paint film had large pieces of debris or it completely peeled off along the cut marks.
5	In more than 50% of the rectangular cut marks, the paint film had large pieces of debris or completely peeled off along the cut marks.

Tab. 11: Results of the paint film adhesion test.

No.	Grade of paint film adhesion	Film thickness (mm)
A	1	0.719
B	3	0.156
C	1	0.146
D	1	0.153
E	2	0.147
F	2	0.145
G	2	0.158
H	5	0.144
I	2	0.142
J	1	0.169
K	3	0.158
L	1	0.149

The analysis of the data indicated the following:

At room temperature and ventilation conditions, the polyurethane resin varnish had the shortest film formation time. In contrast, the film formation time of the alkyd varnish was longest, at one week. The hardening agent used in the polyurethane resin varnish accelerated the solidification process.

All of the samples used in the experiment had no putting, but were sanded. Therefore, the metalized poplar samples had a more even surface and provided a more even paint film after sanding. The film thickness was thinner than that of the untreated wood. Because of metallization of the poplar specimens, the vessels and wood fibrocystic cavities were impregnated with the alloy, which decreased the void ratio of the surface.

Upon crosswise comparison of the untreated poplar and metalized wood, the alkyd varnish, phenolic enamel, and polyurethane resin varnish all exhibited nearly the same film adhering ability. Upon longitudinal comparison, the film adhering ability was larger for the metalized poplar with alkyd varnish, phenolic enamel, and polyurethane resin varnish than for the untreated poplar, This results similar to that of Yu et al. (2007).

CONCLUSIONS

The main conclusions derived from this study are summarized below:

1. Among the factors studied for the impregnation effect, the pressure and time significantly affected the metallization process, and the temperature effect was insignificant. The impregnation effect obviously increased with an increasing pressure and time. The optimum pressure, time, and temperature were determined to be 0.5 MPa, 85°C, and 1h, respectively.

2. For both the untreated and treated poplar, the contact angle change with distilled water exhibited a good exponential regression relationship with time; as the impregnation effect improved, the wettability weakened.

3. Compared with the untreated wood, the film adhering capacity of the metalized poplar improved considerably. After the anti-aging experiment, the metalized poplar samples showed a relatively high film adhering capacity.

ACKNOWLEDGMENTS

REFERENCES

1. Aytin, A., Korkut, S., 2016: Effect of thermal treatment on the swelling and surface roughness of common alder and Wych elm wood. Journal of Forestry Research 27(1): 225–229.

2. BS 3962-6, 1980: Methods of test for finishes for wooden furniture. Assessment of resistance to mechanical damage.

3. GB/T 8170-2008, 2008: Rules of rounding off for numerical values and expression and judgement of limiting values.

4. Gobakken, L.R., Westin, M., 2008: Surface mould growth on five modified wood substrates coated with three different coating systems when exposed outdoors. International Biodeterioration and Biodegradation 62(4): 397-402.

5. Gu, J., 1999: Adhesives and coatings. China Forestry Publishing House, Beijing, China, Pp 33-34.

6. Hakkou, M., Pétrissans, M., Zoulalian, A., Gérardin, P., 2005: Investigation of wood wettability changes during heat treatment on the basis of chemical analysis. Polymer Degradation and Stability 89(1): 1-5.

7. He, M.J., Lam, F., Yang, J., Zhang, S.D. 2008: Wood structural design. Beijing, China Construction Industry Press. 317 pp.

8. Hill, C.A.S., 2006: Wood modification - chemical, thermal and other processes, John Wiley and Sons Ltd., Chichester, England, 260 pp.

9. Homan, W.J., Jorissen, A.J.M., 2004: Wood modification developments. Heron 49(4): 361–368.

10. ISO 3129, 2012: Wood. Sampling methods and general requirements for physical and mechanical tests.
11. ISO 3131, 1975: Wood. Determination of density for physical and mechanical tests.
12. Jirous-Rajkovic, V., Bogner, A., Radovan, D., 2004: The efficiency of various treatments in protecting wood surfaces against weathering. Surface Coatings International Part B: Coatings Transactions 87(1): 15-19.
13. Kart, S., Baysal, E., Kucuktuvek, M., Turkoglu, T., Toker,H., Altay, C., Cibo, C., Peker, H., 2019: Some surface characteristics of varnished thermowood after weathering. Wood Research 64(1): 35-48.
14. Kielmann, B.C., Militz, H., Mai, C., 2016: The effect of combined melamine resin coloring agent modification on water related properties of beech wood. Wood Research 61(1): 1-12.
15. Kou, W.Z., 2006: China's poplar industry has entered a harmonious development road. China Forestry Industry 11: 14-16.
16. Kucuktuvek, M., Baysal, E., Turkoglu, T., Peker, H., Gunduz, A., Toker, H. 2017: Surface characteristics of Scots pine wood heated at high temperatures after weathering. Wood Research 62(6): 905-918.
17. Li, J., 1995: Wood composites for the 21st century. World Forestry Research (3): 34-40.
18. Li, J., Li, G., 1994: Metallic wood. Chinese Wood (6): 19-20.
19. Li, L.F., Yu, L.P., Wu, Z.G., 2018: Delignification of poplar wood with lactic acid-based deep eutectic solvents. Wood Research 64(3): 499-514.
20. Lu, C., Chen, X., 2003: Research progress in preparation of novel composite materials using wood mesoporous structure. Polymer Materials Science & Engineering 19(6): 32-36.
21. Okon, K.E., Lin, F., Chen, Y., Huang, B., 2018: Tin-based metal bath heat treatment: An efficient and recyclable green approach for *Pinus massoniana* wood modification. Journal of Forestry Research 29(6): 1807-1814.
22. Si, N., 2003: Introduction of several kinds of wood and inorganic nonmetal composite materials. Building Materials Industry of Information (6): 55-56.
23. Sun, Y.F., Yang, X.J., 2011: On the development prospect of Chinese wood structural architecture. Building Materials Decoration 6, 22-26.
24. Teng, X., 2009: Surface physicochemistry. Chemical Industry Press, Beijing, China, Pp 47-53.
25. Toker, H., Baysal, E., Turkoglu, T., Kart, S., Sen, F., Peker, H. 2016: Surface characteristics of oriental beech and scots pine woods heat-treated above 200°C. Wood Research 61(1): 43-54.
26. Turkoglu, T., Kabasakal, Y., Baysal, E., Gunduz, A., Kucuktuvek, M., Bayraktar, D.K., Toker, H., Peker, H., 2017: Surface characteristics of heated and varnished Oriental beech after accelerated weathering. Wood Research 62(6): 961-972.
27. Wang, L., Li, J., Liu, Y., 2006: Preparation of electromagnetic shielding wood-metal composite by electroless nickel plating. Journal of Forestry Research 17(1): 53-56.
28. Yildiz, S., Gümüşkaya, E., 2007: The effects of thermal modification on crystalline structure of cellulose in soft and hardwood. Building and Environment 42(1): 62-67.
29. Yu, H.P., Liu, Y.X., Luo, G.H., 2007: The change rule of visual physical quantity of transparent polyurethane coated wood. Journal of building materials (04): 89-94.
30. Zhang, D., Yang, L., 2012: Research progress in modified fast growing poplar wood. Forestry Machinery and Woodworking Equipment 40(3): 16-20.

Ruyuan Yang, Xiaofeng Zhang, Youfu Sun*, Tingting Zhou, Quan Yuan
Nanjing Forestry University
College of Materials Science and Engineering
Nanjing
China
*Corresponding author: yfsun@njfu.edu.cn

A STUDY ON SUITABILITY OF SOME WOOD SPECIES FOR LANDSCAPE APPLICATIONS: SURFACE COLOR, HARDNESS AND ROUGHNESS CHANGES AT OUTDOOR CONDITIONS

Candan Kus Sahin[1], Mehmet Topay[1], Ahmet Ali Var[2]
[1]Suleyman Demirel University
Turkey
[2]Isparta University of Applied Sciences
Turkey

ABSTRACT

In this study, each of the commonly used two types of woods (softwood and hardwood) from five species was studied. All wood species show a systematic trend to change to higher values of surface roughness with natural weathering progress. The Black pine, Calabrian pine and beech wood samples show a more or less smooth trend, whereas basswood gives the highest surface roughness changes under all conditions. However, the hardwood species, except basswood, have higher hardness properties both initially and at the end of weathering process when compared to softwoods. The surface discoloration that occurs is clearly visible as a natural texturing. However, the degree of, and the pattern of texturing, may vary with different kinds of woods; the color changes also vary to some extent. It was revealed that the discoloration is strongly dependent on the botanical origin of wood species. The lower lightness changes (ΔL %) were found for all three pine species (16.2 to 37.2%) when compared to fir (54.9%) and spruce samples (91.8%). The Scotch pine wood showed highest values for the contribution of red color initially and low redness change on the surface after the weathering process, among the other softwood species.

KEYWORDS: Wood, landscape practices, color, weathering, discoloration, CIE lab.

INTRODUCTION

Wood was one of the earliest materials to serve as a source for shelters, weapons, and energy for the early nomadic cultures. The knowledge of early wood use is based on fragments, drawings, and other conserved representations. Indeed, wood as a feature used in the landscape

can be found in nearly all cultures throughout history. Even in very early times (i.e., stone and masonry cultures), it was used in the construction of some garden structures (i.e., pergolas, arbors, boxes, fences) (Winterbottom 2000). Its wide range of versatility includes: warmth and richness, light weight, ability to span long distances, and workability takes people back to the landscape. Thanks in part to its natural origin with aesthetic features, wood is also well suited to apply in many landscape practice implementations (Auer 1982, Cristoforo 1976, Sahin and Onay 2020, Skarvelis and Mantanis 2013, Winterbottom 2000).

However, unprotected wood that absorbs solar UV light undergoes a color, texture and usually, physical changes. These changes result in its degradation when exposed to the weather conditions (Hon, et al. 1985, Kržišnik et al. 2018, Oberhofnerová et al. 2017, Sahin and Mantanis 2011). But, the level of degradation ranges from marginal surface discoloration affecting the aesthetic appeal to extensive loss of mechanical properties. The discoloration of wood at the outside usually called "non-microbial" discolorations, differ from fungal activity (Cassens and Feist 1991, McDonald et al. 1996).

However, one of the important problems when using of wood in atmospheric conditions is the uneven discoloration of the wood surface, which appeared mostly as aged of the outdoor-used woods while the surface layer darkened in natural color (Lykidis et al. 2016, Sahin and Mantanis 2011). Chang et al. (2015) have utilized wood waste with gypsum as binder to produce a new type of bricks for construction purposes. They measured the sunlight effects on those wood-based materials to change the color (hue) characteristics. They reported that these allotropic bricks can be applied to the external walls of buildings, providing landscape friendly buildings. Lo Monaco (2015) performed colorimetric analysis on aging treated (light exposure up to 504 hours) coppices of beech wood with using the CIE L*a*b* system in order to predict the wood color characteristics as a function of the exposure time, and vice versa to assess the exposure time needed to obtain the desired color coordinates. They found that beech wood from aged coppices in central Italy has interesting qualitative features, suggesting a more profitable use of their wood for various outside applications rather than being used for firewood. Tolvaj and Mitsui (2010) investigated irradiation characteristics of beech (*Fagus crenata* Blume), Black locust (*Robinia pseudoacacia* L.), Japanese cedar (*Cryptomeria japonica* D. Don) and spruce (*Picea abies* Karst.) woods by sunlight, xenon light and mercury vapor light. It was found that the samples showed a rapid color change during the initial period of treatment but the rate of change decreased with treatment time. Kannar and his group (2018) found that the yellowness properties of spruce wood's changed (increased) at outdoor conditions while the leaching partly removed the yellow and red chromophore molecules generated by the UV radiation. But the samples shown slightly lighter after water leaching.

Although plenty of literature can be found for color characteristics of wood samples that are used indoors or under outdoor conditions, a better understanding of specific wood discoloration under outside conditions is clearly needed. To find out, selected wood specimens were used to determine resistance against weathering conditions. After specific time to atmospheric exposure, the level of photo-discoloration was determined based on degrees of discoloration, surface roughness and hardness changes of the selected woods listed below.

MATERIALS AND METHODS

In the present study two types of wood (softwood and hardwood) of five species were used. The softwood species of scotch pine (*Pinus sylvestris*), Calabrian pine (*Pinus buritia*), black pine (*Pinus nigra*), Uludag fir, (*Abies bornmulleriana*), spruce (*Picea orientalis*), and the hardwood

species of cherry (*Prunus avium*), chestnut (*Castanea sativa*), beech (*Fagus orientalis*), basswood (*Tilia Americana*) and oak (*Quercus alba*) were selected for the experiments. The three small samples of each wood species were cut in the form of 60 x 60 x 10 mm pieces and conditioned at 20°C and 65% relative humidity in controlled room conditions to reach air dry moisture content of 12% level.

The natural outdoor exposure (weathering process) was conducted at the south side of a park (Cunur park) located in Isparta city, Turkey. The specially prepared samples were aged for a 12 months period. The measurements were taken after of six and 12 months, respectively. For the colour measurements, the radial surfaces of samples were used in order to determine the appropriate colour properties of samples.

To evaluate the surface quality of the wood samples of the different species after natural weathering conditions, there are a range of methods to measure surface roughness of wood species such as; simple touch on surface, macroscopic view and microscopic determination on the surface. However, "true measurement" of surface roughness requires a calibrated means of determining the peaks and valleys of the surface being evaluated. The value given is typically an average based on the distance of the area measured and the heights of the peaks and valleys. For that reason, surface roughness measurements were done with a Contact Stylus Profilometer type Time TR 200 device. With this equipment it is possible to build a two-dimensional surface profile after a direct measurement of the necessary parameters. The root-mean-square deviation of the profile, (Pq) was utilized to analyze surfaces. All the definitions used and parameters measured or calculated in this study are given in ISO 4287 (1998) and DIN 4768 (1990) standards.

The discoloration of wood specimens was determined using a color spectrophotometer (X-Rite SP 968 Spectrophotometer). Measurements were made using standard illumination and a standard observer. The CIE L*a*b* color scale (CIE, 1976), where L* stands for lightness, a* stands for redness, and b* stands for yellowness, was used to quantify the changes in color. The color variables of the surface layer of woods, and the difference in color, ΔE*, between them, were determined. The surface whiteness and yellowness color properties were also determined according to standard ASTM E-313, and ASTMD-1925, respectively.

The shore hardness, like many other tests, measures the depth of an indentation in the material created by a given force on a standardized presser foot. This depth is dependent on the hardness of the material and its viscoelastic properties. A Shore Hardness (Scale D) instrument was utilized to measure the hardness properties of the wood samples. The tests were conducted according to the ASTM D2240 standard. This test allows for a measurement of the initial hardness and for the indentation hardness after a given period of time. The surface hardness properties of wood samples were measured for each direction; five measurements were made of each sample.

RESULTS AND DISCUSSIONS

Tab. 1 summarizes the surface roughness changes against control (%) of wood species (0 months) under natural weathering (six and 12 months) conditions. It is observed that the one month exposure of wood species leads to some level of increase in surface roughness.

Tab. 1: Surface roughness change (%) of wood species at weathering conditions.

	0 month (Control, μm)	1 month	6 months	12 months
Softwoods				
Scoth pine	1.32	21.3	515.9	N/A
Black pine	3.92	18.4	20.9	58.9
Calabrian pine	2.83	37.1	91.3	271.1
Fir	2.33	59.2	95.3	N/A
Spruce	2.13	96.2	165.8	N/A
Hardwoods				
Chestnut	1.13	102.2	155.9	N/A
Cherry	3.54	72.8	75.4	N/A
Beech	3.34	25.8	69.6	74.7
Basswood	6.08	N/A	N/A	N/A
Oak	1.28	31.4	216.3	N/A

The lowest surface roughness changes were observed with Black pine (18.4%) following by scotch pine (21.3%), beech (25.8%), Calabrian pine (37.1%), oak (31.4%), fir (59.2%), cherry (72.8%), spruce (96.2%), and basswood (N/A) respectively. It appears that different wood species undergo considerable different surface roughness (%) changes. However, all wood species show a systematic trend to higher surface roughness values with prolonged natural weathering progress. The maximum surface roughness changes were obtained after 12 months weathering conditions in all wood species. Under those conditions, except Black pine (58.9%), beech (74.7%), and Calabrian pine (271.1%), show theoretically immeasurable surface roughness values (out of measurable range of 400 μm) which is change greater than 1000%). It has already been explained by a number of researchers that the wetting and drying cycles of wood exposed outdoors could result in rough surfaces caused by typically raised grain (Cassens and Feist 1991).

However, the characteristics of surface roughness are very complicated and not well understood for most wood species. To determine the causes of roughness one has to understand factors such as: wood cell wall structure, humidity conditions, annual ring orientation and density. These factors have a pronounced impact on surface roughness changes as reported in literature (Cassens and Feist 1991, McDonald et al. 1996). Hence, variations among surface roughness properties of wood specimens were very complicated and it is not intend to explain all changes. But, it is reasonable to explain that outdoor conditions could cause complex interactions resulting in slowly breaking down wood constituents and weakening fiber bonds. Moreover, moisture fluctuations cause surface layers to swell and shrink in addition to contraction due to degradation, while stable deeper layers restrain these movements, so that weakened fiber bonds fail and result in surface erosion and deformations. But it is noticeable that, black pine, Calabrian pine and beech wood show a more or less smooth trend whereas basswood shows the highest surface roughness changes (very easy to change surface roughness properties) under all conditions.

Fig. 1 shows the comparative hardness changes of wood species against natural weathering process. As seen in Fig. 1, the prolonged outdoor exposure beyond 6 months has further deteriorating effects on all wood species.
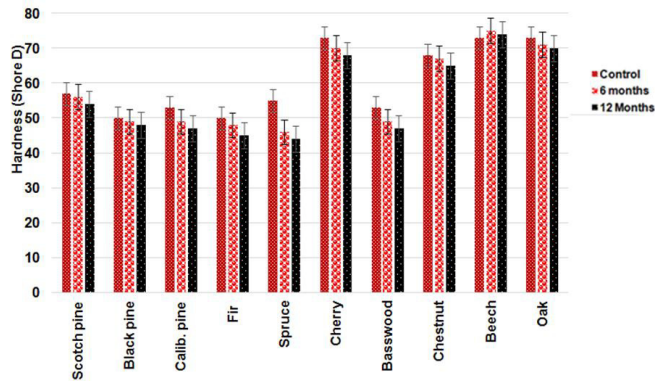
Fig. 1: Surface hardness change of wood species at various conditions.

As expected, hardwood species except basswood have higher hardness properties initially while at the end of weathering process the hardwoods properties compare to those of softwoods. However, after the 12 months natural weathering process, the highest hardness values for hardwoods were determined for both oak (73) and beech (70) and followed by cherry (68), chestnut (65) and basswood (47) species, respectively. On the other hand, after the 12 months natural weathering process, the highest hardness values for softwoods were exhibited by scotch pine (54), followed by Black pine (48), Calabrian pine and fir (47), and spruce (44) species, respectively. It is noticeable that after the 12 months natural weathering process, softwood species showed 4.0 to 20.0% hardness reduction whereas hardwoods showed 4.2 to 11.3% hardness reduction. The results found in this study are clearly consistent with literature findings that the hardwoods usually have higher hardness values initially and are more resistant to outdoor conditions than softwoods.

Wood used in landscape applications, such as; for pergolas, fences, decks, containers, tables, boxes, could create its own appearance. However, it has already been mentioned above that wood used under outside conditions have under gone complex photo degradation reactions to lose of its beauty and aesthetic appearance (discoloration). The brightest woods turn a dark color, but in the short time all species turn into various color combinations. These changes happen because of the action of light, moisture and temperature. It is realized that surface discoloration and erosion, can be visible as natural texturing, takes place. Discoloration of woody material may result in loss of quality and value of the wood. As seen in Fig. 2, even exposure for short duration of time to atmospheric conditions, occasionally produce discolored woods. The degree of, and the pattern of texturing may vary with different kinds of woods, as do the extent of roughness and color modification.

Fig. 2: Surface natural appearance of wood species at various conditions: A– Control, B– one month, C– six months, D– 12 months of natural weathering durations at outside.

For better understanding and quantification of discoloration level of wood species after exposure to atmospheric conditions, spectrophotographic measurements were done and results presented in Tab. 2 for softwood species and in Tab. 3 for hardwood species, respectively. According to the results from the color measurements, the discoloration is strongly dependent on the botanical origin of wood species (Tab. 2, Tab. 3). However, it is important to note that the differences in color values measured in this study were not necessarily all so large that they could be considered to be unacceptable by the end-users of wood.

The lightening as a result of natural weathering was clearly shown in Tab. 2. However, the lower lightness changes (ΔL^*) were found for all three pine species (16.2 - 37.2) compare to fir (54.9) and spruce samples (91.8). It is well known that light-colored wood specimens underwent photo-bleaching reactions when exposed to weathering conditions. The results found in this study are in good agreement with earlier findings (Esteves et al. 2008).

Tab. 2: Surface colour change of softwood species at various conditions (weathered at 12 months duration).

Species	ΔL	Δa	Δb	ΔE (Metric)
Scoth pine	32.3	31.1	44.4	34.3
Black pine	16.2	61.6	35.4	31.2
Calib. pine	37.5	57.8	54.4	48.6
Fir	54.9	41.6	60.5	58.5
Spruce	91.8	40.9	44.1	48.2

The Scotch pine wood showed highest values for the contribution of red color initially and low redness change (Δa^*= +4.4 to +3.03; 31.1% change) on the surface after weathering process, among the other softwood species. However, the color coordinates of yellow (+b) to blue (-b) of wood samples also displayed exhibited a high variations. Interestingly, natural weathering favored a dramatic reduction of yellow color for fir wood (Δb^* = 14.6 to 5.77; which equals a 60.5% change). Tolvaj and Faix (1995) reported that the yellow color of wood was mainly due to the lignin moiety of the wood. However, the effects of wood cell wall chemicals on the color of wood are very complicated and beyond the bounds of this study to explain.

A number of researchers have already proposed that ΔE (total color differences) could be a better predictor than ΔL^*, Δa^* and b^* for most color properties of woods (Chang et al. 2015, Janin et al. 2001, Lo Monaco 2015, Tolvaj and Mitsui 2010). However, the softwood substrates appeared to be better correlated with ΔE than the other color (Δa and b) parameters. Moreover, for softwood species, the ΔE values showed a trend that was somewhat similar to that of ΔL^*, Δa^* and b^* values. The highest ΔE of 58.5 was found for fir wood, followed by Calabrian pine (48.6), spruce (48.2), Black pine (34.3) and Scotch pine (31.1) species, respectively. These comparisons between the surfaces and the measured results clearly reveal that the color-change response of a wood can be accurately predicted based on the ΔE values.

The marked effect of surface color changes for hardwood species with natural weathering conditions are also clearly evident in Tab. 3. However, the results in Tab. 3 confirm that surface color properties of the woods from the hardwood species were found to be very high. This is probably due to the fact that hardwoods have more dark color initially; hence the discoloration is higher compared to softwood species. These results are clearly consistent with literature findings (Kucuktuvek et al. 2017, Oberhofnerová and Pánek 2016).

Moreover, the explanation of discoloration patterns of hardwoods looks like they were complicated since the general characteristics of the smaller the initial L^* value of hardwoods. The high ΔL^* values (changes %) were found for beech (-146.1), followed by oak (-9.7) and cherry (-8.9), respectively. In contrast, basswood and chestnut species show some lightness increases. It has already been explained that the discoloration of dark-colored wood specimens (i.e. hardwoods) are much more complicated, whereas these patterns shifted slightly toward those observed for light-colored woods (Sahin, et al. 2011).

Tab. 3: Surface colour change (%) of hardwood species at various conditions (C– control, W– weathered at 12 months duration).

Species	ΔL	Δa	Δb	ΔE (Metric)
Cherry	-8.9	-18.9	40.9	15.4
Basswood	62.8	48.1	92.2	75.3
Chestnut	23.1	-6.5	36.4	31.3
Beech	-146.7	-254.1	-4.1	63.3
Oak	-9.7	47.9	81.8	49.1

However, the ΔE shows a systematic trend to higher values for hardwoods compared to softwood species. The maximum ΔE changes were found for basswood (75.3), followed by beech (63.3) and oak woods (39.3), respectively. In addition, very low ΔE changes (15.4) were found in the cherry samples.

It is important to repeat that the discolorations are not well understood for most wood species. To determine the causes of discolorations one has to understand factors such as: wood chemical composition, ambient temperature, humidity, and light conditions. Hence, variations

among discoloration patterns of wood specimens are complicated and this study does not intend to explain all these color characteristics. It should be also emphasized that the determination of the Δa* and Δb* values must be considered as being only suggestive.

Fig. 3 shows whiteness and yellowness changes of wood species after a weathering process. It should be realized that the whiteness and yellowness reduction more or less followed a similar trend for both softwood and hardwood species. However, it can be also found that hardwood species (except basswood) have usually less whiteness and yellowness values compared to softwood species.
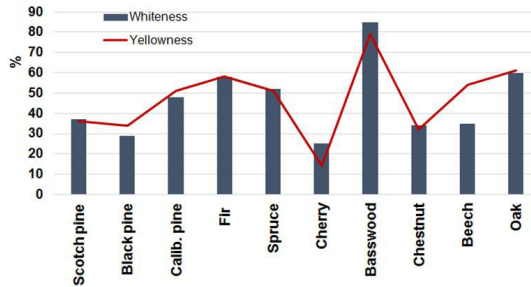
Fig. 3: Whiteness and yellowness properties of woods after weathering process (12 months).

The highest whiteness values were found to be for basswood (84.8%) followed by oak (59.7%), fir (58.2%), spruce (52.4%), Calibrian pine (48.1%), Scotch pine (36.9%), beech (34.5%), chestnut (33.6%), Black pine (29.3%), and cherry (24.8%), in that order. A more or less similar trend was also found for whiteness values. The highest yellowness were found to be for basswood (79.2%) followed by oak (61.3%), fir (58.3%), beech (53.6%), Calabrian pine (51.3%), spruce (51.1%), Scotch pine (36.1%), Black pine (34.3%), chestnut (31.7%), and cherry (14.2%), in that order. As mentioned above, this is also in good agreement with literature findings that the hardwoods that have more dark color initially resulting in discoloration that is usually higher compared to softwood species (Hill 2006, Palashev 1994). But, the discoloration patterns of wood are complicated since many variables affect the natural color of wood. Moreover, a number of attempts were conducted on the effects of outdoor conditions on color modification of woods. Consistently, weathering processes make the wood surface darker (Dirckx et al. 1992, Hill 2006, Palashev 1994, Pastore et al. 2004).

CONCLUSIONS

An attempt was made to analyze wood surface property changes due to exposure to natural outdoor conditions of the most frequently traded wood species in Turkey and all of Europe. However, the natural surface appearance and color of wood are very important quality criteria in the utilization, especially for outdoor applications (i.e., landscape architecture). It has been clearly revealed that the susceptibility to surface appearance change (roughness, hardness and discoloration) is variable and strongly dependent on the botanical origin of species as well the nature of the wood itself.

It is observed different wood species undergo considerable different surface roughness (%) changes. In 12 months, weathering conditions black pine, beech, and Calabrian pine show

very high surface roughness values. However, at this level of weathering, it is also observed that softwood species showed 4.0 to 20.0% hardness reduction whereas hardwoods showed 4.2 to 11.3% hardness reduction. However, the Scotch pine wood showed highest values for the contribution of red color initially and low redness change (Δa^*= +4.4 to +3.03; 31.1% change) on the surface after weathering process, among the other softwood species. The softwoods look like well correlated with ΔE than the other color (Δa and b) parameters while the ΔE shows a systematic trend to higher values for hardwoods compared to softwood species. It can be concluded that except for basswood, hardwoods are more suitable species for using under outdoor conditions rather than softwood species when surface hardness properties are considered.

REFERENCES

1. Auer, M.M. 1982: Wood finishing and refinishing. Creative Homeowner Press, New Jersey, NJ. 142 pp.

2. Cassens, D.L., Feist, W.C., 1991: Exterior wood in the South, selection, application and finishes. U.S. Department of Agriculture, Gen. Tech. Rep. FPL-GTR-69, Madison, WI. 60 pp.

3. Chang, Y.H., Huang, P.H., Wu, B.Y., Chang, S.W., 2015: A study on the color change benefits of sustainable green building materials. Construction and Building Materials 83: 1-6.

4. Cristoforo, R.J., 1976: Wood projects for the garden. Ortho Books, Chevron Chemical Company. San Francisco, CA, 96 pp.

5. Dirckx O., Triboulottrouy, M.C., Merlin, A, Deglise X., 1992: Wood photo discolouration of *Abies grandis* under solar light exposure. Annales Des Sciences Forestieres 49(5): 425-447.

6. Esteves, B., Marques, A.V., Domingos, I., Pereira, H., 2008: Heat-induced colour changes of pine (*Pinus pinaster*) and eucalypt (*Eucalyptus globulus*) wood. Wood Science and Technology 42(5): 369-384.

7. Hill, C., 2006: Wood Modification: chemical, thermal and other processes. John Wiley & Sons, Ltd. NY, 260 pp.

8. Hon, D.N.S., Chang, S.T., Feist, W.C., 1985: Protection of wood surfaces against photooxidation. Journal of Applied Polymer Science 30(4): 1429-1448.

9. Janin, G., Gonzales, J.C., Ananias, R., Charrier, B., Silva, G., Dilem, A., 2001: Aesthetics appreciation of wood colour and patterns by colorimetry. Part 1. Colorimetry theory for the CIELAB system. Maderas: Ciencia y Tecnología 3(1-2): 3-13.

10. Kržišnik, D., Lesar, B., Thaler, N., Humar, M., 2018: Influence of natural and artificial weathering on the colour change of different wood and wood-based materials. Forests 9(8): 488.

11. Kucuktuvek, M., Baysal, E., Turkoglu, T., Peker, H., Gunduz, A., Toker, H., 2017: Surface characteristics of scots pine wood heated at high temperatures after weathering. Wood Research 62(6): 905-918.

12. Lo Monaco, A., Calienno, L., Pelosi, C., Balletti, F., Agresti, G., Picchio, R., 2015: Technical properties of beech wood from aged coppices in central Italy. iForest-Biogeosciences & Forestry 8(1): 82-88.

13. Lykidis, C., Bak, M., Mantanis, G., Németh, R., 2016: Biological resistance of pine wood treated with nano-sized zinc oxide and zinc borate against brown-rot fungi. European Journal of Wood and Wood Products 74(6): 909-911.

14. Mc Donald, K.A., Falk, R.H., Williams, R.S., Winandy, J.E., 1996: Wood decks, materials, construction and finishing. Forest Products Society, Madison, WI, 93 pp.

15. Oberhofnerová, E., Pánek, M., García-Cimarras, A., 2017: The effect of natural weathering on untreated wood surface. Maderas. Ciencia y tecnología 19(2): 173-184.

16. Oberhofnerová, E., Pánek, M., 2016: Surface wetting of selected wood species by water during initial stages of weathering. Wood Research 61(4): 545-552.

17. Palashev, Y. ,1994: Change in the wood colour under the influence of climatic factors. Naukaza Gorata 31(2): 65-71.

18. Pastore, T.C.M., Santos, K.O., Rubim, J.C., 2004: Spectrocolorimetric study on the effect of ultraviolet irradiation of four tropical hardwoods. Bioresource Technology 93(1): 37-42.

19. Sahin, H.T., Arslan, M.B., Sahin, C., 2011. Colour changes of heat-treated woods of Red-bud maple, European hophornbeam and oak. Color Research & Application 36(6): 462-466.

20. Sahin, H.T., Mantanis, G.I., 2011: Colour changes in wood surfaces modified by a nanoparticulate based treatment. Wood research 56(4): 525-532.

21. Sahin, C.K., Onay, B., 2020: Alternative wood species for playgrounds wood from fruit trees. Wood Research 65(1): 149-160.

22. Skarvelis, M., Mantanis, G.I., 2013: Physical and mechanical properties of beech wood harvested in the Greek public forests. Wood Research 58(1): 123-130.

23. Tolvaj, L., Faix, O., 1995: Artificial ageing of wood monitored by drift spectroscopy and CIE Lab color measurements. Holzforschung 49(5): 397-404.

24. Tolvaj, L., Mitsui, K., 2010: Correlation between hue angle and lightness of light irradiated wood. Polymer Degradation and Stability 95(4): 638-642.

25. Winterbottom, D.M., 2000: Wood in the landscape. A practical guide to specification and design, John &Wiley Sons, NY. 216 pp.

Candan Kus Sahin*, Mehmet Topay
Suleyman Demirel University
Faculty of Architecture
Department of Landscape Architecture,
32260 Isparta
Turkey
*Corresponding author: candansahin@sdu.edu.tr

Ahmet Ali Var
Isparta University of Applied Sciences
Faculty of Forestry
Department of Forest Products Engineering
32040 Isparta
Turkey

COMPARISON OF SELECTED PROPERTIES OF NATURAL AGED WOOD AND CONTEMPORARY TIMBER OF *PINUS SYLVESTRIS* L. INVESTIGATED USING STANDARD METHODS AND MEASURING OF TRANSITION SPEED OF ULTRASOUNDS ALONG THE FIBRE

Adam Krajewski, Paweł Kozakiewicz, Piotr Witomski
Warsaw University of Live Science
Poland

ABSTRACT

Scots pine wood (*Pinus sylvestris* L.) is the most common wood material used in historical buildings in many parts of Central and Eastern Europe. Experiments were conducted natural aged wood (263 – 459 years old), extracted from construction elements of four historical buildings (from seven construction elements), and contemporary wood extracted from 5 construction elements. A strong relationship was observed between density and static bending strength (MOR) of natural aged wood (R^2 = 0.5599), and also of contemporary timber (R^2 = 0.7863). Antique wood compared to contemporary wood with the same average moisture content and density is characterized by significantly lower modules (static and dynamic), the speed of ultrasonic waves transitions, and bending strength. Differences in these properties increase with increasing wood density.

KEYWORDS: *Pinus sylvestris*, natural aged wood, physical properties, mechanical properties.

INTRODUCTION

Mechanical properties of natural aged wood have been of great interest among researchers for many years. A great contribution into research on natural aged wood was made between 1950-1955 by Kohara (1952, 1954, 1955, 1956), who tested *Chamaecyparis obtusa* Endl. and *Zelkowa serrata* Thunb. wood taken from very old constructions of Japanese temples (Obataya 2007). Some constructions were even 1300 years old. In the research of Yokoyma et al. (2009), experiments for static bending conducted on *Ch. obtusa* wood samples cut from historical

constructions proved that the technical properties of the wood were still quite good as compared to contemporary wood.

Scots pine (*Pinus sylvestris* L.) is a dominant species of wood in the middle of Central-Eastern Europe. In some regions it has been the main building material (e.g Mazovia and Warmia regions in Poland). However, natural aged coniferous softwood from Europe, including Scots pine wood (Krániz et al. 2010) and spruce wood (Schulz et al. 1984, Krániz et al. 2010, Thaler and Miha 2013), is a relatively rare subject of research on mechanical qualities. Also, European natural aged coniferous wood used in such research is usually much younger – around 100÷200 years old (Rug and Linke 2013, Thaler and Miha 2013, Krániz et al. 2010, Yorur and Yumrutas 2014) – than aged wood of *Ch. obtusa* examined in Japan (Yokoyma et al. 2009). The age of *Ch. obtusa* samples used in that research ranged from 500 to over 1600 years.

Among laboratory tests on mechanical qualities of aged wood from historical constructions, the most common topic is definitely measuring compressive strength parallel to grain (Deppe and Ruhl 1993, Obataya 2007, Witomski et al. 2014, Sonderegger et al.2015). Results of research on other qualities of European aged wood from historical constructions are rather not as common. They include research on shear strength of aged Scots pine heartwood (Yorur and Yumrutas 2014, Krajewski et al. 2016).

Special reviews in this regard are the reviews on the mechanical properties of antique wood (Cavalli et al. 2016, Kránitz et al. 2016). These works, however, focus on other species of wood (properties of Scots pine wood are presented at random mainly in terms of compression strength).

This insufficient research raises the question. How, in the case of naturally aged wood of Scots pine wood, do such properties as wood static bending strength (MOR) and Young modules (dynamic and static MOE), as compared to contemporary timber? This is an important issue, among others, in assessing the safety of the wooden constructions and the decision on the need and scope of conservation work undertaken.

The possibility of using measurements of transition speed of ultrasounds along the fibre in order to estimate wood static bending strength (MOR) seems an interesting option. For this reason, the correlation between static bending strength (MOR) and density of wood, and the correlation between transition speed of ultrasounds along the fibre of wood and density of wood were studied.

MATERIALS AND METHODS

The authors of the present research used natural aged heartwood of Scots pine (*Pinus sylvestris* L.) free from fungal decay or insect attack. The tested wood samples were taken from 4 historical constructions form Poland (Mazovian district and Warmian-Masurian district) dating from 16th-18th century. Samples used in tests were sized 20 x 20 x 300 mm and extracted from 7 constructional elements: (A1) wall beam from the church in Puszcza Mariańska (dating from 1755) – 8 samples, (A2) wall beam from the church in Puszcza Mariańska (1755) – 17 samples, (A3) wall beam from the church in Puszcza Mariańska (1755) – 13 samples, (A4) element of rafter from the monastery in Święta Lipka (German: Heilige Linde, 1703) – 4 samples, (A5) element of rafter from the castle in Lidzbark Warmiński (German: Heilsberg, 1559) – 17 samples, (A6) element of rafter from the church in Cegłów (before 1629) – 10 samples, (A7) element of rafter from the church in Cegłów (before 1629) – 30 samples.

The wood collected for research was dated based on the analysis of the documentation of the objects from which it came. The authenticity of the elements was confirmed on the basis of their appearance and location in the constructions and presence of the original carpentry marks.

The age given is the number of years of use in the construction (the actual age of antique wood is higher). Natural aged wood was represented by a total number of 99 samples taken from constructions aged 263 – 459 years. The wood from the castle in Lidzbark Warmiński was taken from trees cut down at the age of 130 – 140 years. The wood from all the other constructions was taken from trees cut down at the age of 100 – 120 years.

The contemporary timber was taken from 5 Scots pine heartwood timber from tress at the age of around 80 – 100 years. 75 samples of dried and seasoned timber were used for comparative tests (F1 - 5 samples, F2 - 12 samples, F3 - 18 samples, F4 - 20 samples and F5 - 20 samples). Density of natural aged wood and fresh cut and dried and seasoned timber of each sample was calculated using stereometrical method according to standard method ISO 12061-2: 2014.

Moisture content (MC) of the wood was determined using oven-dry method according to ISO 13061-1: 2014. The transition speed of ultrasounds along fibre and dynamic modulus of elasticity (MOEd) were determined using an original ultrasonographic method with the use of material tester UMT-1, connected to specialistic computer software. The tests were conducted using two cylindrical heads of 40 mm diameter: receiving head and transmitting head producing ultrasounds of frequency of 40 kHz. The tester worked in impulse mode (transmission 12 Hz) with 40 dB gain and at the electrical voltage of 60 V, using policrylate gel as coupling substance. The pattern delay time was t0 = 8.9 μs.

After running ultrasound waves parallel to the grain, the time of the main echo was read and the results were used to calculate the speed of longitudinal waves parallel to the grain:

$$c_{\parallel} = \frac{L}{t} \tag{1}$$

where: c - speed of the longitudinal waves parallel to the grain (m·s^{-1})
L - sample length [m] (assuming that L >> λ)
$t = t_1 - t_0$ - real time of the passing through of the longitudinal wave (s)
t_1 - time of the passing through of the wave read from the computer screen (s)
t_0 - lag time (s).

On the basis of speed the elasticity, modulus parallel to the grain was calculated using the formula below:

$$MOE_d = c_{\parallel}^2 \cdot d \cdot \frac{(1 + \mu_o) \cdot (1 - 2 \cdot \mu_o)}{(1 - \mu_o)} \tag{2}$$

where: MOE_d - dynamic modulus of elasticity parallel to the grain (GPa)
μ_o - reduced Poisson's ratio for wood ($\mu_o = 0.3$) (-)
d - density of wood of a known moisture content (kg·m^{-3}).

Average values of transition speed of ultrasounds through and average the dynamic elasticity modulus both aged wood and fresh cut timber were then calculated. Statistical significance of the difference between those values was evaluated using Student test. The relationship between transition speed of ultrasounds along fibre in natural aged wood and contemporary timber and wood density was determined and coefficients of determination (R^2) were calculated.

Static bending strength of wood (MOR) and static modulus of elasticity of wood (MOEs) were tested for each sample according to standard method ISO 13061-3:2014 and ISO 13061-4:2014. To establish those values, a universal testing machine INSTRON (model 3369) was used. The machine is connected to computer program INSTRON Series IX/s Automated Materials Tester Version 8.32.00, allowing the analysis of the results.

Average values of MOR, static MOE and dynamic MOE for both aged wood and contemporary timber were calculated. Also, coefficients of variation were calculated for each of those features for every set of samples from each single construction element, as well as for the whole sets of samples of both natural aged wood and contemporary timber. It was verified whether the obtained groups of results for both aged wood and fresh cut timber exhibit normal distribution. Next, statistical significance of differences between average values of MOR, static MOE and dynamic MOE was evaluated. To determine statistical significance of the differences between those properties of aged wood and contemporary timber, Student test was used, as those values exhibited normal distribution. The relationships between MOR, static MOE and dynamic MOE, and wood density, were determined. Also, coefficients of determination (R^2) were calculated.

RESULTS AND DISCUSSION

The results of measurements and calculations are shown in Tab. 1 in the form of numerical data. The average values of wood properties and their coefficients of variation for each sample of natural aged wood and contemporary timber displayed some differences. The results of statistical verification of significance of the differences between the average values of moisture content, density, transition speed of ultrasounds along fibre dynamic MOE, static MOE, and bending strengths (MOR) for both natural aged wood and contemporary timber are shown in this table too.

Tab. 1: Selected physical and mechanical properties of natural aged heartwood and contemporary heartwood of scots pine (Pinus sylvestris L.).

No of elements	Number of samples	MC (%)	Density of wood (kg·m⁻³)	Transition speed of ultrasounds‖ (m·s⁻¹)	MOEd (MPa)	MOEs (MPa)	MOR (MPa)
Coefficient of variation (in brackets) v (%)							
A1	8	8.9 (3.1)	467 (3.6)	5362 (2.5)	9687 (6.2)	8793 (7.4)	73.9 (15.6)
A2	17	9.1 (2.4)	549 (4.1)	5449 (6.1)	11808 (14.6)	10409(13.3)	89.4 (15.6)
A3	13	8.8 (3.2)	418 (5.5)	5019 (5.5)	7616 (12.6)	7116 (12.0)	63.9 (8.9)
A4	4	8.9 (3.0)	452 (2.1)	5723 (1.1)	10671 (4.1)	9918 (6.7)	84.5 (3.3)
A5	17	8.7 (2.6)	365 (2.1)	5107 (1.6)	6853 (3.4)	6498 (3.8)	62.4 (7.9)
A6	30	9.0 (4.5)	459 (5.2)	5256 (6.9)	9203 (17.1)	8437(13.8)	81.8 (11.2)
A7	10	8.9 (3.8)	389 (6.5)	5026 (3.0)	7108 (10.8)	6678 (12.0)	56.9 (9.3)
Average for natural aged wood		8.9 (5.2)	446 (14.0)	5237 (6.1)	8925 (23.4)	8180 (20.5)	74.4 (19.4)
F1	5	8.9 (4.6)	531 (7.1)	5996 (2.0)	14216 (10.8)	12068(11.4)	111.9 (17.0)
F2	18	9.0 (2.4)	459 (11.2)	5777 (4.0)	11466 (18.0)	9955 (18.6)	91.0 (20.8)
F3	12	9.2 (3.9)	536 (3.4)	5897 (4.1)	13877 (8.8)	12141 (7.2)	108.5 (14.6)
F4	20	8.9 (2.6)	440 (10.1)	5343 (2.1)	9389 (15.6)	8255 (15.3)	83.4 (16.4)
F5	20	9.0 (2.8)	437 (7.1)	5460 (4.5)	9712 (13.3)	8517 (11.9)	84.4 (10.7)

Average for natural aged wood	9.0 (6.3)	465 (11.8)	5610 (5.8)	11013 (21.4)	9609 (20.7)	91.4 (19.7)
Statistical verification						
Differences between natural aged wood and contemporary wood	not significant	not significant	significant	significant	significant	significant

The antique wood, originating from various elements and objects, was characterized by considerable density variability from 365 kg·m⁻³ (element of rafter from the castle in Lidzbark Warmiński) to 549 kg·m⁻³ (wall beam from the church in Puszcza Mariańska). The coefficient of variation of this wood characteristic was 14%. Contemporary construction elements for research have been selected taking into account the similarity of the annual rings (width and arrangement) and density to the elements of historic wood.

The difference between the average density of natural aged wood and the average density of fresh cut timber proved to be statistically insignificant in the case of the tested samples at the assumed probability level. This fact allowed to compare all the other features of the wood. The tested wood did not show differences in moisture content. The differences between transition speed of ultrasounds along fibre, dynamic MOE, static MOE and MOR for both natural aged wood and contemporary timber were in all the cases statistically significant (Tab. 1). Thus, they cannot be explained by the difference in wood moisture content (MC) and density.

The relationship between density and static bending strength (MOR) of wood is shown in Fig. 1, separately for the tested collections of samples of natural aged wood and contemporary timber.
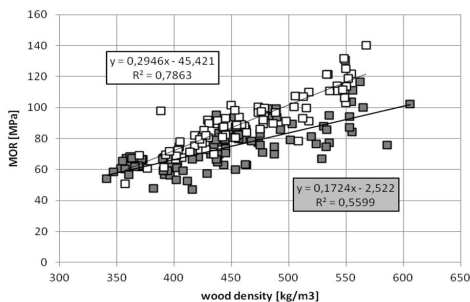

Fig. 1: *The relationship between density and static bending strength (MOR) of natural aged wood (grey points) and contemporary timber (white points).*
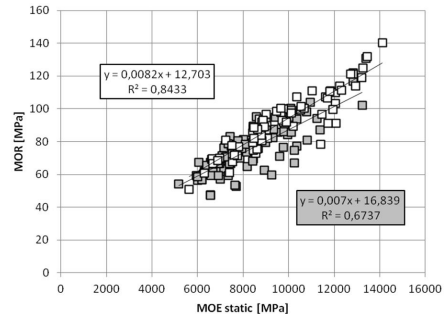
Fig. 2: *The relationship between static MOE and static bending strength (MOR) of natural aged wood (grey points) and contemporary timber (white points).*

Next, the relationship between MOR and static MOE is presented. The relationship between wood static bending strength (MOR) and static modulus of elasticity of wood is shown in Fig. 2. The relationship between wood static bending (MOR) and dynamic modulus of elasticity of wood (MOE) is shown in Fig. 3. The relationships between wood density and ultrasound wave speed inside the wood are shown in Fig. 4, separately for the tested collections of samples of natural aged wood and contemporary timber. The equations of linear correlations and values of determination coefficients are given on all graphs.
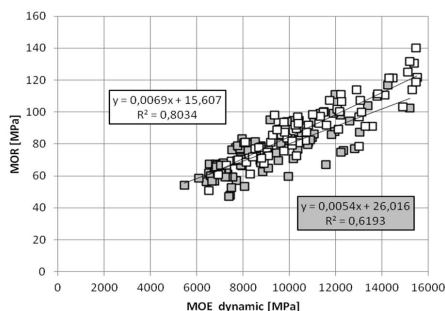
Fig. 3: The relationship between dynamic MOE and static bending strength (MOR) of natural aged wood (grey points) and contemporary timber (white points).
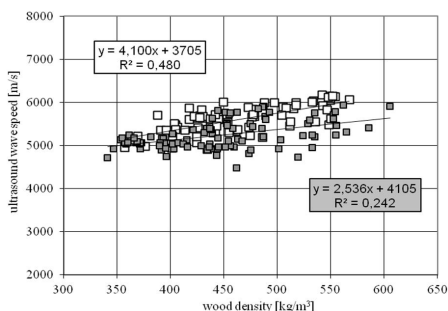
Fig. 4: The relationship between density and wood transition speed of ultrasounds along the fiber of natural aged wood (grey points) and contemporary timber (white points).

As it was mentioned above, among laboratory tests on mechanical properties of aged wood from historical constructions, the most common topic is definitely compressive strength parallel to grain (Deppe and Ruhl 1993, Obataya 2007, Witomski et al. 2014, Sonderegger et al. 2015). This probably results from the fact that samples used in such kind of research are of simple shapes and require relatively small amount of original wood from the construction. It is thus rather easy to obtain a significant number of samples for standard tests. This is why the present research on MOR and MOE of natural aged wood was conducted. It seems that in the present research on static bending strength across fibre (MOR), after many years of work a sufficient number of samples of natural aged wood was collected, and compared with contemporary timber, to obtain representative results for Scots pine heartwood. Big difficulty in obtaining natural aged wood being much older than 100 years resulted in many attempts to use accelerated thermo-hydro aged wood to estimate changes in properties of this material (Matejak et al. 1983, Froidevaux et al. 2011, Jankowska and Kozakiewicz 2014).

Most research on properties of natural aged wood has been so far conducted on Japanese wood species (Kohara 1955, Kohara and Okamoto 1956, Hirashima et al. 2005, Ando et al. 2006, Obataya 2007, Yokoyma et al. 2009), among others because of a big number of well preserved old wooden buildings in Japan.

Normal distribution of wood features for both collections of tested samples of natural aged wood and contemporary timber allowed to apply Student test to verify statistical significance of differences between arithmetic averages calculated for both collections.

Average values of MOR, static MOE and dynamic MOE for natural aged wood and fresh cut timber proved to be statistically different. MOR of natural aged wood (74.4 MPa) was visibly lower than MOR of fresh cut timber (91.4 MPa). The obtained results are thus consistent with research conducted on Japanese wood species. Japanese research on wood of *Ch. obtusa* and *Z. serrata* has proven that natural aged wood more than 300 years old has a lower durability for static bending (MOR) as compared to contemporary timber (Kohara and Okamoto 1956, Obataya 2007). As part of this work on Scots pine wood, the dependence between the age of old wood from individual objects and the decrease in the studied properties has not been captured. The wood was too diverse in density and dating was not precise(no dendrochronological designation).

The transition speed of ultrasounds is a feature related to wood density, yet a more important factor is the anatomical structure of the material. As a result of ageing, gradual changes in the

ultrastructure of cell walls (shortening of cellulose chains and increase of crystallinity – e.g. Guo et al. 2018) in the wood appear, which causes a slight reduction of the transition speed of ultrasounds in old wood (Fig. 4.).

Scots pine wood used in historical constructions preserved to this day in Central and Eastern Europe had always low amount of sapwood, or no sapwood at all. If a constructional element contained some sapwood, it was usually strongly damaged by wood boring insects, especially the old house borer *Hylotrupes bajulus* L. Heartwood of Scots pine has a low content of proteins, which does not provide proper conditions for old house borer larvae to survive, which was ascertained many years ago (Becker 1963a, Becker 1963b). This fact results in predominant amount of heartwood in preserved original constructions of historical buildings. Frequently, structural nodes hold on undamaged heartwood. Unfortunately, good quality of original aged wood tends to be underestimated during conservatory work in historical buildings and recognised as poor. This is because the estimation of the condition of roof construction is typically based on visible damages of constructional elements near the surface, where sapwood dominates, showing damage caused by insect larvae. This does not mean, however, that the entire constructional element, consisting mostly of heartwood, is in poor condition. Especially in the case of ceiling beams and rafters, the most important properties seem to be static bending strength across fibre (MOR) and Young's moduli (dynamic MOE and static MOE).

However, natural aged wood is characterised by higher brittleness, which was earlier proven in research on Japanese natural aged wood (Kohara and Okamoto 1956, Hirashima et al. 2005, Obataya 2007, Yokoyma et al. 2009). Aged wood of Scots pine used in present study was of various age, yet it was much younger than the wood from ancient Japanese temples. The wood from rafter in Lidzbark had been cut at the age 130-140 years and since then spent 458 years in the construction. The wood from the church in Cegłów served in the construction for no less than 388 years since the moment it had been cut down. The wood from wall beams in the Church in Puszcza Mariańska came from trees cut down 262 years ago. However, also in the case of the examined Scots pine wood, a decrease was visible in average durability for static bending (MOR) at around 19%. Dealing with wood 250 – 500 years old, such level of decrease in MOR should be taken into account. Also, coefficient of variation of MOR for natural aged wood used in the experiments was 19.4%, thus very close to coefficient of variation of MOR for fresh cut timber (19.7%).

The calculations of wood static bending strength (MOR) and static MOE (Fig. 2) showed a good level of matching of both properties, with the value of R^2 = 0.843 for contemporary timber and R^2 = 0.674 for natural aged wood. Similarly, in the case of MOR and dynamic MOE, a satisfactory matching was shown by the results (R^2 = 0.803 for contemporary timber and R^2 = 0.619 for natural aged wood).

In the studied range of wood age (262-458 years since cutting down), the value of MOR is also related to the density of wood (Fig. 1). The coefficient of determination for natural aged Scots pine wood is in this case R^2 = 0.560, while for contemporary timber R^2 = 0.786. Thus still around 56% of variation in static bending strength (MOR) in aged wood is caused by the influence of wood density.

The decrease in shear strength parallel to grain of natural aged Scots pine wood was insignificant, as was shown by earlier research. Shear strength of natural aged wood was 8.55 MPa, while shear strength of contemporary timber was 8.64 MPa (Krajewski et al. 2016). Compressive strength parallel to grain was much higher for natural aged wood than for contemporary timber (Witomski et al. 2014). This phenomenon had been studied earlier on Japanese wood (Kohara 1954, Kohara and Okamoto 1956, Obataya 2007, Yokoyma et al. 2009).

Average transition speed of ultrasounds along the fibre was higher for natural aged wood than for contemporary timber and the difference was statistically significant, yet the correlation between transition speed of ultrasounds along the fibre and the density of wood was unsatisfactory – below 0.5 (Fig. 4). However, the experiments were conducted on relatively narrow and short samples (30 cm), which acts in favour of noises resulting from reflections of the wave on the edges. Results allowing much better estimation of capabilities of this test method can be achieved on big-dimensional, long wooden elements. In the light of Japanese research, it seems that transition speed of ultrasounds is conditioned not only to wood density, but also to the degree of crystallinity of cellulose. Based on earlier research, it was ascertained that crystallinity of cellulose is higher in natural aged wood (Kohara and Okamoto 1956, Obataya 2007, Nilsson and Rowell 2012, Guo et al. 2018). It is probable that a stronger conditioning of transition speed of ultrasounds along the fibre to crystallinity of cellulose caused a weaker conditioning of the feature to the density of wood. Due to a wide range of the research, experiments conducted so far did not include studies on crystallinity of cellulose and its impact on transition speed of ultrasounds along the fibre of wood. The authors hope to continue their work in this matter.

CONCLUSIONS

The obtained results show that natural aged Scots pine wood, taken from constructions around 250 – 500 years old, is characterised by a wood static bending strength (MOR) lower by almost 1/5 than in the case of contemporary timber. At the same time, MOR of wood is still significantly related to the density of wood.

There is a strong proportional relationship between bending strength and static and dynamic modulus of elasticity in contemporary and old wood. Regardless of the above, the old wood is characterized by significantly lower values of static and dynamic modulus of elasticity along the fibers.

The coefficient of determination R^2 for correlation between transition speed of ultrasounds along the fibre and the density of wood, resulting from tests on relatively small samples, was as low as 0.24 – 0.48 (thus did not exceed 0.5). For this reason, it seems that the estimation of this method of testing static bending strength (MOR), highly correlated with the density of wood (R^2 = 0.86 – 0.97), should be based on tests performed on big-dimensional construction elements and taking crystallinity of cellulose into account.

REFERENCES

1. Ando, K., Hirashima, Y., Sugihara, M., Hirao, S., Sasaki, Y., 2006: Microscopic processes of shearing fracture of old wood, examined using the acoustic emission technique. Journal of Wood Science 52(6) : 483-489.
2. Becker, G., 1963a: Der Einweis - Gehalts von Holz auf das Hausbocklarven – Wachstum? Zeitschrift für angewandte Entomologie 51: 368-390.
3. Becker, G., 1963b: Holzbestandteile und Hausbocklarven-Entwicklung (Wood components and development of longhorn beetle larvae). Holz als Roh- und Werkstoff 8 (21): 287-93.
4. Cavalli, A., Cibecchini, D., Togni, M., Sousa, H.S., 2016: A review on the mechanical properties of aged wood and salvaged timber. Construction and Building Materials 114: 681-687.

5. Deppe, HJ., Rühl, H., 1993: Zur Beurteilung alter Bauhölzer, Holz als Roh- und Werksoff 41: 379 – 383.
6. Froidevaux, J., Volkmer, T., Gril, J., Fioravanti, M., Navi, P., 2011 : Comparison between accelerated thermos-hydro aged wood. In: 1st Workshop of COST Action FP0904 "Mechano-Chemical transformations of wood during Thermo-Hydro-Mechanical processing", Bienne, Switzerland, hal-00796686, 3 pp.
7. Guo, J., Zhou, H., Stevanic, J.S., Dong, M., Yu, M., Salmén, L., Yin, Y., 2018: Effects of ageing on the cell wall and its hygroscopicity of wood in ancient timber construction. Wood Science and Technology 52: 131-147.
8. Hirashima, Y., Sugihara, M., Sasaki, Y., Kosei, A., Yamasaki, M., 2005: Strength properties of aged wood III: static and impact bending strength properties of aged keyaki and akamatsu woods. Mokuzai Gakkaishi 51: 146–152.
9. ISO 13061-1, 2014: Physical and mechanical properties of wood . Test methods for small clear wood specimens. Part 1: Determination of moisture content for physical and mechanical tests.
10. ISO 13061-2, 2014: Physical and mechanical properties of wood. Test methods for small clear wood specimens. Part 2: Determination of density for physical and mechanical tests.
11. ISO 13061-3, 2014: Physical and mechanical properties of wood. Test methods for small clear wood specimens. Part 3: Determination of ultimate strength in static bending.
12. ISO 13061-4, 2014: Physical and mechanical properties of wood. Test methods for small clear wood specimens. Part 4: Determination of modulus of elasticity in static bending.
13. Jankowska, A., Kozakiewicz, P., 2014: Comparison of outdoor and artificial weathering using compressive properties. Wood Research 59(2): 245-252.
14. Kohara, J.,1952: Studies on the durability of wood I, mechanical properties of old timbers. Bulletin Kyoto Prefectural University 2: 116-131.
15. Kohara, J., 1954: Studies on the permanence of wood VI, the changes of mechanical properties of old timbers, Bulletin Kyoto Prefectural University 6: 164–174.
16. Kohara J., 1955: On performance of wood II, differences between the ageing processes of cypress wood and zelkova wood. Wood Industry 10: 395-399.
17. Kohara, J., Okamoto, H., 1956: Study on the old timber – changes in chemical component. Mokuzai Gakkaishi 2(5): 191 – 195.
18. Krajewski, A., Kozakiewicz, P., Witomski P., 2016: Shear strength of scots pine (*Pinus sylvestris* L.) from historical buildings. Wood Research 61(5): 845-850.
19. Kránitz K., Deublein M., Niemz P., 2010: Strength estimation of aged wood by means of ultrasonic devices. In: The future of Quality Control for Wood & Wood Products, 4-7th May 2010, Edinburgh, The Final Conference of COST Action E53, 9 pp.
20. Kránitz, K., Sonderegger, W., Bues, C.T., Niemz P., 2016: Effects of aging on wood: a literature review. Wood Science and Technology 50(1): 7–22.
21. Matejak, M., Popowska, E., Szejka, E., 1983: Vergleichende Untersuchungen über Methoden des beschleunigen Alterns von Holz. Holzforschung und Holzverwetung 35(5): 117 – 119.
22. Nilsson, R. Rowell, R., 2012: Historical wood – structure and properties. Journal of Cultural Heritage 13, Supplement: S5-|S9.
23. Rug, W., Linke, G., 2013: Untersuchungen zur Holzkorrosion an historishem Bretschichtholz. Bautechnik 90(10): 642 – 650.
24. Schulz, H., von Aufsess, H., Verron, T., 1984: Eigenschaften eines Fichtenbalkens aus alten Dachstuhl. Holz als Roh- und Werkstoff 42(3): 109.

25. Sonderegger, W., Kránitz, K., Bues, C.T., Niemz, P., 2015: Aging effects on physical and mechanical properties of spruce, fir and oak wood. Journal of Cultural Heritage16(6): 883-889.

26. Thaler, N., Miha, H., 2013: Performance of oak, beech and spruce beams after more than 100 years in service International Biodeterioration & Biodegradation 85: 305 – 310.

27. Witomski, P., Krajewski, A., Kozakiewicz, P., 2014: Selected mechanical properties of Scots pine wood from antique churches of Central Poland. European Journal of Wood Products 72: 293-296.

28. Yokoyma, M., Gril, J., Matsuo, M., Yano, H., Sugiyma, J., Clair, B., Kubodera, S., Mistutani, T., Sakamoto, M., Ozaki, H., 2009: Mechanical characteristic of aged Hinoki wood from Japanese historical buildings. Comptes Rendus Physique 10(7): 601-606.

29. Yorur, H., Kurt, S., Yumrutas, I., 2014: The effect of aging on various physical and mechanical properties of Scotch pine wood used in construction of historical Safranbolu houses. Drvna Industrija 65(3): 191-196.

Adam Krajewski, Paweł Kozakiewicz*, Piotr Witomski
Warsaw University of Live Science – Sggw
Institute of Wood Science and Furniture
Department of Wood Science and Wood Preservation
Nowoursynowska Street 159
02-787 Warsaw
Poland
*Corresponding author: pawel_kozakiewicz@sggw.edu.pl

CHARACTERIZATION OF NEW MUTANT *EUCOMMIA ULMOIDES* CONSTITUENTS IN THE DISCOLORATION DURING GROWING

Mengpei Liu
Zhengzhou University of Light Industry
China

Mengpei Liu, Qingxin Du, Panfeng Liu, Jun Qing, Hongyan Du, Lu Wang
Chinese Academy of Forestry
China

ABSTRACT

A new mutant *E. ulmoides* with red xylem is found, and this red color will gradually metabolize over time. Comparisons of chemical properties and metabolites of xylem between the mutant and wild type were analyzed in this study in order to discover the cause of the red mutation. The results showed that the acid-insoluble lignin content of mutant type was about 13.83% higher than that of wild type, but the crude protein of wild type was almost 2 times of mutant type. Meanwhile, 6 most important amino acids and amino acid derivatives were detected, which had significant correlation with crude protein. Additionally, the contents of organic acids, polyphenols and alkaloids in the mutant type were 243%, 316% and 281% of those in the wild type, respectively, while the contents of flavonoids and phenolamines contents were 78.8% and 27.3% of those in the wild type, respectively. These results will provide an important reference for understanding the wood color variation during growing.

KEYWORDS: *Eucommia ulmoides*, mutant xylem, chemical properties, metabolites.

INTRODUCTION

Eucommia ulmoides Oliv. is the only member of Eucommiaceae, existed in the Eocene and therefore is considered a 'living fossil plant' (Sun et al. 2013, Call and Dilcher 1997). It is a traditional and valuable medicinal plant and high-quality natural rubber in China, which accounts for about 99% of the world's total resources (Feng et al. 2016, Nakazawa et al. 2013, Nakazawa et al. 2009, Du 1996). Its bark, as a Chinese medicine, has been used for over 2000

years with the effect of decreasing blood pressure and cholesterol, antibacterial and enhancing the body's nonspecific immune function (Kwan et al. 2003, Tomoda et al. 1990). *E. ulmoides* is also called a 'hard rubber tree' because of the abundant quantities of trans-polyisoprene rubber in its bark, leaf and seed (Wang et al. 2018, Chen et al. 2012). Departments of non-timber forestry research and development center of Chinese academy of forestry, has the world's largest *E. ulmoides* resources with more than 1800, which planted in Xinxiang, Henan Province, China (N35°18´13.71´, E113°55´15.05"). A red-xylem discolored *E. ulmoides* mutant is found at this base. Meanwhile, the grafted varieties of this red-xylem of *E. ulmoides* have the same performance in different places. Studies on wood discoloration are mostly focused on wood drying or processing, but rare in the growth process (Sahin et al. 2011, De Moura et al. 2013, Preklet et al. 2019). Therefore, the color variation of *E. ulmoides* xylem during growing is a very rare phenomenon, which deserves further study.

The extent of the color change of wood depends on specific wood constituents (Rowe 2012). Changes in wood chemical composition are a major cause of wood discoloration, such as lignin and cellulose. Additionally, metabolomics has been defined as the analysis of all metabolites in an organism and simultaneous measurement of all metabolites in a given biological system (Chen et al. 2012, Rowe 1989, Dixon and Strack 2003), and LC-MS has been regarded as a promising metabolomics tool for metabolic profiling of metabolites (Paupiere et al. 2017, Loskutov et al. 2017, Zhang et al. 2016, Lin et al. 2014). Therefore, the different of the new mutant and wild type of *E. ulmoides* was conducted through comparison of chemical properties and metabolites of xylem in this study in order to discover the cause of the red mutation, and the results will provide a reference for wood color variation during growing.

MATERIALS AND METHODS

Materials

The xylem of new mutant and wild type of *E. ulmoides* was collected in August, 2016 from *Eucommia ulmoides* cultivation base, Xinxiang, Henan province, China. The morphological characters between the mutant and wild type of *E. ulmoides* were showed in Fig. 1.
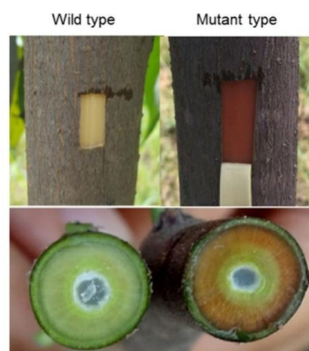

Fig. 1: The morphological characters of the mutant and wild type of Eucommia ulmoides.

Chemical and primary metabolites analysis

Acid-insoluble lignin, α-cellulose and brown cellulose were detected using equipment (NAI-CQW-6, Shanghai Na Ai Precision Instrument Co., Ltd.) in Zhejiang Academy of Forestry

Sciences, according to the China national standards (CNS) GB/T2677.8-1994, GB/T 744-2004 and GB/T2677.10-1995, resp. Near infrared reflectance spectroscopy method was chosen using Near infrared spectrometer (NIRQuest 256-2.1, 900-2050 nm, Boson Technology Co., Ltd.) according to CNS GB/T18868-2002 to detect crude proteins.

The freeze-dried xylem was crushed using a mixer mill (MM 400, Retsch) with a zirconia bead for 1.5 min at 30 Hz. 100 mg powder was weighted and extracted overnight at 4°C with 1.0 mL 70 % aqueous methanol. Following centrifugation at 10,000 g for 10 min, the extracts were absorbed (CNWBOND Carbon-GCB SPE Cartridge, 250 mg, 3 mL; ANPEL, Shanghai, China) and filtrated (SCAA-104, 0.22 µm pore size; ANPEL, Shanghai, China) before LC-MS analysis.

The sample extracts were analyzed using an LC-ESI-MS/MS system (HPLC, Shim-pack UFLC SHIMADZU CBM30A system; MS, Applied Biosystems 4500 Q TRAP). The analytical conditions were as follows, HPLC: column, Waters ACQUITY UPLC HSS T3 C18 (1.8 µm, 2.1 mm*100 mm); solvent system, water (0.04% acetic acid), acetonitrile (0.04% acetic acid); gradient program, 100:0 V/V at 0 min, 5:95 V/V at 11.0 min, 5:95 V/V at 12.0 min, 95:5 V/V at 12.1 min, 95:5 V/V at 15.0 min; flow rate, 0.40 mL·min^{-1}; temperature, 40 °C; injection volume: 5 µL. The effluent was alternatively connected to an ESI-triple quadrupole-linear ion trap (Q TRAP)-MS.

Statistical analyses

All analyses of chemical properties were done using three replicates. Univariate analyses of variance (ANOVA) and least significant differences (LSD) were performed using JMP Pro 12 (SAS Institute, Cary, NC, USA). Biomarker selection was done by partial least squares discriminant analysis (PLS-DA) in MetaboAnalyst 3.5 and heat map was done by MetaboAnalyst 3.5.

RESULTS

Chemical properties

The wood composition of the mutant *E. ulmoides* with wild type as control was showed in Tab. 1. Acid-insoluble lignin, α-cellulose and brown cellulose were detected in this study.

Tab. 1: Acid-insoluble lignin, α-cellulose and brown cellulose of the mutant and wild type of Eucommia ulmoides (%).

	Acid-insoluble lignin	α-cellulose	Brown cellulose
Mutant 1	28.82±0.93[a1]	81.43±0.65[bc]	77.96±0.78[c]
Mutant 2	29.56±0.25[a]	82.56±0.27[ab]	77.84±0.45[c]
Mutant 3	27.52±0.03[b]	81.01±0.71[c]	78.47±0.53[bc]
Average	28.63	81.67	78.09
Wild 1	24.63±0.07[d]	80.67±0.22[c]	79.91±0.33[a]
Wild 2	26.06±0.56[c]	83.32±0.58[a]	79.42±0.57[ab]
Wild 3	24.75±0.05[d]	81.87±0.57[abc]	78.74±0.15[abc]
Average	25.15	81.95	79.36

[1]Data are expressed as mean ± SD (n = 3). Means were separated by LSD p ≤ 0.05.

The results indicated that there were no significant difference in α-cellulose and brown cellulose between the mutant and wild type of *E. ulmoides*. However, significant variation

existed in acid-insoluble lignin of mutant and wild type, with the average 28.63% and 25.15%, respectively. The acid-insoluble lignin content of mutant was 13.83% higher than that of wild type. Discoloration in the cell wall was influenced by photochemical reactions leading to the degradation of wood constituents, mainly lignin (Ozgenc et al. 2012, Li et al. 2017). Lignin contains many chromophores and has an aromatic structure that absorbs sunlight, especially in the UV region. Approximately 80-95% of UV light incident on wood surface is absorbed by lignin, and it is therefore easily decomposed by photo-oxidative processes. UV light interacts with lignin to initiate discoloration and deterioration (Li et al. 2015, Hayoz et al. 2003). However, fiber-rich cellulose with a higher resistance against ultraviolet light degradation remains in the cell wall without significant change (Rowell and Barbour 1989, Feist and Hon 1984).

Crude protein, amino acid and amino acid derivative

The crude protein in mutant type was 1.46-1.90%, which was significantly lower than that in wild type with 3.32-3.44%. It meant the crude protein of wild type was almost 2 times of that in mutant type. Because the red color of xylem of the mutant type would gradually metabolize over time, then amino acid metabolites between the mutant and wild type was analyzed. 50 amino acids and amino acid derivatives were detected in this study as well as the correlation with crude protein. It showed that 15 most important discriminatory biomarkers were detected between the mutant and wild type of *E. ulmoides* (Crude protein, Xanthurenic acid O-hexoside, L-Phenylalanine, L-Asparagine, L-Alanine, Phenylalanine, Oxitriptan, L-Proline, D-3-Methylhistidine, D-Ala-d-ala, N-Acetyl-L-leucine, N-Hydroxy-L-tryptophan, L-Serine, Serotonin and L-Isoleucine) (VIP value>1.1) (Fig. 2a).
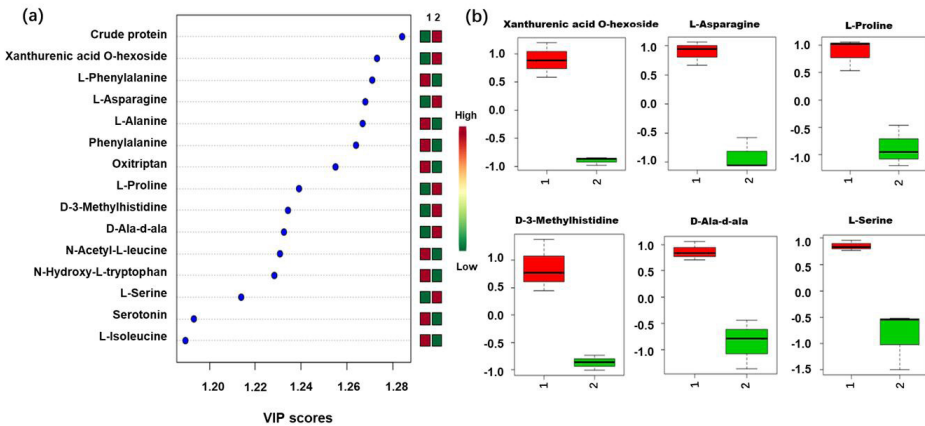

Fig. 2: Amino acid and amino acid derivative analysis between the mutant and wild type of Eucommia ulmoides in VIP scores: (a) the top 15 selected biomarkers based on variable importance in projections (VIP value>1.1), (b) 6 selected biomarkers positively correlated with crude protein. The number 1 and 2 indicates the mutant type and wild type, resp.

There was a significant positive correlation between crude protein and D-Ala-d-ala, L-Serine, with correlation coefficient 0.89 and 0.87, respectively (p<0.05). Meanwhile, extremely significant positive correlation also existed between crude protein and Xanthurenic acid O-hexoside, L-Proline, D-3-Methylhistidine, L-Asparagine, with correlation coefficient

0.98, 0.98, 0.96 and 0.95, respectively (p<0.01) (Fig. 2b). These 6 components may have some correlation with the decrease of crude protein in mutant type of *E. ulmoides*.

Flavonoid, polyphenol, organic acid and other metabolites

Except amino acid and amino acid derivative, other metabolites were also detected between mutant and wild type of *E. ulmoides*, including flavonoid, polyphenol, organic acid, alkaloid, phenolamine and terpenoid (Fig. 3).
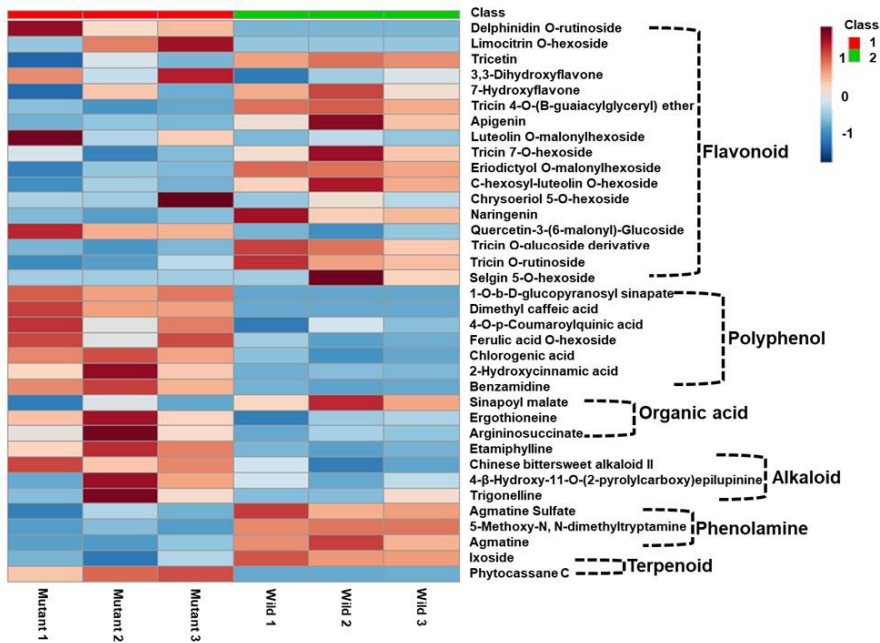

Fig. 3: Flavonoid, polyphenol, organic acid and other metabolites analysis between the mutant and wild type of Eucommia ulmoides in heat map. The number 1 and 2 indicate the mutant type and wild type, respectively.

It showed that 2 flavonoids were higher in mutant type, Delphinidin O-rutinoside and Quercetin-3-(6-malonyl)-Glucoside, respectively, but 10 flavonoids were higher in wild type. The contents of the mutant type flavonoids was 78.8% of that of the wild. Except Sinapoyl malate, the contents of organic acids, polyphenols and alkaloids in the mutant type were 243%, 316% and 281% of those in the wild type, respectively, while phenolamines contents were 27.3% of those in the wild type. With regard to terpenoids, Phytocassane C was higher in mutant type, whereas Ixoside was higher in wild type. Therefore, there were also significant differences in flavonoids, polyphenols, organic acids and other metabolites between the mutant and wild type of *E. ulmoides*.

DISCUSSION

There are many researches on the color change of wood in the process of post-harvest or drying. Wood discoloration is a complex phenomenon, mainly affected by heat, light, physiological and biochemical reactions, as well as from attack by microorganisms (Sandoval et al. 2010, Chang et al. 1999, Salca et al. 2015). However, there is no related research on the color change in the process of wood growth. The mutant *E. ulmoides* with red-xylem during growing is found, but this red color will gradually metabolize over time, which is a rare situation in wood discoloration. The chemical properties of xylem between the mutant and wild type of *E. ulmoides* showed that the acid-insoluble lignin content of mutant type was just about 13.83% higher than that of wild type. However, the crude protein of wild type was almost 2 times of that in mutant type, which had significant positive correlation with D-Ala-d-ala, L-Serine, Xanthurenic acid O-hexoside, L-Proline, D-3-Methylhistidine and L-Asparagine. Moreover, most of the polyphenols, organic acids and alkaloids were higher in mutant type, but flavonoids and phenolamines were higher in wild type.

E. ulmoides is rich in primary and secondary metabolites, such as amino acids, flavonoids and organic acids, which do not only play an important role in the growth and development, but also have the basis of medicinal value of *E. ulmoides*. The color change of the mutant with red-xylem maybe closely related to the variation of its metabolic components. These results provided an important reference for understanding the color variation in *E. ulmoides* during the growing. Further studies on amino acids, flavonoids and polyphenols related pathways can be carried out at the later stage, as well as further validation and analysis in combination with other genomes such as transcriptome.

CONCLUSIONS

(1) There was significant variation in acid-insoluble lignin between the mutant and wild type. The content of acid-insoluble lignin in mutant was 13.83% higher than that in wild type. (2) The crude protein in wild type was almost 2 times of that in mutant type, which had significant positive correlation with D-Ala-d-ala, L-Serine, Xanthurenic acid O-hexoside, L-Proline, D-3-Methylhistidine and L-Asparagine. (3) The contents of organic acids, polyphenols and alkaloids in the mutant type were 243%, 316% and 281% of those in the wild type, respectively, while the contents of flavonoids and phenolamines contents were 78.8% and 27.3% of those in the wild type, respectively.

ACKNOWLEDGEMENTS

REFERENCES

1. Call, V.B., Dilcher, D.L., 1997: The fossil record of *Eucommia* (Eucommiaceae) in North America. American Journal of Botany 84(6): 798-814.

2. Chang, S.T., Wang, S.Y., Su, Y.C., Huang, S.L., Kuo, Y.H., 1999: Chemical constituents and mechanisms of discoloration of Taiwania (*Taiwania cryptomerioides* Hayata) heartwood. Holzforschung 53(2): 142-146.

3. Chen, R., Harada, Y., Bamba, T., Nakazawa, Y., Gyokusen, K., 2012: Over expression of an isopentenyl diphosphate isomerase gene to enhance trans-polyisoprene production in *Eucommia ulmoides* Oliver. BMC biotechnology 12(78): 1-12.

4. De Moura, L.F., Brito, J.O., Nolasco, A.M., Uliana L.R., De Muniz, G.I.B., 2013: Evaluation of coating performance and color stability on thermally rectified *Eucalyptus grandis* and *Pinus caribaea* var. hondurensis woods. Wood Research 58(2): 231-242.

5. Dixon, R.A., Strack, D., 2003: Phytochemistry meets genome analysis, and beyond. Phytochemistry 62(6): 815-816.

6. Du, H.Y., 1996: High quality and high yield cultivation of *Eucommia ulmoides*. China Forestry Publishing. Beijing, China, 55 pp.

7. Feist, W.C., Hon, D.N.S., 1984: Chemistry of weathering and protection. In: The chemistry of solid wood. Advances in Chemistry Series 207 (ed. Rowell Roger M). chapter 11, American Chemical Society, Washington DC. Pp 401-451.

8. Feng, Y.Z., Wang, L., Fu, J.M., Wuyun, T.N., Du, H.Y, Tan, X.F., Zou, F., Li, F.D., 2016: Transcriptome sequencing discovers genes related to fatty acid biosynthesis in the seeds of *Eucommia ulmoides*. Genes & Genomics 38(3): 275-283.

9. GB/T2677.8, 1994: Fibrous raw material. Determination of acid-insoluble lignin.

10. GB/T 744, 2004: Pulps. Determination of alkali resistance.

11. GB/T2677.10, 1995: Fibrous raw material. Determination of holocellulose.

12. GB/T18868, 2002: Method for determination of moisture, crude protein, crude fat, crude fibre, lysine and methinione in feeds. Near infrared reflectance spectroscopy.

13. Hayoz, P., Peter, W., Rogez, D., 2003: A new innovative stabilization method for the protection of natural wood. Progress in Organic Coatings 48(2-4): 297-309.

14. Kwan, C.Y., Chen, C.X., Deyama, T., Nishibe, S., 2003: Endothelium-dependent vasorelaxant effects of the aqueous extracts of the *Eucommia ulmoides* Oliv. leaf and bark: implications on their antihypertensive action. Vascular Pharmacology 40(3): 229-235.

15. Li, N., Chen, Y., Bao, Y., Zhang, Z., Wu, Z., Chen, Z., 2015: Evaluation of UV-permeability and photo-oxidisability of organic ultraviolet radiation-absorbing coatings. Applied Surface Science 332(30): 186-191.

16. Li, N., Chen, Y., Yu, H., Xiong, F., Yu, W., Bao, M., Wu, Z., Huang, C., Rao, F., Li, J., Bao, Y., 2017: Evaluation of optical properties and chemical structure changes in enzymatic hydrolysis lignin during heat treatment. RSC Advances 7: 20760-20765.

17. Lin, H., Rao, J., Shi, J., Hu, C., Cheng, F., Wilson, Z.A., Zhang, D., Quan, S., 2014: Seed metabolomic study reveals significant metabolite variations and correlations among different soybean cultivars. Journal of Integrative Plant Biology 56(9): 826-836.

18. Loskutov, I.G., Shelenga, T.V., Konarev, A.V., Shavarda, A.L., Blinova, E.V., Dzubenko, N.I., 2017: The metabolomic approach to the comparative analysis of wild and cultivated species of oats (*Avena* L.). Russian Journal of Genetics: Applied Research 7(5): 501-508.

19. Nakazawa, Y., Bamba, T., Takeda, T., Uefuji, H., Harada, Y., Li, X., Chen, R., Inoue, S., Tutumi, M., Shimizu, T., 2009: Production of Eucommia-rubber from *Eucommia ulmoides* Oliv. (hardy rubber tree). Plant Biotechnology 26(1): 71-79.

20. Nakazawa, Y., Takeda, T., Suzuki, N., Hayashi, T., Harada, Y., Bamba, T., Kobayashi, A., 2013: Histochemical study of trans-polyisoprene accumulation by spectral confocal laser scanning microscopy and a specific dye showing fluorescence solvatochromism in the rubber-producing plant, *Eucommia ulmoides* Oliver. Planta 238(3): 549-560.

21. Ozgenc, O., Hiziroglu, S., Yildiz, U.C., 2012: Weathering properties of wood species treated with different coating applications. BioResources 7(4): 4875-4888.

22. Paupiere, M.J., Muller, F., Li, H., Rieu, I., Tikunov, Y.M., Visser, R.G.F., Bovy, A.G., 2017: Untargeted metabolomic analysis of tomato pollen development and heat stress response. Plant Reproduction 30(2): 81-94.

23. Preklet, E., Tolvaj, L., Banadics, E.A., Alpar, T., Varga, D., 2019: Coulour modification and homogenisation of larch wood by steaming. Wood Research 64(5): 811-820.

24. Rowe, J.W., 1989: Natural products of woody plants. Chemicals extraneous to the lignocellulosic cell wall. Springer-Verlag, Berlin, Heidelberg, 188 pp.

25. Rowell, R.M., Barbour, R.J., 1989: Archaeological wood: properties, chemistry and preservation. American Chemical Society. Washington DC, 435 pp.

26. Sahin, H.T., Mantanis, G.I., 2011: Colour changes in wood surfaces modified by a nanoparticulate based treatment. Wood Research 56(4): 525-532.

27. Salca, E.A., Gobakken, L.R., Gjerdrum, P., 2015: Progress of discoloration in green, freshly cut veneer sheets of Black alder (*Alnus glutinosa* L.) wood. Wood Material Science & Engineering10(2): 178-184.

28. Sandoval-Torres, S., Jomaa, W., Marc, F., Puiggali, J.R., 2010: Causes of color changes in wood during drying. Forestry Studies in China 12(4): 167-175.

29. Sun, Z., Li, F., Du, H., Zhu, J., Wang, Y., 2013: A novel silvicultural model for increasing biopolymer production from *Eucommia ulmoides* Oliver trees. Industrial Crops and Products 42: 216-222.

30. Tomoda, M., Gonda, R., Shimizu, N., Kanari, M.A, 1990: Reticuloendothelial system-activating glycan from the barks of *Eucommia ulmoides*. Phytochemistry 29(10): 3091-3094.

31. Wang, L., Du, H., Li, T., Wuyun, T.N., 2018: De novo transcriptome sequencing and identification of genes related to salt stress in *Eucommia ulmoides* Oliver. Trees 32(1): 151-163.

32. Zhang, J., Luo, W., Zhao, Y., Xu, Y., Song, S., Chong, K., 2016: Comparative metabolomic analysis reveals a reactive oxygen species-dominated dynamic model underlying chilling environment adaptation and tolerance in rice. New Phytologist 211(4): 1295-1310.

Mengpei Liu
Zhengzhou University of Light Industry
School of Food and Bioengineering
Zhengzhou, 450002
China

Qingxin Du, Panfeng Liu, Jun Qing, Hongyan Du, Lu Wang*
Chinese Academy of Forestry
Non-Timber Forest Research and Development Center
Zhengzhou, 450003
China
*Corresponding author: wanglu181716@163.com

INFLUENCE OF GASEOUS PLASMA TREATMENT ON FUNCTIONAL PROPERTIES OF COATED PAPERS

Matej Holc[1], Igor Karlovits[2], David Ravnjak[3]
Aleš Palatinus[3], Ita Junkar[1]

[1]Jožef Stefan Institute
Slovenia
[2]Pulp And Paper Institute
Slovenia
[3]Vevče Paper Production Mill
Slovenia

ABSTRACT

Three different types of paper with different coatings have been used in order to study the influence of gaseous plasma treatment on surface properties of paper. Radio frequency (RF) oxygen plasma was used for treatment of papers that contain different parts of organic and inorganic components in their coatings. Surface properties like surface morphology, roughness, surface energy, wettability, and chemistry were studied. The influence of plasma modification was also studied in terms of printability and paper gloss, which are one of the key parameters that dictate the use of such paper in desired applications. The results indicate that plasma modification of different types of coatings indeed influences paper printability as well as gloss function, which was shown to be highly connected with surface morphology, as micro- and nanopores were opened or formed due to selective plasma etching of organic part of the coating. Moreover, significant increase in surface energy was observed on all plasma treated papers, however this seemed not to influence much on the printing and gloss properties.

KEYWORDS: Gaseous plasma, paper, coating, surface energy, morphology, surface chemistry, gloss, printability.

INTRODUCTION

Paper is a versatile material, used in a wide variety of applications. Its major bulk component is cellulose, a polysaccharide. For use in specific applications, cellulose-based papers need to be modified to achieve desired qualities, such as weight, color, gloss, printability, or barrier

properties. To this end, coatings may be applied. In the paper industry, there is a clear trend of applying synthetic or bio-based waterborne polymer coatings (Skácelová et al. 2016). These coatings may contain organic polymers, such as styrene-butadiene latex, polyester resins, starch, or various other binders or fillers. Additionally, it is possible to include particles of inorganic materials, such as the minerals kaolin and calcium carbonate ($CaCO_3$), as pigments or fillers, thus forming a polymer-particle matrix.

The inclusion of polymer coatings brings new challenges for printing and product processing, as it affects both surface morphology and chemistry. It improves the barrier properties of paper, but disrupts access to the internal void volumes. The porous structure of a particle-containing coating influences paper qualities such as ink setting and optical properties (Pykönen 2010). The cellulose, as well as any mineral and latex particles on the surface of coatings, are also typically covered by the polymers they are dispersed in, which affects the surface chemistry (Pykönen et al. 2009)

Plasma, as a surface modification method, is one of intriguing ways to alter the surface properties of paper. It is well known that exposure of materials to highly reactive plasma alters their surface properties without influencing the bulk attributes of the material (Vesel et al. 2018). In the case of organic materials, exposure to oxygen plasma will functionalize the materials (Vesel and Mozetič 2017) and increase their surface energy, making the material more hydrophilic, and thus more suitable for application of dyes, inks, etc. (Vesel and Mozetič 2018), (Camargo et al. 2017) or to make it antimicrobial (Vohrer et al. 2001). It can also enable protein immobilization (Zhao et al. 2016) This effect increases with a higher dose of reactive plasma species due to increased exposure time (Friedman 2008) or discharge power (Pawłat et al. 2016). Typically, the effect gradually decreases with time after treatment, which is known as ageing.

Morphology of materials can also be modified by plasma treatment through the process of etching, where matter is removed from the surface of the treated material. Surface morphology can be altered either due to physical sputtering or chemical etching (Vesel and Mozetič 2017) of the surface. Selective etching is also possible, wherein plasma etches away susceptible organic material, such as polymers, while resistant inorganic material remains intact (Cveblar et al. 2005).

So far, paper surfaces were plasma treated mostly to increase wettability through oxidation. Usually, uncoated paper was treated, both at low and atmospheric pressure. Vesel et al. (2007) used an inductively coupled, radio frequency (RF) oxygen plasma at low pressure to treat ink-jet paper, which is cellulose-based and contains alkyl ketene dimer (AKD) and $CaCO_3$. The wettability increased, and X-ray photoelectron spectroscopy (XPS) analysis showed oxidation and increased presence of calcium. Scanning electron microscopy (SEM) images at low magnification showed no visible change in surface morphology (Vesel et al. 2007). Pawłat et al. (2016) used an RF jet at atmospheric pressure to treat cellulose-based paper containing $CaCO_3$ filler, and similarly noted increased wettability and oxidation, without drastic changes in surface morphology and Fourier-transform infrared (FTIR) spectra. Tian et al. (2012) used a commercially available plasma asher at low pressure to successfully increase the wettability of paper-based bioactive sensors, while Skácelová et al. (2016) used a diffuse coplanar surface barrier discharge (DCSBD) to increase wettability and oxidation of paper; ageing was also reported. Cornelius et al. (2017) treated paper handsheets with a dielectric barrier discharge (DBD) at atmospheric pressure. When using helium with a fraction of oxygen, they recorded oxidation, but observed no changes to surface roughness. Wettability increase, as measured by wicking, was observed only when helium with a fraction of C3F6 was used for generation of plasma. On the other hand, increase in surface roughness was reported following DBD treatment in a helium-oxygen mixture at atmospheric pressure. It was attributed to selective etching of organic material (cellulose fibers) over inorganic fillers ($CaCO_3$) (Dimitrakellis et al. 2017).

Plasma treatment of pigment-coated paper was done by Pykönen et al. (2008), who have used different plasma treatments at atmospheric pressure: one corona treatment in air, one pilot scale experimental plasma in argon, and one laboratory scale plasma based on DBD in nitrogen. They found that all treatments increased surface energy, and thus wettability, through oxidation and increase in roughness, as determined by XPS and gloss measurement, respectively. An ageing effect was observed for the surface energy, but not for the oxidation level (Pykönen et al. 2009). Oxidation appeared to primarily affect the polymer dispersants. Further, plasma increased the surface atomic percentage of elements found in the coating pigments, indicating etching of the polymer matrix. The different pigment components of individual coatings also responded differently to the treatments (Pykönen et al. 2009). Tuominen et al. (2014), as well as Bollström et al. (2012) also treated pigment-coated paper with a corona treatment in air and with an atmospheric pressure plasma in argon; both increased wettability. The first study found surface oxidation, and a slight decrease in micro- or nanoscale surface roughness for different paper types; ageing was reported. The second study found increased surface energy with no changes in topography. In a paper by Vaswani, Koskinen and Hess (2005) plasma was used to achieve hydrophobic surfaces with the use of polymerized fluorocarbon films.

Pykönen et al. (2010) also studied offset printability after plasma treatment. While the corona and pilot scale treatments did not have a clear influence on print density, the laboratory scale treatment reduced it. The reason was a reduced surface strength due to micro-picking. Their work further indicates that plasma activation influences ink setting, in a manner which was correlated with the type of ink oil and its interactions with the plasma-treated surface. In the particular case of the pilot scale experimental plasma, the ink setting rate could be adjusted without influencing the final print quality. Karlovits and Lavrič (2018) printed with water based flexo inks on wax coated paper samples after plasma treatment, where the printability was improved. By fine-tuning the plasma treatment parameters, it should be possible to achieve the desired changes to the coating, which could improve its surface properties for specific application. Thus, the main motivation of our work was to systematically study the influence of oxygen plasma treatment of three different types of coatings in terms of altered surface properties, as well as printability and paper gloss.

MATERIAL AND METHODS

Pre-coated papers from different manufacturers and with different type of coatings were used for surface modification. For the purpose of this text, they were assigned the names paper 1, paper 2, and paper 3. Paper 1 is an offset paper made from recycled waste paper and bleached mechanical pulp. This paper consists of about 18% – 24% of inorganic parts, and is coated with 0.5-1 $g \cdot m^{-2}$ of starch. Paper 2, the second offset paper, has deinked pulp, mechanical pulp, and consists of about 28% - 32% of inorganic parts. It is coated by a combination of $CaCO_3$ and pigment coating, and has the highest amount of inorganic components in the coating. Paper 3 is made from a combination of softwood (eucalyptus) and hardwood with production rests. This paper also has higher amount of surface coating (30% of the paper weight), which contains $CaCO_3$, kaolin fillers, as well as a latex binder. In order to study the influence of plasma treatment on these three types of paper, the papers were cut in pieces of 10×10 cm^2 and modified by plasma for 10 s or 60 s.

Weakly ionized oxygen plasma was created in a discharge chamber by an inductively coupled RF discharge. The RF generator operates at a frequency of 27.12 MHz and at about 500 W.

The generated plasma enables rather uniform treatment of the sample inside the reactor chamber. The pressure was set to 30 Pa and the treatment times were 10 s and 60 s. The samples were treated on a glass table in the plasma reactor, as schematically presented in Fig. 1.
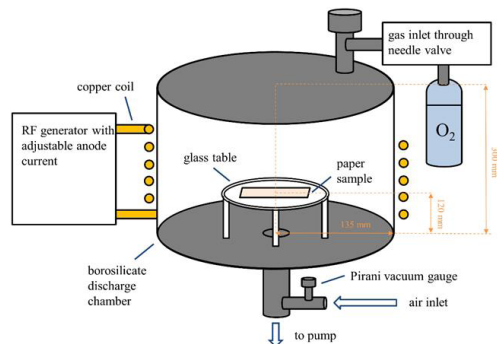

Fig. 1: Schematic representation of the plasma reactor used for treatment of paper.

Morphological properties of the samples were analyzed using SEM. Approximately 5 × 5 mm pieces of treated and untreated paper were cut from the material. They were attached onto aluminum stubs using conductive carbon tape, their edges connected to the stub surface using carbon paste, and coated with a layer of gold approximately 10 nm thick using a Balzers SCD 050 sputter coater (Bal-Tec, Balzers, Liechtenstein). The SEM images were obtained using a Jeol JSM-7600F Schottky Field Emission SEM (Jeol Ltd., Tokyo, Japan).

Topographic changes of papers before and after plasma treatment were monitored with an atomic force microscope (AFM) (Solver PRO, NT-MDT, Moscow, Russia) in the tapping mode in air. The samples were scanned with a standard Si cantilever with a force constant of 22 N.m-1 and at a resonance frequency of 325 kHz.

The surface roughness was measured with a TR200 stylus profilometer using a diamond tip with 2 μm radius. The following measurement parameters were used: sampling length 0.80 mm and traversal speed 0.135 mm·s-1. The measured average surface roughness parameter, Ra, is compliant to the geometric product specification standards (ISO 4287: 1997 and ISO 12218: 1997, 2004). The samples were measured in 3 different areas by measuring the vertical and horizontal scanning lines.

The surface energy was measured with an automated contact angle tester according to the Tappi T 5580 m 97 standards and by using two test liquids. The surface energy was calculated by the harmonic mean method. The influence of ageing was studied on paper 3 in order to observe stability of surface modification. Wettability and surface energy was measured after storage of paper 3 at the room temperature and at constant humidity for one and three weeks.

The surface of the sample was analyzed with the XPS instrument PHI TFA XPS (Physical Electronics, Ismaning, Germany). The base pressure in the XPS analysis chamber was about 6×10-8 Pa. The samples were excited with X-rays over a 400-μm spot area with monochromatic Al source at radiation energy of 1486.6 eV. The photoelectrons were detected with a hemispherical analyzer positioned at an angle of 45˚ with respect to the normal of the sample surface. The energy resolution was about 0.5 eV. Survey-scan spectra were obtained at pass energy of 187.85 eV. Since the samples are insulators, we used an additional electron gun to allow for surface neutralization during the measurements. All spectra were referenced to the main C 1s peak of the carbon atoms,

which was assigned a value of 284.8 eV. The XPS spectra were measured for an untreated sample and samples treated by oxygen plasma after 10 and 60 s of treatment.

The paper gloss levels were measured using a Lehmann gloss meter, which uses the Tappi, ANSI T 480 om-15 standard, where the specular gloss of paper is measured at 75° (15° from the plane of paper) with converging beam geometry.

To test the printability, we have determined the ink levelling and ink absorbency of the untreated and plasma treated samples. The test uses the special porosimetric K&N testing ink, which contains parts of pigments and parts of dyes, therefore the ink is absorbed to different depths in the paper structure. The ink levelling, which is influenced by the surface roughness and porosity, was measured through the print gloss measurement. The method is the same as for paper gloss, except that the samples were printed with suitable inks. The printing was done on a Pruefbau printability tester using the standard inking and printing speed of 1 m.s-1 and a printing pressure of 120 kPa.

To obtain even inking, we have applied the ink using a L&W GFL ink automated wipe off tester and evaluated the luminance factors using an X-Rite directional geometry spectrophotometer. To measure changes in ink absorbency, which influences optical parameters such as ink density, lightness and brightness values as well gloss values, the K&N ink absorption test was carried out according to SCAN-P 70:09. The test samples were printed with a suitable ink and were allowed to absorb the ink for 120 s. The wiped off samples were measured with an i1Pro 2 spectrophotometer with measuring mode M1 (D50 standard illuminant, 2^0 standard observer and 0:45c directional geometry). The appropriate absorbency values were calculated according to Eq. 1 and are reported as a percentage:

$$A = \frac{100 \cdot (R_\infty - R_y)}{R_\infty} \qquad (\%) \tag{1}$$

where: R_y - luminance factor of stained area (%) and R_∞ (%) is the intrinsic luminance factor of paper.

RESULTS AND DISCUSSION

Changes in the surface morphology of the three different paper types were assessed from SEM and AFM images. In Fig. 2, it can be clearly seen that plasma treatment influences the surface morphology of paper, especially after the longer treatment time (60 s). Nice examples of kaolin structures were revealed after plasma treatment, and can be observed on paper 2 and paper 3, especially after 60 s of treatment. In the case of paper 3, plasma obviously opens the micropore structure. Similar open structures were also observed in the case of paper 1, which appears to show a completely different morphology in comparison to paper 2 and paper 3, but nonetheless, pores with a diameter of about 1 µm can be seen on the surface. Additionally, nanostructures appear on the surface of paper 1 and also paper 2. Therefore, paper 1 exhibits a unique combination of nanotopography and micropore structure. In the case of paper 2, no significant changes in surface morphology on the micro scale were observed by SEM analysis, but nanotopography is present, while in the case of paper 3, no nanostructuring of the surface is observed, only opened micro porous structures.
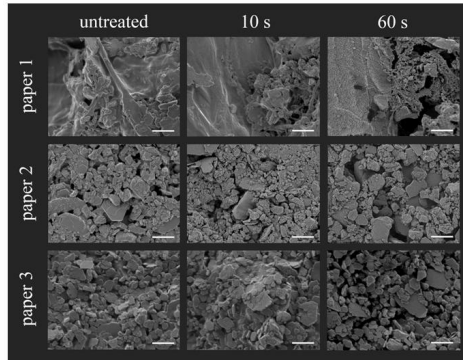
Fig. 2: SEM images of untreated and plasma treated paper surfaces. Taken at 20,000 × magnification. Size of the scale bar is 1 μm.

The morphology of paper 2 was further studied by AFM analysis, as seen in Fig. 3. In this case, surface nanostructuring can be observed already after 10 s of plasma treatment. It is hard to provide reliable information about the surface roughness of untreated and plasma treated samples from AFM measurements, as the surface is not homogeneous, and thus, the measured surface roughness is highly influenced by the area of analysis. For example, if the area of analysis is done on surfaces with more kaolin particles, the change in surface roughness is not as obvious, as kaolin crystals are not etched by plasma. On the other hand, in case of organic parts of the coating, the increase in roughness can be detected, as the surface becomes more nanostructured compared to the untreated surface.
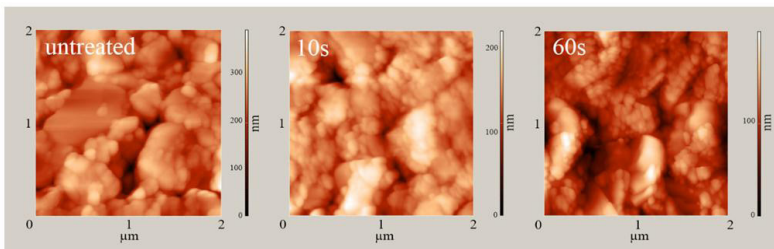

Fig. 3: AFM images of the untreated, 10 s and 60 s plasma treated surfaces of paper 2.

Results of the average surface roughness measurements of unprinted papers before and after plasma treatment are presented in Fig. 4 (a), while the results for the printed papers before and after plasma treatment are presented in Fig. 4 (b).
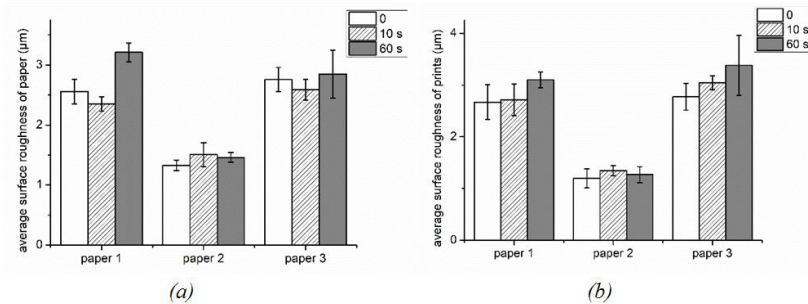
Fig. 4: Average surface roughness (Ra) determined by profilometer analysis. (a) Ra of untreated and plasma treated paper surfaces; (b) Ra of untreated and plasma treated, subsequently printed paper surfaces.

A small decrease in surface roughness of paper 1 was observed after 10 s of plasma treatment, while after 60 s of treatment, a small increase in Ra was observed, as seen in Fig. 4a. A similar trend was observed in the case of paper 3, as seen in Fig. 4a. Paper 2 had the lowest roughness value among all papers, and a different interaction of plasma with this paper was observed. After 10 s of treatment, there was a slight increase in Ra, and no significant changes were observed after 60 s of treatment. When evaluating surface roughness of the printed papers, as seen in Fig. 4b, it can be seen that roughness of paper 2 again is the least influenced by plasma treatment. For the case of paper 1 and 3, an increase in surface roughness from the initial value can be observed after the longer treatment time. The printed paper 1 exhibits an increase in Ra value from 2.67 μm (initial printed sample without plasma treatment) to about 2.72 μm and 3.10 μm for 10 and 60 s treatment, resp. A similar trend was observed in case of paper 3.

Surface wettability and surface energy results are collected in Tab. 1. Differences already exist in the initial wettability of papers. The highest water contact angle (WCA) was measured on paper 1, with a WCA of about 113°, followed by paper 3 with WCA of about 105°, while paper 2 had the lowest WCA of about 63°. Changes in wettability show that all plasma treated surfaces become hydrophilic already after 10 s of treatment. The longer treatment time slightly improves wettability in case of paper 1 and 3, while in case of paper 2, conversely, a slight increase in wettability was observed. The increase in surface energy was also observed on all plasma treated papers. The initial surface energies of paper 1 and 2 were comparable, about 45.7 mN·m^{-1} and 45.3 mN·m^{-1}, respectively, while the surface energy of paper 3 was lower, at 24.9 mN·m^{-1}. A comparable surface energy after 60 s of plasma treatment was measured on the paper 1 and 3, followed by a slightly lower value for paper 2. Interestingly, as paper 3 exhibited the lowest initial surface energy, in this case, the highest increase in surface energy was obtained. It seems that paper 3 was the most influenced by plasma treatment in terms of both surface wettability and energy, as in this case, the highest increases were observed. The offset paper 2 seems to be the least influenced by plasma treatment in terms of surface wettability and energy. The influence of so-called ageing of plasma treated surfaces was also studied on paper 3. It was observed that wettability has slightly decreased with time, as the WCA increased from about 18° for freshly treated paper to about 31° after one week of storage, and after three weeks reached a constant value of about 36°. A similar effect was observed in the case of surface energy, which increased from the initial 69.6 mN·m^{-1} to 64.3 mN·m^{-1} after one week of storage, and finally reached a constant value at about 62.1 mN·m^{-1}. It should also be noted that all plasma treated surfaces were highly

hydrophilic and that both wettability and surface energy were close to the detection limit of our measuring method.

Tab. 1. Recorded WCA values and surface energy for the untreated and plasma treated paper samples.

	paper 1			paper 2			paper 3		
Treatment (s)	0	10	60	0	10	60	0	10	60
WCA (°)	113.0	20.1	14.4	63.3	26.6	32.0	104.9	26.1	18.5
surface energy (mN·m⁻¹)	45.7	68.9	70.9	45.3	66.5	63.7	24.9	66.6	69.6

Chemical analysis of the surface was also studied in order to provide more insights into the surface modification of coated papers by plasma. In all cases, an increase in oxygen content and a decrease in carbon content were observed, as seen in Fig. 5. No significant changes were apparent between the 10 s and 60 s treatment times, thus only results for untreated and 60 s treated surfaces are presented in Fig. 5. The initial O/C ratio is the highest for paper 2, about 0.75, while more comparable, lower O/C ratios are observed in case of paper 1 and 3, about 0.47 and 0.46, resp. After plasma treatment, the highest increase in the O/C ratio was observed in the case of paper 3, from 0.46 to about 1.68, followed by paper 2, where the initial O/C ratio was about 0.75 and increased to 1.89. The smallest increase in the O/C ratio was observed in case of paper 1, from about 0.47 to about 0.83. Moreover, an increase in elements from the inorganic parts of the coating can be observed for all plasma treated samples, as increase in the presence of Ca, Al or Si atoms is apparent.
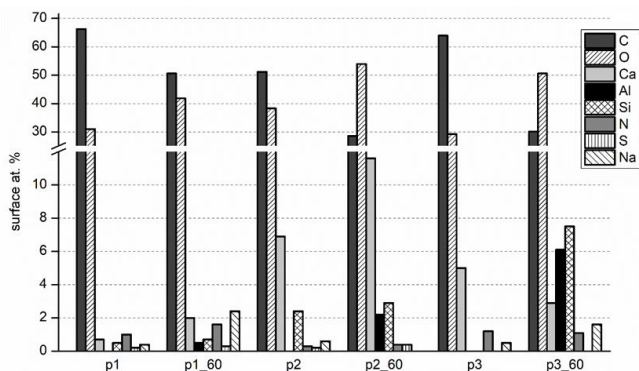

Fig. 5: Concentration of elements (in atomic %) on untreated and plasma treated paper surfaces as determined by XPS. p1: paper 1, untreated; p1_60: paper 1, treated for 60 s; p2: paper 2, untreated; p2_60: paper 2, treated for 60 s; p3: paper 3, untreated; p3_60: paper 3, treated for 60 s.

The results of the unprinted papers before and after plasma treatment are presented in Fig. 6a. It seen that the highest initial gloss is measured for paper 2, but in this case, plasma treatment also seems to reduce the gloss, especially after 10 s of treatment. For paper 1, a slight reduction in paper gloss is also observed after plasma treatment, while in the case of paper 3, an increase in gloss is observed after 10 s of treatment.
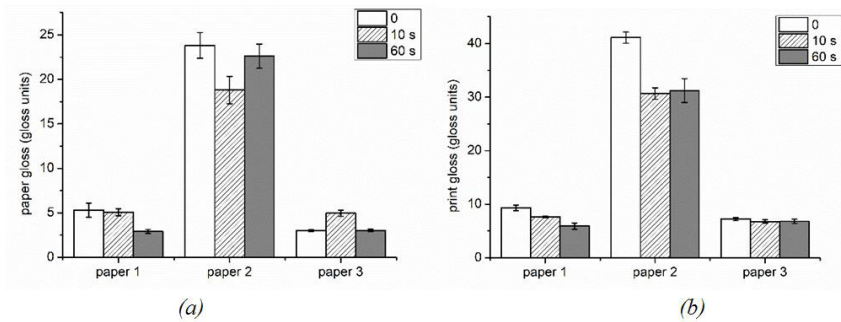
Fig. 6: Gloss values recorded for untreated and plasma treated paper samples. (a) paper gloss values; (b) print gloss values.

For the case of print gloss, as seen in Fig. 6b, paper 2 again has the highest gloss units, which are reduced after 10 and 60 s of plasma treatment. For paper 1 and 3, no significant changes in gloss of printed papers were detected.

The ink absorbency calculated values are presented in Fig. 7. It can be observed that paper 1 has the highest initial ink absorbency value, about 7%, followed by paper 3 with about 6% and paper 2 with about 4%. After 10 s of plasma treatment, increases in absorbency for paper 1 and 3 was observed, while in case of paper 2, the absorbency remains unchanged. Longer plasma treatment (60 s) results in decreases in ink absorbency for papers 1 and 3, practically to the level of the initial absorbency value in case of paper 1. Again, practically no changes in absorbency were detected in the case of paper 2.
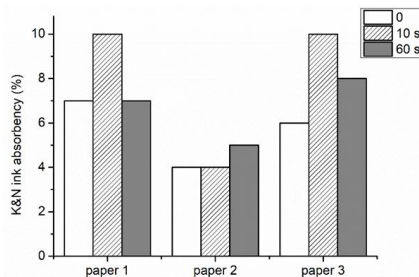

Fig. 7: K&N ink absorbency values calculated for the untreated and plasma treated paper samples.

Plasma treatment significantly influences on surface morphology, especially after longer treatment times. According to SEM analysis, the 60 s treatment time of paper 1 and 3 opens their microporous structure. This occurs due to preferential plasma etching of the organic part of the coating, which masks the inorganic particles of the coating. Paper 1 contains the highest percentage of organic components in its coating, as the coating is mainly composed of starch. Thus, in this case, after the longer plasma treatment time (60 s), etching of the organic part of the coating is the most apparent. Paper 3 also contains a significant amount of organic materials in the coating, therefore similar micropores open, but the $CaCO_3$ and kaolin particles remain intact. Similar effects were found for plasma treatment of uncoated paper, where Dimitrakellis et al. (2017) noted preferential etching of cellulose over $CaCO_3$ particles, as well as coated paper, where plasma oxidation and etching primarily affected the polymer matrix of the coating (Pykönen

et al. 2009). In the case of paper 1 and 2, nanostructuring of the surface was also observed. The morphology of paper 2 is the least influenced by plasma, as even after longer treatment time, no significant changes in microporous structures were observed. However, as revealed by AFM and higher magnification SEM images, slight nanostructuring of the surface does appear. The nanostructuring of the surface is well known in the case of plasma treatment of polymers (Junkar 2013) , where selective etching of the polymer matrix can be observed.

The SEM morphology results can be well correlated with roughness measurements, as the opening of micropores by plasma can be correlated with the increase in the Ra values for papers 1 and 3. On the other hand, almost negligible changes in Ra values were observed in case of paper 2, which correlates with the fact that on this paper, no changes in microporous structures were detected. Similar results were observed on printed papers, as the roughness increased for paper 1 and 3. The increased roughness could be to some extent correlated with the building up of ink due to a rougher surface.

Regarding surface wettability and surface energy, paper 2 again stands out, as it has the lowest increase in wettability as well as in surface energy. However, it should be noted that this paper initially has the most hydrophilic character, as WCA is about 63°, while in case of paper 1 and 3, the WCA is about 113° and 105°, respectively. The highly improved wettability of paper 1 and 3 could be attributed to the opening of micropores on the surface, which allows penetration of water into the porous paper structures. In all cases, the increase in wettability can also be attributed to preferential etching and removal of the organic hydrophobic parts of the coating, as well as to newly formed oxygen functional groups on the surface of coating. This was confirmed by XPS analysis, as in all cases, an increase in oxygen atoms and decrease in carbon content was observed. The SEM and XPS results show that paper 1 has the most organic parts in the coating, which can easily be functionalized and nanostructured by plasma. According to the manufacturers, the coating is mainly made from starch. Thus in case of paper 1, primarily the competition between etching and functionalization of organic parts of the coatings takes place during plasma treatment. However, in case of papers 2 and 3, the high increase in oxygen is not only due to functionalization, but can mainly be assigned to removal of organic parts of the coating (etching) and revealing the inorganic parts of the coatings rich with oxygen, such as calcium carbonate ($CaCO_3$), and kaolin ($Al_2Si_2O_5(OH)_4$) (Jikan et al. 2017).

Moreover, in XPS analysis, presence and increases in atomic concentrations of inorganic components like Ca, Al or Si were observed on the surface after plasma treatment. Differences in chemical composition correspond well with the type of coating. For example, the initial atomic concentration of Ca is about 0.7 at%, 7 at%, and 5 at%, for papers 1, 2 and 3, respectively. This confirms the fact that much lower amount of inorganic parts can be detected in case of paper 1, while higher amounts of inorganic parts are present in papers 2 and 3. Furthermore, the increases in inorganic elements can be nicely correlated with the removal of organic parts of the coating and exposure of the inorganic particles buried underneath the organic film. The elements Si and Al correspond to the chemical composition of kaolin. While no Si or Al atoms were detected on untreated paper 3, , both of these elements were detected after plasma treatment of paper 2 and 3, which further confirms the exposure of kaolin particles. This was also observed from SEM analysis, as the kaolin parts became easily visible after plasma treatment. Furthermore, the influence of plasma treatment on gloss and printing properties was studied as one of the important functional properties of the paper. Interestingly, paper 2 exhibited the most pronounced changes in gloss after plasma treatment, both in case of unprinted and printed papers. Gloss units should be directly connected to macro- and micro-roughness of the surface, however, in our study, this was not observed, as the microporous structure was the least altered

in the case of paper 2. However, it should be noted that paper 2 also had the highest gloss among all studied papers, and that the surface wettability in this case was also the highest. Moreover, to some extent, the nanotopography obtained on paper 2 after plasma treatment could also influence on the paper gloss. Much lower influence of plasma treatment on gloss properties of paper 1 and 3 were observed. However, a slight decrease in gloss was observed on unprinted and printed paper 1 treated for 60 s. This can again be correlated with increased nanotopography or the formation of nanopores due to plasma etching. In the case of paper 3, no changes in gloss of printed papers were detected, although in this case, plasma significantly altered the micropore structure, which became opened. These results appear to indicate that paper gloss is more influenced by nanopore topography than by the presence of micropores. Printing properties evaluated by K&N ink absorbency measurements can be correlated with the porosity values and the pore structure of the paper. The ink absorbency values significantly increase in the case of papers 1 and 3, but only after 10 s of treatment, while after 60 s of treatment, paper 1 exhibits similar ink absorbency as the untreated paper, while the absorbency value of paper 3 is still higher compared to the untreated paper. The increase in ink absorbency after 10 s for papers 1 and 3 could be ascribed to gradual opening of the micropores, which allows for the deeper penetration of ink. The decrease after 60 s of plasma treatment could again be ascribed to formation of nanotopography, especially in the case of paper 1, where the decrease to initial value of ink absorbency could be correlated to nanostructuring of the organic coating and formation of nanoporous morphology. The ink leveling is no longer influenced only by the opened micropore structure, which was obtained already after 10 s of plasma treatment. Instead, it could be presumed that ink absorbency is in this case predominantly influenced by nanopores formed on the surface, as ink no longer penetrates deep into the opened microporous structures, but is significantly retained on the nanoporous surface. In the case of paper 2, a slight increase in ink absorption was observed after 60 s of treatment, which can be correlated to nanostructuring of the surface, as determined from AFM analysis. Again, the nanostructured surface could be the prevailing factor influencing ink absorbency, as no significant changes in the opened microstructure were detected on paper 2. Interestingly, it was also shown that the high increases in surface wettability as well as in surface energy did not influence the ink absorbency, as no significant changes in wettability nor surface energy were detected between papers treated for 10 s and 60 s. Thus, in the present case, gloss and printing properties were mainly influenced by surface nanotopography, which was obtained by plasma etching and is stable with time.

CONCLUSIONS

The results of this study show that different types of coatings react differently to plasma treatment and that significant changes in surface energy or wettability do not necessary lead to significant changes in printing properties. However, plasma treatment was shown to highly influence the micro- and nanoporous structure of the paper, which seems to have the most influence on the functional properties of the paper, such as printing properties. Although the plasma treatment is known to modify only the first few nanometers of the surface, it seems that in case of porous paper structure, plasma treatment selectively etches the organic components of the coating, which opens the porous microstructure also a few micrometers in depth. Such effect is stable with time and can be used in order to specifically tailor printing properties of the paper.

ACKNOWLEDGMENTS

REFERENCES

1. Bollstrom, R., Tuorninen, M., Maattanen, A., Peltonen, J., Toivakka, M., 2012: Top layer coatability on barrier coatings. Progress in Organic Coatings 73: 26-32.

2. Camargo, J., Menezes, A., Cruz, N., Rangel, E., Delgado-Silva, A. , 2017: Morphological and chemical effects of plasma treatment with oxygen (O2) and sulfur hexafluoride (SF6) on cellulose Surface. Materials Research 20(Suppl. 2): 842-850.

3. Cornelius, C., Saquing, C., Venditti, R., McCord, M., Bourham, 2017: The effect of atmospheric pressure plasma on paper and pulps. BioResources 12: 8199-8216.

4. Cvelbar, U., Mozetič, M., Klanjšek-Gunde, M., 2005: Selective oxygen plasma etching of coatings. IEEE Transactions on Plasma Science 33: 236-237.

5. Dimitrakellis, P., Travlos, A., Psycharis, V.P., Gogolides, E., 2017: Superhydrophobic paper by facile and fast atmospheric pressure plasma etching. Plasma Processes and Polymers 14: 8.

6. Fridman, A., 2008: Plasma chemistry. Cambridge University Press: New York, 42 pp.

7. Gorjanc, M., Mozetič, M., 2014: Modification of fibrous polymers by gaseous plasma: Principles, techniques and applications. Lambert Academic Publishing, Saarbrücken, 92 pp.

8. Jikan, S.S., Badarulzaman, N.A., Yahaya, S., Adamu, A.D., 2017: Delamination of kaolinite by intercalation of urea using milling. Materials Science Forum 888: 136-140.

9. Junkar, I., 2013: Plasma treatment of amorphous and semicrystalline polymers for improved biocompatibility. Vacuum 98: 111-115.

10. Karlovits, I., Lavrič, G., 2018: Influence of plasma treatment on properties of waxed papers. In: 9th International Symposium on graphic engineering and design. Novi Sad: Faculty of Technical Sciences, Pp 58-59.

11. Pawłat, J., Terebun, P., Kwiatkowski, M., Diatczyk, J., 2016: Rf atmospheric plasma jet surface treatment of paper. Journal of Physics D: Applied Physics 49(37): 4001..

12. Pykönen, M., Sundqvist, H., Järnström, J., Kaukoniemi, O.V., Tuominen, M., Lahti, J., Peltonen, J., Fardim, P., Toivakka, M., 2008: Effects of atmospheric plasma activation on surface properties of pigment-coated and surface-sized papers. Applied Surface Science 255: 3217-3229.

13. Pykönen, M., Sundqvist, H., Kaukoniemi, O.V., Tuominen, M., Lahti, J., Fardim, P., Toivakka, M., 2008: Ageing effect in atmospheric plasma activation of paper substrates. Surface and Coatings Technology 202: 3777-3786.

14. Pykönen, M., Silvaani, H., Preston, J., Fardim, P., Toivakka, M., 2009: Plasma activation induced changes in surface chemistry of pigment coating components. Colloids and Surfaces A: Physicochemical and Engineering Aspects 352: 103-112.

15. Pykönen, M., 2010: Influence of plasma modification on surface properties and offset printability of coated paper PhD. Åbo Akademi University, 69 pp.

16. Skácelová, D., Kováčik, D., Homola, T., Čech, J., Černák, M., 2016: Surface modification of paper and paperboards using atmospheric pressure plasmas. In: Atmospheric pressure plasmas: processes, technology and applications. Parker, M., (Ed.), Nova Science Publishers, Inc., Hauppauge, New York, Pp 227-236.

17. Tian, J., Jarujamrus, P., Li, L., Li, M., Shen, W., 2012: Strategy to enhance the wettability of bioacive paper-based sensors. ACS Applied Materials & Interfaces 4: 6573-6578.

18. Tuominen, M., Lahti, J., Lavonen, J., Penttinen, T., Räsänen, J., Kuusipalo, J., 2010: The influence of flame, corona and atmospheric plasma treatments on surface properties and digital print quality of extrusion coated paper. Journal of Adhesion Science and Technology 24(3): 471-492.

19. Tuominen, M., Teisala, H., Aromaa, M., Stepien, M., Makela, J.M., Saarinen, J.J., Toivakka, M., Kuusipalo, J., 2014: Creation of superhydrophilic surfaces of paper and board. Journal of Adhesion Science and Technology 28: 864-879.

20. Vaswani, S., Koskinen, J. and Hess, D., 2005: Surface modification of paper and cellulose by plasma-assisted deposition of fluorocarbon films. Surface and Coatings Technology 195(2-3): 121-129.

21. Vesel, A., Mozetič, M., Hladnik, A., Dolenc, J., Zule, J., Milošević, S., Krstulović, N., Klanjšek-Gunde, M., Hauptmann, N., 2007: Modification of ink-jet paper by oxygen-plasma treatment. Journal of Physics D: Applied Physics 40(12): art. No. 3689.

22. Vesel, A., Mozetič, M., 2017: New developments in surface functionalization of polymers using controlled plasma treatments. Journal of Physics D: Applied Physics 50(29), art. No. 293001.

23. Vesel, A., Zaplotnik, R., Kovac, J., Mozetic, M., 2018: Initial stages in functionalization of polystyrene upon treatment with oxygen plasma late flowing afterglow. Plasma Sources Science & Technology 27(9): art. No. 094005.

24. Vohrer, U., Trick, I., Bernhardt, J., Oehr, C., Brunner, H., 2001: Plasma treatment - an increasing technology for paper restoration? Surface and Coatings Technology 142-144: 1069-1073.

25. Zhao, M., Li, H., Liu, W., Guo, Y., Chu, W., 2016: Plasma treatment of paper for protein immobilization on paper-based chemiluminescence immunodevice. Biosensors and Bioelectronics 79: 581-588.

Matej Holc, Ita Junkar*
Jožef Stefan Institute
Jamova Cesta 39
1000 Ljubljana
Slovenia
*Corresponding author: ita.junkar@ijs.si

Igor Karlovits
Pulp And Paper Institute
Bogišićeva 8
1000 Ljubljana
Slovenia

David Ravnjak, Aleš Palatinus
Vevče Paper Production Mill
Papirniška Pot 25
1251 Ljubljana-Dobrunje
Slovenia

EFFECT OF AGRICULTURAL RESIDUE FIBERS
ON NEWSPRINT STRENGTH PROPERTIES

Ivana Plazonić, Željka Barbarić-Mikočević, Nikola Španić
University of Zagreb
Croatia

ABSTRACT

As newsprints, mostly made from recycled wood pulp, are not high quality papers according to its optical, mechanical and chemical characteristics, in this research the usage of straw pulp as an alternative raw material was analyzed. For that purpose, straw pulp was mixed with recycled wood pulp and strength properties of laboratory made papers were determined according to TAPPI standards. Selection of agricultural waste for preparing straw pulp was based on annual yield of crop species (*Triticum spp.*, *Hordeum vulgare* L. and *Triticale sp.*). Results indicated that straw pulp can be efficiently used in portions up to 20% as a substitute for wood fibers or as an additive in order to obtain particular newsprint properties.

KEYWORDS: Straw, pulp, newsprint, fibers length, strength properties.

INTRODUCTION

In the context of challenging environmental issues, such as reducing deforestation and natural disasters availability of virgin cellulose fibers from wood raw materials is significantly decreased. The global deforestation rate is still high (Indarto and Mutaqin 2016), so there is a potential shortage of conventional wood raw material for the pulp industry. On the other hand, the demand for pulp and paper fiber resources has increased significantly due to increased consumption of various types of paper products and the fast population growth rate (Azeez 2018). In developed countries the rate of paper recycling is growing continuously and many of the mills worldwide use as much as 100% waste paper as raw material base (Rhyner et al. 1995). However, the lack of such raw material is a paper as a final product with poorer mechanical properties due to a decrease in the interfiber bonding (Ibrahim 2003, Fišerová et al. 2013). Therefore, during papermaking process from recycled pulp, definite percentage of pulp with virgin wood fibers must be added to provide the desired strength of paper (Minor and Atalla 1992). For reducing hardwood consumption, either as basic raw material or as supplement, paper industry is forced to find alternative sources of fibrous raw material, particularly those based on agricultural

products (Samariha et al. 2013). Considering that all plants contain cellulose in a greater or lesser percentage, pulp can be produced from any wood or non-wood plant. Although the grain of corps is important agricultural product for many countries all around the world, the residues from the corps are largely wasted. One of the most abundant and renewable lignocelullosic agricultural residues is the straw, which is left in the fields, burned or plugged back into the fields after harvesting (Ren et al. 2019). Converting this lignocellulosic residue to pulp for paper would be an advantageous way to utilize it as the consumption of paper is increasing rapidly in in all developed countries.

A rational waste management in some part of the world is recognized because it hides many candidates for paper feedstock. Researches all over the world are dealing with alternative non-wood raw materials for pulp and paper industry, due its: chemical compositions, appropriate process of fibers isolation which will provide quality pulp, usage for different grades of paper products, possibility to provide adequate, optical, mechanical and reproduction quality and recycling efficiency of such products. Until now, only about 2% of the raw materials involved in papermaking in USA and Europe are non-wood fibers (Grossmann 2009), where they are used mainly for cardboards and fluting papers (Schall et al. 2009). One of the most investigated agricultural residues for the pulp and paper industry is wheat straw (Potůček and Gurung 2014). This is understandable as wheat is the most widely cultivated crop in the world (Curtis 2016) which consequently generates substantial quantities of residues of about 529 million tons worldwide every day (Govumoni et al. 2013). Utilization of wheat straw for the pulp and paper production has some deficiencies such as low pulp yield and problems with the recovery of spent pulping liquors by soda pulping process (Veisi and Mahdavi 2016). On a global scale so far wheat straw pulp, carried out by soda-anthraquinone process, has proven to be a good substitute for old corrugated cardboard (OCC) pulp for making fluting paper. Namely, blending of wheat straw soda – anthraquinone pulp with OCC pulp in different ratios significantly improved all the paper properties, except tear index, compared to 100% OCC pulp (Schall et al. 2009).

In previous research (Plazonić et al. 2016) conducted chemical component analysis showed that wheat, barley and triticale straw contain high amounts of cellulose, which was the first step of its valorization as a source of fibers in papermaking industry. In this research, emphasis was placed on the potential value of straw for pulp and papermaking based on strength properties of newsprint produced at laboratory scale. As newsprint represents a lower grade paper, along with accepting four-color printing (CMYK) paper strength properties are important indicators of the quality of newsprint as a printing substrate. For that purpose, the tensile index, tear index and burst index of newsprint, formed from recycled pulp in admixture with a variable content of straw pulp, were determined.

MATERIAL AND METHODS

Materials (straw – pulp – paper)

The straw of three most common crop species in Croatia e.g. wheat (*Triticum spp.*), barley (*Hordeum vulgare* L.) and triticale (*Triticale sp.*) was collected after the harvest. Cleaned straw was manually cut using scissors into approximately 3 cm long pieces and conducted into semi-chemical pulp according soda pulping method (Plazonic et al. 2016) by degrading the lignin and hemicelluloses into small water-soluble molecules which were washed away from the cellulose fibers.

After the thermal treatment which was carried out in automatic autoclave (Kambič) under the controlled and defined conditions (Tab. 1), the pulp slurry was removed from black process liquor by decantation. Thereafter, softened pulp was rinsed in two cycles with tap water and had been transferred into Valley beater (Techlab Systems (TLS)) where appropriate amount of tap water was added in order to maintain the pulp suspension at 1.5% consistency. The fiberization was occurred at pH 9, 24°C and 500 rpm for 40 min. Finally, the pulp was drained and allowed to dry to moisture content of approximately 7% at the room temperature.

Tab. 1: Soda pulping conditions.

Straw	Pulping conditions
Wheat	Temperature of 120°C, alkali level of 16% for 60 min and a 10:1 liquid-biomass ratio.
Barley	
Triticale	

In disintegration stage of paper production process, obtained unbleached straw pulp was added in proportions of 10%, 20% and 30% to reference pulp. Reference pulp was recycled pulp, used for newsprint in many printing presses for printing newspapers, supplied in the form of dry sheets. In order to estimate the effect of straw fibers on newsprint strength properties, laboratory sheets of approximately 45 g·m^{-2} were formed in a Rapid-Köthen sheet former (FRANK-PTI) according to standard EN ISO 5269-2:2001. In total, according to its composition 10 different laboratory made newsprints were formed (Tab. 2).

Tab. 2: Pulp proportions for laboratory made newsprint.

Pulp blends	Proportions
recycled wood	100
recycled wood : wheat	90:10; 80:20; 70:30
recycled wood : barley	90:10; 80:20; 70:30
recycled wood : triticale	90:10; 80:20; 70:30

Methods

Fiber length determination

According to slightly modified Franklin's method (Chaffey 2002), each specimen intended for fiber length determination was macerated in 1:1 (v/v) mixture of glacial acetic acid and 30% hydrogen peroxide. Maceration took place in 35 ml scintillation vials that have been heated for 48 h to 60°C using dry block heater (IKA, Dry block heater 1). After the specified time elapsed almost pure white delignified samples were obtained. Macerating solution was then carefully decanted, and the samples were rinsed with distilled water for several times. In order to neutralize the remaining traces of acetic acid small amounts of sodium carbonate were added to half-filled vials containing samples in distilled water. Sodium carbonate was added in small amounts at the time ensuring that effervescence is not so vigorous that it breaks up the delignified straw samples. When the effervescence has stopped the liquid from the vials was decanted and samples were rinsed several times with distilled water in order to remove the traces of sodium carbonate. Finally, individual fibers were produced by vigorously shaking the delignified straw samples in vials half-filled with distilled water. Such fibers were then dyed using Toluidine Blue O dye and observed using Zeiss AXIO Zoom V16 microscope. For each specimen type, the lengths of 50 randomly selected fibers were measured using AxioVision SE64 (Rel. 4.9.1) software. All the

chemicals used in the pulp preparation were purchased from Kemika Ltd., Croatia. Toluidine Blue O dye was purchased from Sigma-Aldrich, Germany.

Strength properties of laboratory made newsprint

All strength properties of laboratory prepared newsprints were tested in accordance with appropriate TAPPI standards (Tab. 3). Each test was repeated ten times and the average of these tests was used to determine the effect of addition of fibers from each straw pulp on newsprint strength properties prepared from recycled wood pulp at laboratory scale. Standard deviation (SD) for each measured and calculated strength property was also noted.

Tab. 3: Analysis of strength properties.

Strength property	TAPPI standard method of analysis
Tensile breaking properties	T494 om-01
Tearing resistance	T414 om-12
Bursting strength	T403 om-97 (Mullen tester)
Surface strength (wax picking test)	T459 om-93

RESULTS AND DISCUSSION

The strength properties of paper samples are substantially influenced by individual characteristics of cellulose fibers as well as by the paper network structure. It is important to say how this research was studied at laboratory scale. Namely, in laboratory made newspapers fibers are not properly oriented as in commercial papers, due to the way of functioning semi-automatic Rapid-Kothen sheet former used for making laboratory sheets. However, lengths of those individual fibers surely define structure of laboratory papers and thus its strength properties (Plazonić et al. 2016). Microscopic images of fibers from each cereal straw captured during fiber length determination are presented at Fig. 1.
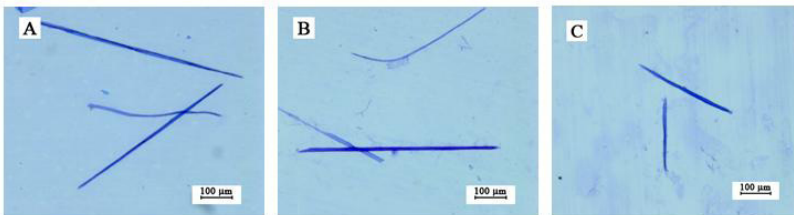
Fig. 1: Micro images of fibres (168x magnification): wheat (A), barley (B) and triticale (C).

Newsprint is predominantly recycled fiber based paper where it is important to emphasize how by each recycling process fibers become shorter. So, blending with longer fibers is extremely important during newsprint production because length is one of the most important fiber properties which effects on the strength properties of the pulp and the paper made of it. A long fiber pulp is good to blend with short fiber pulp to optimize on fiber cost, strength and formation

of paper. In general, usage of longer fibers will increase the number of bonds per fiber, which will lead to more strongly bound of fibers into the network, thereby increasing the strength of fiber network in paper (Keränen and Retulainen 2016). As virgin straw fibers should be used as enrichment for recycled fibers instead wood fibers, fibers length determine for each analyzed straw is listed in Tab. 4. The differences among straw of crop species in fiber length are visible.

Tab. 4: Fibers length of straw conducted to pulp for newsprint production.

Raw material	Species	Fibers length (mm)*			
		Mean	SD	Min	Max
Straw	Wheat (*Triticum spp.*)	0.83	0.26	0.45	1.62
	Barley (*Hordeum vulgare* L.)	0.91	0.29	0.40	1.62
	Triticale (*Triticale sp.*)	0.93	0.61	0.27	2.63

*Values based on lengths of 50 fibers measured for each examined species.

If mean values in Tab. 4 are observed it can be concluded that all corps straw contained short fibers with a mean length of 0.83 mm for wheat, 0.91 mm for barley and 0.93 mm for triticale one. It was noted that straw fibers are heterogeneous in a character, with a considerably large range in fiber length. Namely, wheat and barley straw consist of fibers whose length ranges from 0.45 to 1.62 mm, while the range for triticale fibers is much wider (0.27 – 2.63 mm). However, for all analyzed straws most fibers are in the range from 0.5 to 0.9 mm, approximately 76 % of the wheat, 68 % of barley and only 36 % of the triticale fibers (Španić et al. 2018). Generally, gained results for fiber length are in correlation with other researches reports. The most studied straw is wheat straw and consequently the most information about fiber length is available for this type of straw. Mean fiber length of wheat straw publish by Deniz is 0.738 mm by Deniz et al. (2004), by Guo is 0.68 mm by Guo et al. (2009) while by Favadi and by Singh is 1.18 mm (Fadavi et al. 2012, Singh et al. 2011). El Mansouri has published that average length of triticale fibers is 0.926 mm (El Mansouri et al. 2012).

After the experiment data processing, the effects of varies blending levels of two pulp types (straw pulp and recycled pulp) on the strength properties (tensile index, tear index, burst index and critical wax strength number (CWSN) of the laboratory made newsprint sheets was established. All gained strength properties results are summarized in Tab. 5. The effect of each straw pulp on strength properties of laboratory newsprint sample were shown by comparison with reference sample (0% of straw pulp). It is observed that inhomogeneity of all laboratory made newsprint samples affects the results of the mechanical properties measurements and shows results, which have a high standard deviation.

Tab. 5: Strength properties of the laboratory made pulp sheets: a) wheat, b) barley, c) triticale.

a) Wheat		Pulp (%)							
		Straw	*Recycled*	*Straw*	*Recycled*	*Straw*	*Recycled*	*Straw*	*Recycled*
		0	**100**	**10**	**90**	**20**	**80**	**30**	**70**
Tensile index (Nm·g⁻¹)	Mean	43.61		41.80		41.02		41.02	
	SD	3.45		2.01		2.40		1.61	
	Range	36.62 – 46.23		40.36 – 47.60		39.07 – 47.08		38.26 – 43.35	
Elongation (%)	Mean	1.23		1.35		1.4		1.4	
	SD	0.25		0.18		0.09		0.12	
	Range	0.7 – 1.5		1.1 – 1.6		1.3 – 1.5		1.2 – 1.6	
Tear index (mN·m²·g⁻¹)	Mean	9.20		10.18		9.12		9.57	
	SD	1.05		0.83		1.01		0.50	
	Range	7.95 – 11.00		9.05 – 11.13		7.97 – 10.50		9.11 – 10.21	
Burst index (kPa·m²·g⁻¹)	Mean	13.54		13.69		13.07		13.41	
	SD	0.27		0.25		0.32		0.85	
	Range	13.19 – 13.97		13.26 – 14.23		12.44 – 13.70		12.69 – 15.60	
CWSN		7A		7A		7A		6A	

b) Barley		Pulp (%)							
		Straw	*Recycled*	*Straw*	*Recycled*	*Straw*	*Recycled*	*Straw*	*Recycled*
		0	**100**	**10**	**90**	**20**	**80**	**30**	**70**
Tensile index (Nm·g⁻¹)	Mean	43.61		43.17		42.52		40.31	
	SD	3.45		2.25		2.15		1.99	
	Range	36.62 – 46.23		39.85 – 48.03		38.97 – 45.33		37.37 – 43.14	
Elongation (%)	Mean	1.23		1.26		1.34		1.30	
	SD	0.25		0.12		0.13		0.18	
	Range	0.7 – 1.5		1.1 – 1.4		1.2 – 1.6		1.1 – 1.5	
Tear index (mN·m²·g⁻¹)	Mean	9.20		11.52		9.53		8.54	
	SD	1.05		1.75		0.79		0.72	
	Range	7.95 – 11.00		9.97 – 13.75		7.84 – 9.80		7.93 – 9.76	
Burst index (kPa·m²·g⁻¹)	Mean	13.54		13.34		13.17		13.05	
	SD	0.27		0.23		0.70		0.46	
	Range	13.19 – 13.97		12.90 – 13.66		12.50 – 14.98		12.60 – 13.96	
CWSN		7A		7A		7A		6A	

c) Triticale		Pulp (%)							
		Straw	*Recycled*	*Straw*	*Recycled*	*Straw*	*Recycled*	*Straw*	*Recycled*
		0	**100**	**10**	**90**	**20**	**80**	**30**	**70**
Tensile index (Nm·g⁻¹)	Mean	43.61		44.37		41.69		41.15	
	SD	3.45		3.77		1.0		1.91	
	Range	36.62 – 46.23		38.04 – 49.12		39.74 – 42.93		37.63 – 43.43	
Elongation (%)	Mean	1.23		1.37		1.37		1.32	
	SD	0.25		0.28		0.17		0.18	
	Range	0.7 – 1.5		1.0 – 1.9		1.0 – 1.6		1.1 – 1.7	

Tear index (mN·m²·g⁻¹)	Mean	9.20	9.95	9.10	10.03
	SD	1.05	1.80	0.32	0.82
	Range	7.95 – 11.00	8.28 – 12.55	8.78 – 9.55	9.50 – 11.40
Burst index (kPa·m²·g⁻¹)	Mean	13.54	13.61	12.88	13.03
	SD	0.27	0.25	1.42	0.64
	Range	13.19 – 13.97	13.24 – 14.09	10.00 – 15.43	12.31 – 14.56
CWSN		7A	7A	6A	6A

In general, addition of straw pulp, regardless to the crop type, has not shown any significant negative influence on strength properties of paper. Furthermore, reference sample with 0% of straw pulp has the minimum measured tensile index 36.62 Nm·g⁻¹, while all samples with straw pulp have the higher value of minimum measured tensile index (in range 37.37 – 40.36 Nm·g⁻¹). The maximum measured tensile index of reference sample was 46.23 Nm·g⁻¹; while for samples with straw pulp this parameter was in range 43.14 – 48.03 Nm·g⁻¹. There were no significant differences between tensile index of sheets made of pure recycled pulp and those with 10%-30% straw pulp/90% -70% recycled pulp blended. From tensile index results, it could be expected that commercial papers with addition of straw pulp (wheat, barley or triticale) would have similar or even better tensile index as papers made only from recycled wood pulp. During tensile breaking properties determination, elongation of the strip of each laboratory newsprint sample is recorded as well as an insight into the percentage increase in length of the test strip when fracture occurs divided by the original length of the test strip. From gained results, it is evident that addition of all straw pulp types in all observed shares increases the relative elongation of laboratory newsprint samples. The recorded relative elongation average value of reference sample was 1.21%, while for papers with 10% - 30% wheat pulp was 1.35% - 1.40%; barley pulp was 1.26% - 1.34% and triticale pulp was 1.37% - 1.32%. Again, the minimum measured relative elongation 0.7% was for reference sample, while all samples with straw pulp have the higher value of minimum measured relative elongation (in range 1.0% – 1.3%).

It was noted that the minimum tear index value of all sheets produced with addition of straw pulp was higher comparable with value obtained for reference sample (7.95 mN·m²·g⁻¹). Results displayed on Tab. 5 showed that the addition of straw pulp produce laboratory newsprint with similar or slightly lower average burst index value compare to recycled pulp in reference sample. In general, from all analyzed straw pulp, wheat pulp has shown the most positive influence on burst index of laboratory newsprint sheets. This result could be connected with fiber length results as the longer and stronger fibers provide higher strength properties. Namely, the smallest measured fiber in macerated wheat straw was 0.45 mm; while in barley and especially in triticale straw the smallest fiber was significantly shorter (min length of barley fiber was 0.40 mm and triticale fiber 0.27 mm).

Since wax sticks are used as analogues for hot melt adhesives, measurements were made of their tensile strength using the pull-off test to determine how well they replicate the properties of the adhesives. The tensile strength of the wax appears to increase with wax number, which means that the higher the CWSN indicate the stronger paper surface strength or its resistance to picking. As newsprint is grade of paper, which is intended entirely for printing, surface strength is an important parameter as it relates to the forces created during printing. Picking denotes damaging the paper surface during printing operation due to forces imposed by lifting-off the printing equipment from the paper surface. These forces depend on ink viscosity and printing speed. If they exceed the surface strength of paper, picking begins. In other words, a low surface strength of paper may create picking problems (Drobchenko 2004). The CWSN results indicate

that addition of straw pulp into recycled pulp does not significantly change surface strength of laboratory made newsprint. In comparison with reference sample, where determinate CWSN was 7A, only papers with triticale pulp have shown some lower surface strength (CWSN = 6A) when the share of straw pulp was higher than 10%. Surface strength is the ability of paper to resist a force pulling fibers or fiber bundles from its surface and is strongly influenced by the type of fibers used in papermaking process. As long fibers are improving the surface strength properties of the paper, it is evident why papers with triticale pulp have shown the lower surface strength. Namely, in macerated triticale straw the shortest fibers were detected (fibers with length of 0.27 mm). However, acceptable pick level for commercial uncoated papers is at least 7A (Board 2003) and all laboratory newsprint papers without any surface treatment have sufficient surface strength for printing process.

CONCLUSIONS

The straw as agricultural residues, in general, and wheat straw, in particular, can be successfully considered as an alternative, replacing the pulp produced from recovered paper. It has been noticed from this study that straw pulp gained from wheat, barley and triticale agricultural species can act as a good strength fiber enrichment of paper sheets made from repulped recycled newsprint when added in portions up to 20%, while in range from 20% to 30% strength properties vary depending on straw source. Overall, fiber length of all analyzed straw fibers is satisfactory for papermaking, although, they would be classified as short fibers. Based on gained results it could be concluded that straw fibers can be efficiently used in small portions as a substitute for more expensive wood fibers or as an additive in order to obtain particular paper properties.

ACKNOWLEDGMENTS

REFERENCES

1. Azeez, M.A., 2018: Pulping of non-woody biomass. Chapter 3. In: Pulp and Paper Processing (ed. Kazi, S.N). IntechOpen, London, Pp 55-86.
2. Board, N., 2003: The complete book on printing technology. Asia Pacific Business Press Inc. India, 742 pp.
3. Chaffey, N., 2002: Wood microscopical techniques. In: Wood formation in trees: cell and molecular biology techniques (ed. Chaffey, N.). CRC Press, Boca Raton, Pp 23-24.
4. Deniz, I., Kırcı, H., Ates, S., 2004: Optimization of wheat straw triticum drum kraft pulping. Industrial Crops and Products 19(3): 237-243.
5. Drobchenko, A., 2004: Automated picking assessment using machine vision. MSc (Diploma) thesis, Lappeenranta University of Technology, 71 pp.
6. El Mansouri, N.E., Espinach, F.X., Julian, F., Verdaguer, N., Torres, L., Llop, M. F., Mutje, P., 2012: Research on the suitability of organosolv semi-chemical triticale fibers as reinforcement for recycled HDPE composites. BioResources 7(4): 5032-5047.
7. Fadavi, F., Kermanian, H., Resalat, H., 2012: Effect of fiber fractionation on refinability and strength properties of wheat straw soda-aq pulp. Lignocellulose 1(2): 153-163.

8. Fišerová, M., Illa, A., Boháček, Š., Kasajová, M., 2013: Handsheet properties of recovered and virgin fibre blends. Wood Research 58(1): 57- 66.

9. Govumoni, S.P., Koti, S., Kothagouni, S.Y., Venkateshwar, S., Linga, V.R., 2013: Evaluation of pretreatment methods for enzymatic saccharification of wheat straw for bioethanol production. Carbohydrate Polymers 91(2): 646–650.

10. Grossmann, H., 2009: The limits of paper recycling – an European approach to identify and extend the limits of paper recycling. In: 2007 TAPPI 8th Research Forum on Recycling. Pp 1-8.

11. Guo, S., Zhan, H., Zhang, C., Fu, S., Heijnesson-Hultén, A., Basta, J., Greschik, T., 2009: Pulp and fiber characterization of wheat straw and eucaluptus pulps - a comparison. BioResources 4(3): 1006-1016.

12. Ibrahim, R., 2003: Structural, mechanical and optical properties of recycled paper blended with oil palm empty fruit bunch pulp. Journal of Oil Palm Research 15(2): 28-34.

13. Indarto, J., Mutaqin, D.J., 2016: An overview of theoretical and empirical studies on deforestation. Journal of International Development and Cooperation 22(1-2): 107-120.

14. Keränen, J.T., Retulainen, E., 2016: Changing quality of recycled fiber material. Part 1. Factors affecting the quality and an approach for characterisation of the strength potential. BioResources 11(4): 10404-10418.

15. Minor, J.L., Atalla, R.H., 1992: Strength loss in recycled fibers and methods of restoration. In: Proceedings of Materials Research Society symposium. San Francico, CA. Pittsburg, PA: Materials Research Society, vol. 266: Pp 215-228.

16. Plazonić, I., Barbarić-Mikočević, Ž., Antonović, A., 2016: Chemical composition of straw as an alternative material to wood raw material in fibre isolation. Drvna industrija 67(2): 119-125.

17. Plazonić, I., Barbarić-Mikočević, Ž., Bates, I., 2016: Strength properties of newsprint from recovered paper in admixture with wheat pulp. Proceedings of 8th international symposium on graphic engineering and design (ed. Pavlović, Ž.). Novi Sad: Grafički centar GRID, Serbia, Pp 201-206.

18. Plazonic, I., Bates, I., Barbaric-Mikocevic, Z., 2016: The effect of straw fibers in printing papers on dot reproduction attributes, as realized by UV inkjet technology. BioResources 11(2): 5033-5049.

19. Potůček, F., Gurung, B., 2014: Strength characteristics of chemi-mechanical pulp from rapeseed straw. Acta Facultatis Xylologiae Zvolen 56(1): 51–57.

20. Ren, J., Yu, P., Xu, X., 2019: Straw utilization in China - status and recommendations. Sustainability 11(6): 1762.

21. Rhyner, C.R., Schwartz, L.J., Wenger, R.B., Kohrell, M.G., 1995: Waste Management and Resource Recovery. CRC Press. Boca Raton, 544 pp.

22. Samariha, A., Khakifirooz, A., Nemati, M., Ravanbakhsh, F., Kiaei, M., Saghafie, A., 2013: Newsprint from NSSC bagasse pulp mixed with hardwood CMP pulp and bleached softwood kraft pulp. BioResources 8(4): 5561-5569.

23. Schall, N., Kruger, E., Blum, R., Rubenacker, M., 2009: Soda-AQ pulping of wheat straw and its blending effect on old corrugate cardboard (OCC) pulp properties. Tappsa Journal: 35-39.

24. Singh, S., Dutt, D., Tyagi, C. H., 2011: Complete characterization of wheat straw (*Triticum aestivum* PBW-343 l. EMEND. FIORI & PAOL.). A renewable source of fibres for pulp and papermaking. BioResources 6(1): 154-177.

25. Španić, N., Plazonić, I., Jambreković, V., Barbarić-Mikočević, Ž., 2018: Wood and nonwood fibres length as main factor affecting their suitability as raw materials for papermaking industry. In: Proceedings of Natural resources, green technology and sustainable development/3. University of Zagreb, Croatia, Pp 121-125.

26. Veisi, A., Mahdavi, S., 2016: Mixing bleached white poplar and wheat straw chemimechanical pulps to improve the mechanical and optical characteristics. BioResources 11(2): 2987-2997.

Ivana Plazonić*, Željka Barbarić-Mikočević
University of Zagreb
Faculty of Graphic Arts
Department of Fundamental and General Knowledge
Chair of Applied Chemistry
10 000 Zagreb
Croatia
*Corresponding author: ivana.plazonic@grf.hr

Nikola Španić
University of Zagreb
Faculty of Forestry
Department of Wood Technology
10 000 Zagreb
Croatia

BLENDING IMPACT OF HARDWOOD PULPS WITH SOFTWOOD PULP ON TISSUE PAPER PROPERTIES

Monika Stankovská, Mária Fišerová, Juraj Gigac, Elena Opálená

Pulp and Paper Research Institute
Bratislava, Slovak Republic

ABSTRACT

The influence of proportions of bleached birch, eucalyptus, beech kraft pulps as well as the bleached aspen chemi-thermomechanical pulp (BCTMP) in the mixture with bleached pine kraft pulp on tissue paper properties was compared. Increase of bleached beech kraft pulp and aspen BCTMP proportion in a mixture with bleached pine kraft pulp leads to significant rise of porosity ε as well as bulk. The water absorption after immersion increased significantly with increase of aspen BCTMP content in the mixture while other hardwood pulps in the mixture had only moderate impact. Increasing of bleached beech and eucalyptus kraft pulps content in the mixture continually increased initial water absorption. As a result of blending of bleached birch kraft pulp with bleached pine kraft pulp, bulk softness improved and the tensile index increased slightly. The increased content of bleached birch and beech kraft pulp in the mixture increased the brightness while the addition of aspen BCTMP and bleached eucalyptus kraft pulp increased of coordinate b* value. Mixed pulps with properties suitable for different types of hygienic products were selected.

KEYWORDS: Hardwood kraft pulp, softwood kraft pulp, chemi-thermomechanical pulp, water absorption, tensile index, bulk softness, optical properties, tissue paper.

INTRODUCTION

The expenses of fibre typically accounts for more than 50% of the total cost of hygienic papers production, depending on their properties such as softness, bulk density, strength and absorption capacity. The highest quality tissue paper products are mainly made of pulp, usually a mixture of long-fibre pulp of softwood wood with short-fibre pulp of hardwood wood. Hygienic products made of 100% hardwood pulp can be very soft, but are less rigid than from softwood pulp. Their disadvantage is also the degradation of strength during embossing. Additives may be used to increase the strength, but they affect the cost and the resulting properties of tissue paper.

Tissue hygiene products are produced to meet the desired properties for a particular application within the market. Overall, absorbency, softness and strength are the most important characteristics used to assess the quality of pulp products. Wet strength and absorbency are considered to be the most important functional properties of kitchen towel products (de Assis et al. 2018). Other properties such as softness, brightness and appearance are commonly considered as secondary properties in this case. But as determined by Kim et al. (1994), there are customers who are sensitive to softness in case of kitchen towels and do not demand a perfect drying of the surface.

Bleached pulps are often added to bleached softwood pulps to improve printability of speciality papers. Because of the price difference between softwood and hardwood pulps, it makes sense to optimize the softwood pulp blending in paper without compromising the desired end product properties of the hygienic product and production efficiency. Together, pulp, producing technology and know-how provide quality to the final hygienic product. Kraft pulp of softwood varies in tensile strength and strength at beating is also different. Higher strength at a given degree of beating allows a reduction in its blending while maintaining the resulting strength. If a higher strength is obtained by using less energy for beating and less blending of the softwood pulp, it becomes an additional advantage which results in lower costs. If the fine content of the pulp is high, dewatering will be impaired and dust will be generated on the paper machine. For soft and bulky tissue papers, only beating of softwood pulp is recommended.

The use of bleached kraft hardwood pulp has long been increasing due to it special suitability for the production of hygienic paper, especially eucalyptus pulp, but also because of the price difference between bleached softwood and hardwood kraft pulp. Another advantage of bleached hardwood pulps is that they do not need to be milled. Higher proportion of hardwood pulp also improves formation, resulting in drying energy savings (Haynes 1990). The beating of hardwood and softwood pulps to obtain mixed pulp can be carried out separately or together. Hardwood pulps are more sensitive to beating process of higher intensity (Annergren and Hagen 2009) while softwood requires sufficient degree of force (Biermann 2018). Practice has shown that both a separate and mixed beating can be successfully used to produce a high quality end product. Generally, mixed refining is being performed on smaller machines, where the flow of individual components is small. Measured fibre strength properties and energy consumption indicate that some fibres are better to be beaten separately but some fibres favour mixed beating (Lumiainen 1996). For this reason, a combined system with separate beating for different pulps followed by mixed beating, offers a good alternative because of the benefits from both separate and mixed systems. Chauhan et al. (2011) studied beating behaviour of three hardwood pulps and one softwood pulp mixed in different proportion. The results showed that fibre length was not affected either beated together or separately in PFI mill and strength properties of mixed beated pulps were either slightly better or comparable to these of separately beated pulps.

Absorbency and softness are mostly influenced by porosity, creping and fibre composition. Papers with a low bulk density have high porosity leading to increased absorbency and softness. Other properties affecting water absorption and softness are type of wood, delignification processes, stiffness, bulk, additives, wet strength, basis weight, thickness, etc. For example, specialty types of mechanical pulp can produce highly porous tissue paper compared to chemical pulps. In addition to selecting the pulp type itself, the functional properties of tissue papers can be improved in several ways. Nanocellulose can also improve absorbency and strength. The refining of the fibrous raw material is a critical operation of the papermaking process and has significant effect on fibre properties. It often determines how well the technical requirements of the product are met. Subsequent processes, such as forming and drying, are influenced

highly by the conditions used in refining. Applying of higher specific edge load for refining of bleached kraft birch and eucalypt pulp leads to better absorbency of tissue paper (Gigac and Fišerová 2008). Removal of xylan in the eucalyptus pulp slurry was found to increase bulk and absorbency and to decrease the tear and tensile strength (Gomes et al. 2011). The effect of xylan removal and sorption on fibre properties of pine pulp was also studied (Schonberg et al. 2001). The location and the charge of xylan have a considerable impact on the formation of interfibre bonds. Scott Bond-values correlated with the amount of surface xylan on fibre surfaces, whereas tensile strength was affected by the total amount of xylan and particularly by the total charge of the fibres.

In addition to the question of whether to beat the pulps separately or mixed, it is important to set the optimum blending of hardwood pulp to softwood. The effect of higher blending of eucalyptus pulp with pine pulp on tensile strength, hand-felt softness, bulk and water absorbency (capillary rise of water) using an on-site paper machine was studied by Chang et al. (2018). The results of their study showed that the increase of hardwood pulp content (75-85%) had no effect on water absorption or bulk, while the effect on tensile strength was modest and hand-felt softness only changed at the highest hardwood pulp content. However, Chang et al. (2018) only studied the effect of hardwood pulp addition within a small range of content (75-85%).

Mechanically treated pulps which have harder fibres provide greater paper bulk and thus higher water absorption capacity. On the other hand, high content of fines present in mechanical pulps increases the density of tissue paper and creates problems with dusting and linting (Axelsson 2001). Bleaching of mechanical pulps with peroxide can improve absorbency rate due to reduction of extractives content and provide higher brightness, lower fibre stiffness, better fibre bonding, lower dusting, better brightness stability (Johnson 1978).

Chemically treated fibres have elastic fibres, resulting in better binding and softness. In the chemi-thermomechanical pulp (CTMP) processing process, wood chips are impregnated with a weak sodium sulphite solution at alkaline pH prior to overpressure. The effect of this treatment is to make lignin softer and thus the fibre breakage during refining will be concentrated to the middle lamella rich in lignin. This leads to the formation of a higher amount of long fibres and a lower amount of fine particles and chips at a certain power in comparison to thermomechanical pulp (TMP). The high content of long fibres is important for all products requiring high density, so CTMP technology is especially suitable for such products. CTMP is one of the fastest growing products in the pulp and paper industry and has balanced properties of hardwood and softwood (Nanko et al. 2005). However, long fibres can cause problems with poor formation on the machine, which can result in poor surface properties, therefore shorter fibres are desirable. Short and stiff fibres can be obtained from hardwood CTMP such as birch pulp or by cutting long fibres in softwood CTMP with low consistency beating. CTMP provides better strength than TMP pulps due to higher binding strength; while at the same time it has better absorbency and absorption rate. The disadvantage of using CTMP is their low opacity. Therefore, such types of pulp are mainly used to produce paper with low added value and short durability, because they turn yellow in the light. This is due to the oxidation of phenolic groups of lignin to quinones under the light and air influence. However, bleached chemi-thermomechanical pulp (BCTMP) from weakly coloured wood species as aspen can be a good option. BCTMP is increasingly used in the manufacture of woodfree printing (Hu et al. 2009) and office papers and multi-layer folding cartons as well as tissue papers. The highest potential market for aspen BCTMP is in growing printing and writing paper grades (Cheyne 1990, Granndfeldt and Dahlin 2003). The content of aspen BCTMP typically used in specialty paper ranges from 15% to 30%, depending on the paper grade.

The objective of the work was to determine the effect of the addition of hardwood pulps to softwood pulp on properties of tissue paper in order to select the composition of mixed pulp with an optimal balance between water absorption, softness and tensile index.

MATERIAL AND METHODS

Bleached kraft pulps

Bleached pine kraft pulp made from young pine wood Södra Black (Pine), bleached beech kraft pulp from Bukocel (beech), bleached birch kraft pulps Södra Gold (birch), TCF bleached eucalyptus kraft pulp Pontevedra (eucalyptus) and bleached aspen chemi-thermomechanical pulp (Aspen BCTMP).

Methods

Pulp beating and preparation of handsheets

All types of pulp were separately beaten to 20°SR in a laboratory Jokro mill according to ISO 5264-3 (1979). Low drainage resistance was chosen for all tested pulps as pulp beating markedly reduces the water absorption, bulk softness and brightness (Fišerová et al. 2019). The hand sheets (60 g·m^{-2}) were prepared in the sheet former Rapid Köthen according to the standard ISO 5269-2 (2004).

Preparing of mixed pulps

Bleached pine kraft pulp was mixed with 20, 40, 80 and 100% of bleached birch, eucalyptus and beech kraft pulps or aspen BCTMP.

Analysis

Porosity ε was calculated according to the equation given in literature (Daub et al. 1986).

The bulk was calculated from the apparent bulk density determined according to ISO 534:2011. W*ater absorption after immersion for time of 10 s* was determined according to the standard ISO 5637 (1989).

The tensile index was determined according to ISO 1924-2a.

The bulk softness was calculated from the bending stiffness determined at 15° and 10 mm distance between the clamp and the knife-edge according to the TAPPI T 556 pm-95 method.

The brightness was determined according to ISO 2470-1:2016 and coordinate b* value according to ISO 5631-1:2015.

Water penetration dynamics were measured by the ultrasound device PDA C.02 (Emtec, Radnor, PA, USA) with a frequency of 2 MHz. Water with a surface energy of 72 mJ·m^{-2} was used as the test liquid. Ultrasound signal intensity (USI) change was obtained at 43 ms - 60 s using the SC algorithm. The algorithms for calculating initial water absorption was designed from the USI drop in 200 ms and. A more detailed description of this method as well as an evaluation process of the initial water absorption has already been published (Stankovská et al. 2019).

RESULTS AND DISCUSSION

Handsheets properties of mixed pulps

The porosity and bulk of pulp handsheet significantly influences the water absorption after immersion and initial water absorption (Stankovská et al. 2019) as well as softness (Morais et al. 2019). The effect of hardwood pulp blending on porosity ε is shown in Fig. 1a. The porosity ε of birch pulps, having higher flexibility and thus fibre flattening, was lower than the porosity of other pulps and decreased slightly from 0.59 to 0.54 with increasing of birch pulp content in the mixture with pine pulp. As the eucalyptus pulp content in the mixed pulp increased, there was only a slight change in porosity ε. A more pronounced effect of hardwood pulp addition to pine pulp on porosity ε was shown at higher content (80 and 100%) of beech pulp and of aspen BCTMP. The bleached aspen kraft pulp had the highest porosity ε (0.66). Aspen BCTMP has more flexible fibres due to higher lignin content and lower porosity ε, resulting in a more rigid structure with low tendency to collapsiveness of fibres which leads to less binding and higher porosity. Bulk of handsheets (Fig. 1b) is an important property for tissue paper because the thickness and volume of the paper correlate well with the absorbency as well as bulk softness. Blending of hardwood pulps with pine pulp, with the exception of birch pulp led to bulk increasing. The bulk rose particularly rapidly with increased aspen BCTMP content by about 3-23% and of beech pulp by 5-15%.
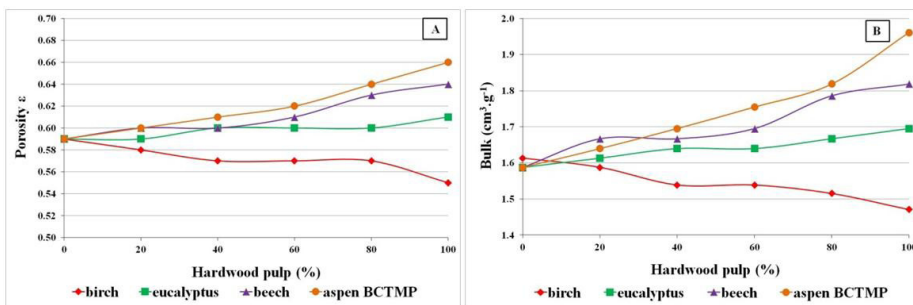

Fig. 1: Blending impact of bleached birch, eucalyptus, beech kraft pulp and bleached aspen BCTMP with bleached pine kraft pulp on porosity (a) and bulk (b).

The effect of the bleached birch, eucalyptus, beech kraft pulp or aspen BCTMP blending with bleached pine kraft pulp on water absorption after immersion (WA) is shown in Fig. 2a. Mixed pulp from aspen BCTMP had significantly higher water absorption after immersion (282-514%) than other mixed pulps (243-311%). The water absorption after immersion of aspen BCTMP was 1.8-1.9 times higher, which also corresponds to high bulk and porosity ε (Fig. 1a, b). The water absorption after immersion increased significantly (by 17-113%) with increasing of aspen BCTMP content in the mixed pulp. Increasing of the eucalyptus pulp content resulted in a 12-29% increase in water absorption after immersion; while for beech pulp, the impact of blending was less pronounced (7-12%). With higher beech pulp content (60-100%) in the mixed pulp, the water absorption after immersion remained unchanged.

Fig. 2b shows the effect of hardwood pulp addition to pine kraft pulp on initial water absorption. Increasing the hardwood pulp content in the mixed pulp resulted in the increase of initial water absorption by 1.6 to 3.2 times for beech pulp, by 1.4 to 2.4 times for aspen BCTMP, and 1.2 to 2.4 times for eucalyptus pulp.
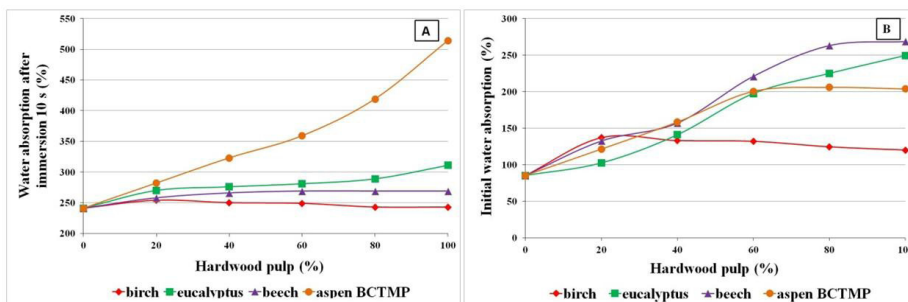
Fig. 2: Blending impact of bleached birch, eucalyptus, beech kraft pulp and bleached aspen BCTMP with bleached pine kraft pulp on water absorption after immersion (A) and initial water absorption (B).

Fig. 3a shows the effect of the hardwood pulp blending with the pine pulp on the tensile index. As a result of birch pulp blending, the tensile index increased slightly by 2-6%. With increase content of other type of hardwood pulps, the tensile index decreased. Tensile index of beech pulp blending dropped significantly already at its content of 20% (by 21%), and with a further content increase of 40-80%, the decrease was less pronounced (by 29-37%). On the contrary, the tensile index of aspen BCTMP decreased by 6% with its content of 20% in the mixture, while it declined more markedly at higher content (by 21-59%). The tensile index of the eucalyptus pulp blending declined evenly with content increasing by 4-17%. At 20% of content in the mixture, the tensile index of eucalyptus and aspen pulp was similar. The higher tensile index of birch pulp blending is due to the presence of longer fibres and a lower Runkel ratio. The effect of birch pulp blending with pine pulp has not been demonstrated significantly as both pulps have a similarly low Runkel ratio. Our results are different than those of published by Finn (Finn 1991), where the effect of birch pulp blending with pine pulp on tensile strength was also studied. However, in their work, °SR between pine pulp and birch pulp in the mixture differed.

The softness of the tissue paper can be measured directly as surface softness, e.g. by the tissue softness analyzer (TSA Emtec) or indirectly by the photoclinometric method with oblique surface illumination to determine the optical surface variability of tissue paper products (Gigac et al. 2019 a, b). The subjective pairwise method can also be used to determine the softness of hygiene products (Gigac et al. 2018). In our work, softness was determined as the bulk softness, calculated from the bending stiffness determined at 15° and 10 mm distance between the clamp and the knife-edge. The effect of hardwood blending on the bulk softness of the mixed pulps is shown in Fig. 3b. The addition of aspen BCTMP had no effect on bulk softness of mixed pulp. With content of 20% and 40% birch pulp in the mixture, the bulk softness increased slightly by 3%, and further addition had no effect. Increasing content (from 40%) of beech and eucalyptus pulp caused a significant decrease in bulk softness of mixed pulp; the curve of slope for both pulps was identical.
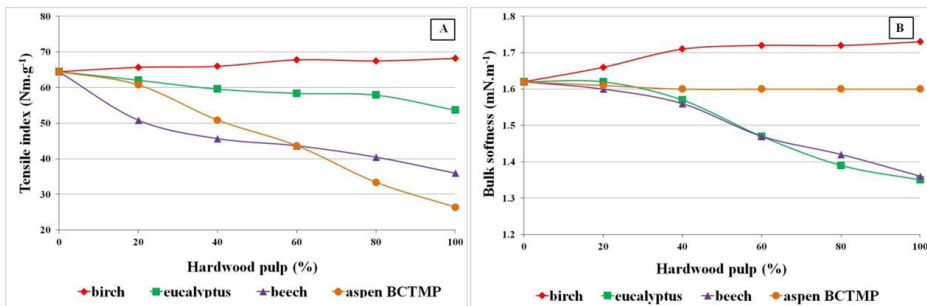
Fig. 3: Blending impact of bleached birch, eucalyptus, beech kraft pulp and bleached aspen BCTMP with bleached pine kraft pulp on tensile strength (a) and bulk softness (b).

Fig. 4a illustrates the effect of blending hardwood pulps with softwood pulp on the brightness. The brightness of bleached pine kraft pulp was 82.5% ISO. With birch and beech pulp addition, brightness increased by 0.1-1.5% ISO (birch) and by 0.1-0.7% (beech). Increased content of eucalyptus pulp resulted in a slight decrease in brightness by 0.4-1% ISO. In case of aspen BCTMP, a significant decrease in brightness by 3.8% ISO at content of 20% occurred, and further addition in the mixture led only to a minimal change. Fig. 4b shows the blending effect of hardwood pulps with pine pulp on the coordinate b* value, which indicates the yellowness. Bleached pine kraft pulp had the coordinate b* value of 6.02. Increasing the eucalyptus content lead to a slight increase in the coordinate b* value, while a significant increase in the coordinate b* occurred with increasing of aspen BCTMP content in the mixed pulp. Increasing of beech and birch pulp proportion in the mixture resulted in a decrease in the coordinate b* value, the shape of both curves was identical.
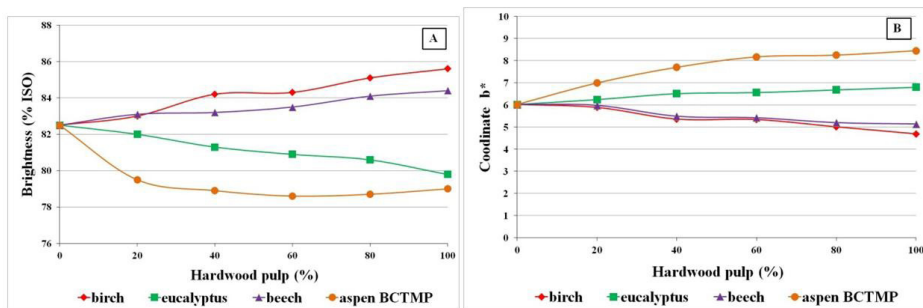
Fig. 4: Blending impact of bleached birch, eucalyptus, beech kraft pulp and bleached aspen BCTMP with bleached pine kraft pulp on brightness (a) and coordinate b (b).*

Selection of mixed pulp for tissue paper

Fig. 5 shows a relationship between tensile index and water absorption after immersion (A); and between tensile index and the initial water absorption (B) of mixed pulps. Bleached pine kraft pulp had the high tensile index (64.5 $\mu m \cdot g^{-1}$) but water absorption after immersion (241%) and the initial water absorption (85%) were low. The aim of blending of hardwood beech, eucalyptus or aspen BCTMP with pine pulp was to increase the tensile index and retain good water absorption.

The most suitable pulp appears to be eucalyptus pulp of 20-80% content in the mixture when higher water absorption after immersion of 270-289% and tensile index of 57.9-62.1 Nm·g^{-1} as well as brightness of 80.6-82% ISO were found (Fig. 4a). The initial water absorption at this eucalyptus pulp content in the mixture was high (198-225%; Fig. 5b). With increasing content of the aspen BCTMP, the water absorption after immersion markedly increased (323-514%), but the tensile index dropped significantly to 26.4-50.9 Nm·g^{-1} even with content of 40%. A content of 20% aspen BCTMP enabled higher water absorption after immersion (282%) as well as high tensile index of 60.8 Nm·g^{-1} and coordinate b* value (6.99, Fig. 4b), whereas brightness was lower (79.5% ISO, Fig. 4a). For tissue papers, however, the water absorption after immersion is more beneficial than the initial water absorption. The mixture with bleached birch kraft pulp had high tensile index (65.7-68.2 Nm·g^{-1}), but low water absorption after immersion as well as the initial water absorption, which were not affected by increased its content (243-254% and 120-137%). The mixture of beech pulp with pine pulp had high initial water absorption (221-269%) at higher content of beech pulp, but very low tensile index (36-43.7 Nm·g^{-1}). The water absorption after immersion of this mixture was lower than of the mixture of eucalyptus kraft pulp or aspen BCTMP with pine kraft pulp.

Fig. 5: Relationship between tensile index and water absorption after immersion (a); and between tensile index and initial water absorption (b) of the mixture of bleached birch, eucalyptus, beech kraft pulps and aspen BCTMP (20, 40, 60, 80 and 100%) with bleached pine kraft pulp.

In Fig. 6 is a relationship between bulk softness and water absorption after immersion (A); and between bulk softness and initial water absorption (B) of the mixed pulps. Bleached pine kraft pulp with high tensile index had higher bulk softness (1.62 m·N^{-1}) but low water absorption after immersion as well as initial water absorption. Although birch pulp of 40-100% content in the mixture had higher bulk softness (1.69-1.73 mN^{-1}) and tensile index (59.7-68.2 Nm·g^{-1}) and brightness (84.2-85.6% ISO, Fig. 4a), absorption properties were low (243-250% and 120-133%). The mixture of birch pulp with pine pulp is suitable for the production of tissue paper which requires high softness and dry strength, but the drawback is low water absorption. After addition of 20% beech pulp to pine pulp, higher bulk softness (1.60 mN^{-1}) with good water absorption after immersion (258%) was reached (Fig. 6a), but the tensile index was low (50.9 Nm·g^{-1}, Fig. 5). The addition of aspen BCTMP to pine pulp resulted in a high bulk softness (1.60-1.65 mN^{-1}) and also water absorption after immersion (282-514%); and at the aspen BCTMP content of 20%, higher tensile index (60.8 Nm·g^{-1}, Fig. 5) was also obtained.

Mixed pulp with a 20% of eucalyptus pulp had high tensile index of 62.1 Nm·g^{-1} as well as bulk softness of 1.63 mN^{-1} and brightness of 82% ISO (Fig. 4a), although water absorption after immersion was slightly lower (270%) compared to aspen BCTMP, but was still higher than other

types of hardwood pulps in the mixture. Thus the mixture of low content of eucalyptus pulp can be more preferably used for toilet paper and facial papers production where softness is the most important property while absorbency is not being targeted as the most important. However, water absorption can be further increased by rising of eucalyptus pulp proportion to 60%, when the water absorption after immersion of 281% and tensile index of 58.4 Nm·g^{-1} were reached; the disadvantage was reduction of bulk softness (1.47 mN^{-1}). Thie higher eucalyptus content blending could be suitable for the manufacture of tissue papers, where not such a high softness is required as kitchen towels or napkins, or higher softness could be achieved after subsequent treatment of the paper e.g. by creping.
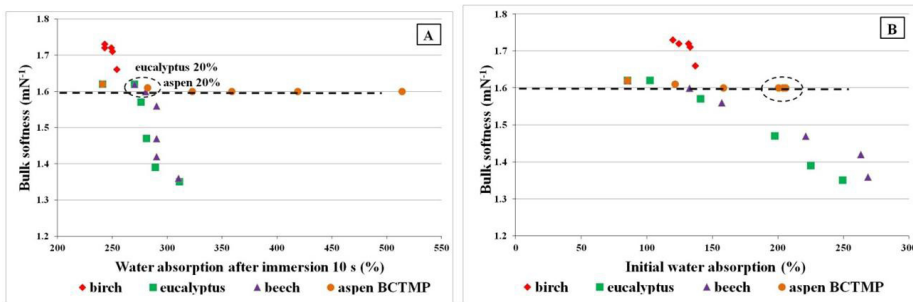

Fig. 6: Relationship between bulk softness and water absorption after immersion (a); and between bulk softness and initial water absorption (b) of the mixture of bleached birch, eucalyptus, beech kraft pulps and aspen BCTMP (20, 40, 60, 80 and 100%) with bleached pine kraft pulp.

CONCLUSIONS

The mixed pulp from bleached beech kraft pulp and bleached pine kraft pulp had good initial water absorption but low bulk softness, the problem also was a low tensile index, even at very low content of beech pulp in the mixture. The mixture of bleached birch kraft pulp with bleached pine kraft pulp had high tensile index as well as bulk softness, but a very poor absorbency, even at low content of birch pulp. The mixed pulp with 20% of aspen BCTMP has proven to be suitable for the production of tissue papers with high tensile index, bulk softness as well as high absorption capacity. This type of mixed pulp is optimal for the production of tissue products where high brightness is not required, but on the contrary, where higher yellowness is desired. Further increasing of aspen BCTMP content in the mixture with bleached pine kraft pulp has shown to be undesirable as it has an adverse effect on the tensile index. Bleached eucalyptus kraft pulp with a 20% addition to bleached pine kraft pulp has shown to be suitable for the production of tissue papers with higher bulk softness and tensile index and moderately high absorbency and high brightness. Higher content (40-60%) of bleached eucalyptus kraft pulp in the mixture increased the water absorption as well as tensile index but it reduced the bulk softness. The mixed pulp with a higher proportion of bleached eucalyptus kraft pulp can be used to produce kitchen towels that do not require such high softness; also after subsequent treatment e.g. creping can be used to produce other types of tissue paper.

ACKNOWLEDGMENTS

REFERENCES

1. Annergren, G., Hagen, N., 2007: Industrial beating/refining. In: Pulp and Paper Chemistry and technology. Vol.3., Paper Chemistry and technology, Ek, M., Gellerstedt, G., Henriksson, G, eds., Pp 121-137.
2. Assis, T.D, Reisinger, L. W., Pal, L., Pawlak, J., Jameel, H., Gonzalez, R. W., 2018: Understanding the effect of machine technology and cellulosic fibers on tissue properties - A Review. Bioresources 13(2): 4593-4629.
3. Axelsson, B., 2001: Pulp for high absorption tissue products. Paper Technology 42(7): 24-26.
4. Bajpai, P. 2018: Biermann's handbook of pulp and paper. Vol. 2: Paper and board making. Marinakis, H.K. ed, Elsevier, UK, Pp 1-34.
5. Chauhan, V.S. Kumar, N., Kumar, M., Chakrabarti, S.K., Thapar, S.K., 2011: Effect of separate and mixed refining of hardwood and softwood pulps on paper properties. Journal of Korea TAPPI 43(4): 1-10.
6. Chang, C.I., Yu, S.T., Perng, Y.S., 2018: Effect of furnish and refining on properties of household paper. Cellulose Chemistry and technology 52(5-6): 433-440.
7. Cheyne, D.A., 1990: An introduction to market aspen bleached chemi-thermomechanical pulp and thermomechanical pulp. Aspen Symposium '89: Proceedings. General Technical Report NC-140. North Central Forest Experiment Station Forest Service, U.S. Department of Agriculture St. Paul, Minnesota, Pp 275-281.
8. Daub, E., Sindel, H., Göttsching, L., 1986: Absorption von Flüssigkeiten in Papier, Das Papier 40(5): 188-197.
9. Finn, D.K., 1991: Increasing the hardwood content on the furnish by separate refining. Paper Engineering Senior Theses 118, Western Michigan University, Pp 1-22.
10. Fišerová, M., Gigac, J., Stankovská, M., Opálená, E., 2019: Influence of bleached softwood and hardwood kraft pulps on tissue paper properties, Cellulose Chemistry and Technology 53(5-6): 469-477.
11. Gigac, J., Fišerová, M., 2008: Influence of pulp refining on tissue paper properties. Tappi Journal 7-8: 27-32.
12. Gigac, J., Fišerová, M., Stankovská, M., Opálená, E., 2018: Correlation between subjective and objective assessment of hygienic paper products softness (in Slovak), Papír a celulóza 73(3-4): 52-56.
13. Gigac, J., Fišerová, M., Stankovská, M., Maholányiová, M., 2019a: Prediction of water-absorption capacity and surface softness of tissue paper products using photoclinometry. O Papel 80(8): 91-97.
14. Gigac, J., Stankovská, M. Fišerová, M., 2019b: Evaluation of water-absorption capacity and surface softness by optical surface variability (in Slovak). Papír a celulóza 74(1): 12-16.
15. Gomes, V.J., Ribeiro, A., Colodette, J.L., 2011: Alteration in the content of xylan in eucalyptus pulp for tissue paper production. In: 5th International Colloquium on Eucalyptus Pulp, Porto Seguro, Brazil, Pp 1-6.

16. Grandfeldt, T., Dahlin, H., 2003: Hardwood BCTMP - improves bulk, smoothness and opacity. Paper Technology 2003: 43-46.

17. Haynes, R. W. 1990. An analysis of the timber situation in the United States: 1989-2040. Gen. Tech. Rep. RM-GTR-199. Fort Collins, CO: U.S. Department of Agriculture, Forest Service, Rocky Mountain Forest and Range Experiment Station. 268 pp.

18. Hu, K., Ni, Y., Zou, X., Zhou, Y., 2006: Impact of aspen BCTMP applying to wood-free LWC on its performance. Part I. Synergy basestock properties. Tappi Journal 5(3): 21–26.

19. Johnsson, G.E., 1978: Mechanical pulp in tissues, fine papers, and boards. Paper Age 14(5): 14-34.

20. Kim, J.J., Shalev, I., Barker, R.L., 1994: Softness properties of paper towels. Tappi Journal 77(10): 83-89.

21. Lumiainen, J.J., 1996: Refining of fine paper fibres-separate or mixed refining? Papermakers Conference Proceedings, Atlanta, USA, Pp 175-186.

22. Morais, F.P., Bértolo, R.A.C., Curto, J.M.R., Amaral, M.E.C.C., Carta, A.M.M.S., Evtyugin, D.V., 2019: Comparative characterization of eucalyptus fibers and softwood fibers for tissue papers applications. Materials Letters: X 4:100028-100032.

23. Nanko, H., Button, A., Hillman, D., 2005: The world of market pulp. Swann, C.E: Ed., Appleton, Wisconsin, USA: WOMP, LLC. TAPPI Press, 274 pp.

24. Schönberg, C., Oksanen, T., Suurnäkki, A., Kettunen, H., Buchert, J., 2001: The importance of xylan for the strength properties of spruce kraft pulp fibres. Holzforschung 55(6): 639-644.

25. Stankovská, M., Gigac, J., Fišerová, M., Opálená, E., 2019: Relationship between structural parameters and water absorption of bleached softwood and hardwood kraft pulps. Wood Research 64(2): 261-272.

*Monika Stankovská, Mária Fišerová, Juraj Gigac, Elena Opálená
Pulp and Paper Research Institute
Dúbravská Cesta 14
841 04 Bratislava
Slovak Republic
*Corresponding author: stankovska@vupc.sk

GENE POOL OF SCOTS PINE (*PINUS SYLVESTRIS* L.)
UNDER REFORESTATION IN EXTREME ENVIRONMENT

Yulai Yanbaev, Rida Sultanova, Liubov Blonskaya
Svetlana Bakhtina
Bashkir State Agrarian University
Russia

Albina Tagirova, Vadim Tagirov
Bashkir State University
Russia

Aleksey Kulagin
Ufa Institute of Biology of Ufa Research Center of Russian Academy of Sciences
Russia

ABSTRACT

The article is devoted to the study of the gene pool formation mechanisms of arboreal plant populations at the sites of mining and processing of mineral resources and may be useful in managing the processes of natural forest remediation of disturbed lands. The aim of the research is to study the genetic diversity and spatial differentiation of the Scots pine (*Pinus sylvestris* L.) undergrowth thriving on the industrial waste discharge of the Uchaly Mining and Processing Plant (the Southern Urals).

Isoenzymes of 7 enzymes were used as markers (encoded by 10 polymorphic loci Aat-1, Aat-2 and Aat-3, Gdh-1, Fdh-1, Lap-1, Lap-1, Skdh-1, 6-Pgdh-1 and Dia-1), separated by polyacrylamide disc electrophoresis. Genetic variability of the undergrowth under the forest canopy (7 samples, average number of avenues per locus A = 2.3-2.8, the observed heterozygosity was $H_O = 0.207 - 0.260$, the expected heterozygosity $H_E = 0.201 - 0.273$) and in industrial waste discharges (4 samples, A = 1.9 - 3.1, $H_O = 0.225 - 0.277$; $H_E = 0.240 - 0.298$) varies over a wide range. In the parent stand, the observed heterozygosity ($H_O = 0.203$) was lower than in any of the undergrowth samples. A comparatively high genetic differentiation of the undergrowth was found (the between-sample subdivision F_{ST} index was 3.8%, the average Nei genetic distance $D_{Nei} = 0.015$ with changes in individual pairs from 0.003 to 0.032), comparable with genetic differences in geographically separated populations.

KEYWORDS: Gene pool, *Pinus sylvestris*, undergrowth, enzymes, markers, heterozygosity.

INTRODUCTION

Industrial pollution of environment today has reached menacing proportions. Particularly serious are the consequences of the activities of mining and processing enterprises in mineral production region. According to official data *State report on natural resources condition and the environment of the Republic of Bashkortostan. Ministry of Environment and Ecology of the Republic of Bashkortostan (2017)*, in the Republic of Bashkortostan (Russia) about 3,000 deposits and manifestations of 60 types of mineral raw materials are discovered. The reserves of the main metal minerals are: copper – 4,686.3 thousand tons, zinc – 5005.5 thousand tons. Here, from the middle of the last century, the Uchalinsky Mining and Processing Plant, its branch in Sibay, the Bashkir Copper-Sulfur Plant, the Buribaevsky Mining and Processing Plant, the 'Bashkir Med' Ltd Enterprise and other mine 10-12% of copper and about 50% of zinc of all the mineral production in Russia. The large scale and duration of the mining and processing of ore, the open method of mining (Fig. 1) led to significant environmental pollution by such highly toxic components of ores (Chudzińska et al. 2014) as copper, zinc, iron, cadmium, lead, bismuth, cobalt, selenium, tellurium, sulfur, antimony, fluorine, etc. for example, compared to background values, wastewater in the area of industrial waste discharges of zinc and copper are 31-102 times and 374-6074 times more, respectively (Belan 2005). In soils bulk compounds of zinc are 5-50 times more than background indicators, copper are more than up to 10 times. The concentration of active forms of Cu in the soil reaches 12 and Zn –3.3 admissible concentration limit. Heavy metals, migrating through the food chain, pose a threat to plants and animals and human health. For this reason, the work on the remediation of such man-made territories is extremely important (Mahar et al. 2016).

Taking into consideration the high cost of such works, in the conditions of Russia in the forest zone, the use of natural overgrowing of man-made territories by trees and shrubs is promising. Such a pioneer species as Scots pine (*Pinus sylvestris* L.), which is one of the main forest formers of Eurasia, has a particularly high potential (Gabdrakhimov et al. 2018, Sultanova et al. 2018). For this reason, studies of plant adaptation mechanisms to extreme environmental conditions in man-made areas are relevant (Kulagin and Tagirova 2015). The effect of industrial pollution on genetic variability, intra- and inter-population differentiation in scots pine stands has been studied in sufficient detail (Yanbaev 2002, Chudzińska et al. 2014, Prus-Głowacki and Nowak-Bzowy 1992, Sherameti and Varma 2015). We studied the subpopulations of the same stand, damaged by industrial pollutants in varying degrees (groups of "resistant" and "sensitive" trees). The indicators of genetic polymorphism of different generations of populations were also compared. But the reproduction peculiarities of the population's gene resources in young stand with the overgrowing of man-made territories by this species have little if any been studied. In Poland, comparative studies of polymorphism of 10 isoenzyme loci of 10-15 years old young stand growth that thrive under zinc contamination conditions and 9 natural crops outside the territory of technogenic pollution have been carried out (Prus-Głowacki and Nowak-Bzowy 1992). The revealed significant differences in the genotypic composition of these age groups indicate the prospects of such research for studying the adaptive strategy of a species under the conditions of technogenesis. Knowledge of the genetic structure formation mechanisms of the new generation of pine forests in the man-made areas can be useful not only for science, but also for managing the necessary processes of natural forest remediation of disturbed lands. The purpose of this research is to study the genetic diversity and differentiation of the common pine undergrowth, which grows under the conditions of heavy metals contamination.

MATERIALS AND METHODS

On the territory of the Uchaly Mining and Processing Plant (hereinafter UMPP, geographic coordinates of its center: N 54°18′33″ and E 59°25′22′), natural pine and birch forests (Fig. 1) come from the northern and eastern sides of the quarry, which are the source of seed supply and reforestation of industrial waste discharge. Basically, undergrowth of Scots pine of different thickness and age is available at the foot and slopes of industrial waste discharge.

Fig. 1: Territory of the Uchaly mining and processing plant. Red arrow – the location of collected samples.

In this part of their perimeter in 7 clumps of trees (trial plots are designated as SDU1, SDU2, SDU3, SDU4, SDU5, SDU6 and SDU7), 32 samples of undergrowth were selected from which winter buds were collected for laboratory analysis. The samples were also collected from 32 trees of a nearby pine stand (TSU), located northeast at a distance of about 300 m from the waste discharges. 32 samples of buds were divided into 4 groups of undergrowth (SSU1, SSU2, SSU3, SSU4) growing under the canopy of this plantation, which stretches for 5 km along the eastern side of the waste discharges. One more sample (SDS) of the same size is the undergrowth of industrial waste discharge of another enterprise located about 200 km to the south of the Bashkir Copper-Sulfur Plant. The age of the undergrowth in all cases was up to 20 years.

Molecular and genetic DNA markers are increasingly being used for population genetic studies of arboreal plants (Forrest et al. 2000), including the use of highly efficient methods of new generations (Blanc-Jolivet et al. 2018). However, in this research, we used enzyme electrophoresis and isoenzyme markers. This allowed us to compare the data obtained with the previously obtained extensive results of studying the genetic structure of natural populations of Scots pine in the Southern Urals (Yanbaev 2002), as well as from scientific literature (Chudzińska et al. 2014, Forrest et al. 2000, Goncharenko et al. 1993, Larionova and Ekart 2011, Prus-Głowacki and Nowak-Bzowy 1992, Savolainen and Hedrick 1995, Sherameti and Varma 2015, Wójkiewicz et al. 2016). The enzymes were extracted using 0.1 M Tris-HCl (pH 8.0) buffer containing 17% of sucrose, 0.1% 2-mercaptoethanol and 0.05% of sodium diethyldithiocarbamate. A portion of 200 mg hybernaculum pieces was ground in a porcelain mortar with the addition of 1 ml of chilled extraction buffer. To bind polyphenols, about 200 mg of insoluble Polyclar AT polyvinylpyrrolidone was added before. The homogenate was centrifuged for 20 minutes at 15-17 thousand rpm in the refrigerator. The separation of isoenzymes was carried out by

the method of disk electrophoresis in vertical plates of 7.5% polyacrylamide gel with a pH of separating gel of 8.9 (Davis 1964, Ornstein 1964) using a tris-glycine electrode buffer with a pH of 8.3. Histochemical detection of enzyme activity zones in gels was carried out according to standard methods (Larionova and Ekart 2011) with minor modifications. We studied the variability of aspartate aminotransferase (AAT, E.C. 2.6.1.1), glutamate dehydrogenase (GDH, 1.4.1.2), formate dehydrogenase (FDH, E.C. 1.2.1.2.), Leucine aminopeptidase (LAP, 3.4.11.1), shikimate dehydrogenase (SKDH, 1.1.1.25.), 6-phosphogluconate dehydrogenase (6-PGD, 1.1.1.44) and diaphorase (DIA, 1.6.4.3).

To characterize the variability and the level of division of populations, 10 polymorphic loci were used: Aat-1, Aat-2 and Aat-3, Gdh-1, Fdh-1, Lap-1, Lap-1, Skdh-1, 6-Pgdh-1 and Dia-1 (Yanbaev 2002). To analyze the level of genetic variability and differentiation of samples, the indicators determined by the BIOSYS-1 program (Swofford and Selander 1981) are used – the frequency of alleles, their number per locus (including using the 5% criterion), the observed and expected heterozygosis, the level indicator of the inter-election subdivision of F_{ST} of Wright's F statistics, M. Nei's genetic distance D (Nei 1972). The differences in the observed distributions of genotypes and their expected frequencies at the Hardy-Weinberg equilibrium were determined using the standard - criterion. In addition, for this purpose, a test was also used with a combination of genotypes into three classes: 1) a homozygous for the main allele, 2) a heterozygote for the main allele, 3) all other genotypes. These calculations were performed using the GSED program (Genetic Structures from Electrophoresis Data (GSED) (Elizabeth M. Gillet).

RESULTS

In the studied samples, only two loci were diallel – Aat-1 and Dia-1. The remaining loci had three alleles (3 loci), four alleles (3 loci), and five alleles (3 loci). The maximum number of alleles, six, was detected at 1 locus (Tab. 1). In the remaining three loci with 4 alleles, not only rare allozymes were revealed - polymorphism was also found for more frequent alleles. In the reforestation of anthropogenic land of UMPP involved not only the nearby stand, but also other, more distant, pine stand. This is proved by the fact that almost half of the identified alleles of young undergrowths (18 out of 39 or 46.2%) are not found in the trees of the nearby stand. As a pioneer species, scotch pine is capable of efficiently spreading seeds over relatively long distances, which should lead to the formation of a genetically homogeneous seed pool. However, a particularly high concentration of certain alleles in individual habitats was noted.

Tab. 1: The number of alleles at the given Loci.

Locus	No. of Alleles
Aat-1	2
Dia-1	2
GDH	3
Lap-1	4
Lap-2	4
Skdh-1	4
Aat-2	5
Aat-3	5
Fdh-1	5
6Pgdh-1	6

For example, the 6-Gdh-1[3] allele was not found in 8 undergrowth samples, in 2 of them, two plants are carriers of the allele with a frequency of 0.016. But in one sample it is found with a frequency of 0.125. In loci that showed a particularly high inter-sampling subdivision, deviations of the observed distributions of genotypes from theoretically expected frequencies were revealed (Tab. 2).

Tab. 2. Loci with deviations of genotype distribution.

Sample	Locus	Deviation from expected genotype distribution, significance level
SDU3	6-Pgdh-1	$p < 0.01$
SSU3	Lap-2	$p < 0.01$
	Skdh- 1	$p < 0.01$
SSU4	Lap-2	$p < 0.05$
	6-Pgdh-1	$p < 0.01$
SDU1	6-Pgdh-1	$p < 0.05$

In our opinion, this phenomenon is associated with a relatively large contribution of individual mother trees to the formation of undergrowth in one or another part of industrial waste discharges. The parent stand adjacent to the waste discharges is pine-birch, in which the proportion of Scots pine varies greatly. In some places, the 'wall' of the stand is very dense due to thick birch and young pine forest. Fruit-bearing Scots pine trees of the reproductive age are sometimes rarely represented along the planting boundary. Under these conditions, a local concentration of certain parent alleles, less frequent in the entire population, or a decrease in their frequencies can be observed.

The average sample of undergrowth in the area of UMPP reveals a relatively high allelic diversity compared with the parent stand. This superiority is due to rare alleles. With the introduction of a 5% polymorphism criterion, the indicator ($A = 1.7 \pm 0.1$) decreases even to a lower level compared to a sample of trees. The expected heterozygosity of the undergrowth on the man-made lands of UMPP ($H_E = 0.264 \pm 0.007$) and the trees in the parent stands are almost the same. But in the parent stands, the observed heterozygosity ($H_O = 0.203$) was lower than in any of the undergrowth samples. This phenomenon may be the result of a relatively high proportion of rare alleles in the reforestation of industrial waste discharges and adjacent man-made lands (for statistical reasons, the probability of their meeting in a homozygous state is less).

Genetic variability in groups of undergrowth samples under the forest canopy ($A = 2.5 \pm 0.1$, changes from 2.3 to 2.8; $H_O = 0.234 \pm 0.011$, 0.2007-0.260; $H_E = 0.247 \pm 0.016$, 0.0101.2.273) and on industrial waste discharges ($A = 2.4 \pm 0.2$ 1.9-3.1; $H_O = 0.244 \pm 0.007$, 0.225-0.277; $H_E = 0.262 \pm 0.007$, 0.240-0.298) varies over a wide range.

Tab. 3: Frequencies and proportion of genetic variation in Loci.

Locus	Frequency of change in genetic composition	Proportion of genetic variation, F_{ST} (%)
Skdh-1	0.844-0.969	1.9
Aat-2	0.625-0.766	2.4
Fdh-1	0.828-0.969	2.0
Lap-2	0.844-1.000	6.5
Aat-3	0.604-0.800	1.2
Dia-1	0.625-0.875	3.6
Gdh-1	0.594-0.908	6.1
6Pgdh-1	0.438-0.906	6.9

The studied samples of common pine undergrowth are located at a short distance from each other – on a plot of about twelve square kilometres. However, the allele frequencies revealed a relatively high level of differences in the undergrowth samples. Only at the Aat-1 and Lap-1 locus practically invariant alleles were found (Tab. 3). Some alleles show a particularly large genetic subdivision of the undergrowth samples of the man-made area of UMPP zone (Fig. 2).
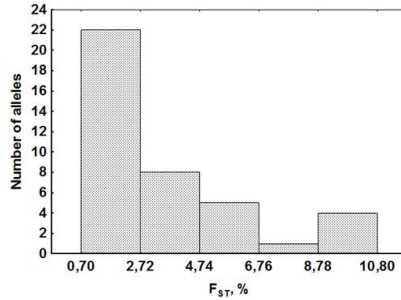

Fig. 2: Distribution of alleles by intersectional division.

For example, F_{ST} values were 0.070 (6-Pgdh-12 allele), 0.089 (6-Pgdh-16), 0.100 (6-Pgdh-11), 0.092 (Gdh-13), 0.108 (Lap-22). The relatively large heterogeneity of the studied samples according to the number and frequency of alleles is not a consequence of the inclusion the stand (TSU sample) and undergrowth from industrial waste discharges of another mining enterprise (SDS) into the analysis. Confirmation of this was obtained when calculating not only the indicator of inter-sampling subdivision of F_{ST} (on average, per one locus 3.8%), but also genetic distances between samples. On average, a value of D = 0.015 is obtained with changes in individual pairs from 0.003 to 0.032.

Tab. 4: The number of pairwise genetic distances between samples.

Pairwise genetic distance between samples, D	Nº of cases
0.001-0.006	15
0.006-0.013	29
0.013-0.019	26
0.019-0.026	13
0.026-0.032	5

With the exclusion from the analysis of the parent stand and the selection of undergrowth from the Bashkir copper-sulfur plant waste discharges, this value decreases insignificantly to D = 0.012 (0.003-0.028). The pairwise genetic distances between the samples varied significantly (Tab. 4).

DISCUSSION

Scotch pine (*Pinus sylvestris* L.) is a well studied species from the population-genetic point of view (Prus-Głowacki et al., 2006, Savolainen et al. 2011, Kujala et al. 2017, Wachowiak et al. 2011, Wójkiewicz et al. 2016). Comparison with the literature data allowed us to conclude that the level of inter-sampling differentiation of undergrowth identified by us on the man-made lands of the Uchaly Mining and Processing Plant was typical for differences in geographically separated populations: South Urals, North-West Russia (Yanbaev 2002), Eastern Europe and Siberia (Goncharenko et al. 1993), Krasnoyarsk Territory, Khakassia, Tuva and Altai Mountains (Larionova and Ekart 2011). The main cause of this phenomenon may be a large variability of sites in man-made polluted lands and industrial waste discharges.

Technogenic ecotopes here are highly differentiated topographically, according to the degree of phytotoxicity of soils, and also differ in the physical, chemical, mechanical, fractional and particle-size properties of rock formations, in the rates of primary soil formation (in many reforestation areas, there is physical weathering and accumulation of organic matter). Undoubtedly, such differences in environmental conditions should have a strong influence on the survival rate and growth course of the undergrowth. To demonstrate this phenomenon, we measured the value of the annual increase in height for the undergrowth of four samples located on the surface of the waste discharges (SDU1, SDU2 and SDU3) at their foot at the edge of the stand (SSU4). The obtained data were compared with a one-year increase in the height of the undergrowth groups growing also in well-lit conditions, but outside the direct impact of industrial pollution of the UMPP at a distance of about 20 km from the enterprise. On average, annual growth in technogenic conditions ranged from 9.5 ± 1.5 cm (differences between plants within 4.1–20.2 cm, coefficient of variation is 50.6%) to 56.7 ± 1.6 cm (50.2-63.5 cm, 8.8%). In the control outside the industrial pollution zone, the following results were obtained: 57.2 ± 3.2 cm, 39.2-72.4 cm and 17.5%, respectively. Under natural conditions, as shown by a study, the annual growth of 28 undergrowth samples on abandoned agricultural lands (Tagirov et al. 2015) outside the direct impact of UMPP variability is much lower. Therefore, it is the contrast of the environmental conditions of the man-made lands of the enterprise that could cause such large differences in the growth of the young trees from different habitats of the man-made lands. Accordingly, plants from such different ecotopes should be subjected to different pressures of natural selection, which may lead (Prus-Głowacki and Nowak-Bzowy 1992) to a more pronounced differentiation in terms of genotypic composition. In this case there is a definite parallel with the effect of increasing the level of genetic differences in populations located in natural conditions in ecologically contrasting habitats. For example, 8 stands in the Tomsk region (the distance between 7 of them did not exceed 16 km, and one is located 130 km from them) differed in the frequencies of alleles of isozyme loci even more than the populations of different regions - Krasnoyarsk Territory, Khakassia, Tuva and Altai Mountains (Larionova and Ekart 2011). However, in these researches, inter-sampling differences were determined at the population level.

Reproduction issues of the natural populations' gene pool of forest trees in technogenic conditions have attracted the researchers' attention all the time. A review of the results in this field obtained in 1991–2013 is given in the publication (Sherameti and Varma 2015). It has been

shown that acute technogenic pollution leads to an increase in the heterozygosity of populations, partly owing to the peculiarities of the Scots pine breeding system. The species is characterized by inbreeding, the level of which depends on many environmental conditions (density of stands, climatic and weather conditions, flowering intensity, etc.) (Forrest et al. 2000). Young inbreeding individuals having a reduced viability and weaker growth due to inbreeding depression. In relatively favorable environmental conditions they are able to survive the early stages of ontogenesis (embryos, seedlings, undergrowth). But under extreme environmental conditions for Scots pine, the process can be eliminated more quickly, which leads to a greater increase in the observed heterozygosity of the surviving individuals. Perhaps this mechanism partially explains the greater heterozygosity of the undergrowth of industrial landfills compared with the maternal population, which arose more than 50 years ago till the creation of UMPP before the increase in pressure of natural selection due to its action. This process can be the cause of the revealed increase in allelic diversity in young growth on industrial dumps, since rare alleles from a theoretical point of view should be more often in a heterozygous state.

The selective advantage possibility of individuals of various isozyme loci which are heterozygous for the alleles is discussed in the literature (Chudzińska et al. 2014). On the other hand, the evaluation of the association of 6 quantitative characteristics with heterozygosis in 12 isozyme loci did not reveal their relationship (Savolainen and Hedrick 1995). This paper argues that a positive association can only be found with a very small population size, inbreeding, and high intrapopulation spatial structuring. In this case, the phenomenon of the 'apparent' advantage of heterozygotes, caused by other factors, and not the selectivity of alleles of isozyme loci in the heterozygous state, can manifest itself. At the same time, it is not excluded that under conditions of acute technogenic pollution of Scots pine stand with heavy metals, metabolically important enzymes can influence the formation of homo- and heterozygosity of populations (Chudzińska et al. 2014). But testing this possibility requires a separate study, involving genes that have a selective role. Our work, apparently, is the only research containing the evidence of increased intrapopulation differentiation and the formation of a relatively high genetic diversity of the Scots pine undergrowth in technogenic conditions on isozyme loci. Only in one paper (Prus-Głowacki and Nowak-Bzowy 1992) the polymorphism of ten isozyme loci of one sample of 10–15 year-old young growth growing under conditions of zinc contamination was studied. But the results obtained were not compared with similar data on the parent stand, but with the genetic diversity of 9 natural stands of Poland in areas outside the direct impact of industrial pollution.

Technogenic pollution of land is currently becoming a problem of the planetary level. In (Mahar et al. 2016) there is the information that there are more than 3.5 million polluted habitats in the European Union alone and about 600 thousand hectares are polluted with heavy metals in the USA is given The scale of the problem, the high cost of technical remediation methods stimulate the development of methods of phytoremediation for the extraction of heavy metals from the environment with plants and their accumulation in the roots and the aerial parts in metabolites in a less dangerous form. A recent review plants of 414 species - the hyperaccumulators of a heavy metal are listed (Midhat et al. 2019). Herbaceous plants dominate in this recommended list, although arboreal plants such as Scotch pine are well-known by the advantages for phytoremediation of polluted lands. Among them are resistance to heavy metals, the ability to grow in a wide range of environmental conditions, a developed root system and a large above-ground biomass, growth rate, etc. Particularly important are such bioecological properties as the abundance and long range of seed dispersal, their high germination capacity, which make it possible to effectively colonize new man-made habitats without human intervention. As a result of this study, it was shown that, in the technogenic zone of the mining enterprises, the undergrowth

also forms a rich gene pool reproducing the gene resources of the local Scots pine population. It is spatially structured, which increases the resistance of the entire population to the effects of harsh industrial pollution. This is another argument for the point of view (Kulagin and Tagirova 2015) that leaving man-made lands for forest remediation — natural reforestation is promising, and this process should also be facilitated.

CONCLUSIONS

In extreme environment, the living organisms can form specific adaptation mechanisms not only to survive but also to multiply successfully. Thus, species with a broader range of ecological requirements are likely to reach domination.

This study is devoted to a phenomenon when the Scots pine not only survives under extreme conditions but also becomes genetically heterogeneous within one population and this heterogeneity is greater than it is usually observed in natural communities.

Such an adaptability enables the spread across territories that are extremely unfavorable for other plant species and exploited by humans. Findings may be used in large-scale cost-effective forest growing. Pine seedlings with a high adaptive potential and genetic heterogeneity are able to form stable communities in other technologically polluted areas. As a core of such pioneer communities, the emerging plant associations will be gradually enriched by other species of plants and animals that inhabit them. Thus, biodiversity in technologically polluted area will increase.

The continuation of this study seems necessary to answer such important questions: how widespread can be this scenario, how is it implemented on industrial lands with other availability of seeds? Moreover, the use of DNA markers that can detect the level of genetic population differentiation more informatively will be a promising solution.

REFERENCES

1. Belan, L., 2005: Ecological and geochemical state of the mining regions of the Bashkir Zauralye. Bulletin of the Orenburg state 6(44): 113-117.
2. Blanc-Jolivet, C., Yanbaev, Y., Kersten, B., Degen, B., 2018: A set of SNP markers for timber tracking of *Larix* spp. in Europe and Russia. Forestry 91(5): 614-628.
3. Chudzińska, E., Diatta, J., Wojnicka-Półtorak, A., 2014: Adaptation strategies and referencing trial of Scots and Black pine populations subjected to heavy metal pollution. Environmental Science and Pollution Research 21(3): 2165-2177.
4. Davis, B., 1964: Disc electrophoresis XI. Methods and application to human serum proteins. Annals of the New York Academy of Sciences 121: 404-427.
5. Forrest, I., Burg, K., Klumpp, R., 2000: Genetic markers: tools for identifying and characterizing Scotch pine populations. Forest Systems 9: 67-88.
6. Gabdrakhimov, K., Khayretdinov, A., Sultanova, R., Konashova, S., Konovalov, V., Sabirzyanov, I., Gabdelkhakov, A., Isyanyulova, R., Martynova, M., Blonskaya, L., 2018: Reproduction of stable pine forests in the Southern Urals. Journal of Engineering and Applied Sciences 13: 6494-6499.
7. Goncharenko, G., Silin, A., Padutov, V., 1993: Analysis of gene structure and differentiation in central and marginal *Pinus sylvestris* populations of Eastern Europe and Siberia. Silvae Genetica 29: 2019-2038.

8. Kujala, S.T., Knürr, T., Kärkkäinen, K., Neale, D.B., Sillanpää, M.J., Savolainen, O., 2017: Genetic heterogeneity underlying variation in a locally adaptive clinal trait in *Pinus sylvestris* revealed by a Bayesian multipopulation analysis. Heredity (Edinb) 118(5): 413-423.

9. Kulagin, A., Tagirova, O., 2015: Forest plantations of the Ufa industrial center: current state in the conditions of anthropogenic impacts Ufa. Gilem, Pp 66-71.

10. Larionova, A., Ekart, A., 2011: Isoenzyme diversity and differentiation of marsh Scotch pine (*Pinus sylvestris* L.) populations in the Western Siberia. Eurasian Journal of Forest Research 14(1): 21-28.

11. Mahar, A., Wang, P., Ali, A., Awasthi, M.K., Lahori, A.H., Wang, Q., Li, R., Zhang, Z., 2016: Challenges and opportunities in the phytoremediation of heavy metals contaminated soils: a review. Ecotoxicology and Environmental Safety 126: 111-121.

12. Midhat, L., Quazzani, N., Hejjaj, A., Ouhammou, A., Mandi, L., 2019: Accumulation of heavy metals in metallophytes from three mining sites (Southern Centre Morocco) and evaluation of their phytoremediation potential. Ecotoxicology and Environmental Safety 160: 150-160.

13. Nei, M., 1972: Genetic distance between populations. American Naturalist 106: 283-291.

14. Ornstein, L., 1964: Disc-electrophoresis I. Background and theory. Annals of the New York Academy of Sciences 121: 321-349.

15. Prus-Głowacki, W., Nowak-Bzowy, R., 1992: Genetic structure of a naturally regenerating Scots pine population tolerant for high pollution near a zinc smelter. Water, Air & Soil Pollution 62(3-4): 249-259.

16. Prus-Głowacki, W., Chudzińska, E., Wojnicka-Półtorak, A., Kozacki, L., Fagiewicz, K., 2006: Effects of heavy metal pollution on genetic variation and cytological disturbances in the *Pinus sylvestris* L. population. Journal of Applied Genetics 47(2): 99-108.

17. Savolainen, O., Hedrick, P., 1995: Heterozygosity and fitness: no association in Scots pine. Genetics 140: 755-766.

18. Jovanović V.S., Mitić V., Mandić S.N., Ilić M., Simonović S., 2015: Heavy metals in the post-catastrophic soils. In: Sherameti I., Varma A. (eds): Heavy metal contamination of soils. Soil Biology, Springer, Cham 44: 3-21.

19. Savolainen, O., Kujala, S.T., Sokol, C., Pyhäjärvi, T., 2011: Adaptive potential of northernmost tree populations to climate change, with emphasis on Scots pine (*Pinus sylvestris* L.). The Journal of Heredity 102(5): 526-536.

20. Sultanova, R., Gabdrahimov, K., Khayretdinov, A., Konashova, S., Konovalov, V., Blonskaya, L., Sabirzyanov, I., Martynova, M., Isyanyulova, R., Gabdelkhakov, A., 2018: Evaluation of ecological potential of forests. Journal of Engineering and Applied Sciences 13: 6590-6596.

21. Swofford, D., Selander, R., 1981: Biosys-1: a Fortran program for the comprehensive analysis of electrophoresis data in population genetics and systematic. Journal of Heredity 72: 281-283.

22. Tagirov, V., Yanbaev, Y., Tagirova, A., 2015: On environmental and genetic components of differences in growth in height of scotch pine on former farmlands. Bulletin of Bashkir University 20(3): 889-891.

23. Wachowiak, W., Salmela, M.J., Ennos, R.A., Iason, G., Cavers, S., 2011: High genetic diversity at the extreme range edge: nucleotide variation at nuclear loci in Scots pine (*Pinus sylvestris* L.) in Scotland. Heredity (Edinb) 106(5): 775-787.

24. Wójkiewicz, B., Cavers, S., Wachowiak, W., 2016: Current approaches and perspectives in population genetics of Scots Pine (*Pinus sylvestris* L.). Forest Science 62(3): 343-354.

25. Yanbaev, Y.A., Bairamgulov, N.R., Redkina, N.N., Mullagulov, R.Y., 2007: Differentiation among populations of the *Rhodiola iremelica* Boriss. (*Grassulaceae*) in the Southern Urals. Russian Journal of Genetics 43(11): 1314-1318.

Yulai Yanbaev*, Rida Sultanova, Liubov Blonskaya
Svetlana Bakhtina
Bashkir State Agrarian University
Federal State Budgetary Educational Institution of Higher Education
50-Letiya Octyabrya Street 34
450001 Ufa
Russia
*Corresponding author: Yanbaev_ua@mail.ru

Albina Tagirova, Vadim Tagirov
Bashkir State University
Federal State Budgetary Educational Institution of Higher Education
Zaki Validi Street 32
450076 Ufa
Russia

Aleksey Kulagin
Ufa Institute of Biology of Ufa Research Center of Russian Academy of Sciences
Prospect Octyabrya, 69
450054 Ufa
Russia

HEAT-INDUCED INKLESS ECO-PRINTING INSPIRED BY PAPER DISCOLORATION: A REVIEW

Peixing Wei
Southeast University
China

Wanyong Tuo
Anyang Institute of Technology
China

Sheng He
China National Bamboo Research Center
China

Guohua Liu
Jiangsu Vocational College of Agriculture and Forestry
China

ABSTRACT

In this paper, the art-of-the-state of heat-induced inkless eco-printing (HIEP) technology in recent years was summarized and prospected, mainly from the printing effect, degree of carbonization, environmental impact and feasibility. The main results were as following: (1) The paper used in HIEP is predominantly yellow in color, which enables a practical printing effect. (2) After HIEP, the paper exhibits no significant carbonized microstructure and keeps its high strength. (3) HIEP is an ecologically and environmentally preferable technology. Only a small amount of toxic products is generated, and no carcinogens are emitted. (4) No significant damage to the paper is evident following HIEP, as the degree of heat experienced during HIEP is far below that experienced during a thermogravimetric (TG) experiment. Additionally, the evaporated water has a buffering effect. Based on the previous research results, this paper finally pointed out the possible research direction in terms of discoloration mechanism and printing effect, environmental impact improvement, paper damage mechanism and strength during HIEP, high-temperature printing head installation and relevant techniques, optimization of printing process parameters.

KEYWORDS: Heat-induced inkless eco-printing (HIEP), carbonized microstructure, pyrolysis products, environmental impact.

INTRODUCTION

The histories of paper-making and printing go back approximately two thousand and one thousand years, respectively (Wang 2017). These inventions have made invaluable contributions to the recording of human history, the dissemination of culture and the advancement of science and technology and have laid the groundwork for modern printing. Based on thousands of years of improvement and the computer's emergence in the mid-twentieth century in particular, the printer has developed rapidly. In the 1960s, commercial dot matrix (White et al. 1984) and laser printers (Boutopoulos et al. 2014) were created, followed by the first inkjet printer in the 1970s (Park et al. 2007) and, later, thermal printing (Kishimura et al. 2005) and 3D printing (Gill and Kaplas 2009). These printing technologies can print not only varied patterns but also many complicated real 3D objects (Gill and Kaplas 2009, Henke and Treml 2012, Xin et al. 2013, Wang and Liu 2014). The authors classify printing techniques into two main types of methods: methods based on bump technology, including stone carving techniques and 3D printing, and coloring methods, which rely on the distribution of dye (typically involving the application of a "paint color" to a "base material", e.g., word printing in ancient China, laser printing and inkjet printing). Laser and inkjet printers can release significant volumes of fine particles, heavy metals, benzene, formaldehyde, styrene, and other carcinogens in the form of gases during printing (Jensen and Rold-Petersen 1979, Gallardo 1994, Bar-Sela and Shoenfeld 2008, Theegarten et al. 2010, Morawska et al. 2009, Yoo et al., 2009, Saraga 2011, Wang et al. 2012, Gigac et al. 2015), and there is currently no effective recycling system for printing waste. The disposal of these wastes can damage the environment and harm human health. The recycling of paper is also adversely affected when the paper is colored by toner or ink (Chantigny et al. 2000).

Thus, in recent years, the printing industry has conducted extensive research on inkless or zero-ink (Zink) eco-printing technologies, with a focus on developing a new and distinct type of printing paper (Comiskey et al. 1998, Garai et al. 2016, Hays 2015, Sun et al. 2015). For example, ZINK Imaging Incorporation introduced a printing paper containing a significant amount of crystalline dye (Song and Wang 2010). Based on the color changes in this paper induced by the creation of dye in response to the application of heat during the printing process, ZINK developed the Pandigital inkless printer (Song and Wang 2010). In the water-spraying-based inkless printing process, the paper used for printing must be pretreated with special chemicals. Below 35°C, the paper turns black upon contact with water. This black color vanishes after 22 hours, enabling this special paper to be reused (Sheng et al. 2015). Dell Incorporated introduced photographic printing based on the application of a special layer onto photo paper that can reflect light of different wavelengths and developed the Wasabi PZ310 mini-printer based on this technology. Other printing techniques have also been introduced that rely on inducing changes in the nanostructures of special materials on the surfaces of paper (Shestopalov et al. 2007, Choi and Park 2010, Shestopalov et al. 2010, Garai et al. 2016) or the use of liquid polymers (Yow and Routh 2006). All of the technologies mentioned above involve tailor-made printing paper. By contrast, Sun et al. (2009) proposed a new concept of inkless laser printing, whose mechanism was that paper color was changed instantaneously at ultra-high temperature. Additionally, laser carbonization printing (Yao and Zhao 2007) and the use of natural pigments (Rentschler 2005, El-Hennawi et al. 2012, Wataoka 2012) with ordinary printing paper represent different approaches to eco-printing technology. The severe carbonization induced in the printing region of the paper after laser carbonization printing and natural pigments can also be viewed as special inks, leading to the classification of these approaches as traditional coloring methods.

Inspired by the yellowing discoloration of plant fibers (Carter 1996, Davidson 1996, Beyer et al. 2005, Fromageot et al. 2006, Wang et al. 2015), the radically new concept of heat-induced inkless eco-printing (HIEP) was proposed in 2010 (Chen et al. 2010, Chen et al. 2012), which obviates the need for ink during the printing process while achieving the same printing results using an ordinary sheet of office paper (Chen et al. 2012). This technology takes advantage of the tendency for paper to yellow, which is usually considered to be a disadvantage of printing paper. Although laser inkless printing (Sun et al. 2009) and heat-induced inkless printing achieved the same result, its damage of paper and environmental impact was not further studied. This paper reviews the research progress in HIEP (Chen et al. 2012, Chen et al. 2014a, Chen et al. 2014b, Chen et al. 2016), including the printing effect, degree of carbonization, environmental impact and feasibility (Wei et al. 2015, Chen et al. 2016a, Chen et al. 2016b), and then proposes potential research directions for HIEP.

The definition and printing effect of HIEP

HIEP is a type of printing that does not require any toner or ink. Using a special printer head composed of a high-temperature printing dot matrix or heat-inducing printing stylus to transfer heat, the required text or graphics can be formed on the paper via the yellowing and blackening caused by thermal or laser energy (Chen et al. 2012). Among traditional printing methods, thermal printing and rice paper pyrography also rely on this approach (Liu 1999). Thermal printing on dedicated thermal paper is based on a heat-induced chemical reaction and the coating of a compound onto the paper to cause a color change. Similarly, the rice paper used for pyrography must be sprayed or brushed in advance with a thin slurry composed of a variety of chemicals (Chen et al. 2014). Thus, both of these techniques involve the painting or writing of one or more colored materials (a coating) onto a base material of another color to form words or patterns. By contrast, HIEP requires only a single "base material" to achieve the effect of printing using the "coloring method".
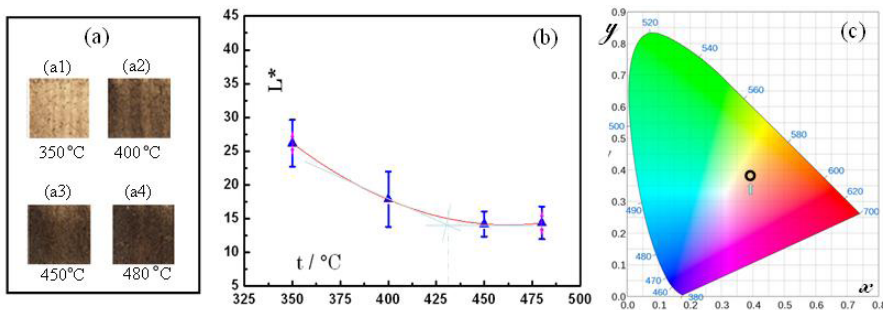

Fig. 1: Heat–induced blocks: (a) photographs of scan printing results, (b) corresponding lightness (L*), and (c) corresponding chromaticity (x, y) (Chen et al. 2012).

The study of the printing effect of HIEP still remains at the stage of laboratory investigation through manual simulation. Heat-induced color blocks produced in such an investigation are shown in Fig. 1a.

Fig. 2a-d and Fig. 2e,f present the experimental results of simulated heat-induced printing by means of clicking and writing, respectively (Xie et al. 2014). The heat-induction temperature was above 500°C for the tests whose results are shown in Fig. 2c and Fig. 2d.
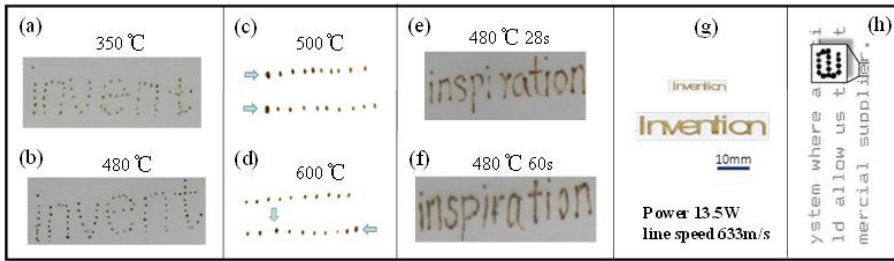
Fig. 2: HIEP simulated printing results (Chen et al. 2012, Xie et al. 2014): (a–d) the print–click method, (e, f) the scan method, (g) LIEP, and (h) dot matrix printing (1970).

From Fig. 2a-f, it is clear that although the heat-induced method has some disadvantages relative to the current state of the art in laser printing because of the current lack of research on the optimization of the printing technology parameters and the accurate control of the printing process, the text formed on the paper is clearly visible, and the printing effect of HIEP is similar to that of a dot matrix printer manufactured in the 1970s, as shown in Fig. 2g. For comparison, Fig. 2h shows the results of simulated printing via laser inkless eco-printing (LIEP) using heat induction on normal A4 office paper (Chen et al. 2012). Although the characters formed by LIEP are yellow in color, heat-induction technology can achieve the desired level of discoloration for printing. Therefore, by bridging the gaps in chromaticity and lightness between HIEP and current printing through the optimization of the printing parameters and precise control of the printing process, HIEP can achieve a practical printing effect.

Paper microstructure after HIEP and environmental impact

HIEP does not require ink during the printing process and can achieve reliable printing results using an ordinary sheet of office paper. However, HIEP may damage the paper and may produce a small amount of harmful gases when the temperature is sufficiently high. Thus, the microstructure of the paper after HIEP and the categorization, quantification, and environmental assessment of volatiles require investigation and analysis to provide a scientific basis for the design of safe HIEP technology. The research progress on these topics is reviewed in this section.

Carbonized paper microstructure after HIEP

The first and second columns in Fig. 3 show sets of microstructure images obtained after simulated scan printing and click printing, respectively (Chen et al. 2014a, Chen et al. 2014b, Chen et al. 2016a,b). In the first column of Fig. 3, it is seen that slight scratches remained on the paper surface after scan printing (as indicated by a "w"). However, the basic characteristics of the paper were retained, namely, the large number of recesses and voids formed through the mutual superposition of fibers, whose main ingredients are cellulose and hemicelluloses (Nathan et al. 2005). Several particles or slightly larger lumps can also be observed in the images in Fig. 3, as indicated by the squares. Most of these substances are inorganics (filler or addition agents) added during the paper-making process, which are usually classified as "ash" (Ren et al. 2009). Very obvious concave indentations remained after click printing (as indicated by a "u" in the second column of Fig. 3). The microstructures did not differ markedly depending on the heat-induction temperature used (Fig. 3a-d).
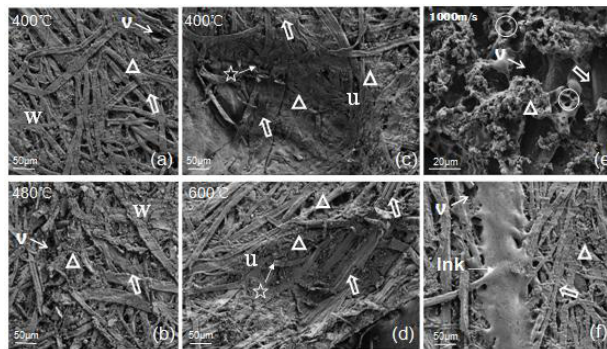
Fig. 3: Paper microstructures after various forms of printing (Chen et al. 2014a, Chen et al. 2014b, Chen et al. 2016a, Chen et al. 2016b): (a, b) scan printing, (c, d) click printing, (e) LIEP, and (f) state-of-the-art laser printing.

The distinct features of HIEP can be appreciated from a comparison with the results of LIEP (Fig. 3e) and current laser printing technology (Fig. 3f) (Chen et al. 2014a). After LIEP, the fine structure looks like that of a microsludge material, with a texture similar to that of a softening substance generated by fiber carbonation decomposition, and a number of small holes (indicated by circles) and cauliflower core-like clots (indicated by triangles) can be clearly observed. In current laser printing (Fig. 3f), the paper surface adsorbs a large amount of ink powder. By contrast, the simulated HIEP samples, for both scan printing and click printing, showed no serious carbonization such as that seen with LIEP nor any residual ink powder such as that currently used in laser printing. Therefore, for paper recycling, the printing paper used for HIEP requires the removal of the least amount of colored material.

Pyrolysis products and environmental impact of HIEP

Fig. 4a and Fig. 4b presents content area percentages of the main pyrolysis products in air at each temperature and the pyrolysis volatiles with an area content exceeding 2 % at 250-700°C under an air atmosphere (Chen et al. 2014b). The products shown in the figure are those that represent more than 2% of the area in the mass spectral analysis; the Y coordinate is the area percentage. And the numbers represented different pyrolysis products: 1-CO_2, 2-C_2H_4O, 3-C_3H_6O, 4-$C_2H_4O_2$, 5-$C_3H_4O_2$, 6-C_5H_{10} (cis-2-Pentene), 7-C_5H_{10} (Trans-2-Pentene), 8-$C_3H_4O_2$, 9-CH_2Cl_2, 10-$C_5H_{10}O$, 11-$C_2H_{14}N_2$, 12-$C_5H_4O_2$, 13-$C_5H_6O_2$, 14-$C_4H_6O_3$, 15-$C_6H_6O_3$, 16-C_7H_5NS, 17-$C_8H_8O_3$, 18-$C_{10}H_{10}O_3$, 19-$C_6H_{12}O_6$, 20-$C_9H_{10}O_4$, and 21-$C_{16}H_{22}O_4$.

The volatiles are divided into six classes according to their harmful effects: Class I includes only CO_2; Classes II and III include irritants and flammable products, respectively (Fig. 5a); Class IV includes corrosive products; and Classes V and VI include moderately and highly toxic products, respectively. According to Fig. 5, the pyrolysis volatiles do not include any carcinogens. For Class I, 1-CO_2 is the most common product, followed by the lightly polluting Class II and III products, which include a number of different volatiles. The main toxic products included in Classes V-VI are 2-C_2H_4O, 3-C_3H_6O, 5-$C_3H_4O_2$, 9-CH_2Cl_2, 12-$C_5H_4O_2$, 13-$C_5H_6O_2$, 16-C_7H_5NS, and 21-$C_{16}H_{22}O_4$ (Fig. 5b). In general, two types of products in Classes V and VI are produced at each temperature (Fig. 5a).
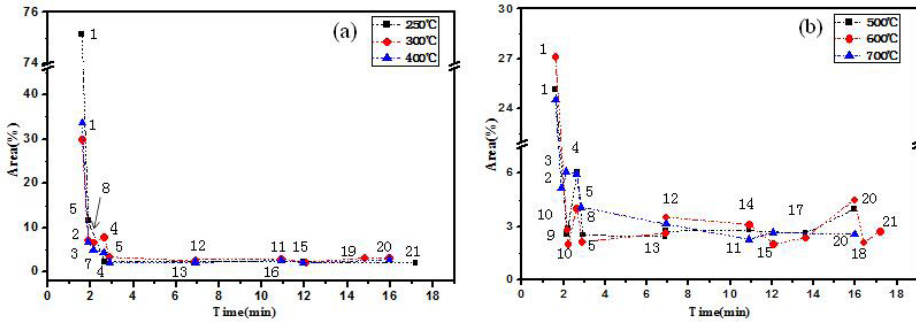
Fig. 4: The main pyrolysis products of the HIEP paper printing process at (a) 250–400°C and (b) 500–700°C.
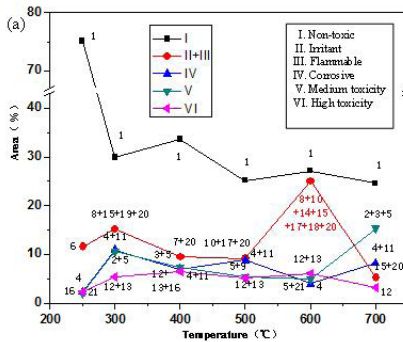

Fig. 5: The content area percentages of main pyrolysis products in air generated at various temperatures, representing the environmental impact of the printing process.

Generally speaking, CO_2 (Class I) and lightly polluting products (Classes II and III) account for a significant amount of the volatiles observed. The sum of Classes I-III is approximately 50%. The proportion of each class of toxic products (Classes V and VI) is approximately 5% at most temperatures (Fig. 5a). In current laser printing technology, the paper surface adsorbs a substantial amount of ink powder (Fig. 3f); by comparison, HIEP leaves only a number of concave indentations and recesses on the paper's surface and does not generate a significant amount of pyrolysis volatiles. HIEP also significantly reduces the waste paper recycling costs associated with ink processing, and its use therefore provides excellent economic and environmental benefits.

Nondestructive printing mechanism of HIEP

Although it is well known that paper cannot withstand fire, it has been shown that no damage is evident after HIEP for a heat-induction temperature of 600°C. Based on an analysis of the thermal and physical properties and the printing contact time, the feasibility of the precise control of HIEP for industrial applications has been validated (Xie et al. 2014). Fig. 6 presents the TG thermal physical properties of the paper (Xie et al. 2014). The TG curves can be separated into six stages (Fig. 6a) below 600°C.
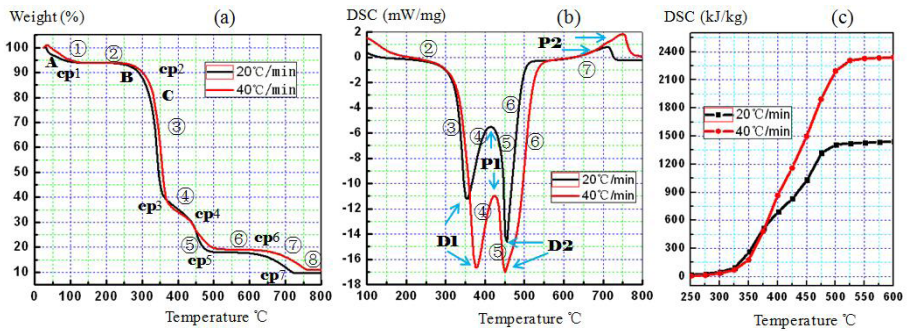
Fig. 6: Thermal analysis of the paper (Xie et al. 2014): (a) TG curves, (b) DSC curves, and (c) endothermic curves.

The pyrolysis of the paper predominantly occurs during the third to fifth stages of the TG curves (Fig. 6a). The differential scanning calorimetry (DSC) curve (Fig. 6b) features two endothermic peaks (D1 and D2) and one exothermic peak (P1). The locations of these peaks depend on the heating rate. The temperatures of the critical points increase with an increasing heating rate (Fig. 6). According to Li et al. (2005) and Wang et al. (2009) who investigated the TG behavior of wood and biomass in air, these two endothermic peaks (Fig. 6b, D1 and D2) primarily arise from the pyrolysis of hemicelluloses and cellulose. The exothermic peak P1 forms for two reasons. First, the material burns at a high temperature (referred to as "secondary combustion"), releasing the heat generated in the third stage of weight loss (Wang et al. 2009, Tan et al. 2006). Second, a transitional stage in the TG curve can be observed (see Fig. 6a), because hemicellulose pyrolysis and cellulose pyrolysis occur at different temperatures. The total thermal solution in this stage absorbs less than the required amount of heat, which contributes to the formation of the exothermic peak. Overall, the pyrolysis process is endothermic, as the endothermic contribution exceeds the exothermic contribution (Fig. 6c).

According to Fig. 6a, the paper experiences significant weight loss when the temperature reaches approximately 350°C. During HIEP, why does the paper not incur serious damage when the temperature exceeds 600°C? The reason, according to the author, is that the vaporization of the moisture in the paper (greater than 5%) serves as a buffer, and furthermore, the heating time is very short: in the experiment presented in Fig. 6, even at a high heating rate of 40°C·min⁻¹, the time required to heat the paper from 300°C to 400°C was 150 s, whereas during the simulated HIEP process, the time required to print each dot at 450°C was approximately 30 ms. In other words, the degree of heat transfer differed between the HIEP and TG experiments by at least 2-3 orders of magnitude (Xie et al. 2014).

Feasibility of HIEP

As seen from the effect of the heating rate on the weight loss (pyrolysis) of the paper (Fig. 6), heating paper at a lower heating rate requires a longer heating time to reach a given temperature and thus leads to greater weight loss (Fig. 6a) and less heat absorption (Fig. 6c). Although pyrolysis requires much more heat at a higher heating rate, such rapid heating can significantly shorten the time needed to reach a specific temperature. In addition, rapid heating can reduce the weight loss of the paper, which is desirable for the manufacturability and commercialization of the HIEP process (Xie et al. 2014). In other words, it is clear that the paper loses weight quickly

between 400 and 600°C. The paper weight-loss rate can be closely controlled by monitoring the heat-induction temperature and time. These findings provide a scientific basis for controlling the weight loss of paper during yellowing and discoloration and for preventing damage based on the TG behavior of the paper (Xie et al. 2014).

However, if the heat-induction temperature is excessively high, the requirements concerning the material of the print head, printer security and other HIEP parameters are also high. Temperatures ranging between 400 and 600°C are reasonable for heat-induced printing. As mentioned above, HIEP can achieve a practical printing effect within a sufficiently short time interval to maintain the strength of the paper and avoid any obvious carbonation. In summary, HIEP, a new inkless eco-printing technology, has been shown to be viable.

Moreover, the environmental impacts of the pyrolysis volatiles produced from newsprint and silk have also been analyzed (Wei et al. 2015). At HIEP temperatures (400-600°C), the toxicity of the pyrolysis volatiles in the printing paper was found to be the lowest, with the best environmental friendliness, whereas the impact of newspaper is the worst and that of silk is in the middle.

The printing effect on all three kinds of materials was expected to be desirable (Wei et al. 2015). However, the color could be clearly observed through the back of the newsprint because of its higher permeability. Of the three materials, printing paper was found to be the most suitable for HIEP, and newsprint, the least suitable. Silk may still be used in HIEP for the production of art, name cards and clothing nameplates in small amounts (Wei et al. 2015).

Potential research directions

Over the past five years, the printing effect, environmental impact, and damage mechanism of HIEP and the suitability of printing materials for HIEP have been studied and some progress has been achieved. However, further investigations are needed to improve this new technology. To this end, a greater understanding of the pyrolysis of biomass (considering the relevant biological, heat transfer, and chemical aspects) and color science will be required. Meanwhile, cross-disciplinary research including laser technology (for instance, LIEP), nanoscience (with regard to nano-level pyrolytic carbonization on the paper surface), photochemistry (with regard to the behavior of chromophores in photo-oxidization and photodegradation), paper-manufacturing science (including information regarding biomass hydrolysis, enzyme treatment, graft changes and other chemical treatments to make paper more suitable for HIEP), high-temperature materials science, and mechanical and transmission-related developments (because the printer heads will require sophisticated transmission and electronic control) will be essential for solving the next generation of research problems.

Discoloration mechanism and printing effect

As mentioned above, the printing effect of HIEP is similar to that of an early dot matrix printer. Although the yellowing discoloration of paper is a well-known phenomenon, the mechanism that drives it is not yet clear. Moreover, HIEP is performed under high-temperature and short-duration conditions. According to chemical theory, therefore, the relevant discoloration mechanisms should be different. According to preliminary observations, no obvious carbonization occurs during HIEP; thus, the discoloration of HIEP is not caused by paper carbonization. Because the tendency for paper to yellow at room temperature is generally considered to be a disadvantage, researchers have tended to focus on the elimination of the yellow coloration. However, discoloration is an essential component of the HIEP process. Thus, the mechanism of paper discoloration and the identification of the post-pyrolysis color groups need to be studied in depth.

As a new technology, HIEP should offer adequate resolution, color-fastness and opacity. The resolution of HIEP should be similar to that of current inkjet (Stankovska et al. 2014) and thermal printing. Early samples produced using the manual simulated printing processes have been preserved for more than 4 years. Their color-fastness and opacity can visually meet the requirements of practical applications, but quantitative research on these samples has not yet been performed.

Environmental impact

Although the environmentally friendly qualities of HIEP have been preliminarily studied, this process might release a small quantity of harmful gases. The volatiles emitted from paper during 1s of high-temperature pyrolysis have been determined in a previous study. In HIEP, the use of a shorter heat-induction time should result in less pyrolysis, making this technique more environmentally friendly. In addition, the chemical compositions of paper differ by mill, and the heat transfer of HIEP is different from that in a paper pyrolysis experiment. Thus, comprehensive studies on HIEP's environmental impact should be conducted.

Paper damage mechanism and strength during HIEP

No significant damage to the paper was evident following HIEP, as the degree of heat experienced during HIEP is low and the evaporating water has a buffering effect. No serious carbonization was observed during a simulated HIEP experiment, even when the temperature reached 600°C. If the duration of contact between the printing head and the paper were to be too long, however, the paper could certainly be burnt. Thus, the relationships between the process parameters, such as heat-induction temperature and contact time, and paper quality parameters, such as carbonization degree and strength, need to be determined. To achieve this goal, an unsteady heat transfer analysis (electronic simulation) could be conducted along the longitudinal and lateral directions of the paper with the development of a three-dimensional model.

High-temperature printing head installation and relevant techniques

By drawing lessons from the control systems for the current inkjet and thermal printing methods and using new manufacturing methods, the patterning and precision of HIEP can be improved. However, several new questions related to high-temperature operation may follow, such as those related to machine cooling, device complexity, stability and energy consumption. Although these problems can be solved using modern technologies, the final results will require quantitative analysis and experimental validation.

Optimization of process parameters

The process parameters, such as heat-induction temperature, printing speed, and printing-head pressure on the printing paper, need to be optimized both in general and for specific printing materials, such as silk.

In addition to the problems discussed above, the printing color of HIEP is dull compared with what can be achieved in current laser printing, which should also be addressed. Further studies on HIEP will pursue the research directions described above, and relevant findings will be reported in turn.

CONCLUSIONS

HIEP is capable of achieving the same results as traditional printing using only a single "base material" (i.e., paper). Issues that arise during the life cycle of printed products, such as environmental pollution and human health risks caused by toner or ink and the challenges involved in the recycling and reuse of waste paper, are obviated by this process. The development of this printing method also constitutes a cross-study platform involving the fields of biology, photochemistry, nanoscience, paper-manufacturing science and color science. Thus, the development of HIEP represents a significant technological improvement and could be a landmark technology in the current era of worsening environmental pollution.

ACKNOWLEDGEMENTS

REFERENCES

1. Beyer, M., Koch, H., Fischer, K., 2005: Role of hemicelluloses in the formation of chromophores during heat treatment of bleached chemical pulps. Macromolecular Symposia 232(1): 98-106.
2. Bar-Sela, S., Shoenfeld, Y., 2008: Photocopy machines and occupational antiphospholipid syndrome. Israel Medical Association Journal 10(1): 52-54.
3. Boutopoulos, C., Kalpyris, I., Serpetzoglou, E., Zergioti, I., 2014: Laser-induced forward transfer of silver nanoparticle ink: time-resolved imaging of the jetting dynamics and correlation with the printing quality. Microfluidics and Nanofluidics 16: 493-500.
4. Carter, H.A., 1996: The chemistry of paper preservation: Part 2. The yellowing of paper and conservation bleaching. Journal of Chemical Education 73(12): 1068-1073.
5. Comiskey, B., Albert. J.D., Yoshizawa, H., Jacobson, J., 1998: An electrophoretic ink for all-printed reflective electronic displays. Nature 394: 253-255.
6. Chantigny, M.H., Angers, D.A., Beauchamp, C.J., 2000: Decomposition of de-inking paper sludge in agricultural soils as characterized by carbohydrate analysis. Soil Biology and Biochemistry 32: 1561-1570.
7. Chen. J.X., Xie, J., Chen, F., 2010: A heat-inducing eco-printing method and print head device. China Patent 201010218623.8-ZL.
8. Chen, J.X., Wang, Y., Xie, J., Meng, C., Wu, G., Zu, Q., 2012: Concept of heat-induced inkless eco-printing. Carbohydrate Polymers 89(3): 849-853.
9. Chen, J.X., Xie, J., Pan, L., Wang, X., Xu, L.N., Lu, Y., 2014a: The microstructure of paper after heat-induced inkless eco-printing and its features. Journal of Wood Chemistry and Technology 34(3): 202-210.
10. Chen, J.X., Pan, L., Xie, J., Wu, G., Ren, H., Wang, Y., 2014b: Pyrolysis volatiles and environmental impacts of printing paper in air. Cellulose 21: 2871-2878.
11. Chen, J.X., Meng, C., Xie, J., Lan, L., Zhou, D., Chen, J.N., 2016a: Laser eco-printing technology for silk fabric patterns. Indian Journal of Fibre and Textile Research 41: 78-83.

12. Chen, J.X., Xu, L., Xie, J., Wang, Y., Zu, Q., 2016b: The effect of laser inkless eco-printing on the carbonized microstructure of paper. Cellulose Chemistry Technology 50(1): 101-108.

13. Choi, S.J., Park, J.Y., 2010: High-aspect-ratio imageable top-surface lithography using UV-assisted inkless contact printing. Small 6(3): 371-375.

14. Davidson, R.S., 1996: The photodegradation of some naturally occurring polymers. Journal of Photochemistry and Photobiology B: Biology 33(1): 3-25

15. El-Hennawi, H., Ahmed, K., El-Thalouth, I., 2012: A novel bio-technique using laccase enzyme in textile printing to fix natural dyes. Indian Journal of Fibre and Textile Research 37(3): 245-249.

16. Fromageot, D., Pichon, N., Peyron, O., Lemaire, J., 2006: Thermal yellowing sensitised by pre-photo-oxidation of non-deacidified paper. Polymer Degradation and Stability 91(2): 347-357.

17. Gallardo, M., 1994: Siderosilicosis due to photocopier toner dust. Lancet 344: 412-413.

18. Gill, S.S., Kaplas, M., 2009: Comparative study of 3D printing technologies for rapid casting of aluminum alloy. Materials and Manufacturing Processes 24(12): 1405-1411.

19. Gigac, J., Stankovska, M., Fiserova, M., Opalena, E., 2015: Improvement of inkjet print quality via hydrophilic polymers and base. Wood Research 60(5): 739-746.

20. Garai, B., Mallick, A., Banerjee, R., 2016: Photochromic metal-organic frameworks for inkless and erasable printing. Chemical Science 7(3): 2195-2200.

21. Hays, D.A., 2015: Paper documents via the electrostatic control of particles. Journal of Electrostatics 51: 57-63.

22. Henke, K., Treml, S., 2012: Wood based bulk material in 3D printing processes for applications in construction. European Journal of Wood and Wood Products 71: 139-141.

23. Jensen, M., Rold-Petersen, J., 1979: Itching erythema among post office workers caused by a photocopying machine with wet toner. Contact Dermatitis 5(6): 389-391.

24. Kishimura, A., Yamashita, T., Yamaguchi, K., Aida, T., 2005: Rewritable phosphorescent paper by the control of competing kinetic and thermodynamic self-assembling events. Nature Materials 4(7): 546-549

25. Li, A.M., Sun, L.J., Li, R.D., Wang, L., 2005: Characteristics of combustion and pyrolysis for decorative woods in poor-oxygen atmosphere. Journal of Engineering Physics and Thermophysics 26: 237-240.

26. Liu, Z.W., 1999: One method for rice paper pyrography. China Patent 99122434.5-CN.

27. Lou, Q., Qu, S., Jing, P., Ji, W.Y., Cao, J.S., Zhang, H., Liu, L., Zhao, J.L., Shen, D.Z., 2015: Water-triggered luminescent "nano-bombs" based on supra - (carbon nanodots). Advanced Materials 27: 1389-1394.

28. Morawska, L., He, C., Johnson, G., Jayaratne, R., Salthammer, T., Wang, H., Uhde, E., Bostrom, T., Modini, R., Ayoko, G., McGarry, P., Wensing, M., 2009: An investigation into the characteristics and formation mechanisms of particles originating from the operation of laser printers. Environmental Science and Technology 43(4): 1015-1022.

29. Mosier, N., Wyman, C., Dale B., Elander, R., Lee, Y.Y., Holtzapple, M., Ladisch, M., 2005: Features of promising technologies for pretreatment of lignocellulosic biomass. Bioresource Technology 96(6): 673-686.

30. Park, J.U., Hardy, M., Kang, S.J., Barton, K., Adair, K., Mukhopadhyay, D., Lee, C.Y., Strano, M., Alleyne, A., Georgiadis, J., Ferreira, P., Rogers, J., 2007: High-resolution electrohydrodynamic jet printing. Nature Materials 6(10): 782-789.

31. Ren, P.X., Jiang, J.C., Yang, X.S., Liu, J.L., 2009: Research progress on production of ethanol as fuel from fast pyrolysis products of lignocellulose. Biomass Chemical Engineering 43: 47-51.

32. Rentschler, T., 2005: New approaches in papermaking with small particles. Wochenblatt für Papierfabrikation 133: 1385-1393.

33. Song, X., Wang, S., 2010: Simple analysis about inkless printing technology. Publishing and Printing 3:74.

34. Shestopalov, A.A., Clark, R.L., Toone, E.J., 2007: Inkless microcontact printing on self-assembled monolayers of fmoc-protected aminothiols. Journal of the American Chemical Society 129(45): 13818-13819.

35. Sun, X.L., Zhao, Z., Bai, Z., 2009: A new no ink laser printing technology. Mechatronics 15: 84-86.

36. Shestopalov, A.A., Clark, R.L., Toone, E.J., 2010: Catalytic microcontact printing on chemically functionalized h-terminated silicon. Langmuir 26(3): 1449-1451.

37. Saraga, D., Pateraki, S., Papadopoulos, A., Vasilakos, Ch., Maggos, Th., 2011: Studying the indoor air quality in three non-residential environments of different use: A museum, a printery industry and an office. Building and Environment 46: 2333-2341.

38. Stankovska, M., Gigac, J., Letko, M., Opalena, E., 2014: The effect of surface sizing on paper wettability and on properties of inkjet prints. Wood Research 59(1): 67-76.

39. Sun, H., Gao, N., Ren, J., Qu, X., 2015: Polyoxometalate-based rewritable paper. Chemistry of Materials 27(22): 7573-7576.

40. Sheng, L., Li, M.J, Zhu, S.Y, Li, H., 2015: Hydrochromic molecular switches for water-jet rewritable paper. Nature Communications 5: 55-55.

41. Tan, H., Wang, S.R., Luo, Z.Y., Cen, K.F., 2006: Pyrolysis behavior of cellulose, xylan and lignin. Journal of Fuel Chemistry Technology 34(1): 61-65.

42. Theegarten, D., Boukercha, S., Philippou, S., Anhenn, O., 2010: Submesothelial deposition of carbon nanoparticles after toner exposition: Case report. Diagnostic Pathology 5: 77-81.

43. White, C.W., Brussell, E.M., Williams, T.T., Eog, S.J., 1984: Gray-scale graphics using dot matrix printers. Behavior Research Methods Instruments and Computers 16: 273-276.

44. Wang, G., Li, W., Xue, Q.Z, 2009: Thermogravimetric behaviors of biomass' chemical components under air or syngas. Journal of Fuel Chemistry Technology 37(2): 170-176.

45. Wang, H., He, C.R, Morawska, L., 2012: Ozone-initiated particle formation, particle aging, and precursors in a laser printer. Environmental Science and Technology 46(2): 704-712.

46. Wataoka, I., 2012: Ink-jet printing using natural dyes. Journal of the Society of Fiber Science and Technology 68(6): 176-179.

47. Wang, L., Liu. J., 2014: Liquid phase 3D printing for quickly manufacturing conductive metal objects with low melting point alloy ink. Science China Technological Sciences 57: 1721-1728.

48. Wang, N., Tahmasebi, A., Yu, J., Huang, F., Mamaeva, A., 2015: A comparative study of microwave-induced pyrolysis of lignocellulosic and algal biomass. Bioresource Technology 190: 89-96.

49. Wei, P., Zhou, M., Pan, L., Wei, P., Zhou, M., Pan, L., Xie, J., Chen, J., Wang,Y.: Suitability of printing materials for heat-induced inkless eco-printing. Journal of Wood Chemistry and Technology 36(2): 129-139.

50. Wang, Q., 2017: The formation of "four great inventions" in ancient China and other issues. Studies in Dialectics of Nature 8: 72-77.

51. Xin, Z.Q, Wang, S., Li, F.Y., Zhang, X.Y., Zhang, Z.L., Song, Y.L., 2013: The preparation of nanoparticles and their applications in ink-jetting and printing fields. Scientia Sinica (Chimica) 43: 677-686.

52. Xie, J., Chen, J.X, Wang, Y., Liu, Y.F., Noori, M., Pan, L., 2014: Weight loss phenomenon of paper and the mechanism for negligible damage of heat-induced inkless eco-printing. Cellulose Chemistry and Technology 48(5-6): 577-584.

53. Yow, H.N., Routh, A.F., 2006: Formation of liquid core-polymer shell microcapsules. Soft Matter 2: 940-949.

54. Yao, N.M., Zhao, X.L., 2007: Printing paper carbonization method with laser high temperature. China Patent 200710071837.5-ZL.

55. Yoo, S., Hsieh, J.S., Zou, P., Kokoszka, J., 2009: Utilization of calcium carbonate particles from eggshell waste as coating pigments for ink-jet printing paper. Bioresource Technology 100: 6416-6421.

Peixing Wei*
Southeast University
School of Civil Engineering
Nanjing, 210096
P. R. China
*Corresponding author: wayne0448123@163.com

Wanyong Tuo*
Anyang Institute of Technology
School of Civil & Architectural Engineering
Anyang, 455000
P. R. China
*Corresponding author: twy2014@163.com

Sheng He
China National Bamboo Research Center
Hangzhou, 310012
P. R. China

Guohua Liu
Jiangsu Vocational College of Agriculture and Forestry
Jurong, 212400
P. R. China

EFFECT OF THE FABRIC REINFORCEMENT OF
STRUCTURAL HOLES IN WOOD BASED PANELS

Nurdan Cetin Yerlikaya
Yalova University
Turkey

Abdurrahman Karaman
Usak University
Turkey

ABSTRACT

The objective of this study was to determine the effects of the glass fiber fabric reinforced holes in MDF, PB, OSB, and PL. The fabrics of 19 mm or 50 mm wide were used to reinforce the edge or flat surface of test specimens. The experimental sample groups were formed in 34 different ways. Three different holes configurations were prepared. The samples were subjected to the 3 points bend testing in the flatwise and edgewise directions. As a result of tests, bending strength and modulus of elasticity were determined. The data obtained separately in flatwise and edgewise bending tests were subjected to multiple variance analysis. According to experiment results, the lowest values were obtained in the "fabricless" in both tests. The lowest value was obtained as 12.35 N·m^{-2} (in PB material) in the group 12, which has samples with the fabric on the edge and 2 holes on the surface in the flatwise test, while the highest value was obtained as 49988 N·m^{-2} (in PL material) in the group 19, which has samples with the fabric on the bottom edge and holeless in the edgewise test. According to the materials, the lowest values were as 18.32 N·m^{-2} in PB material, while the highest values were 49988 N·m^{-2} in PL material. It was determined that the BS and MOE values decreased between 0.3 and 49% in terms of the effect of the hole with fabric on the edge. In the holeless groups, the lowest values 18.32 N·m^{-2} in flatwised were obtained in fabricless group in PB, while the highest values 49988 N·m^{-2} in edgewised were obtained in the group of fabric on top surface in PL. The results showed that the fabric reinforcement has a positive impact on the strength.

KEYWORDS: Wood based panel, bending strength, modulus of elasticity, glass fiber fabric, reinforced.

INTRODUCTION

The use of the panel products such as medium-density fiberboard (MDF), particleboard (PB), oriented strandboard (OSB), and plywood (PL) for application areas such as all type furniture or roof and wall sheathing increased in recent years. These panel products need to be drilled several holes during their production. In particular, as Cai and Ross (2010) stated, the bending strength (BS) and modulus of elasticity (MOE) of the panel products are important for the performance characteristics of the panels. As a result, they point out that to understand the effect of holes on strength properties is very important. Eckelman (1975) stated that when constructing furniture frames, it is normally necessary to bore holes through the members to join them together by means of fasteners such as dowels and screws. He specified that these holes must be expected to have a weakening effect upon the members, particularly if they occur at points of high stress. He points out that it is important to take into account any such reductions in strength in the design process to ensure that members are sufficiently designed to withstand the force that would be applied to them in service.

In relation to the BS and MOE of wood-based materials, a lot of research has been done to determine the BS and MOE values of the different panels (Hosseinpourpia et al. 2019, Chen et al. 2019, Ghasemi and Moradi 2017, Akgul et al. 2017, Yoshihara 2016, Xu and Que 2016, Chen et al. 2015, Gao et al. 2015, Svoboda et al. 2015, Yildirim et al. 2015, Baidaea et al. 2015, Zhou et al. 2012, Ayrılmış et al. 2010, Bekhta and Marutzky 2007, Alfredsen and Larnoy 2006, and Eckelman 1975). But there is not another information about the effects of the hole on the BS and MOE of the MDF, PB, OSB, and PL in the literature. Eckelman (1975) developed and presented the expressions which were required to calculate the residual strength of members with holes in them. He carried out static bending tests to determine their BSs on both douglas-fir and PB beams of rectangular cross section to evaluate the predictive power of the expressions which had been developed. He determined by the test results that observed results dropped nearly 15% to 20% below predicted values when holes were drilled near the edge of PB beams tested on edge. In these results obtained, he stated that stress concentrations around the hole in the PB beams could occur. Chen et al. (2019) analyzed the effects of hole sizes on mechanical properties (BS and MOE) of the spruce and Douglas fir samples with and without open-hole. They were prepared four groups (one group without open-hole, and three groups with open-hole which had 13, 16, and 20 mm diameters). They found that open-hole had significant impact on the bending strength.

A lot of researches have been done to determine the effect of drilled holes on the BS of lumber (Falk et al. 2003), timber (Franke et al. 2015), laminated veneer lumber (LVL) (Ardalany et al. 2013a,b). Falk et al. (2003) concluded that hole location may be as important as hole size. Ardalany et al. (2013a, b) state that the larger holes decreased the capacity of the LVL members by up to 52%. Some researcher was investigated the effect of the laminated timber beams (Hallström 1996) or LVL (Ardalany et al. 2013b) reinforced with glass fiber fabric on the holes. Hallström (1996) stated that when the beams were reinforced, a significant increase of the strength. He indicated that great improvements of strength were obtained with the glass fibers.

In this study, in addition to Eckelman's work, the effect of the hole reinforced with glass fiber fabric (hereinafter referred to as "fabric") on the BS was investigated. The aims of this study were to determine the effect of some factors (material, the hole, the fabric, and the reinforced with the fabric of the negative effect of the hole) on the BS and MOE at the wood based materials (hereinafter referred to as "panels").

MATERIALS AND METHODS

Materials

In the preparation of the test samples, 18 mm thick MDF, PB, OSB, and 11-ply PL, were used. The fabrics 19 mm and 50 mm wide were used to reinforce the test specimens. These fabrics were fastened with the DTE 1000 epoxy resin and DTS 1105 hardener on the panels. DTE 1000 epoxy resin is a solvent-free epoxy resin. DTS 1105 hardener is a solvent-free epoxy hardener. The epoxy adhesive mixture was prepared by mixing 3 parts of epoxy resin and 1 unit of hardener.

Methods
Preparation of samples

All panels were cut the 50 mm x 410 mm using the CNC cutting machine. Pre-tests on MDF were carried out to decide the length (100, 200, 300, and 400 mm) of the fabric (wide 50 mm) to be glued. The samples were subjected to bending test according to TS EN 310 and ASTM D 1037 standards. According to the test results, it was decided to use the 200 mm long fabric. Fabrics wide 19 mm were glued to be 410 mm long (from one end to the other) on the edge of the samples which having the dimensions of 50 x 410 mm. The experimental sample groups were formed in 34 different ways. Thus, in total 680 samples were prepared for this study (4 different materials, 34 configurations, 5 repeats).

The samples to be applied to the fabric were treated as follows: 50 mm wide fabrics were cut 200 mm long. The mixture of epoxy adhesive was applied on the areas, where the fabric was to be placed, with a brush by a mold. Then, the fabric was placed on these areas and then epoxy adhesive was applied again. Then the nylon bag was laid on. Then the bag was laid on the samples so that the samples would not stick together. After that these specimens were left to dry 2 days. And then, these samples were removed from the molds and they were allowed to dry thoroughly for 2 more days. Then the excess parts overflowing from the edges of the samples were cleaned by cutting with a circular saw machine. The hole locations and dimensions to be opened on the parts is shown in Fig. 1.
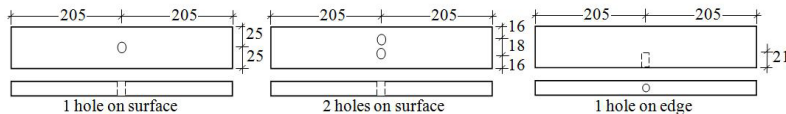

Fig. 1: Hole locations in boards (18 x 50 x 410 mm).

Testing procedures

The specific gravity (SG), and moisture content (MC), BS, and MOE of the samples were determined according to TS EN 323, TS EN 322, TS EN 310, and ASTM D 1037 standards, respectively. The samples were subjected to the 3 points bend testing in the flatwise and edgewise directions shown in Fig. 2. The samples were placed and were bent in the middle of the length (in the flat and edge position) on the Universal test machine Zwick Roel/Z200 at the Mechanical Laboratory of the Yalova University.

Fig. 2: Bending strength test setup.

The loading speed was adjusted so that failure would occur within an average of 60 ± 30 sec. The F_{max}, BS and MOE values were calculated automatically by the computerized testing device. The BS was calculated in accordance to Eq.1:

$$BS = 3*F_{max}*l_1/2*b*t2 \qquad (N \cdot mm^2) \qquad (1)$$

where: BS - bending strength (N·mm²); F_{max} - the maximum force (N); l_1 - the distance between supports (mm); b - the width of the sample (mm); t - the height (thickness) of the sample (mm).

The MOE were calculated in accordance with Eq. 2:

$$MOE = l_1^3 (F_2-F_1)/4*b*t^3(a_2-a_1) \quad (N \cdot mm^2) \qquad (2)$$

where: MOE - modulus of elasticity (N·mm⁻²); F_2-F_1 - the load increase in the proportional section of the load-deflection diagram (N); F_1 = approx. 10% of the largest force (N); F_2 = approx. 40% of the largest force (N); a_2-a_1 - the deflection increase in the half of the sample length corresponding to the load increase (mm).

In determination of the MOE in bending, the 1/3 amount of the greatest force obtained in the BS test was chosen as the elastic region. Load-deflection graphs measured with ± 0.01(unit) sensitivity corresponding to each 50 N force applied were plotted. And the 10% and 40% values of the failure load were recorded. And the 10% and 40% values of the failure load were recorded. The MOE was calculated by using the recorded these values in the elastic deformation zone of the drawn curve.

Analyses of the data
The data obtained separately in flatwise and edgewise bending tests were subjected to multiple variance analysis in SPSS program. And 16 (in flatwise) or 18 (in edgewise) experimental groups, 4 material types, 4 hole groups, 3 (in flatwise) or 4 (in flatwise) hole location groups, 3 fabric groups and 4 fabric location groups on BS and MOE effects were determined. The relationship between these main factors was determined at $p < 0.001$ significance level. When these main factors or their interactions with each other were found to be statistically significant, Duncan test was applied to determine the differences between the groups and to establish homogeneous groups.

RESULTS AND DISCUSSION

Some physical and mechanical properties of the panels used in the experiments were given in Tab. 1. The BS and MOE values of the raw materials (control samples) were in parallel with the values given in chapter 12 of the wood handbook written by Cai and Ross (2010).

Tab. 1: Density and moisture content of wood-based panels.

	MDF	PB	OSB	PL
Moisture content (%)	6.9	8.1	8.6	10.9
Density (g·cm⁻³)	0.759	0.642	0.564	0.62
BS (N·mm⁻²)	35.99	18,29	22,73	63.9
MOE (N·mm⁻²)	3410	3241	4848	8894

The results obtained from the pre-tests were given in Tab. 2. As shown in the table, it was determined that the results of the samples of 20, 30, and 41 cm long glued fabric were almost the same. Therefore, the length of the fabric to be glued to the surfaces of the test samples was determined to be 20 cm.

Tab. 2: Pre-test bending test results (MDF).

Fabric length	Flatwised						Edgewised					
	Control	5 cm	10 cm	20 cm	30 cm	41 cm	Control	5 cm	10 cm	20 cm	30 cm	41 cm
F max (N)	1030	1050	1330	1650	1440	1530	2600	2570	2630	2780	2960	3100
MOE (N·mm⁻²)	3350	3480	3380	3910	3890	3890	20300	21600	22700	21300	21300	22900

The BS and MOE results obtained in experiments were given in Tab. 3. The results show that, in the flatwise test, the lowest value as 12.35 N·m⁻² (in PB material) was obtained in the group 12, which has samples with the fabric on the edge and 2 holes on the surface, while the highest value as 12912 N·m⁻² (in PL material) was obtained in the group 2, which has samples with the fabric on the bottom surface and holeless. On the other hand, in the edge test, the lowest value was obtained as 30.27 N·m⁻² (in PB material) in the group 29, which has samples fabricless and 1 hole on the bottom edge, while the highest value was obtained as 49988 N·m⁻² (in PB material) in the group 19, which has samples with the fabric on the bottom edge and holeless.

In the flatwise tests, according to the tests groups, the highest BS and MOE values were obtained in the "holeless-fabric on bottom surface" group (group no 2) for MDF, PB, and PL materials, and in the "holeless-fabric on top surface" group (group no 3) for OSB material. Additionally, the lowest BS values for MDF and PB materials and the lowest MOE values for PB material were obtained in the "2 holes on surface-fabric on edge" group (group no 12), while other lowest values were obtained in the "2 holes on surface-fabricless" group (group no 9).

On the other hand, in the edgewise tests, the highest BS values for MDF and PB materials were obtained in the "1 hole on surface-fabric on bottom edge" group (group no 23), while other highest values were obtained in the "holeless-fabric on bottom edge" group (group no 19). Additionally, the lowest BS values were obtained; in the "1 hole-fabric on bottom edge" group (group no 33) for PL material, and in the "1 hole on bottom edge-fabricless" group (group no 29) for other material, while the lowest MOE values were determined in the "1 hole on top edge-fabric on surface" group (group no 32) for MDF material, in the "1 hole on surface-fabricless" group (group no 21) for PB material, in the "2 holes-fabric on surface" group (group no 26) in OSB material, and in the "1 hole on top edge-fabricless" group (group no 30) for PL material.

Tab. 3: Test results (N·m⁻²).

Group No	Hole	Glass fiber fabric	Scheme	MDF		PB		OSB		PL	
				BS	MOE	BS	MOE	BS	MOE	BS	MOE
					(Flatwised)						
1	No	No		35,99	3410	18,32	3214	22,73	4848	63,9	8894
2	No	on bottom surface		47	4423	33	4098	32	5832	73,02	12912
3		on top surface		40	4315	32	3918	33	5928	69	10480
4	No	on edge		39	3710	20,9	3518	23	5000	64,1	9003
5	1 hole on surface	No		26,5	3294	14,12	2988	22,54	5124	53,90	8555
6	1 hole on surface	on bottom surface		37,73	3620	26,88	3495	22,95	4875	62,70	9260
7		on top surface		28,6	3710	14,93	3250	26,53	5460	59,07	9077
8	1 hole on surface	on edge		26,25	3455	16,18	3347	20,53	4383	57,15	8475
9	2 holes on surface	No		22,56	3260	12,74	3044	18,04	4130	45,8	7894
10	2 holes on surface	on bottom surface		33	3677	21,18	3320	24,17	5023	53,5	8683
11		on top surface		24	3447	12,57	3283	20,17	5207	52,03	8967
12	2 holes on surface	on edge		21,98	3380	12,35	2962	19,4	4225	53	8400
13	1 hole on edge	No		35,32	3364	17,22	2976	19,75	4408	57,26	9560
14	1 hole on edge	on bottom surface		44,7	3870	31,6	3625	30,45	5150	66	9040
15		on top surface		35,03	3967	17,3	3440	23,05	5150	64,63	9380
16	1 hole on edge	on edge		36,43	3443	18,5	3223	20,1	4350	51,55	8978
					(Edgewised)						
17	No	No		82,2	20147	34	14553	46,1	19200	194,6	39440
18	No	on surface		93	23587	40	16010	57	22010	209	43014
19	No	on bottom edge		88	25365	47	23282	60	28918	230	49988
20		on top edge		86	24387	43	21025	58	27825	225	48783
21	1 hole on surface	No		82,12	19800	32,36	13640	42,46	21220	184,6	37820
22	1 hole on surface	on surface		97,83	21333	37,77	13800	53,8	20133	198,67	39767
23	1 hole on surface	on bottom edge		98,93	22867	56,07	18867	55,45	24250	204,4	43300
24		on top edge		90,90	22933	41,23	19200	49,45	23550	206,33	46533
25	2 holes on surface	No		77,44	20280	33,56	15480	42,58	20140	156,6	38700
26	2 holes on surface	on surface		82,68	19825	37,7	14700	45,25	18600	170	40933
27	2 holes on surface	on bottom edge		90,87	23567	53,07	18933	49,1	23000	165,67	43500
28		on top edge		85,2	23500	33,7	18700	53,65	24400	170	43600
29	1 hole on bottom edge	No		58,65	19750	30,27	14333	38,2	19733	173,67	40767
30	1 hole on top edge			61,65	18900	32,3	14000	44,33	20067	161	34550
31	1 hole on bottom edge	on surface		63,33	19100	34,57	14900	57,55	21300	162,33	40267
32	1 hole on top edge	on surface		70,25	18700	40	14450	58,7	19500	160,5	35300
33	1 hole on bottom edge	on bottom edge		62,5	20667	37,9	16533	47,3	23900	150	41433
34	1 hole on top edge	on top edge		75,77	21267	41,80	18133	55,65	23950	174,33	37900

In Tab. 3, according to the flatwise tests, the presence of 2 holes on the surface of the sample caused much more strength decrease. On the other hand, according to the edgewise tests, the

presence of 1 hole on the edge of the sample caused much more strength decrease than others.

When the test results were evaluated in terms of materials, in both flatwise and edgewise tests, the BS and MOE values were the lowest in PB, the highest in the PL. The reason why these values are high or low can be explained as the BS and MOE values of the material itself are higher or lower than others. According to the results of variance analysis, it was determined that 4 different homogeneous groups were formed (Tab. 4).

Tab. 4: Homogenous groups (HG) according to the materials (N·mm⁻²).

Materials	Flatwised				Edgewised			
	BS	**HG**	**MOE**	**HG**	**BS**	**HG**	**MOE**	**HG**
MDF	33.38	B	3647	C	80.41	B	21443	C
PB	19.99	D	3356	D	39.24	D	16697	D
OSB	23.65	C	4943	B	50.81	C	22317	B
PL	59.16	A	9222	A	183.15	A	41422	A

The test results of the "fabricless" groups (group 1, 5, 9, and 13 in flatwise tests and group 17, 21, 25, 29, and 30 in edgewise tests) were evaluated to determine the effect of the hole. As a result, BS values were found generally that in the flatwise tests, the "holeless" groups was high and the "2 holes on surface" groups was low, whereas, in the edgewise tests, the "holeless" groups was high and the "1 hole on edge" groups was low. The MOE values were determined generally; the "holeless" was high in both tests; the "2 holes on surface" in flatwise tests, and also "1 hole on edge" in edgewise tests were low. According to these results, it was clear that the existence of a hole on the material and the increase in the number of such holes reduces the strength. The reason for this decrease can be explained as the reduction of the cross-section area of the material to react to the applied load. In parallel with the results obtained in the studies of Eckelman (1975), Falk et al. (2003), and Chen et al. (2019), the hole was determined to reduce strength. The effect of the hole was evaluated statistically and their homogeneous groups in Tab. 5 were obtained according to variance analysis. 4 homogeneous groups were obtained for BS in PB and MDF and for MOE in MDF and PL in the flatwise tests and for BS in MDF and for MOE in PB in the edgewise tests. 3 homogeneous groups were observed in others.

Tab. 5: Homogenous groups (HG) according to the hole.

Groups	Flatwised								Edgewised							
	MDF		PB		OSB		PL		MDF		PB		OSB		PL	
	BS	**HG**	**BS**	**HG**	**BS**	**HG**	**BS**	**HG**	**BS**	**HG**	**BS**	**HG**	**BS**	**HG**	**BS**	**HG**
1	41	A	26	A	28	A	68	A	87	B	41	A, B	55	A	215	A
2	30	C	18	C	23	B	58	B	93	A	42	A	50	B	199	B
3	25	D	15	D	21	C	51	C	84	C	40	B	48	C	166	C
4	38	B	21	B	23	B	60	B	65	D	36	C	50	B	164	C
	MOE	**HG**	**MOE**	**HG**	**MOE**	**HG**	**MOE**	**HG**	**MOE**	**HG**	**MOE**	**HG**	**MOE**	**HG**	**MOE**	**HG**
1	3965	A	3687	A	5402	A	10322	A	23371	A	18718	A	24488	A	45306	A
2	3520	C	3270	B	4961	B	8842	C	21733	B	16377	C	22288	B	41855	B
3	3441	D	3153	C	4646	C	8486	D	21793	B	16953	B	21535	C	41683	B
4	3661	B	3316	B	4764	B, C	9239	B	19731	C	15392	D	21408	C	38370	C

Groups: 1= holeless, 3 = 2 holes on surface, 4 = 1 hole on edge.
Groups: 1= holeless, 2 = 1 hole on surface, 3 = 2 holes on surface, 4 = 1 hole on edge.

When the results were analyzed statistically according to the hole location, homogeneous groups were obtained as seen in Tab. 6.

Tab. 6: Homogenous groups (HG) according to the hole location.

Groups	MDF		PB		OSB		PL		MDF		PB		OSB		PL	
Flatwised																
	BS	HG	BS	HG	BS	HG	BS	HG	MOE	HG	MOE	HG	MOE	HG	MOE	HG
1 (holeless)	41	A	26	A	28	A	68	A	3965	A	3687	A	5402	A	10322	A
2 (on surface)	28	C	17	C	22	B	55	C	3480	C	3211	C	4803	B	8664	C
3 (on edge)	38	B	21	B	23	B	60	B	3661	B	3316	B	4764	B	9239	B
Edgewised																
Groups	MDF		PB		OSB		PL		MDF		PB		OSB		PL	
	BS	HG	BS	HG	BS	HG	BS	HG	MOE	HG	MOE	HG	MOE	HG	MOE	HG
1 (holeless)	87	A	41	A	56	A	215	A	23371	A	18718	A	24488	A	45306	A
2 (on surface)	88	A	41	A	49	C	182	B	21763	B	16665	B	21912	B	41769	B
3 (on bottom edge)	62	C	34	C	48	C	162	C	19839	C	15256	C	21644	B, C	40822	C
4 (on top edge)	69	B	38	B	53	B	165	C	19622	C	15528	C	21172	C	35917	D

In the flatwise tests, 2 different homogeneous groups were formed in both BS and MOE values of OSB. In edgewise tests, 4 different homogeneous groups were obtained for the MOE values of PL. In the others, 3 different homogeneous groups were formed. The highest values were obtained mostly in the "holeless" groups both tests. The lowest BS and MOE were obtained in the "on surface" groups in the flatwise tests. the lowest BS were determined mostly the "bottom edge" groups and the lowest MOE were determined generally in the "top edge" group in the edgewise tests. As a result, Falk et al. (2003) stated that the hole location affects the bending strength.

The groups without holes (in groups 1-4, 17-20) were evaluated to determine the effect of the fabric (Tab. 3). The lowest values were obtained as 18.32 N·m^{-2} (in flatwised) and as 34 N·m^{-2} (in edgewised) in fabricless groups in PB, while the highest values were obtained as 10480 N·m^{-2} (in groups of fabric on top surface in flatwised) and 49988 N·m^{-2} (in groups of fabric on bottom edge in edgewised) in PL. The highest BS and MOE were obtained; in the "on top surface" group for OSB and PL and in the "on bottom surface" group for MDF and PB in the flatwise tests (in groups 1-4); in the "on bottom edge" group in all materials except for the BS value (was obtained in the "on surface" group) of the OSB in edgewise tests. In flatwise tests, as can be seen, in all materials, the sample group which was "fabric on surface" was seen to cause higher strength. However, in OSB, it was determined that the fabric on the bottom surface of the sample was more effective than the fabric on the top surface. The reason for this is due to the structural features of the OSB as seen in the failure shapes. It can be confirmed as the top surface of the material was swelled and deformed by the fabric on the bottom surface.

When the test results were analyzed statistically in terms of the effect of fabric, homogeneity groups that obtained according to variance analysis results were obtained as shown in Tab. 7. In all materials, the highest values were obtained; in the "fabric on surface" in the flatwise tests; in the "fabric on edge" in the edgewise tests. The lowest values were obtained in the "fabricless" in both tests. It was determined that the fabric on surface provided compared to the fabricless samples an increase of; between 12 and 52% in the flatwise tests; between 1 and 28% in the edgewise tests. Statistically, it was seen that the "fabric on surface" was in the highest. It was also clearly seen that the effect of the fabric on surface was higher than the effect of the fabric on edge. Similar to

these results, Hallström (1996) stated that when the beams were reinforced, a significant increase of the strength.

Tab. 7: Homogenous groups (HG) according to the fabric.

Groups	Flatwised								Edgewised							
	MDF		PB		OSB		PL		MDF		PB		OSB		PL	
	BS	HG	BS	HG	BS	HG	BS	HG	BS	HG	BS	HG	BS	HG	BS	HG
1	30	C	16	C	21	B	55	B	72	C	33	C	43	B	174	C
2	36	A	24	A	27	A	63	A	81	B	38	B	55	A	180	B
3	31	B	17	B	21	B	57	B	85	A	44	A	54	A	191	A
	MOE	HG	MOE	HG	MOE	HG	MOE	HG	MOE	HG	MOE	HG	MOE	HG	MOE	HG
1	3332	C	3056	C	4628	B	8726	B	19775	C	14401	B	20072	B	38255	C
2	3879	A	3554	A	5328	A	9725	A	20509	B	14772	B	20309	B	39856	B
3	3497	B	3263	B	4490	B	8714	B	23069	A	19334	A	24974	A	44380	A

Groups: 1=fabricless, 2= fabric on surface, 3= fabric on edge.

The tests results were evaluated statistically in terms of the fabric location. And the obtained homogeneous groups were given in Tab. 8.

Tab. 8: Homogenous groups (HG) according to the fabric location.

Groups	Flatwised								Edgewised							
	MDF		PB		OSB		PL		MDF		PB		OSB		PL	
	BS	HG	BS	HG	BS	HG	BS	HG	BS	HG	BS	HG	BS	HG	BS	HG
1	30.09	D	15.6	D	20.77	B	55.22	B	72.41	C	32.5	D	42.73	B	174.09	D
2	40.61	A	28.16	A	27.39	A	63.81	A	81.42	B	38.01	C	54.46	A	180.1	C
3	31.91	B	19.2	B	25.69	A	61.18	A	85.08	A	48.51	A	52.96	A	187.52	B
4	30.91	C	16.98	C	20.76	B	56.45	B	84.47	A	39.93	B	54.19	A	193.92	A
	MOE	HG	MOE	HG	MOE	HG	MOE	HG	MOE	HG	MOE	HG	MOE	HG	MOE	HG
1	3332	D	3056	D	4628	B	8726	C	19775	C	14401	B	20072	B	38255	C
2	3897	A	3635	A	5220	A	9974	A	20509	B	14772	B	20309	B	39856	B
3	3860	B	3473	B	5436	A	9476	B	23116	A	19404	A	25017	A	44555	A
4	3497	C	3263	C	4490	B	8714	C	23022	A	19265	A	24931	A	44204	A

Groups: 1=fabricless, 2=on bottom surface, 3=on top surface, 4=on edge.

Furthermore, the results were examined in terms of the effect of the hole with fabric on the edge (groups 4, 8, 12, and 16) in the flatwise tests. And, the BS and MOE values were as follows respectively it was found. It decreased in the "1 hole on edge" group, 7% and 7% for MDF, 12% and 8% for PB, 13% and 13% for OSB, and 20% and 0.3% for PL. It decreased in the "1 hole on surface" group, 49% and 7% for MDF, 23% and 5% for PB, 11% and 12% for OSB, and 11% and 6% for PL. It decreased in the "2 holes on surface" group, 44% and 9% for MDF, 41% and 16% for PB, 16% and 19% for OSB, and 17% and 7% for PL. According to these ratios, the presence of 2 holes on the surface was seen to cause the most decrease in strength.

Failure mode

In the "fabricless" groups, all samples except MDF and OSB samples in edgewise were cracked. MDF samples in edgewise were broken. Any deformation was seen in OSB samples. However, a cracking sound was heard during the experiment. Possibly separations in the inner layers of the OSB have occurred.

Only MDF samples in groups 17, 21, 23, 24, 25, 27-30, 33, and 34 were broken. On the other hand, in the groups 6, 14, and 23 in OSB was surged by squeeze from the side of the load

line applied to the top surface. In PL, in groups 1, 5, 6-11, 14-16, 22, and 32, the layers of the PL were separated from each other. Besides, the almost other samples were cracked.

The failure shapes of the "fabric on edge" samples (in groups 4, 8, 12, and 16) in flatwise tests similar. The fabric was separated from the edge and the material was cracked. On the other hand, it was found that the reduction ratio in strength for the samples with hole on the edge was less than the others (Tab. 3). As it was understood from the shape of deformation, the fabric on the edge carried more load than the others and as a result, the fabric was opened by wriggle from below to the hole. It also appears that the samples were broken up to the hole and cracked upwards through the hole. On the other hand, in other materials, the fabric was slightly opened and the material was cracked on the bottom surface. In addition, it was seen that the PL samples were separated from its layers.

The "hole on edge" group had been determined to have higher strength than the "1 hole on surface" group and "2 holes on surface" group. In addition, in the "1 hole on edge" group, the material was cracked by being squeezed from the hole to both upwards and towards the side of the load line applied on the top surface. This was shown that the fabric was higher than the strength of the material. In the "fabric on bottom surface" and "1 hole on edge" groups, in the MDF, OSB, and PL, the fabric was not deformed, and the material was not also cracking. In PL, the material was separated from the layer at the level of the hole. The fabric in PB was opened and torn and the material was cracked.

CONCLUSIONS

According to the results, in the flatwise test, the lowest value was obtained as 12.35 $N \cdot m^{-2}$ in the samples with the fabric on the edge and 2 holes on the surface for PB material, while the highest value was obtained as 12912 $N \cdot m^{-2}$ in the samples with the fabric on the bottom surface and holeless for PL material. On the other hand, in the edge test, the lowest value was obtained as 30.27 $N \cdot m^{-2}$ in the samples fabricless and 1 hole on the bottom edge for PB material, while the highest value was obtained as 49988 $N \cdot m^{-2}$ in the samples with the fabric on the bottom edge and holeless for PB material.

According to the materials, for the BS and MOE values in both tests, the lowest values were as 18.32 $N \cdot m^{-2}$ for BS and as 2962 $N \cdot m^{-2}$ for MOE in PB, while the highest values were as 230 $N \cdot m^{-2}$ for BS and as 49988 $N \cdot m^{-2}$ for MOE in the PL.

In the holeless groups, the lowest values were obtained as 18.32 $N \cdot m^{-2}$ (in flatwised) and as 34 $N \cdot m^{-2}$ (in edgewised) in fabricless groups in PB, while the highest values were obtained as 10480 $N \cdot m^{-2}$ (in groups of fabric on top surface in flatwised) and 49988 $N \cdot m^{-2}$ (in groups of fabric on bottom edge in edgewised) in PL.

It was determined that the BS and MOE values of the samples with hole in terms of the effect of the hole with fabric on the edge decreased between 0.3 and 49%. The existence of a hole on the material and the increase in the number of such holes reduces the strength. The presence of hole on the sample caused much more strength decrease.

The lowest values were obtained in the "fabricless" in both tests. It has been determined that the fabric on the surface increases resistance up to 52% compared to fabricless samples. The fabric on the bottom surface of the sample was more effective than the fabric on the top surface. The effect of the fabric on the surface of the sample was higher than the effect of the fabric on the edge of the sample. The effect of the fabric on the edge of the sample was cause for increase compare to the samples the fabricless. If the sample has any holes, it may be advisable to reinforce, for example, with a fabric.

ACKNOWLEDGEMENTS

REFERENCES

1. Alfredsen, G., Larnoy, E., 2006: Dynamic MOE testing of wood: the influence of wood protecting agents and moisture content on ultrasonic pulse and resonant vibration. Wood Research 51(1): 11-20.
2. Ardalany, M., Fragiacomo, M., Carradine, D., Moss, P., 2013a: Experimental behavior of laminated veneer lumber (LVL) joists with holes and different methods of reinforcement. Engineering Structures 56: 2154-2164.
3. Ardalany, M., Fragiacomo, M., Moss, P., Deam, B., 2013b: An analytical model for design of reinforcement around holes in laminated veneer lumber (LVL) beams. Materials and Structures 46: 1811-1831.
4. Akgul, M., Uner, B., Camllibel, O., Ayata, Umit., 2017: Manufacture of medium density fiberboard (MDF) panel from agribased lignocellulosic biomass. Wood Research 62(4): 615-624.
5. ASTM D 1037, 1973: Evaluating the properties of wood-base fiber and particle panel materials.
6. Ayrılmış, N., Buyuksarı, U., As, N., 2010: Bending strength and modulus of elasticity of wood-based panels at cold and moderate temperatures. Cold Regions Science and Technology 63: 40-43.
7. Bekhta, P., Marutzky, R., 2007: Bending strength and modulus of elasticity of particleboards at various temperatures. Holz als Roh-und Werkstoff 65: 163-165.
8. Biadaea, T., Czarnecki, R., Dukarska, D., 2015: Attempt to produce flexible plywood with use of Europe wood species. Wood Research 60(2): 317-328.
9. Cai, Z., Ross, R.J., 2010: Wood handbook. Chapter 12: Mechanical properties of wood-based composite materials, 12 p. Report GTR-190. Forest Products Laboratory. Madison. WI, U.S.
10. Chen, D., Zhang, W., Shen, W., Jin, Z., Zhang, Q., 2019: Investigation on the mechanical properties of open-hole spruce and Douglas fir. Wood Research 64(1): 155-164.
11. Chen, H.T., Li, T., Zhou, C.L., Li, Y.Q., Song, R.X., 2015: Experimental evaluation on mechanical performance of OSB webbed parallel strand bamboo I-joist with holes in the web. Construction & Building Materials 101: 91-98.
12. Eckelman, C.A., 1975: Effects of holes on the bending strength of wood and particleboard parts. Wood Research Laboratory. Research Bulletin No. 922, 8 pp.
13. Falk, R.H., DeVisser, D., Plume, G.R., Fridley, K.J., 2003: Effect of drilled holes on the bending strength of large dimension Douglas-fir lumber. Forest Products Journal 53(5): 55-60.
14. Franke, F., Franke, B., Harte, A.M., 2015: Failure modes and reinforcement techniques for timber beams-state of the art. Construction and Building Materials 97: 2-13.
15. Gao, H., Yang, X.C., Zhang, C., 2015: Experimental and numerical analysis of three-point bending fracture of pre-notched asphalt mixture beam. Construction & Building Materials 90: 1-10.

16. Ghasemi, A.R., Moradi, M., 2017: Effect of thermal cycling and open-hole size on mechanical properties of polymer matrix composites. Polymer Testing 59: 20-28.
17. Hallström, H., 1996: Glass fibre reinforced holes in laminated timber beams. Wood Science and Technology 30: 323-337.
18. Hosseinpourpia, R., Mai, C., Taghiyari, H.R., 2019: Properties of medium-density fibreboards bonded with dextrin-based wood adhesive. Wood Research 64(2): 185-194.
19. Svoboda, T., Ruman, D., Gaff, M., Gasparik, M., Miftieva, E., Dundek, L., 2015: Bending characteristics of multilayered soft and hardwood materials. Bioresources 10(4): 8461-8473.
20. TS EN310, 1999: Wood-based panels. Determination of modulus of elasticity in bending and of bending strength.
21. TS EN322, 1999: Wood-based panels. Determination of moisture content.
22. TS EN323, 1999: Wood-based panels. Determination of density.
23. Xu, W.T., Que, Z.L., 2016: Stress performance analysis of laminated veneer lumber (LVL) with holes and plywood reinforcement methods. China Forest Products Industry (11): 30-34.
24. Yildirim, M.N., Uysal, B., Ozcifci, A., Ertas, A.H., 2015: Determination of fatigue and static strength of scots pine and beech wood. Wood Research 60(4): 679-686.
25. Yoshihara, H., 2016: Analysis of the open-hole compressive strength of spruce. Holzforschung 70(5): 449-455.
26. Zhou, J., Hu, C., Hu, S., Yun, H., Jiang, G., and Zhang, S., 2012: Effects of temperature on the bending performance of wood-based panels. BioResources 7(3): 3597-3606.

Nurdan Cetin Yerlikaya*
Yalova University
Faculty of Art And Design
Department of Interior Design
Central Campus, Cinarcik Road 77200
Yalova
Turkey

Abdurrahman Karaman*
Usak University
Banaz Vocational School
Department of Forestry
Usak
Turkey
*Corresponding authors: nurdan.yerlikaya@yalova edu.tr, abdurrahman.karaman@usak.edu.tr

STUDY ON COLD/WARM SENSATION OF MATERIALS

USED IN DESKTOP OF FURNITURE

Wen-Gang Hu, Na Liu, Lu Xu, Huiyuan Guan
Nanjing Forestry University
China

ABSTRACT

The aim of this study was to investigate the cold/warm sensations of materials used in desktop when forearms touching desktop. Both experimental tests and subjective evaluations were conducted in this study. A device was developed used to simulate forearm in order to replace subjects. Five men and five women were selected and introduced to six types of materials and two types of environmental temperatures in the tests. The results showed that the effects of environmental temperature on contact temperature of all tested materials were statistically significant, and the differences among wood and wood based materials, plastic materials, and artificial stone were also statistically significant. The device developed in this study was qualified to measure the contacting temperature between forearm and desktop sustainably and steadily, which can reduce the error introduced by subjects. Although qualitative relation was found between contact temperature and subjective evaluations, no quantitative correlation was proved.

KEYWORDS: Desktop, furniture, forearm, cold/warm sensation.

INTRODUCTION

Man has a very effective temperature regulatory system, which keeps the body's core temperature at approximately 37°C. Sweating is an effective cooling tool because the energy required for the sweat to evaporate is taken from the skin. Man considers the environment comfortable if no type of thermal discomfort is present. The first comfort condition is thermal neutrality, which means that a person feels neither too warm nor too cold. Franger (1972) regarded thermal neutrality as thermal comfort. Gagge and Gonzalez (1974) thought thermal comfort is a comfortable condition that you do not feel cold or hot. It was defined in the ISO 7730 (1994) standard as being "That condition of mind which expresses satisfaction with the thermal environment". A definition most people can agree on, but also a definition which is not easily converted into physical parameters.

Thermal environments are considered together with other factors such as air quality, light, noise level and interior decoration, when we evaluate our working environment (Song et al. 2016). If we do not feel the everyday working environment is satisfactory, our working performance will inevitably suffer. Thus, thermal comfort also has an impact on our work efficiency. Furniture is the most frequent device we touch in daily life and working and occupies most spaces of room. Therefore, it directly influences the thermal environment and comfort.

Some studied the effects of furniture arrangement on the whole thermal environment of room by computational fluid dynamics (Zukowska et al. 2012, Zhuang et al. 2014, Horikiri et al. 2015, Li et al. 2020). Others investigated the thermal comfort of human body when touching furniture (Zhou et al. 2018). Wang et al. (2007) studied how upper extremity skin temperatures correlate with overall-body thermal sensation by measuring skin temperatures at the finger, hand, and forearm. The results showed that finger temperature and finger-forearm temperature gradients are very similar in their correlation to overall sensation. Wang et al. (2000) investigated the relation between the skin temperature of the palm and sensory cold-warmth after contact with some materials. Results showed that it is possible to evaluate the contacted sensory cold-warmth relying on the basic thermal properties of material. In addition, gender difference in thermal comfort for Chinese people was investigated through two laboratory experiments by Lan et al. (2007). The results show that there are gender differences in thermal comfort for Chinese people. Female comfortable operative temperature (26.3°C) is higher than male comfortable operative temperature (25.3°C). Pasut et al. (2013) evaluated the effect of heated/cooled chair on thermal sensation and comfort. The results show that the heated/cooled chair strongly influences the subjects' thermal sensation and comfort. Vlavić et al. (2012a) studied temperature and moisture as the contributing factors to sitting comfort during performance of usual tasks under controlled conditions. The study method employed temperature and moisture measurements on five different office chairs using the probes placed on or in the seats. At the same year, they further studied the thermal discomfort of five different office chairs as subjects performed their usual jobs in controlled conditions by sensation differential technique (Vlaović et al. 2012b).

Forearm is the part touching the desktop most frequently, and the skin is most sensitive to temperature when contacting with desktop, therefore, sensations of forearm for temperature contacting with desktop plays an important role in thermal comfort of man.

The aim of this study was to evaluate the cold/warm sensation of materials commonly used in desktop when forearm contacts with desktops using experimental test and subjective evaluation. The specific objectives are to 1) evaluate the changes of temperature when forearm contacting different desktop materials by subjects; 2) develop a simple device to simulate the forearm used to measure the changes of temperature when forearm contacting desktop; 3) evaluate the cold/warm by seven-point thermal sensation scale semantics differential method; 4) compare the results of experimental tests measured by subjects, device and subjective evaluation.

MATERIAL AND METHODS

Test materials

Six types of materials commonly used in desktop (Chen and Zhu 2019, Guo et al. 2020) were chosen in this study including medium density fiberboard (MDF), laminated bamboo lumber (LBL) rubber wood (RW), melamine resin surfaced particleboard (MRSP), acrylonitrile butadiene styrene plastic (ABS), and marble (MARB). The dimensions of specimens are all measured 300 mm long, 150 mm wide and 18 mm thick. All samples were conditioned in a humidity chamber controlled at 20°C ± 2°C and 50% ± 3% relative humidity (RH) for two weeks.

Equipment and device

Thermocouple thermometers (Xinsite, HT-9815, China) was used to measure the changes of temperature, which contains four channels, and the measuring range is from 50ºC to 300ºC with accuracy of 0.1ºC.

Fig. 1 shows the device developed in this study to simulate forearms of subjects with outline dimensions of 250 mm × 100 mm × 70 mm. It is composed of seven parts: (1) digital display temperature controller used to control temperature, (2) power supply, (3) temperature probe used to measure internal temperature of the device, (4) heating plate, (5) elastic silicone rubber sheet used to simulate skin of man, (6) Aluminum alloy U-groove is supporting structure, and (7) thermal insulation cotton used to keep internal temperature of device.

The work principle of device is to simulate the temperature of forearm by internal temperature of the device, and the surface of elastic silicone rubber sheet is used to simulate skin of forearm.

(a)   *(b)*
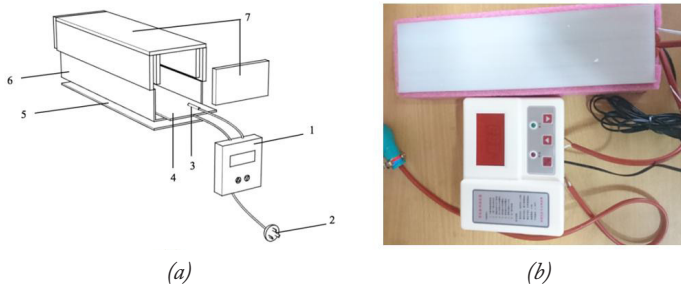
Fig. 1: The device used to simulate forearm (a) diagram and (b) the physical photo.

Test methods

The thermal comfort is seriously influenced by environmental temperature. Therefore, two environmental temperatures were set to investigate the sensations of cold/warm for different desktop materials, the high temperature (HT) and low temperature (LT) are 25ºC and 18ºC, respectively. The relative humidity keeps at a constant 50% ± 3%. The experiment includes two parts to conduct, the first one is to measure the temperature changes of forearm by subjects and device developed in the study respectively, and the second one is subjective evaluation on cold/warm sensation by subjects with semantics differential (SD) method (Zhagn et al. 2020).

Test measured by subjects

Ten healthy subjects with five males and five females were selected in this study. All of them are between 23-25 years old staffs. In order to minimize the effect of clothing, the subjects all wore the same cotton T-shirts, and jeans. Measurements were carried out in the air-conditioned room. Prior to measurement, the environmental temperature was turned to the specified temperature (HT or LT), and subjects went into the laboratory 30 min before conducting test to make the body temperature adjust to the environment.

Fig. 2 presents the setup of test. The tested specimen was laid on two foam strips to prevent from conducting heat through lab table, and the thermocouple probe was attached to the center of the forearm of subject with breathable tape. The temperature of subjects' forearm skins were measured before started testing. Subjects put their forearm right upon the tested specimen and kept in naturally reading postures. Each test lasted for 30 min, the temperature changes were record by the thermocouple thermometer with 1 min interval within the first 6 min of test, and recorded with increment of 3 min after 6 min. Each subject took 10 min break after finishing

each type of material test, each subject was tested in high and low temperature environment, respectively, in morning and afternoon. All tests were conducted throughout 10 days.
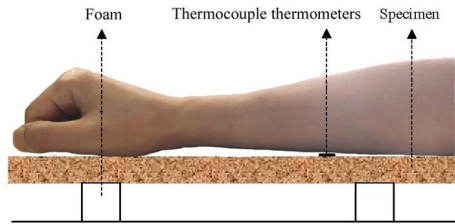

Fig. 2: Setup for measuring the temperature between desktop and forearm.

Test measured by device

Forearm of subject was replaced by the device developed in this study and the same test was repeated using the above testing method. Prior to measurement, the temperature of elastic silicone rubber sheet must be close to that of forearm skin as much as possible. In order to achieve this goal, correction must be done to make sure the correlation between internal temperature of device and the temperature of elastic silicone rubber sheet. The internal temperature of device was set as T_0 with values 35°C, 36°C, 37°C, 38°C, and 39°C respectively, and then the temperature of elastic silicone rubber sheet was set as T, and the values of T corresponding to each T_0 can were measured by thermocouple thermometer. Finally, the correlation between T_0 and T was figured out by regression method.

Subjective evaluation

During the experimental test by subjects, the subjects were also asked to evaluate the thermal comfort of tested materials by SD method after starting the test 1 min, 5min, 15min, and 30 min.

Tab. 1: Seven-point thermal sensation scale.

Semantic	Cold	Cool	Slightly cool	Neutral	Slightly warm	Warm	Hot
Scale	-3	-2	-1	0	1	2	3

Tab. 1 is the 7-point thermal sensation scale used to evaluate the thermal sensation according to Franger (1972) and ISO 7730 (1994). Fanger found that being thermally neutral guarantees comfort, because in optimal condition, no specific sensation of feeling warm or cold is to be expected by the subjects (Candas 2005).

RESULTS AND DISCUSSION

Results of experiments measured by subjects

Fig. 3 shows the temperature changes of six types of materials in HT and LT environments. The temperature-time curves all present the same trends, the temperature increased proportionally with time dramatically within the first 1 min, and then the curve increased slowly and temperature tended to be a constant at the end of test. In addition, the temperature of MARB was lower than other materials no matter in HT or LT environment, especially in LT environment.
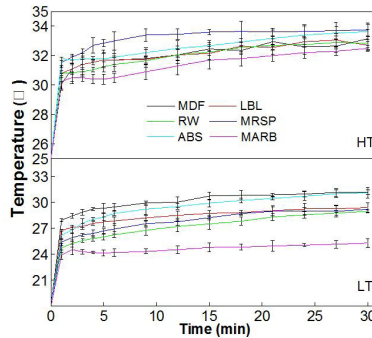
Fig. 3: Results of experiments measured by subjects.

An analysis of variation (ANOVA) was conducted to analyze the effects of material type and environmental temperature on contacting temperature of forearm at the time point of 30 min. The results showed the effects of environmental temperature on contacting temperature of forearm with all tested materials were statistically significant, and the differences between wood/wood based materials (MDF, WR, and LBL), plastic materials (ABS, and MESP), and artificial stone (MARB) were also statistically significant with their p-values all below 0.05.

Results of experiments measured by device

The correlation between T and T_0 was regressed by Origin pro 9.1 software (OriginLab, 1991), the regression equations in high and low temperature environments are shown in Eq. 1 and Eq. 2 respectively.

$$T_{HT} = 0.1171 \, T_0^2 - 7.8246 \, T_0 + 161.79 \qquad R^2 = 0.99988 \qquad (1)$$

$$T_{LT} = 0.0857 \, T_0^2 - 5.7569 \, T_0 + 125.5 \qquad R^2 = 0.99553 \qquad (2)$$

where: T_{HT}/T_{LT} - temperature of elastic silicone rubber sheet in high/low environment, (ºC),
   T_0 - is internal temperature of the device, (ºC).

The temperature-time curves of all six types of materials measured by device are all in the same trends compared with those determined with subjects, which is shown in Fig. 4. In addition, the temperature of MARB was still the lowest of all materials, which was consistent with results measured by subjects.
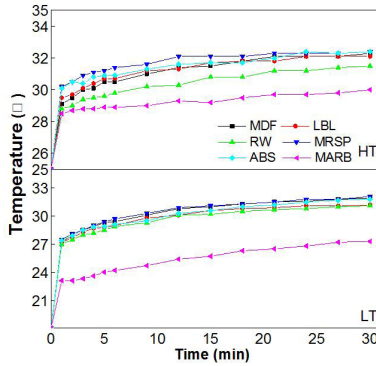
Fig. 4: Results of experiments measured by device.

Comparison of experimental results measured by subjects and device

The comparisons of results measured by subjects and device in HT and LT environments are shown in Fig. 5 and Fig. 6, resp.
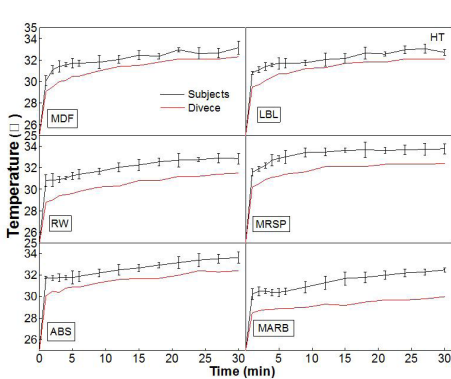
Fig. 5: Comparison of the results measured by subjects and device in high temperature environment.
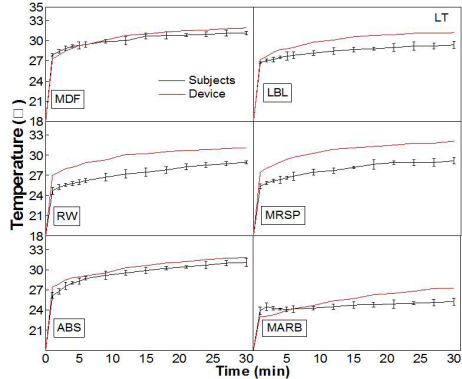
Fig. 6: Comparison of the results measured by subjects and device in low temperature environment.

The trends of temperature-time curves of them were similar to each other. However, the temperatures measured by subjects were all bigger than those measured by device in HT environment. By contrast, the results measured by device were bigger than those determined by subjects in LT environment. Furthermore, the temperatures of every measured time point of subject and device were compared in HT and LT environments, and the average errors and coefficients of variation (COV) are shown in Tab. 2. It suggested that the errors between the results of subjects and those of device were all within 10%, which means that device developed in this study can be used to measure the temperature between forearm and desktop sustainably and steadily.

Tab. 2: Errors of device measurement in high and low temperature environments.

Error	HT	LT
MDF	3.04% (38.4)	1.51% (56.8)
GLB	2.89% (33.4)	5.09% (32.8)
RW	5.04% (12.7)	9.21% (10.0)
MFCB	4.43% (10.4)	9.72% (8.8)
ABS	3.46% (20.4)	2.68% (35.1)
MARBLE	6.48% (16.5)	4.35% (60.6)

Results of subjective evaluation

Fig. 7 and Fig. 8 are results of mean values of subjective evaluations scored by subjects at time point of 1min, 5 min, 15 min and 30 min after starting tests in HT and LT environments respectively. According to the definition of thermal comfort (Franger 1972), subjects feel thermal comfort, when condition is not too hot or cold. In other words, the subjects are in thermal neutrality when sensation scale is equal to 0. Thus, the order of thermal comfort for all materials is: LBL, MDF, WR, MARB, MRSP, and ABS successfully in HT environment. The order in LT environment is: WR, MDF, MRSP, LBL, ABS, and MARB. Although the gender of subject is different, there is no gender difference in thermal sensation near neutral conditions (Lan et al. 2007).
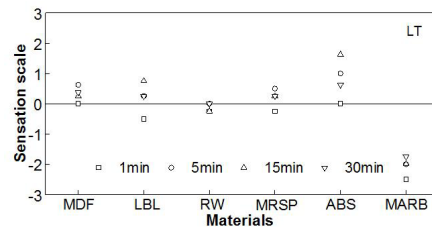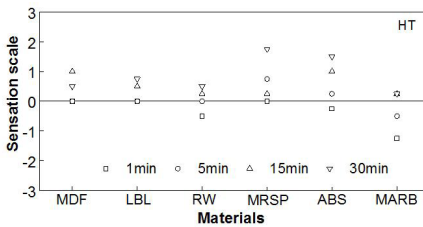
Fig. 7: Results of subjective evaluations of subjects in high temperature environment.

Fig. 8: Results of subjective evaluations of subjects in low temperature environment.

To be specific, the RW and MDF performed better thermal comfort than other tested materials both in HT and LT environments. The reason is that the thermal conductivities of wood and wood based materials are smaller than those of the other tested materials used in this study, because of the porosity of timber. The thermal comfort of MARB in HT environment was better than LT environment. The thermal conductivity of MARB is bigger than those of the other tested materials used in the study (Wang et al. 2001, Yang et al. 2016, Wang et al. 2020, Tang and Fu 2020), which made it adjusted to the environment temperature soon. Therefore, in HT environment, subjects felt cool at first, and then felt neutral with the temperature increasing. By contrast, in LT environment, the subjects felt more and more cold sensation with the temperature decreasing. In addition, in HT environment, the average sensation scale of ABS was -0.25 at 1 min, which means subjects felt slightly cool. However, with time increasing, the sensation scale increased fast to 1.5 at the end of test, which means the subject felt warm. It suggests that the sensation of cold/warm of material is not absolute but relative, which seriously influenced by environmental temperature and contacting time (Gagge et al. 1967, Höppe 2002).

To some extent, it can be found that there was a qualitative relationship between contact temperature and sensation of cold/warm. However, no correlation was found between the temperature and subjective evaluations of subjects, which was also confirmed by Vlaović et al. (2012b).

CONCLUSIONS

The cold/warm sensations of forearm when contacting different desktop materials in HT and LT environments were studied by experimental and subjective methods. Following conclusions were drawn: (1) The effects of environmental temperature on contacting temperature of forearm contacting all desktop materials were statistically significant. In specific, the differences between wood and wood based materials (MDF, WR, and LBL), plastic materials (ABS, and MESP), and artificial stone (MARB) were all statistically significant respectively. (2) The device developed in this study was qualified to measure the contacting temperature between forearm and desktop sustainably and steadily, which can be used to replace the subjects, and reduce the error introduced by subjects. (3) Although some qualitative relation was found between contacting temperature and subjective evaluations, no quantitative correlation was proved between them.

The thermal comfort is so complex and important for man that further studies are worth being done. The influences of different veneer materials on thermal comfort of desktop and how to choose materials of desktop for different types of furniture are two interesting topics to further study.

ACKNOWLEDGMENTS

REFERENCES

1. Candas, V., 2005: To be or not to be comfortable: Basis and prediction. Environmental ergonomics: The ergonomics of human comfort, health and performance in the thermal environment. In: Tochihara, Y., Ohnaka, T. (Eds.), Elsevier ergonomics book series, Vol. 3, Elsevier Ltd., Pp 207-215.
2. Chen Y.S., Zhu J., 2019: Study on bending characteristics of fast growing eucalyptus bookcase shelves by using burgers model. Wood Research 64(1): 137-144.
3. Fanger, P.O., 1972: Thermal comfort. McGraw Hill. New York, 25 pp.
4. Gagge, A.P., Gonzalez, R.R., 1974: Physiological and physical factors associated with warm discomfort in sedentary man. Environmental Research 7(2): 230-242.
5. Gagge, A.P., Stolwijk, J.A.J., Hardy, J.D., 1967: Comfort and thermal sensations and associated physiological responses at various ambient temperatures. Environmental Research 1 (1): 1-20.
6. Guo, Y., Guo, C.X., Shi, X., Shen, L.M., 2020: Adaptability of study desks and chairs based on analysis of sitting posture using OpenPose. Journal of Forestry Engineering 5(2): 179-185.

7. Höppe, P., 2002: Different aspects of assessing indoor and outdoor thermal comfort. Energy and Buildings 34(6): 661-665.
8. Horikiri, K., Yao, Y.F., Yao, J., 2015: Numerical optimization of thermal comfort improvement for indoor environment with occupants and furniture. Energy and Buildings 88: 303-315.
9. ISO 7730, 1994: Moderate thermal environments. Determination of the PMV and PPD indices and specification of the conditions for thermal comfort.
10. Lan, L., Lian, Z.W., Liu, W.W., Liu, Y.M., 2007: Investigation of gender difference in thermal comfort for Chinese people. European Journal of Applied Physiology 102(4): 471-480.
11. Li, X.X., Shen, L.M., Gao, J.S., 2020: Investigation of influence mechanism of temperature-controlled mattress on human thermal comfort in winter. Journal of Forestry Engineering 5(3): 175-182.
12. Pasut, W., Zhang, H., Kaam, S., Arens, E., Zhai, Y., 2013: Effect of a heated and cooled office chair on thermal comfort. HVAC&R Research 19(5): 574-583.
13. Song, S.S., Wan, Q., Wang, G.G., 2016: Eye movement evaluation of different wood interior decoration space. Wood Research 61(5): 831-843.
14. Tang, T.L., Fu, Y.C., 2020: Formation of chitosan/sodium phytate/nano-Fe_3O_4 magnetic coatings on wood surfaces via layer-by-layer self-assembly. Coatings 10(1): 51.
15. Vlaović, Z., Domljan, D., Grbac, I., 2012a: Research of temperature and moisture during sitting on office chairs. Drvna Industrija 63(2):105-112.
16. Vlaović, Z., Domljan, D., Župčić, I., Grbac, I., 2012b: Thermal comfort while sitting on office chairs-subjective evaluations. Drvna Industrija 63 (4): 263-270.
17. Wang, D., Zhang, H., Arens, E., Huizenga, C., 2007: Observations of upper-extremity skin temperature and corresponding overall-body thermal sensations and comfort. Building and Environmental 42(12): 3933–3943.
18. Wang, S.Y., Lin, F.C., Lin, M.Y., 2000: Thermal properties of interior decorative material and contacted sensory cold-warmth I: Relation between skin temperature and contacted sensory cold-warmth. Journal of Wood Science 46: 357-363.
19. Wang, S.Y., Lin, F.C., Lin, M.Y., 2001: Thermal properties of interior decorating material and the sensation of cold/warm by contact II: the relations among heat flux, temperature change of material, and sensation of cold/warm by contact. Journal of Wood Science 47: 109-114.
20. Wang, W.L., Peng, J.D., Zhao, Z.Y., Zhou, X.J., Zhang, J., Du, G.B., 2020: Modification of melamine-formaldehyde resin for decoration board. Journal of Forestry Engineering 5(2): 42-47.
21. Yang, B.S., He, S.J., Wang, F., Que, Z.L., Pan, B., Zhu, Y.X., 2016: Thermal performance of electrically heated flooring prepared by thin Chinese fir glulam. Journal of Forestry Engineering 1(1): 46-50.
22. Zhagn, Z.H., Xu, B.M., 2020: Tang dynasty chair feature design based on kansei evaluation and eye tracking system. Wood Research 65(1): 161-174.
23. Zhou, C.M., Yu, M.N., Zhou, T., 2018: Experimental study on three-dimensional shape mapping of complex furniture. EURASIP Journal on Image and Video Processing 9: 89.
24. Zhou, Z.B., Li, X., Ding, J.W., Guo, X.L. Cao, P.X., 2019: Structure design and process analysis of internal heating engineered wood flooring. Journal of Forestry Engineering 4(1): 165-169.

25. Zhuang, R., Li, X., Tu, J., 2014: CFD study of the effects of furniture layout on indoor air quality under typical office ventilation schemes. Building Simulation 7: 263-275.
26. Zukowska, D., Melikov, A.K., Popiolek, Z., 2012: Impact of personal factors and furniture arrangement on the thermal plume above a sitting occupant. Building and Environmental 49: 104-116.

Wen-Gang Hu, Na Liu, Lu Xu, Huiyuan Guan*
Nanjing Forestry University
Co-Innovation Center of Efficient Processing and Utilization of Forest Resources
College of Furnishings and Industrial Design
Nanjing
China
*Corresponding author: hwg@njfu.edu.cn

ECONOMICAL DESIGN OF TIMBER-CONCRETE COMPOSITE BEAMS

Nikola Velimirović[1], Ivan Stanimirović[2], Dragoslav Stojić[2], Nemanja Marković[2,3]
Milivoje Milanović[1]

[1]State University of Novi Pazar
Serbia
[2]University of Niš
Serbia
[3]Ruhr-University Bochum
Germany

ABSTRACT

The aim of the presented study is to find the best solution for the cross-sectional dimensions of timber-concrete composite (TCC) beam by focusing on serviceability limit state verification and cost of the beam, simultaneously. The population of 10.000 samples of the observed variables according to the predetermined ranges using Monte Carlo sampling method was generated. In order to find a number of Pareto-optimal solutions on the Pareto front, the weighted sum method was employed using original algorithm. The results have shown that minimum relative cost of the TCC beam can be increased even by 26.6% if the rheological effects that are neglected by the Effective modulus method are counted in the calculation of the final deflection. The presented trade-off strategy in design of the TCC beams has shown that with the slight increase of relative cost compared to the minimum, it is possible to get Pareto optimal design solution of the TCC beam that has drastically decreased final deflection and therefore is a more reliable design solution.

KEYWORDS: Timber-concrete composite, multi-criteria decision-making, Pareto optimality, weighted sum method.

INTRODUCTION

The timber-concrete composite (TCC) structure is a structural system in which a timber beam is connected to an upper concrete flange using different types of connectors (Dias et al. 2015). They were able to exploit the best properties of both materials due to bending and tensile

forces induced by gravity loads that are resisted primarily by the timber and compression by the concrete topping systems, while the connection system transmits the shear forces between the two components. Yeoh et al. (2011) provides survey on the timber-concrete composite research in the recent years. All around the world TCC systems have been used in structures during the last two decades. The main reason being that applications that could not have been built by timber alone now become possible with a use of TCC solution. In residential and office buildings, TCC systems have been extensively used for new floors and for upgrading and enhancing the performance of existing timber floors as the traditional timber floors may have excessive deflection, insufficient acoustic separation, and low fire resistance. TCC floors help in resolving all of these problems. Dias et al. (2016) gives a short overview of the use of TCC structural system in construction and then presents several case studies of its applications.

In structural design process, the design engineer has a task to offer the best technical solution of structure in accordance with the previously established terms and conditions. Civil engineering structures are generally designed based on prior work and experience, which often leads to the adoption of uneconomical solutions, because design engineers usually tend to maximally meet given design conditions. This comes as a direct result of the large safety and financial risks associated with civil engineering project because adopted structural design solution could drastically depart from the most favourable solution. Due to this fact, it is necessary to apply some of the optimization techniques in structural design process. However, the wide range of disparate and complex design requirements becomes a huge technical challenge when applying structural optimization within the design process of structures (Christensen and Klarbring 2009). Many of the structural design problems in civil engineering may be considered as multi objective problems. Design solution should satisfy confronting objectives at the same time. In order to solve this kind of problems, multi-criteria decision-making should be employed. In most cases, the ideal solution is not achievable. The problem of finding the best non-ideal solution usually does not have a unique solution. The level of optimality of a specific solution depends on the preferences made by the decision maker. The objective is the solution to be accepted as an effective result by the decision maker. In order to extent that objective, it is mandatory to contain those preferences as much as possible, in the computation process. There are numerous decision-making algorithms available in the literature. Probably the most known methods are the weighted sum method, ELECTRE method, TOPSIS method and PROMETHEE method. These algorithms vary in used normalization and weighting subroutines, which leads to the different complexities of these methods.

MATERIAL AND METHODS

Problem formulation

The market potential of the TCC systems is reflected in its application in construction of multi-storey residential and commercial buildings, which is presented in (Knauf 2017). The design guidelines of TCC structures are not explicitly given in any of the available structural design standards, except EN 1995-1-1 (2004). This standard does not consider design procedure in depth, but this should be changed with the development of new code generations. The future revision of Eurocode 5 should include a section dedicated to TCC systems (Dias et al. 2016). In design procedures for TCC systems, both serviceability and ultimate limit states under short-term and long-term loading should be considered. Although serviceability is generally considered less important than safety, the consequences of the serviceability failure may be significant in terms

of costs (Honfi et al. 2012). In many design situations, particularly in residential and office buildings, acceptable performance of the structural system is seldom defined by ultimate limit state, but rather by serviceability requirements, especially by final deflection limit (Fragiacomo and Schänzlin 2013, Fragiacomo and Lukaszewska 2013).

The aim of the present study is to find the best solution for cross-sectional dimensions of the TCC beam by focusing on serviceability limit state (SLS) verification and cost of the TCC beam, simultaneously. The main goal of this process is to minimize the material being used in a structure and to reduce its overall weight without compromising its performances. Therefore, the size optimization study of TCC beams may present an opportunity to find material and cost savings within construction of the structures and it can be of practical value to structural designers.
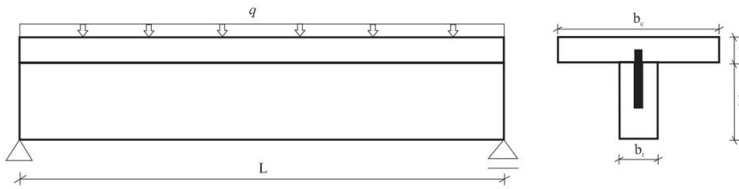
Fig. 1: Simply supported timber–concrete composite beam with mechanical fasteners.

In this study is considered simply supported TCC beam with mechanical fasteners as it is shown in Fig. 1. The input data of this optimization model shows geometrical characteristics of TCC cross section, observed connection system, mechanical characteristics of the componential materials and fasteners as well as loading and boundary conditions. Timber beam considered in this study has rectangular cross-section and it is performed of the spruce, sawn softwood timber structural strength class C27 with mechanical characteristics in accordance with the classification of structural timber with rectangular cross section (EN 338 2016). The concrete slab is made of concrete strength class C25/30 with characteristics according to EN 1992-1-1 (2004). Connection system, considered in this research, was achieved using glued-in steel rods made of the steel grade S235, which are often used to enhance old timber floors as well as for new construction works. In the pre-drilled holes, perpendicular to the grain and coated with epoxy resin, steel rods ϕ 20/150 mm are embedded at constant intervals of s = 240 mm. We have considered TCC beams in indoor conditions, where temperature (T) is 22 ± 4°C and relative humidity (RH) is 50 ± 5%. Based on Eurocode 5, these conditions correspond to the service class 1. According to the Eurocode recommendations (EN 1991-1-1 2002), for the areas for domestic and residential activities, the imposed load of 2 kN·m^{-2} is suggested.

Optimization variables

In this study, geometrical characteristics of the cross-section of the TCC beam are observed as independent optimization variables: width of timber beam (*bt*), height of the timber beam (*ht*), height of the concrete slab (*hc*) and width of the concrete slab (*bc*). For the chosen optimization variables, it is necessary to define some constraints in terms of lower and upper bound that should define our research area. The appropriate range of optimization variables was defined based on EN 1995-1-1 (2004), recommendations of the EOTA (ETA-11/0270 2013) as well as based on the empirical recommendations. The other design parameters that are used for the calculation, such as material properties, characteristics of connection system, loading and boundary conditions are fixed during the optimization.

Tab. 1: The constraints of optimization variables.

Optimization variable	Symbol	Dimension	Lower bound	Upper bound
Width of timber beam	b_t	*mm*	50	150
Height of timber beam	h_t	*mm*	100	500
Height of concrete slab	h_c	*mm*	50	100
Width of concrete slab	b_c	*mm*	600	1000

Typical spans for this type of constructions where the timber beam is made of sawn softwood are up to 8 m (ETA-11/0270 2013). According to that, we will conduct an optimization study on TCC beams with spans ranging between 4 m and 8 m.

Objective functions

The most important SLS verification of the TCC beams is the control of the final deflection. The long-term behaviour of the TCC system is a very complex problem and it is not only affected by the long-term load but also by the long-term behaviour of the constituent materials. The variation of the environmental conditions such as temperature and relative humidity significantly affects the behavior of the materials employed in TCC system. The differential shrinkage/swelling of the concrete flange and timber beam cannot freely occur due to the connection system that restrains the possibility of either part to move relative to the other. Consequently, additional deformations will be induced in the composite beam. Therefore, the design of such structures is usually conditioned by the maximum deflection in service. According to this fact, the first objective function is to minimize final mid-span deflection of the TCC beam.

The aim of the economical design is a cost-effective choice of shapes and sizes of structural elements. Therefore, the second objective function is to minimize the cost of the TCC beam. Considering that this composite system is still in the phase of development and introduction onto the market, cost estimation is a very difficult task. There are currently still learning effect costs, which make a calculation of the costs that exist on a long-term basis more difficult (Knauf 2017). Therefore, we defined cost of the TCC beam as follows:

$$C(\boldsymbol{x}) = c_c \cdot V_c + c_t \cdot V_t = (c_c \cdot b_c \cdot h_c + c_t \cdot b_t \cdot h_t) \cdot L \tag{1}$$

where: c_c and c_t denote the relative costs of the manufacturing and embedding concrete and timber material per cubic meter, respectively.

Considering the current state of the market, we have assumed that relative cost of the timber is three times higher than relative cost of the concrete per cubic meter. The considered cost of the TCC beam does not contain cost of fasteners, since it is assumed that the number of fasteners for a particular beam length is constant for all optimization alternatives.

Design constraints

In order to avoid the deformations and other undesirable effects in service such as appearance/comfort/functioning of the structure, the maximum deflection of the horizontal structural elements should be limited. According to the EN 1995-1-1 (2004), for the simply supported TCC beam, the limiting value of the final deflection is L/200, where L is the span of the TCC beam. In addition, based on the design recommendations presented in ETA-11/0270 (2013), we assumed that the ratio of the height of the concrete slab (h_c) and the height of the timber beam (h_t) is less than 70%.

Multi-criteria decision-making background

Weighting coefficients are often utilized for purpose of the criteria importance (Jahan et al. 2012, Zardari et al. 2015). Let us consider a multi-criteria model for ranking the alternatives $(A_1,...,A_m)$ using n criteria $(C_1,...,C_n)$, where the value used to depict the alternative Ai satisfying the criterion C_j, is denoted by a_{ij}. The coefficients of alternatives with respect to criterion C_j are given in the jth column of the decision matrix $DM = [a_{ij}]_{m \times n}$. Obviously, these standards may have dissimilar significance for the decision maker. For each criterion, the values of alternatives may be expressed using unequal units. Therefore, the decision matrix needs to be normalized in order to provide meaningful decisions. We have considered the vector normalization method, although there are many other normalization methods, and they can be found in (Jahan and Edwards 2015). Using this method, the normalized decision matrix $NDM = [q_{ij}]_{m \times n}$ is determined. Each element in this matrix belongs to the real unit interval [0, 1]. However, all the criteria, which are of the minimization kind, are translated to the maximization kind by multiplying the values by -1.

The ranking of alternatives

For $i = 1, 2,..., m$, $j = 1, 2,..., n$, elements qij determine the new normalized values of the alternative Ai using the criterion C_j. Now, if W_j is the weight joined to the criterion C_j, then we can consider the following equations to determine preference elements e_{ij} associated with criteria C_j.

$$e_{ij} = W_j \cdot q_{ij}, \qquad i = 1,..., m; \qquad j = 1,..., n. \tag{2}$$

Next, the elements e_{ij} ($j = 1,2,...,n$) should be summed to obtain the overall value of the alternative A_i given by:

$$V(A_i) = \sum_{j=1}^{n} e_{ij} \tag{3}$$

Finally, ranking of the alternatives A_i is constructed on the value of the aggregation (3) and the completion of criteria in the order of significance. For each two alternatives A_i and Aj it is said that Aj is preferred over A_i, notated as $Aj \rightarrow A_i$, if and only if:

$$
\begin{aligned}
&V(A_i) < V(A_j) \\
&V(A_i) = V(A_j), \quad e_{i1} < e_{j1} \\
&... \\
&V(A_i) = V(A_j), \quad e_{i1} = e_{j1},...,e_{i,n-1} = e_{j,n-1}, \quad e_{in} < e_{jn}
\end{aligned}
\tag{4}
$$

The best possible values for each criterion define ideal point in objective space:

$$f^* = (f_1^*, f_2^*,..., f_n^*) \tag{5}$$

If there is solution x^* that minimizes all objective functions simultaneously:

$$f_j(x^*) \le f_j(x), \quad \forall x \in X, \; j=1,...,n \tag{6}$$

where $f_j^* = f_j(x^{(j)*})$, then such a solution is called the ideal solution:

$$x^* = \{x \mid f_j(x) = f_j^*, j=1,...,n\} \tag{7}$$

However, in real conditions there is no ideal solution, because in most of the cases multi-criteria decision-making considers problem of conflicted objectives that cannot be satisfied simultaneously, therefore finding the optimal solution is very complicated. Pareto optimality has the main role in solving multi-criteria decision-making. Solution $x^* \in X$ is Pareto optimal of multi-criteria decision making if there is no other feasible solution $x \in X$ that it is:

$$f_j(\boldsymbol{x}) \le f_j(\boldsymbol{x}^*), \qquad \forall j = 1,...,n \tag{8}$$

and that for at least one criterion there is no other feasible solution $x \in X$ that it is:

$$f_j(\boldsymbol{x}) < f_j(\boldsymbol{x}^*) \tag{9}$$

However, Pareto optimality in most of the cases provides not just one solution, but a set of solutions where selecting any of them will sacrifice the quality of selection at least one of the criteria, while simultaneously improving least one. This set of solutions is often called Pareto optimal set or Pareto front. The choice of the final solution of multi-criteria decision-making problem could be made either by decision maker or by corresponding to scalarization method.

RESULTS AND DISCUSSION

Optimization alternatives

The design procedure for TCC systems provided in EN 1995-1-1 (2004) is based on an approximate solution of the differential equation for beams with partial composite action. The proposed design method, *γ-method*, could be applied for the short-term verifications. For the long-term verifications, the Effective modulus method presented by Ceccotti (2002) is usually employed in order to account for the effect of creep of the constituent materials of the TCC. Based on the research carried out in recent years, it has been recognized that this approach has certain shortcomings and that is presented in the literature by different authors, Fragiacomo and Cecotti (2004), Fragiacomo (2006), Jorge et al. (2010), Kanócz et al. (2013), Kanócz and Bajzecerová (2014). The Effective Modulus method neglects phenomena such as the concrete shrinkage and inelastic strains of concrete and timber due to thermo-hygrometric environmental variations. Therefore, inclusion of all long-term effects related to constituent materials is highly recommended when accurate long-term analysis of TCC is required (Dias et al., 2018).

In order to generate relevant samples of optimization variables according to the predetermined ranges of optimization variables, Monte Carlo Sampling method (Kroese et al. 2014) was employed. Using this sampling method, we have generated the population of 10.000 samples of the observed optimisation variables. In order to investigate the effects of beam spans on the economical design of TCC beams, we have considered medium and long-span beams with spans ranging between 4 m and 8 m. The optimization alternatives were formed on the basis of the observed criteria, the cost of the TCC beam and the final mid-span deflection. In order to analyze the influence of the phenomena, that are neglected in the Effective modulus method, on the economical design, we have formed two groups of alternatives. In the first group of alternatives (EC-SC1), the final deflection of the TCC beams was calculated according to the Effective modulus method, but in the second group of alternatives (INDOOR) using rigorous approach presented by Kanócz et al. (2013). Fig. 2 presents the trade-off charts of calculated optimization alternatives for the observed ranges of TCC beams.
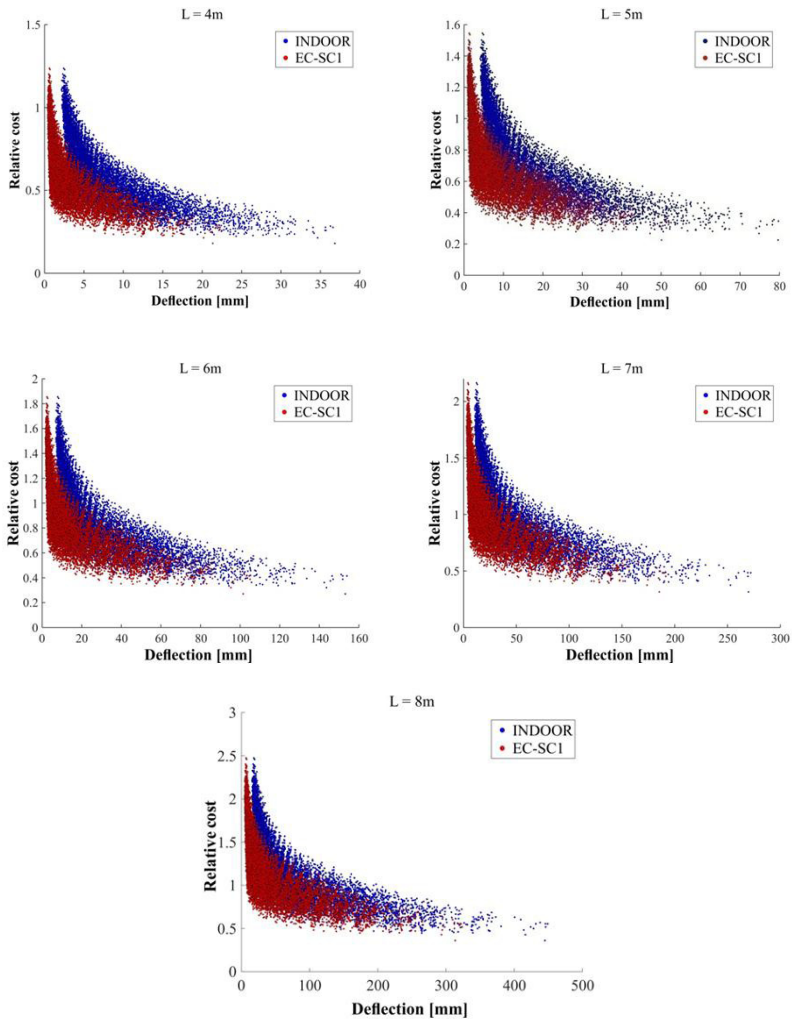
Fig. 2: Trade-off charts of alternatives for the considered spans of TCC beams.

Additionally, it provides us with a comparative analysis of the two observed approaches to calculate the final mid-span deflection of the TCC beams. In order to rank the alternatives, we have used a variation of the Weighted sum method as explained before. At the beginning, the decision matrix is given and weighting coefficients are specified for the cost and for deflection values. The implementation was performed based on generated algorithm:

Algorithm: Calculation of the best alternatives

Input: Weights w_1 and w_2 for the cost and deflection, respectively; the number of alternatives m

1:    Perform the normalization of the decision matrix C:

$$c'_{ij} = \frac{c_{ij}}{\sum\limits_{k=1}^{m} c_{kj}}, \quad 1 \le i \le m, \quad 1 \le j \le 2$$

2:    **For** each alternative i, $1 \le i \le m$ calculate the weighted sum of the cost and deflection as:

$$d_i = w_1 \cdot c_{i1} + w_2 \cdot c_{i2}$$

3:    Sort the alternatives (rows in matrix C) by the value of di , from largest to smallest values, and denote the new matric by D.

4:    **Return** the first n rows of the matrix D as the result.

Minimum relative cost of the TCC beam

Firstly, we have conducted optimization analysis using generated algorithm, where the weighting coefficient for the beam cost was adopted equal to 1. The result of this analysis is the minimum relative cost of the TCC beam so that the serviceability requirements are satisfied. This analysis has also considered the two different approaches for the calculation of the final mid-span deflection, which were previously exposed. In the Tab. 2 are summarized the second-order polynomial fits between the minimum relative costs and the spans of the TCC beams. These results can be used to get an initial estimation of the costs under a given span length.

Tab. 2: Polynomial best–fit equations for minimum relative cost of the TCC beams.

Model	Polynomial best-fit equation	Coefficient of determination (R^2)
EC–SC1	$0.008853 \cdot L^2 - 0.07567 \cdot L + 0.1131$	0.9994
INDOOR	$0.005708 \cdot L^2 + 0.06426 \cdot L - 0.1195$	0.9966

Fig. 3 shows the results of the conducted optimization analysis and the polynomial best fits of those results.
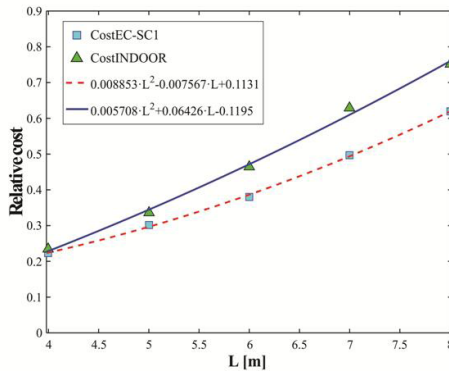

Fig. 3: Minimum relative cost of the TCC beam.

The first curve gives an overview of the obtained results based on the Effective modulus method (CostEC-SC1), while the other curve is formed using results gained by the advanced rigorous approach (CostINDOOR). It is noticeable that both curves have the same non-linear trend that increases with the beam span. Based on the presented analysis results, we can conclude that the minimum relative cost of the TCC beam can be increased even by 26.6% if the rheological effects that are neglected by the Effective modulus method are counted in the calculation of the final deflection. The benefit of the conducted optimization analysis could be the required TCC beam depth. Polynomial best-fits of these results are tabled in Tab. 3.

Tab. 3: Polynomial best–fit equations for required TCC beam depth.

Model	Polynomial best-fit equation	Coefficient of determination (R^2)
EC-SC1	$2.417 \cdot L^2 + 5.53 \cdot L + 129.1$	0.9829
INDOOR	$-1.042 \cdot L^2 + 70.84 \cdot L - 63.45$	0.9991

Based on the Fig. 4, we can see that the required depth of the TCC cross section should be increased even by 36.7% compared to the case where the differential shrinkage is neglected. Therefore, the usual practice of neglecting differential shrinkage leads to a significant underestimation of the final deflection. This analysis gives us the opportunity to offer the recommended span/depth ratio for the TCC beams.

Based on the results obtained using the Effective modulus method, this ratio is approximately 23.4. However, if we include all the long-term effects related to constituent materials that are ignored by this method, the average value of the span/depth ratio is 18.7. These results should prove useful to structural designers and is expected to advance existing design practices of TCC beams.
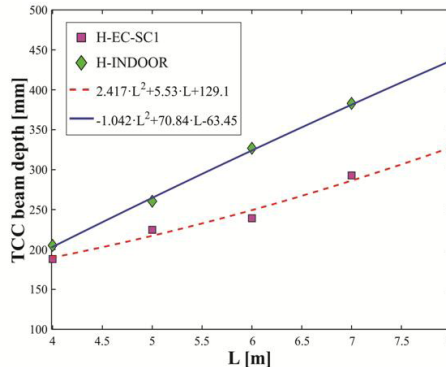

Fig. 4: Required TCC beam depth.

Trade-off strategy in design of the TCC beams

When the large number of design options need to be evaluated according to the considered criteria, it is very helpful to present them in the objective space, as it is shown in Fig. 2. The outer boundary of this set of optimization alternatives would define the borderline limit beyond which design cannot be further improved. In the multi-objective decision-making, this borderline presents the Pareto front that separates the feasible and infeasible regions. The feasible region is defined as the set of feasible solutions, for which all constraints are satisfied. When the value of one objective function of the Pareto-optimal solution is decreasing, while keeping the value of the

other objective function constant, this would move that design option into the infeasible region. Increasing the value of one objective function, while keeping the value of the other objective function constant, would no longer make the design optimal. In order to find a number of Pareto-optimal solutions on the Pareto front, the weighting coefficients for both objectives have been varied using previously presented algorithm.

In this study, we have carried out the multi-criteria decision making process using alternatives where final deflection of the TCC beam is obtained by advanced approach that include all the long-term effects related to constituent materials.
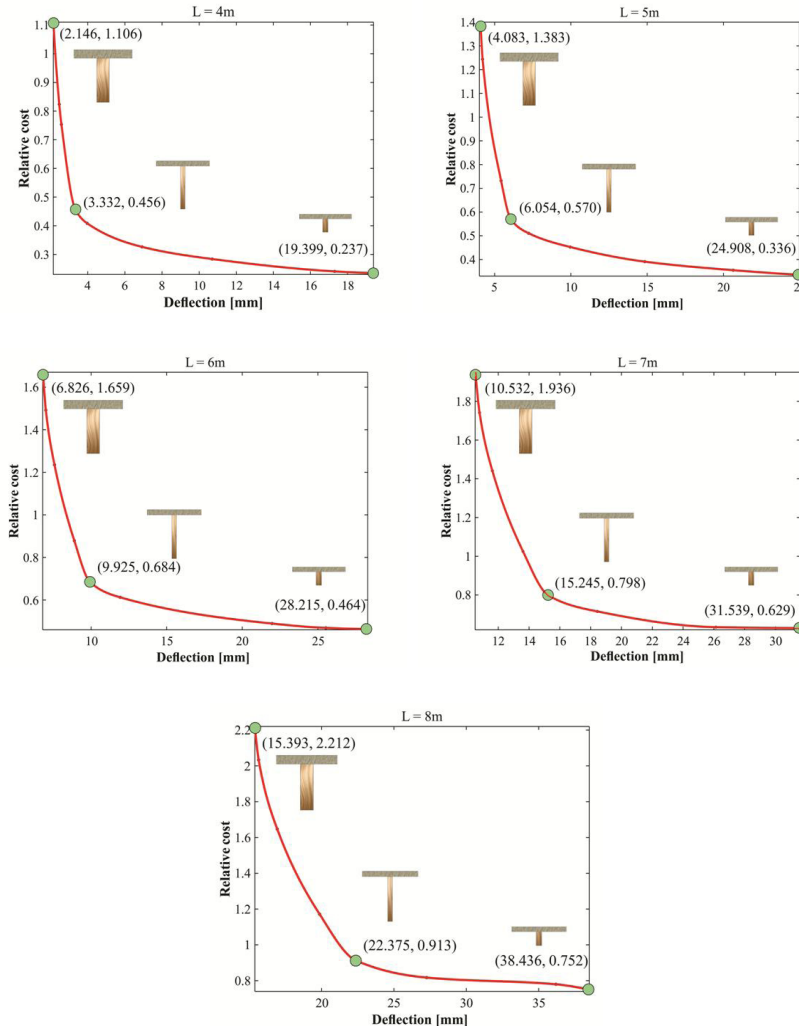
Fig. 5: Design proposals of TCC beams obtained by selecting different solutions of the Pareto front.

Fig. 5 shows Pareto fronts for different beam spans and some possible designs of TCC cross section obtained by selecting different Pareto-optimal solutions of the Pareto front. We can see that the first objective function, deflection, dominates the design process compared to the relative cost function. Fig. 5 provides some samples of changing geometry of the TCC cross section along the Pareto front and allows us to see how becomes robust when taking Pareto-optimal solutions from the right to the left part of the Pareto front.

Analyzing the results of the performed size optimization, we can see that with an increase in the relative price of the TCC beam with span 4 m for only 2.62% compared to the minimum relative cost of the beam, we could obtain the Pareto optimal solution for which the mid-span deflection of the beam is reduced by 10.81%. A similar situation is with the 5-meter long beam. When the relative cost of the beam is increased by 5.77% compared to its minimum value, we can have composite beam which maximum deflection in the end of the service life is reduced by 17.14%. Using trade-off strategy in the design of the TCC beam with span of 6 m, we could get even better improvements in design process. Increasing the relative cost for only 1.09% related to its minimum value, we will get TCC beam which final deflection is reduced by 9.52%, or with an increase of 5.48% of the relative cost, the final deflection is reduced by 22.14%. In the case of the TCC beam of 7m, we have the possibility to get the design option of the cross-section whereby the final deflection could be decreased by 17.15% with an increase of the minimum relative cost for only 0.73%, or even better design option with cost increase of 13.63% to get TCC beam with decreased final deflection for even 41.54%. Finally, in the case of the longest observed TCC beam with the span of 8m, we could improve design of the beam with an increase of the relative cost for 8.69%, but we could get the composite beam which final deflection is decreased by 29.08%.

Financial savings are an obvious potential driver for use of the structural optimization. However, based on the presented trade-off strategy in design of the TCC beams, we can see that with the slight increase of relative cost it is possible to get Pareto optimal design solution of the TCC beam that has drastically decreased final deflection and therefore is a more reliable design solution.

CONCLUSIONS

In order to find economical solution for cross-sectional dimensions of the timber-concrete composite (TCC) beam, size optimization has been conducted by focusing on final mid-span deflection and cost of the TCC beam, simultaneously.

Based on the presented analysis results, it was concluded that the minimum relative cost of the TCC beam can be increased even by 26.6% if the rheological effects that are neglected by the Effective modulus method are counted in the calculation of the final deflection. In addition, it can be seen that the required depth of the TCC cross section should be increased even by 36.7% compared to the case where the differential shrinkage is neglected. This analysis gives the opportunity to offer the recommended span/depth ratio for the TCC beams. Based on the results obtained using the effective modulus method, this ratio is approximately 23.4. However, if we include all the long-term effects related to constituent materials that are ignored by this method, the average value of the span/depth ratio is 18.7. Therefore, we can conclude that the usual practice of neglecting differential shrinkage leads to a significant underestimation of the final deflection. Therefore, inclusion of all long-term effects related to constituent materials is highly recommended when accurate long-term analysis of TCC is required. The weighted sum method was applied in order to find a number of Pareto-optimal solutions on the Pareto front using presented original algorithm. Financial savings are an obvious potential driver for use of

the structural optimization. However, based on the presented trade-off strategy in design of the TCC beams, we can see that with the slight increase of relative cost compared to the minimum, it is possible to get Pareto optimal design solution of the TCC beam that has drastically decreased final deflection and therefore more reliable design solution. The Pareto fronts for different considered beam spans were presented as well as some representative samples of TCC cross section obtained by selecting different Pareto-optimal solutions.

REFERENCES

1. Ceccotti, A., 2002: Composite concrete-timber structures. Progress in Structural Engineering and Materials 4(3): 264-275.
2. Christensen, P.W., Klarbring, A., 2009: An introduction to structural optimisation. Springer Science & Business Media. Netherlands, 214 pp.
3. Dias, A.M.P.G., Martins, A.R.D., Simões, L.M.C., Providência, P.M., Andrade, A.A.M., 2015: Statistical analysis of timber-concrete connections-Mechanical properties. Computers & Structures 155: 67-84.
4. Dias, A., Skinner, J., Crews, K., Tannert, T., 2016: Timber-concrete-composites increasing the use of timber in construction. European Journal of Wood and Wood Products 74(3): 443-451.
5. Dias, A., Schänzlin, J., Dietsch, P. (eds.), 2018: Design of timber-concrete composite structures: A state-of-the-art report by COST Action FP1402 / WG 4, Shaker Verlag Aachen, 228 pp.
6. EN 1991-1-1, 2002: Eurocode 1: Actions on structures. Part 1-1: General actions - Densities, self-weight, imposed loads for buildings.
7. EN 1992-1-1, 2004: Eurocode 2: Design of Concrete Structures. Part 1-1: General Rules and Rules for Buildings.
8. EN 1995-1-1, 2004: Eurocode 5: Design of timber structures. Part 1-1: General - Common rules and rules for buildings.
9. EN 338, 2016: Structural timber. Strength classes.
10. ETA-11/0270, 2013: Self-tapping screws for use in wood-concrete slab kits.
11. Fragiacomo, M., 2006: Long-term behavior of timber–concrete composite beams. II: Numerical analysis and simplified evaluation. Journal of Structural Engineering 132(1): 23–33.
12. Fragiacomo, M., Ceccotti, A., 2004: A simplified approach for long-term evaluation of timber-concrete composite beams. In: Proceedings of the 8th World Conference on Timber engineering. Finnish Association of Civil Engineers RIL. Lahti, Finland. Pp. 537-542.
13. Fragiacomo, M., Lukaszewska, E., 2013: Time-dependent behaviour of timber–concrete composite floors with prefabricated concrete slabs. Engineering Structures 52: 687-696.
14. Fragiacomo, M., Schänzlin, J., 2013: Proposal to account for concrete shrinkage and environmental strains in design of timber-concrete composite beams. Journal of Structural Engineering 139(1): 162-167.
15. Honfi, D., Martensson, A., Thelandersson, S., 2012: Reliability of beams according to Eurocodes in serviceability limit state. Engineering Structures 35: 48-54.
16. Jahan, A., Edwards, K.L., 2015: A state-of-the-art survey on the influence of normalization techniques in ranking: Improving the materials selection process in engineering design. Materials and Design 65: 335–342.

17. Jahan, A., Mustapha, F., Sapuan, S.M., Ismail, M.J., Bahraminasab, M., 2012: A framework for weighting of criteria in ranking stage of material selection process. The International Journal of Advanced Manufacturing Technology 58(14): 411-420.

18. Jorge, L.F., Schänzlin, J., Lopes, S.M.R., Cruz, H., Kuhlmann, U., 2010: Time-dependent behaviour of timber lightweight concrete composite floors. Engineering Structures 32(12): 3966–3973.

19. Kanócz, J., Bajzecerová, V., Šteller, Š., 2013: Timber - concrete composite elements with various composite connections part 1: screwed connection. Wood Research 58(4): 555-570.

20. Kanócz, J., Bajzecerová, V., 2014: Parametric analysis of long-term behaviour of timber-concrete composite bended elements. Wood Research 59(3): 379-388.

21. Knauf, M., 2017: Market potentials for timber-concrete composites in Germany's building construction sector. European Journal of Wood and Wood Products 75(4): 639–649.

22. Kroese, D.P., Brereton, T., Taimre, T., Botev, Z.I., 2014: Why the Monte Carlo method is so important today. WIREs Computational Statistics 6(6): 386–392.

23. Lukaszewska, E., Johnsson, H., Fragiacomo, M., 2008: Performance of connections for prefabricated timber-concrete composite floors. Materials and Structures 41(9): 1533-1550.

24. Yeoh, D., Fragiacomo, M., De Franceschi, M., Boon, K.H., 2011: State of the art on timber-concrete composite structures: literature review. Journal of Structural Engineering 137(10): 1085–1095.

25. Zardari, N.H., Ahmed, K., Shirazi, S.M., Yusop, Z.B., 2015: Weighting methods and their effects on multi-criteria decision making model outcomes in water resources management. Springer. Cham, 166 pp.

Nikola Velimirović*
State University of Novi Pazar
Department of Technical Sciences
36300 Novi Pazar
Serbia
*Corresponding author: velimirovic.nikola@gmail.com

Ivan Stanimirović
University of Niš
Faculty of Science and Mathematics
18000 Niš
Serbia

Dragoslav Stojić, Nemanja Marković
University of Niš
Faculty of Civil Engineering and Architecture
18000 Niš
Serbia

Ruhr-University Bochum
Faculty of Civil and Environmental Engineering
44801 Bochum
Germany

Milivoje Milanović
State University of Novi Pazar
Department of Technical Sciences
36300 Novi Pazar
Serbia

AN EXPERIMENTAL STUDY ON SUSTAINABILITY OF HISTORICAL WOODEN BUILDINGS EXPOSED TO OPEN SEA STREAMS

Esra Celik, Ismail Cengiz Yilmaz, Deniz Yilmaz
Istanbul Arel University
Turkey

ABSTRACT

This research deals with the impact of the microclimate on historical wooden buildings exposed to open sea streams. The Florya Ataturk Marine Mansion in Istanbul, erected on the sea, totally defenceless to weather and sea effects, has been selected as representative case study for many other buildings located in Bosphorus line. In order to address the effect of the environment on the building exposed to open sea streams microclimatic data were collected for one year. The synergistic effect of the sea-salt aerosol and microclimatic conditions were discussed for the assessment of the impact of the marine environment on the durability of the Mansion, identifying the more vulnerable parts of the building as well as the more critical periods. The results indicate that while moisture content changes from 20.9% to 36.7% and temperature changes from 14.1°C to 28.7°C, thermal conductivity coefficient changes from 0.18 $W \cdot m^{-1}K^{-1}$ to 0.26 $W \cdot m^{-1}K^{-1}$, according to the facade of the building and the season as similar to previous studies.

KEYWORDS: Wood structures, historical buildings, thermal conductivity, sustainability.

INTRODUCTION

Finely worked wood was the predominant construction material for the majority of traditional Turkish houses, including yalıs, a house constructed at immediate waterside and usually built with an architectural concept that takes into account the characteristics of the coastal location. The hundreds of waterside residences, mostly dating from the 19th century, sprinkled along the Bosphorus in Istanbul, constitute one of the city's landmarks.

It is well known that the marine microclimate is extremely dangerous for the conservation of movable and immovable heritage assets, especially which are constructed by wood material, because it intensifies natural weathering through the deposition of sea-salt particles that is controlled by various environmental parameters. Marine aerosol intensifies the natural

weathering through the deposition of sea-salt particles that may react with the surfaces and structures depending on the environmental parameters. Relative humidity variations can cause crystallization-dissolution cycles of salts which could penetrate into the material and generate decay. Buildings in marine environment are also vulnerable to biodegradation that is very effective in humid environments. As a consequence, structures and objects exposed to sea water and high moisture levels required frequent maintenance and restoration works.

Fig. 1: Florya Ataturk Marine Mansion (experimental object).

The importance of microclimatology in the preservation and restoration of cultural heritage is widely recognized (Bernardi 2008, Camuffo 2014, Thomson 1986). The study of microclimate is fundamental in the assessment of the weathering surfaces exposed to outdoor and indoor environments (Becherini et al. 2010, Becherini et al. 2013, Camuffo et al. 2004, Fojtik 2018) as the microclimatic conditions play a key role in the starting and developing not only of physical processes, but also chemical and biological ones, often acting in synergism. Moreover, in literature are reported several examples of unsuitable thermal-hygrometric conditions in historical buildings that are usually built with traditional materials, generally stone and wood, that have a bad thermal and hygrometric behaviour (Thomson 1986, Donovan 1986, Mills et al. 1987, Michalski 1990, Grinzato et al. 2002, Abuku et al. 2009, Moradias et al. 2012). In addition, the marine environment can be considered particularly critical for conservation issues, as the atmosphere is enriched with particles that are naturally generated by the action of wind on the seawater surface. Several authors have showed that marine environments that are charged with salts cause deterioration of the construction materials (Davide 2014, Meira et al. 2006, Morcillo et al. 2000, Erkal et al. 2012). Anyhow, most of the literary studies are focused on concrete structures and stone materials (Alao et al. 2014, Chabas et al. 2000), or they address only the chemical weathering due to sea-salts aerosol (Chabas et al. 2000, Zezza et al. 1995, Stefanis et al. 2005). Nevertheless, a deep and comprehensive research about microclimate and sea effects on historical structures is rather lacking in literature. The present study wants to provide an integrated approach to the problem of the impact of microclimate and sea streams on historical buildings, following the example of other studies in literature applied to other topics (Nava et al. 2010).

In this paper it is aimed at studying the impact of the microclimate on historical buildings exposed to open sea streams, through the representative case study of the Florya Ataturk Marine Mansion (Fig. 1), a historic presidential residence located offshore in the Sea of Marmara in the Florya neighbourhood of the Bakirkoy district in Istanbul. Built in 1935 by the municipality of Istanbul for Atatürk's recreational use, it is erected on steel piles driven into the seabed and linked to the mainland by a wooden pier of about 70 m in length. The building is totally defenceless to weather and sea effects, therefore periodically and costly restoration work is made. The damage patterns observed are similar to other historical buildings located nearby the Bosphorus strip mainly because of sea effect and salt deterioration.

The research is aimed at studying the impact of the marine microclimate on the Florya Ataturk Marine Mansion in Istanbul, selected as reference for the huge number of wooden buildings alongside the Bosphorus exposed to open sea streams.

The impact of the marine environment on the durability of the mansion was assessed by the analysis of the meteorological and microclimatic data in synergy with the severe sea effects. The more vulnerable parts of the building as well as the more critical periods were identified. The ambient conditions that the material is exposed to each season are different, which leads to different deformations on the material. These deformations can also affect the heat permeability of the material positively or negatively. The microclimate and sea effects were investigated for the environmental risk assessment of the Florya Ataturk Marine Mansion. The microclimate nearby the mansion was monitored continuously for one year taking also into account the local climatology. Moisture content and surface temperature of the walls were measured outside. Moisture and temperature figures were analysed on daily, weekly, monthly and yearly basis. Also, thermal conductivity coefficients were measured at certain periods during the year by placing wood materials of the same properties on the building facades where on-site measurements were made.

MATERIAL AND METHODS

In this study, the temperature and humidity values of the surface of the building were measured with hand-held measuring instruments that do not damage the building since it is a historical building. Moisture measurement (moisture meter Testo-616) and for the surface temperature measurement Testo 905-T2 was used. For heat conduction coefficient measurements; the samples are subjected to the equinox periods determined as critical periods, in June-July-August, September-October-November, December-January-February, March-April-May, the front and left side facades selected as vulnerable partitions (the front with the most sunbathing time and the left side with the least sunshine duration). Then the samples were subjected to a thermal conductivity test in the laboratory with a thermal conductivity meter (thermal conductivity meter Cole-Parmer) by comparison method according to the test standard (Fig. 2). In this measurement device using the comparison method, the heat conduction coefficient of the sample is determined using a reference body whose heat conduction coefficient is known. The temperature difference was established by placing the sample and reference body between the heat source and the heat sink. The amount of heat energy passing through the sample and reference body is the same. The heat transfer coefficient of the sample was determined by using the upper and lower thermal values of the sample and the heat conduction coefficient of the reference body.

The wooden material used in the building is scots pine. When the literature is examined, holocellulose, alpha cellulose and lignin content were found to be approximately 71-74%, 47-49% and 26-29% respectively (Tutus et al. 2010, Kılıc et al. 2010, Abuamoud et al. 2018, Zborowska et al. 2007) (Tab. 1). Standard sized samples of this pine material are produced and placed on the front and side of the building. Specimens produced according to the test device have a circular cross-section of 11.28 cm in diameter (Fig. 2).

Tab. 1: Main chemical components of scots pine (Tutus et al. 2010, Kılıc et al. 2010, Abuamoud et al. 2018, Zborowska et al. 2007).

Chemical components	Holocellulose	Alpha cellulose	Lignin
Ratio	71-74%	47-49%	26-29%

Fig. 2: A cross-section of pinewood specimen.

Fourier law was used to calculate the heat transfer coefficient by using the temperature values obtained from the comparison method. Assuming that there is no heat transfer in the radial direction from the sample and reference body, the amount of heat passing through the sample is equal to the amount of heat passing through the reference material.

RESULTS AND DISCUSSION

All the data collected during the first year with automatic and manual devices was analysed in their spatial and temporal trends in order to have a complete picture of the microclimate inside the mansion and outside on the basis of weekly, monthly and yearly periods. The monitoring of the microclimate on the Florya Ataturk Marine Mansion was performed for one year with automatic devices. The moisture content of the outer and inner walls of the building was measured manually in the different seasons. In addition, in summer and winter the thermal behaviour of inner wall surfaces differently oriented was investigated by means of thermography. The measured moisture, temperature and calculated thermal conductivity coefficient values are presented in Tabs. 2, 3 and 4, resp.

Tab. 2: Monthly moisture content (MC) values measured in site.

Year	Months	Facade	MC (%)
2018	June-July-August	Front	36.7
2018	June-July-August	Left side	32.9
2018	September-October-November	Front	27.8
2018	September-October-November	Left side	24.7
2018	December-January-February	Front	22.8
2018	December-January-February	Left side	20.9
2018	March-April-May	Front	33.1
2018	March-April-May	Left side	27.4

Tab. 3: Monthly temperature degrees measured in site.

Year	Months	Facade	Temperature (°C)
2018	June-July-August	Front	28.7
2018	June-July-August	Left side	24.1
2018	September-October-November	Front	21.9
2018	September-October-November	Left side	20.3
2018	December-January-February	Front	18.7
2018	December-January-February	Left side	14.1
2018	March-April-May	Front	22.8
2018	March-April-May	Left side	19.3

Tab. 4: Monthly calculated thermal conductivity coefficients.

Year	Months	Facade	k (W·m⁻¹K⁻¹)
2018	June-July-August	Front	0.26
2018	June-July-August	Left side	0.24
2018	September-October-November	Front	0.21
2018	September-October-November	Left side	0.20
2018	December-January-February	Front	0.19
2018	December-January-February	Left side	0.18
2018	March-April-May	Front	0.24
2018	March-April-May	Left side	0.21

According to this; the difference in temperature and moisture between the front and left side facades is clearly visible. Accordingly, the heat transfer coefficient is significantly higher in the samples placed on the facade, which is heavily exposed to microclimate effects, than the samples placed on the other facade. According to this; it is important for building sustainability to concentrate the protection methods and frequency on the front facade compared to the side facade.

Graphs summarizing the variation of the thermal conductivity coefficient depending on temperature and air humidity are presented in Fig. 3 and Fig. 4.
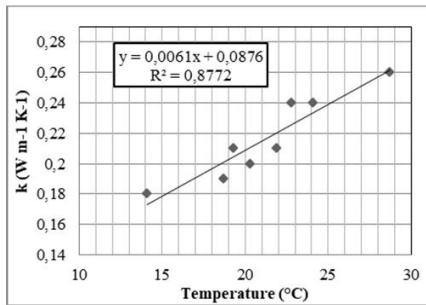
Fig. 3: Thermal conductivity coefficient according to temperature.
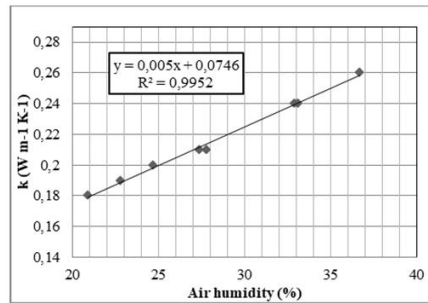
Fig. 4: Thermal conductivity coefficient according to air humidity.

When we compare these values with the studies in the literature, it can be seen that similar results are obtained. In their study which analyses the variations of thermal conductivity under various temperatures, Dell'Isola et al. (2012) experimentally showed that the thermal conductivity coefficient of pinewood increased with increasing temperature and water content ratios (Fig. 5 and Fig. 6).
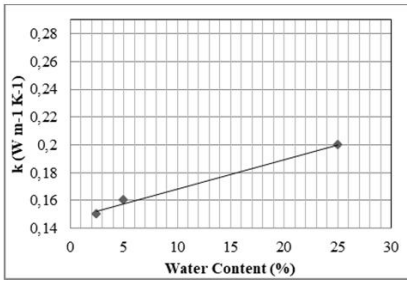
Fig. 5: Thermal conductivity coefficient according to water content at 10°C. (Dell'Isola et al. (2012)).
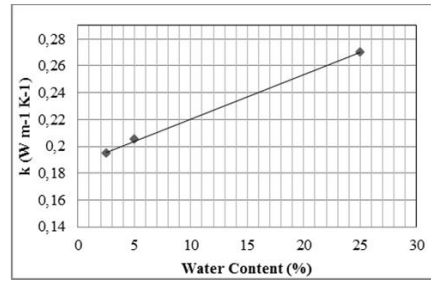
Fig. 6: Thermal conductivity coefficient according to water content at 30°C. (Dell'Isola et al. (2012)).

Troppova et al. (2015) examined in their study the variability of the thermal conductivity coefficient of wood-based fibreboards according to the increase in temperature depending on air humidity from -10°C to 60°C. It was found that the moisture content of material increases from 0% to 14.29% and they also determined that the conductivity coefficient increased (Figs. 7 and 8).
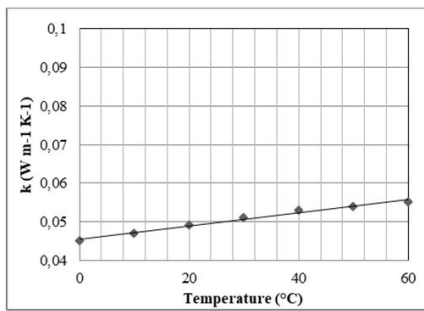
Fig. 7: Thermal conductivity coefficient according to temperature at 0% moisture content. (Troppova et al. (2015)).
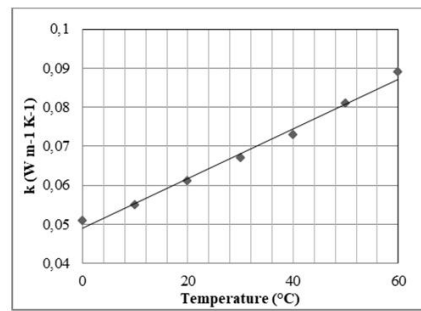
Fig. 8: Thermal conductivity coefficient according to temperature at 14.29% moisture content. (Troppova et al. (2015)).

In addition, Esen et al. (2012) stated in their study that the increase in temperature and humidity values would lead to an increase in the thermal conductivity coefficient in the wood material and they determined that the thermal conductivity coefficient of the fir wood material exposed to the sea effect increased compared to the original sample (Fig. 9). Kol (2009) in her study determined that the thermal conductivity coefficient of 5 different wood species changed with the effect of temperature and humidity and stated that the thermal conductivity of all wood species increased with the increase of temperature and humidity (Fig. 10).
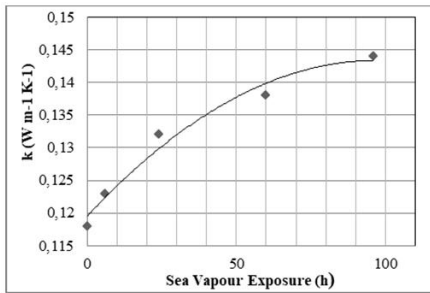
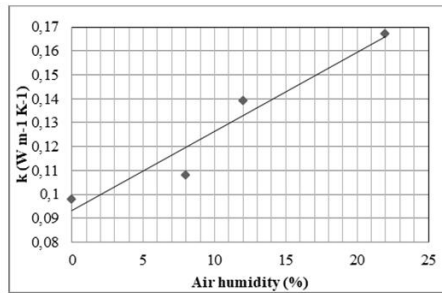Fig. 9: Thermal conductivity coefficient according to sea vapour exposure. (Esen et al. (2012)).

Fig. 10: Thermal conductivity coefficient according to sea vapour exposure. (Kol (2009)).

Trochonowicz et al. (2018) examined the change in air temperature and humidity and thermal conductivity coefficients of the wood based materials and he selected and showed similarly to the studies in the literature that thermal conductivity is dependent on humidity and temperature values (Fig. 11 and Fig. 12).
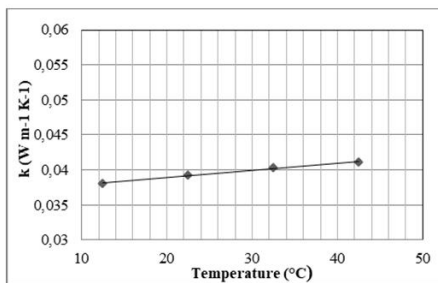

Fig. 11: Thermal conductivity coefficient according to temperature. (Trochonowicz et al. (2018)).
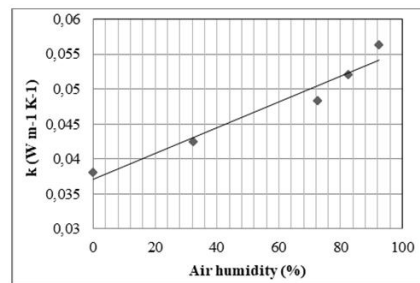
Fig. 12: Thermal conductivity coefficient according to air humidity. (Trochonowicz et al. (2018)).

Examples can be increased with this and similar studies. The common result is that the thermal conductivity coefficient of wood materials is directly related to humidity and temperature. In addition, being open to the sea effect, salinity, wind, etc. are also effective on the thermal conductivity values of wood materials.

CONCLUSIONS

Every historical building is a unique research subject with its inestimable cultural value; nevertheless the Florya Ataturk Marine Mansion can serve as a reference for the huge number of buildings alongside the Bosporus that suffers similar problems. As the mansion is opened to public as "Atatürk Museum" since 1993, the internal microclimate was also monitored and evaluated according to the recommended values for the materials preserved and human comfort requirements. The thermo-hygrometric conditions outside were measured for one year, whilst

specific campaigns were performed to investigate indoor surface temperature and wall moisture content. According to obtained results, it was well understood that thermal conductivity coefficient of the building facade material, pinewood, varies in direct proportion to outside temperature and the moisture content of the material. As a result of the measurements taken from the mansion, a linear correlation was observed between the heat transfer coefficient of the wood and the temperature. This correlation ($y = 0.0061x + 0.0876$, $R^2 = 0.8772$) is compatible with the Fourier heat equation.

Similarly, a linear relationship ($y = 0.05x + 0.0746$, $R^2 = 0.9952$) between air humidity and heat transfer coefficient was observed according to measurements. Therewithal, while the maximum "k" value ($k = 0.26$ W m^{-1}·K^{-1}) as obtained at summer months and front facade (as having most sunbathing time), the minimum one ($k = 0.18$ W m^{-1}·K^{-1}) was obtained at winter months and left facade as exactly opposite. The results of this research could provide useful information for the future better preservation of the building and its content, thus reducing maintenance and restoration work and improving the internal conditions in terms of conservation requirements and human comfort issues. Also, the results which are obtained in this project can contribute to elaborate the more appropriate conservation strategy for the Mansion and also for other similar buildings threatened by the risks related to the marine environment.

REFERENCES

1. Abuamoud, M., Ates, S., Durmaz, E., 2018: Comparison of some anatomical, chemical and fibrous characteristics of Turkish Red pine (*Pinus brutia* Ten.) sampled from different region. Kastamonu University. Journal of Forestry Faculty 18(1): 75-82.
2. Abuku, M., Janssen, H., Roels, S., 2009: Impact of wind driven rain on historic brick wall buildings in moderately cold and humid climate: Numerical analyses of mould growth risk, indoor climate and energy consumption. Energy and Buildings 41(1): 101-110.
3. Alao, O., Alexander, M., Beushausen, H., 2014: Understanding the influence of marine microclimates on the durability performance of RC structures. In: Construction materials and structures (Eds. Ekolu SO, et al.). IOS Press, Pp 1537.
4. Becherini, F., Bernardi, A., Frassoldati, E., 2010: Microclimate inside a semi-confined environment: valuation of suitability for the conservation of heritage materials. Journal of Cultural Heritage 11(4): 471-476.
5. Becherini, F., Bernardi, A., Vivarelli, A., Pockelé, L., De Grandi, S., Gandini, A., García, O., Zubiaga, M., Espada Suárez, J.C., Sperandio, B., 2013: Environmental risk assessment and preventive conservation strategy for the porch of the glory. Santiago of Compostela Cathedral. Journal of Environmental Science and Engineering B2, Pp 299-303.
6. Bernardi, A., 2008: Microclimate inside cultural heritage buildings. Prato, Padova, 171 pp.
7. Camuffo, D., 2014: Microclimate for cultural heritage. Elsevier, Amsterdam, 560 pp.
8. Camuffo, D., Pagan, E., Bernardi, A., Becherini, F., 2004: The impact of heating, lighting and people in re-using historical buildings: a case study. Journal of Cultural Heritage 5(4): 409-416.
9. Chabas, A., Jeannette, D., Lefevre, R.A., 2000: Crystallization and dissolution of airborne sea-salts on weathered marble in a coastal environment at Delos (Cyclades Greece). Atmospheric Environment 34(2): 219-224.

10. Davide, B., 2014: Salt deterioration and microclimate in historical Buildings. Intermediary report of the project. Institut für Denkmalpflege, Forschungsstelle Technologie und Konservierung, ETH Zürich, Pp 1-10.

11. Dell'Isola, M., D'Ambrosio Alfano, F.R., Giovinco, G., Ianniello, E., 2012: Experimental analysis of thermal conductivity for building materials depending on moisture content. International Journal of Thermophysics 33(8-9): 1674-1685.

12. Donovan, P.D., 1986: Protection of metals from corrosion in storage and transit. Wiley, New York, 228 pp.

13. Erkal, A., D'Ayala, D., Sequeira, L., 2012: Assessment of wind-driven rain impact, related surface erosion and surface strength reduction of historic building materials. Building and Environment 57: 336-348.

14. Esen, R., Ozcan, C., Likos, E., Ozkan, O.E., 2012: The effects of exposure to sea water steam on thermal conductivity of varnished fir wood. Kastamonu University. Journal of Forestry Faculty, special issue, Pp 217-220.

15. Fojtik, R., 2019: Moisture content analysis of wooden bridges. Wood Research 64(3): 529-536.

16. Grinzato, E., Bison, P.G., Smarinetti, S., 2002: Monitoring of ancient buildings by the thermal method. Journal of Cultural Heritage 3(1): 21-29.

17. Kılıc, A., Sarıusta, S.E., Hafızoglu, H., 2010: Chemical structure of compression wood of *Pinus sylvestris*, *P. nigra* and *P. brutia*. Journal of Bartin Faculty of Forestry 12(18): 33-39.

18. Kol, H.S., 2009: Pine thermal, dielectric properties. BioResources 4(4): 1663-1669.

19. Meira, M.C., Andrade, I.J., Padaratz, M.C., Alonso, J.C., Borba, J.R., 2006: Measurements and modelling of marine salt transportation and deposition in a tropical region in Brazil. Atmospheric Environment 40: 5596-5607.

20. Michalski, S., 1990: Towards specific lighting guidelines. International Commission of Museums-Committee for Conservation. 9th Triennial Meeting, Dresden, Pp 583-588.

21. Mills, J., White, R., 1987: The organic chemistry of museum objects. London, 165 pp.

22. Moradias, P.A., Silva, P.D., Castro-Gomes, J.P., Salazar, M.V., Pires, L., 2012: Experimental study on hygrothermal behaviour of retrofit solutions applied to old building walls. Construction and Building Materials 35: 864-873.

23. Morcillo, M., Chico, B., Mariaca, L., Otero, E., 2000: Salinity in marine atmospheric corrosion: its dependence on the wind regime existing in the site. Corrosion Science 42(1): 91-104.

24. Nava, S., Becherini, F., Bernardi, F., Bonazza, A., Chiari, M., Garcia, I., Lucarelli, F., Ludwig, N., Migliori, A., Sabbioni, C., Udisti, R., Valli, G., ve Vecchi, R., 2010: An integrated approach to assess air pollution threats to cultural heritage in a semi-confined environment: The case study of Michelozzo's Courtyard in Florence (Italy). Science of the Total Environment 408: 1403-1413.

25. Stefanis, A., Theoulakis, P., Pilinis, C., 2005: The decay effects of sea-salt aerosol on the surface of historic buildings. In Proceedings of the 9th International Conference on Environmental Science and Technology. Rhodes Island, Greece, 1-3 September 2005, Pp 432-437.

26. Thomson, G., 1986: The museum environment. 2nd edition. London, 293 pp.

27. Trochonowicz, M., Galas, M., 2018: Influence of air humidity and temperature on thermal conductivity of wood-based materials. Budownictwo i Architektura 17(4): 77-86.

28. Troppova, E., Svehlık, M., Tippner, J., Wimmer, R., 2015: Influence of temperature and moisture content on the thermal conductivity of wood-based fibreboards. Materials and Structures 48(12): 4077-4083.

29. Tutus, A., Kurt, R., Alma, M., Meric, H., 2010: Chemical analysis of Scotch pine wood and its thermal properties. In: Proceedings of the 3rd National Black Sea Forestry Congress. Artvin, Turkey, 20-22 May 2010, Pp 1845-1851.

30. Zborowska, M., Babinski, L., Gajewska, J., Waliszewska, B., Pradzynski, W., 2007: Physical and chemical properties of contemporary pine wood (*Pinus Sylvestris* L.). In: Conditions of a wet archaeological site in Biskupin. Folia Forestalia Polonica, Series A 38(1): 13-26.

31. Zezza, F., Macrì, F., 1995: Marine aerosol and stone decay. The Science of Total Environment 167(1): 123-143.

Esra Celik, Ismail Cengiz Yilmaz*
Istanbul Arel University
Faculty of Engineering and Architecture
Department of Civil Engineering
Istanbul
Turkey
*Corresponding author: cengizyilmaz@arel.edu.tr

Deniz Yilmaz
Istanbul Arel University
Faculty of Engineering and Architecture
Department of Mechanical Engineering
Istanbul
Turkey